BASIC ELEMENTS OF CRYSTALLOGRAPHY

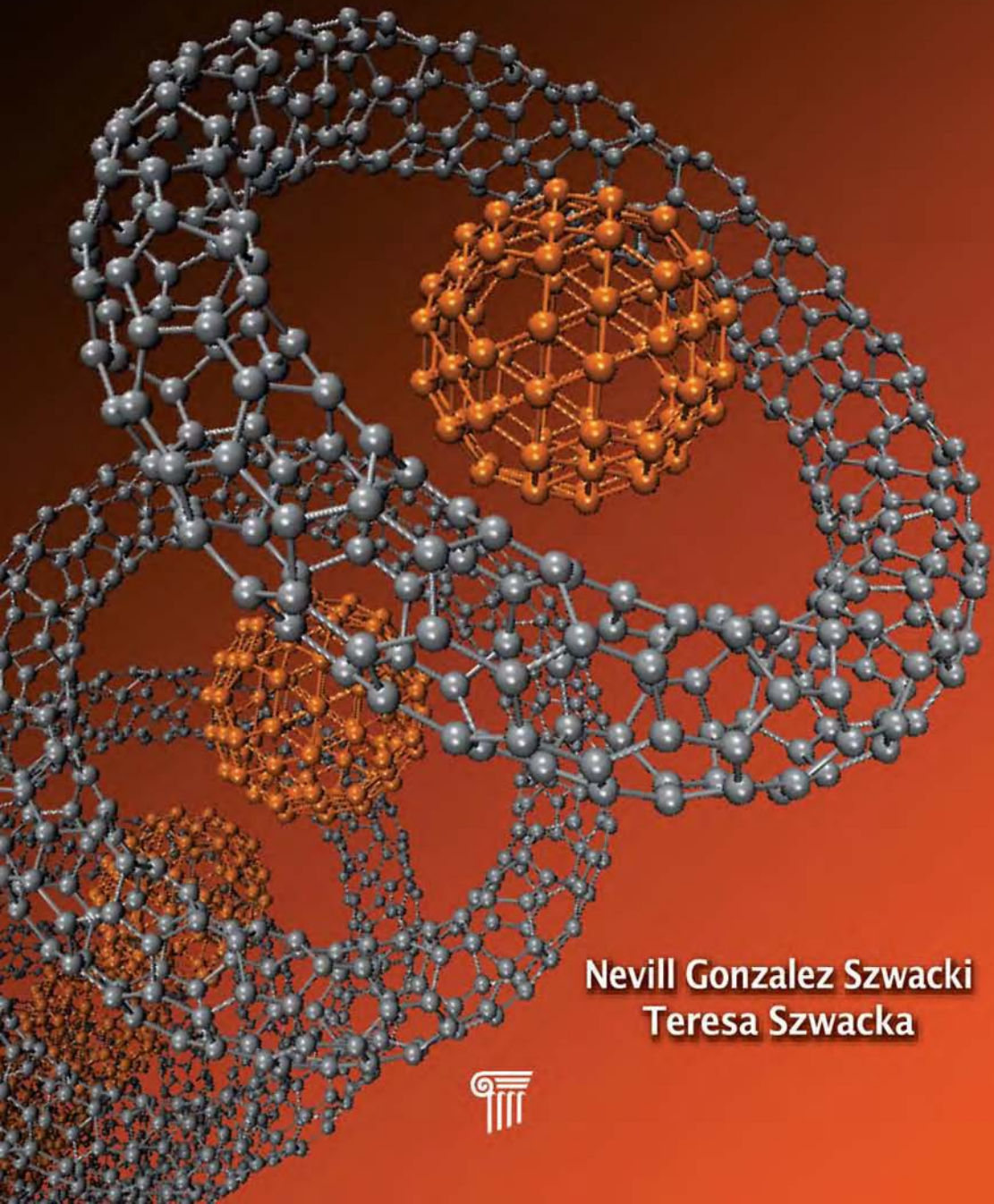

Nevill Gonzalez Szwacki
Teresa Szwacka

BASIC ELEMENTS OF CRYSTALLOGRAPHY

BASIC ELEMENTS OF CRYSTALLOGRAPHY

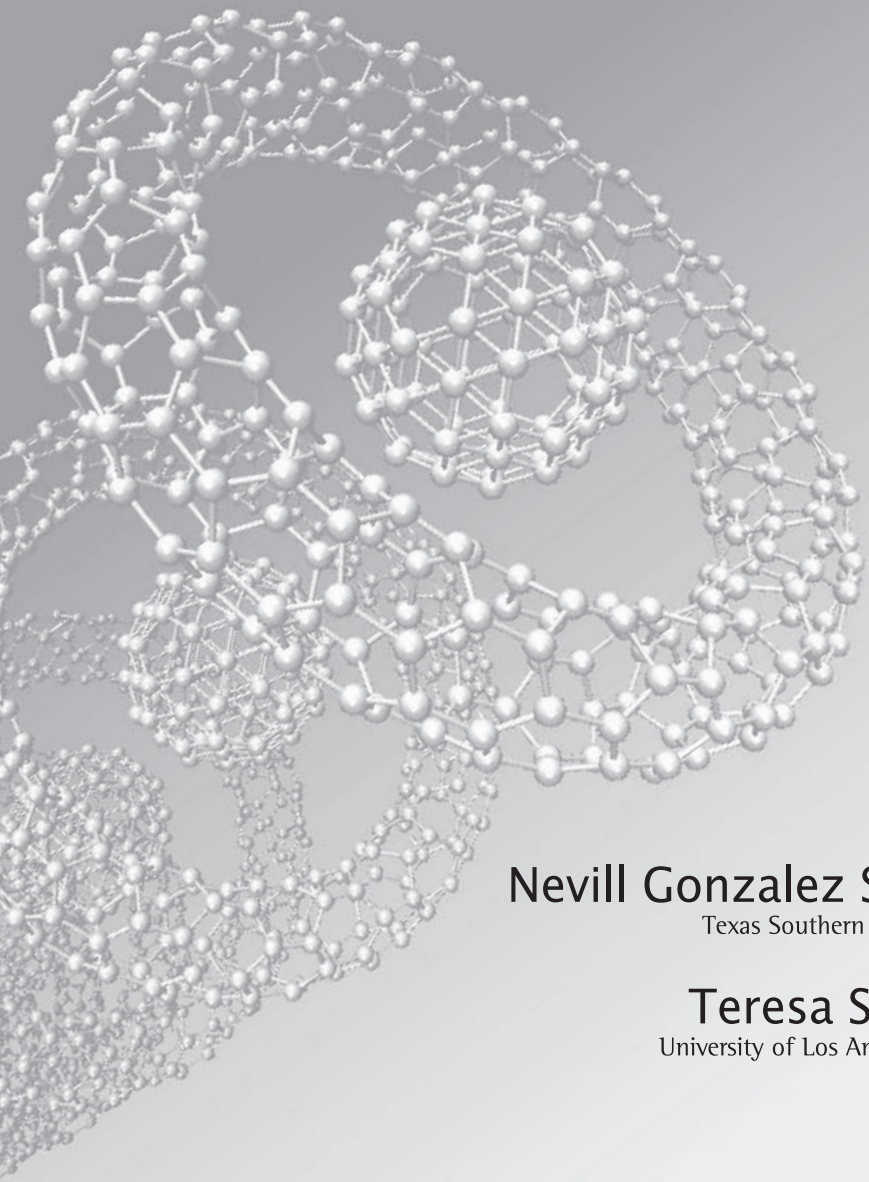

Nevill Gonzalez Szwacki
Texas Southern University, USA

Teresa Szwacka
University of Los Andes, Venezuela

PAN STANFORD PUBLISHING

Published by

Pan Stanford Publishing Pte. Ltd.
Penthouse Level, Suntec Tower 3
8 Temasek Boulevard
Singapore 038988

Email: editorial@panstanford.com
Web: www.panstanford.com

British Library Cataloguing-in-Publication Data
A catalogue record for this book is available from the British Library.

BASIC ELEMENTS OF CRYSTALLOGRAPHY

Copyright © 2010 by Pan Stanford Publishing Pte. Ltd.

All rights reserved. This book, or parts thereof, may not be reproduced in any form or by any means, electronic or mechanical, including photocopying, recording or any information storage and retrieval system now known or to be invented, without written permission from the Publisher.

For photocopying of material in this volume, please pay a copying fee through the Copyright Clearance Center, Inc., 222 Rosewood Drive, Danvers, MA 01923, USA. In this case permission to photocopy is not required from the publisher.

ISBN-13 978-981-4241-59-5
ISBN-10 981-4241-59-8

Printed in Singapore.

PREFACE

This book is intended to be a complete and clear introduction to the field of crystallography for undergraduate and graduate students and lecturers in physics, chemistry, biology, materials and earth sciences, or engineering. It includes an extensive discussion of the 14 Bravais lattices and the reciprocal to them, basic concepts of point group symmetry, the crystal structure of elements and binary compounds, and much more. Besides that, the reader can find up-to-date values for the lattice constants of most elements and about 650 binary compounds (half of them containing rare earth metals). The entire notation in this book is consistent with the International Tables for Crystallography.

We have made all possible effort to attract the reader with high quality illustrations showing all basic concepts in this area. Our purpose was to show rather than describe "using many words" the structure of materials and its basic properties. We believe that even readers who are completely not familiar with the topic, but still want to learn how the atoms are arranged in crystal structures, will find this book useful.

The text is organized into six chapters. Chapter I introduces basic concepts and definitions in the field of crystallography starting with one- and two-dimensional structures. Chapter II provides a detailed description of the 14 Bravais lattices. Chapter III describes the most important crystal structures of the elements with special emphasis on the close-packed structures and the interstices present in them. Chapter IV presents the structures of the most important binary compounds and reports the lattice constants of about 650 of them. Chapter V is devoted to the reciprocal lattice. Chapter VI, which is the final one, shows the relation between a direct lattice and its reciprocal.

All chapters are accompanied by exercises designed in such a way to encourage students to explore the crystal structures he/she is learning about. Our goal always is to help the reader to develop spatial intuition by solving the exercises graphically. Since computers are an essential part of today's education, we invite the reader to make use of crystallographic databases. In most of the database web pages, it is possible to visualize crystal structures in 3D either directly from the web browser or by downloading input files with the coordinates of the structures. Some of the freely available (or with open access options) databases are:

- ICSD for WWW-interface with free demo access (http://icsd.ill.fr)
- American Mineralogist Crystal Structure Database (AMCSD) (http://rruff.geo.arizona.edu/AMS/amcsd.php)
- Crystal Lattice Structures (http://cst-www.nrl.navy.mil/lattice/index.html)
- Crystallography Open Database (COD) (http://cod.ibt.lt).

We also encourage more advanced readers to create their own input files with crystal structure coordinates or download them from the web. The structures can be then viewed with, e.g., the freely available software called Jmol (http://www.jmol.org). This program allows for the structure to be manipulated, i.e., rotated, scaled, and translated, and allows for the measurement of internal coordinates, e.g., bond lengths and angles.

We hope the reader will enjoy this book and will use it as a gateway for understanding more advanced texts on this topic.

N. Gonzalez Szwacki
Houston, USA
T. Szwacka
Mérida, Venezuela
July 2009

CONTENTS

PREFACE v
ABBREVIATIONS xi
I. CRYSTAL STRUCTURE
1. Introduction 1
2. One-Dimensional Crystal Structures 1
3. Two-Dimensional Crystal Structures 4
4. Problems 13
II. THREE-DIMENSIONAL CRYSTAL LATTICE
1. Introduction 17
2. Examples of Symmetry Axes of Three-Dimensional Figures 17
3. Symmetry Axes of a Cube 20
4. Symmetry Axes of a Set of Points 22
5. Crystal Systems 24
6. Conventional Cell for the Trigonal System 27
7. The 14 Bravais Lattices 28
7.1. Introduction 28
7.2. The Triclinic System 29
7.3. The Monoclinic System 29
7.4. The Orthorhombic System 32
7.5. The Tetragonal System 34
7.6. The Cubic System 34
7.7. The Trigonal and Hexagonal Systems 35
7.8. Symbols for Bravais Lattices 35
7.9. Conclusions 36
8. Coordination Number 38
9. Body Centered Cubic Lattice 39
10. Face Centered Cubic Lattice 42
11. Rhombohedral Unit Cell in a Cubic Lattice 46
11.1. Rhombohedral Unit Cell of the *sc* Lattice 46
11.2. Simple Cubic Crystal Structure 48
11.3. Interpretation of Data for As, Sb, Bi, and Hg 49
12. Trigonal Lattice 50

13. Triple Hexagonal Cell *R* in a Cubic Lattice 55
14. Wigner-Seitz Cell 56
14.1. Construction of the Wigner-Seitz Cell 56
14.2. The Wigner-Seitz Cell of the *bcc* Lattice 56
14.3. The Wigner-Seitz Cell of the *fcc* Lattice 58
15. Problems 58
III. CRYSTAL STRUCTURES OF ELEMENTS
1. Introduction 67
2. Pearson Notation and Prototype Structure 68
3. The Filling Factor 69
4. Simple Cubic Structure 69
5. Body Centered Cubic Structure 71
6. Face Centered Cubic Structure 73
7. Close-Packed Structures 75
8. Double Hexagonal Close-Packed Structure 79
9. Samarium Type Close-Packed Structure 81
10. Hexagonal Close-Packed Structure 83
11. Interstices in Close-Packed Structures 87
12. Diamond Structure 92
13. Atomic Radius 98
14. Problems 102
IV. CRYSTAL STRUCTURES OF IMPORTANT BINARY COMPOUNDS
1. Introduction 107
2. The Ionic Radius Ratio and the Coordination Number 107
3. Zinc Blende Structure 112
4. Calcium Fluoride Structure 114
4.1. Fluorite Structure 114
4.2. Anti-Fluorite Structure 117
5. Wurtzite Structure 118
6. Nickel Arsenide Related Structures 124
6.1. NiAs Structure 124
6.2. TiAs Structure 133
7. Sodium Chloride Structure 134
8. Cesium Chloride Structure 144
9. Problems 149

V. RECIPROCAL LATTICE
1. Introduction 153
2. The Concept of the Reciprocal Lattice 153
3. Examples of Reciprocal Lattices 162
3.1. Reciprocal of the Triclinic Lattice 162
3.2. Reciprocal of the Simple Cubic Lattice 162
3.3. Reciprocal of the Face Centered Cubic Lattice 164
4. Problems 165
VI. DIRECT AND RECIPROCAL LATTICES
1. Introduction 169
2. Miller Indices 169
3. Application of Miller Indices 175
4. Problems 180
REFERENCES 185
INDEX 187

ABBREVIATIONS

The following abbreviations are used throughout this book:

bcc	body centered cubic
ccp	cubic close-packed
dhcp	double hexagonal close-packed
fcc	face centered cubic
hcp	hexagonal close-packed
sc	simple cubic
thcp	triple hexagonal close-packed
NN	Nearest Neighbors
NNN	Next Nearest Neighbors
TNN	Third Nearest Neighbors
RE	Rare Earth
TM	Transition Metal

I. CRYSTAL STRUCTURE

1. Introduction

Many of the materials surrounding us (metals, semiconductors, or insulators) have a crystalline structure. That is to say, they represent a set of atoms distributed in space in a particular way. Strictly speaking, this is the case when the atoms occupy their equilibrium positions. Obviously, in the real case they are vibrating. Below we will see examples of crystal structures, beginning with one-dimensional cases.

2. One-Dimensional Crystal Structures

A one-dimensional crystal structure is formed by a set of atoms or groups of them distributed periodically in one direction. In Fig. 1 there are three examples of one-dimensional crystal structures. In all three cases, the whole crystal structure may be obtained by placing atoms (or groups of them), at a distance $a = |\vec{a}|$ one from the other, along a straight line. When we translate an infinite structure by vector $\vec{a}$ we obtain the same structure. The same will occur if we translate the structure by a vector equal to the multiple of vector $\vec{a}$, that is, $n\vec{a}$, where $n \in \mathbb{Z}$. The vector $\vec{a}$ is called a *primitive translation vector*. A clear difference can be seen between the crystal structure from Fig. 1a and the other two structures in this figure. In the structure from Fig. 1a all the atoms have equivalent positions in space, while in the case of structures from Figs. 1b and 1c this does not occur. It can be easily observed that in the structure from Fig. 1b the nearest neighbor (NN) atoms of the atom labeled as 1 (open circles) are of another type (filed circles) and the NNs of the atom labeled as 2 are atoms of type 1. In the case of the structure from Fig. 1c, the atom labeled as 1 has its NN on the right side, while the atom labeled as 2, on the left side.

The fact that after translating an infinite crystal structure by the primitive translation vector $\vec{a}$ or its multiple, $n\vec{a}$, we obtain the same structure characterize all crystal structures. This is the starting point to introduce a certain mathematical abstraction called *lattice* – a periodic arrangement of points in space, whose positions are given by vectors $n\vec{a}$ which can have as an initial point any point of the one-dimensional space.

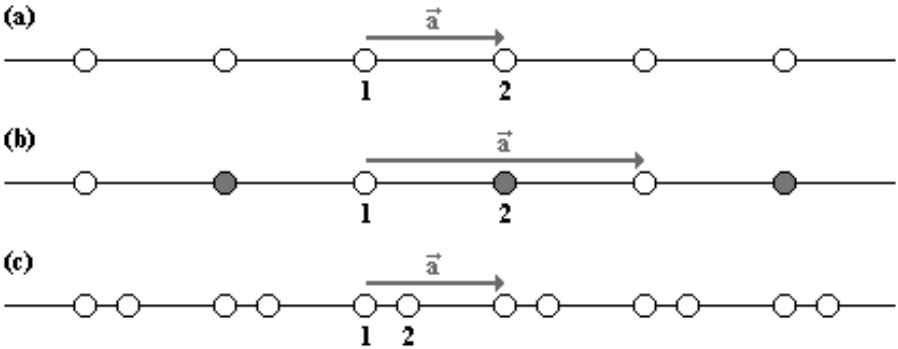

Figure 1 Three different one-dimensional crystal structures: **(a)** periodic repetition of identical atoms, **(b)** periodic repetition of a building block composed of two different atoms, and **(c)** periodic repetition of a building block composed of two identical atoms.

The atomic arrangement in the crystal structure looks the same from any point (node) of the lattice, what can be seen in Fig. 2, where we show two different arrangements of lattice points respect to atoms of the crystal structures from Fig. 1. Therefore, all lattice points have equivalent positions in the crystal structure, what we cannot say in general about the atoms. As it is shown, e.g., in Fig. 1b the equivalency between the neighborhood of the atoms does not exist when the crystal structure is made up of more than one type of atoms. Fig. 1c shows that the distribution of atoms in space can be another possible source of inequivalency between the atoms. The lattice is a mathematical object that possesses the information about the translation symmetry of the crystal structure. The relation between the structure and its lattice will be discussed in details below.

Let us now determine the number of atoms in a volume defined by vector $\vec{a}$. When the initial and final points of vector $\vec{a}$ coincide with the center of atoms (see Fig. 2a), one half of each atom belongs to the volume in consideration, so the volume possesses one atom. Besides that, segment a may have other atoms, what is shown in Figs. 2b and 2c. The volume defined by vector $\vec{a}$ always contains the same number of atoms, independently on the position of the initial point of the vector.

The primitive translation vector $\vec{a}$ called also the *basis vector* of the lattice defines a *unit cell* of this lattice, which contains exactly one lattice point. This cell is called a *primitive cell* and its "volume" is equal to $a = |\vec{a}|$. From now on, the volume of the primitive unit cell will be denoted by Ω_0. The entire space lattice with all lattice points can be obtained duplicating an infinite number of times the primitive cell. The position of each cell replica

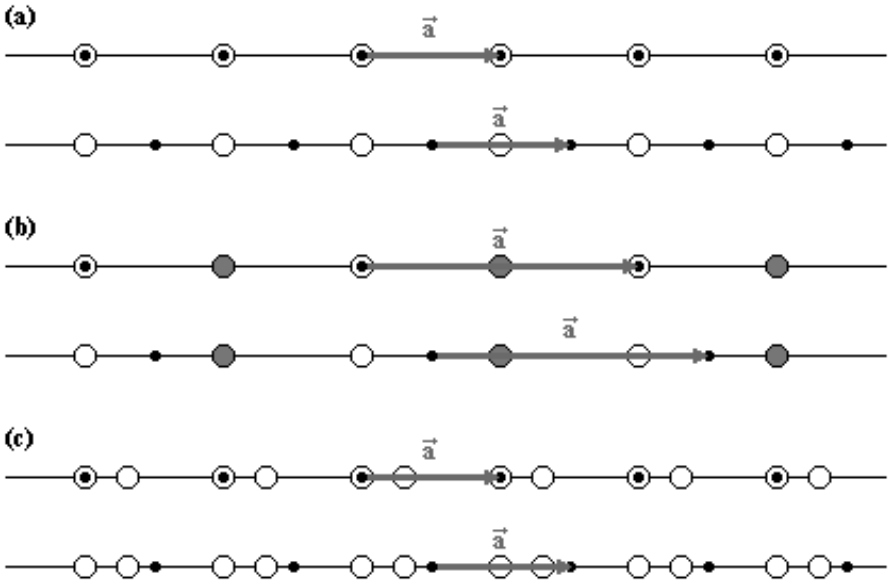

Figure 2 Two different arrangements of lattice points with respect to atoms of the crystal structure, for structures from Fig. 1. In both cases, the atomic arrangement in the crystal structure looks the same from any point of the lattice. The lattice basis vector $\vec{a}$ defines its primitive cell.

is given by a vector $n\vec{a}$. The crystal structure is obtained when we attach to each lattice point a group of atoms, which are within the volume of the primitive cell. This group is called the *basis*. In the case of the crystal structure from Fig. 2a the basis consists of one atom, while in the case of Figs. 2b and 2c of two atoms.

It is obvious that there is more than one way to propose a lattice for a certain crystal structure. For example, the lattice shown in Fig. 3 could be another option for the structure from Fig. 1a. The basis vector of this lattice is two times longer than that defining the lattice proposed in Fig. 2a. We can see in Fig. 3 that the atomic basis of the structure has now two atoms instead of one we had in the previous case. In general we use the lattice in

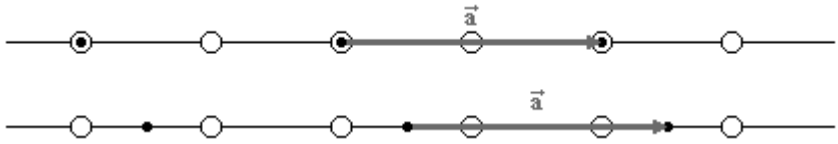

Figure 3 A lattice for the crystal structure from Fig. 1a. In this case, the basis is composed of two atoms. Two different arrangements of lattice points with respect to atoms of the structure are shown.

which the atomic basis of the crystal structure is the smallest one, but sometimes it is convenient to use a different lattice, as we will see farther on.

3. Two-Dimensional Crystal Structures

We will now look at the two-dimensional case, beginning with the example shown in the Fig. 4. In this figure vectors $\vec{a}_1$ and $\vec{a}_2$ are primitive translation vectors. If the infinite crystal structure is translated to a vector $\vec{R}$, that is a linear combination of vectors $\vec{a}_1$, $\vec{a}_2$, given by the formula

$$\vec{R} = n_1\vec{a}_1 + n_2\vec{a}_2 \ , \ \text{where} \ n_1, n_2 \in \mathbb{Z}, \tag{I.1}$$

then the same structure as the original one is obtained. The vectors $\vec{a}_1$, $\vec{a}_2$ can be used to define a lattice. The lattice points may overlap with the centers of atoms like in the Fig. 4. By translating the replicas of the cell I, defined by vectors $\vec{a}_1$, $\vec{a}_2$ in Fig. 4, through all the vectors $\vec{R}$, we can reproduce the entire space lattice.

The cell I in Fig. 4 is not the only one that can reproduce all the space lattice. There is an infinite number of such cells. For example, the cell II, defined by vectors $\vec{a}_1'$ and $\vec{a}_2'$ in Fig. 4, can also reproduce the entire lattice. The volumes of cells I and II are

$$\Omega_0 = a_1 a_2 \sin\sphericalangle(\vec{a}_1, \vec{a}_2) = a_1 h \ \text{ and } \ \Omega_0' = a_1' a_2' \sin\sphericalangle(\vec{a}_1', \vec{a}_2') = a_1 h, \tag{I.2}$$

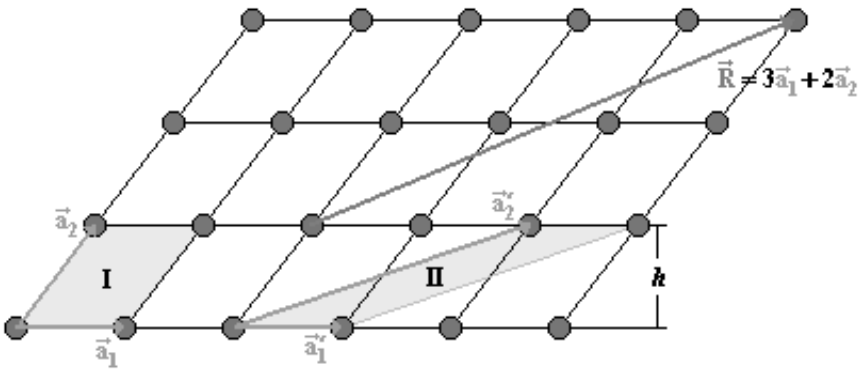

Figure 4 A two-dimensional crystal structure. The lattice points overlap with atom centers. I and II are examples of two unit cells that can reproduce the lattice.

respectively, where $a_1' = a_1$ and $a_2 \sin\sphericalangle(\vec{a}_1, \vec{a}_2) = a_2' \sin\sphericalangle(\vec{a}_1', \vec{a}_2') = h$. So, the two volumes are identical.

We will demonstrate now that the cells I and II from Fig. 4 are primitive, since they only contain one lattice point. Those cells and also the cell 1 in Fig. 5 have 4 atoms at the vertices whose centers represent points of the lattice. Both, the atoms and the lattice points, are shared with neighboring cells. This is shown in Fig. 5, where a highlighted atom (lattice point) is shared by cells 1 to 4. Each cell has a fraction of an atom (lattice point) and the sum of the fractions is 1, giving one atom (lattice point) per cell. The points from the vertices of any cell that is a parallelogram contribute exactly with one lattice point to the cell. All primitive cells have the same volume. This volume corresponds to one point of a lattice. The most commonly used primitive cell is the one which is defined by the shortest or one of the shortest primitive translation vectors of the lattice (e.g. $\vec{a}_1$, $\vec{a}_2$ from Fig. 4). These vectors are called *basis vectors*. Note that the choice of basis vectors is not unique, since even the shortest vectors can be chosen in several different ways. The parallelogram I in Fig. 4 is an example of a *conventional primitive cell* and vectors $\vec{a}_1$, $\vec{a}_2$ are the *conventional basis vectors.*

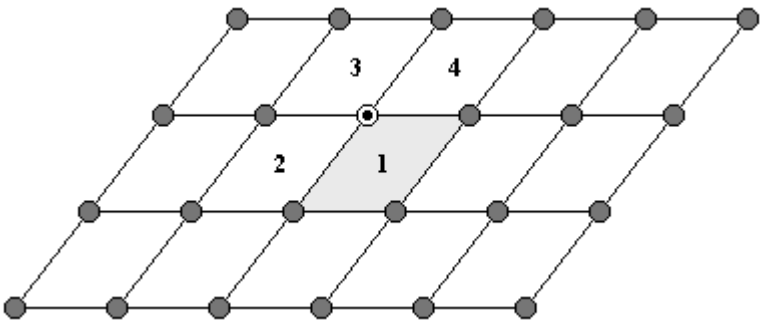

Figure 5 The highlighted atom (lattice point) belongs to four cells which are marked from 1 to 4, therefore only a fraction of this atom (lattice point) belongs to the highlighted cell 1.

For the two-dimensional lattice that we are discussing in this section, we can choose a non primitive unit cell. An example of such a cell is shown in Fig. 6. The cell in this figure possesses two lattice points inside, so the total number of points belonging to it is three.

Let us now place an additional atom in the middle of each parallelogram of type I from Fig. 4. The resulting structure is shown in Fig. 7. The additional atoms are of the same type as the atoms of the original structure.

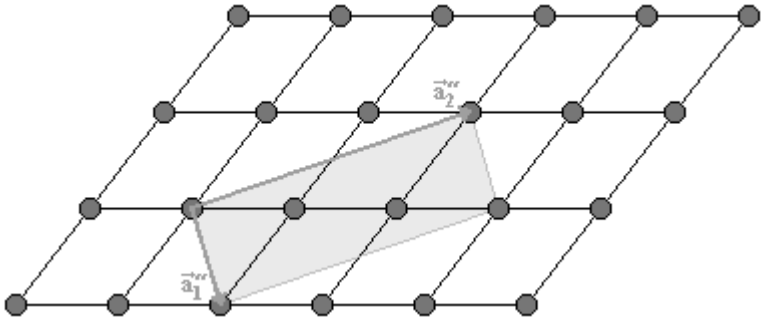

Figure 6 A unit cell that can reproduce the whole lattice. This cell is not primitive since contains 3 lattice points. The lattice points overlap with the centers of atoms.

In Fig. 7 we can observe that the resulting crystal structure is of the same type as the original one, since in both cases the lattices can be chosen in such a way that the atomic basis of each structure possesses only one atom. The vectors $\vec{a}_1$ and $\vec{a}_2$ in Fig. 7 are the primitive translation vectors of such a lattice. Of course we could keep vectors $\vec{a}_1$ and $\vec{a}_2$ defined in Fig. 4 as the primitive translation vectors of the lattice for the structure from Fig. 7, but then the atomic basis would contain two atoms instead of one.

If we place atoms in the middle of the parallelograms of Fig. 4 that are of a different type than the atoms of the host structure then the resulting crystal structure will look as shown in Fig. 8. In this case, the smallest atomic basis contains two atoms (one of each type) and the cell of type I from Fig. 4 represents the conventional primitive cell of the lattice.

Finally, we will consider the case in which we place an additional atom of the same type as the host atoms in the cell of type I from Fig. 4,

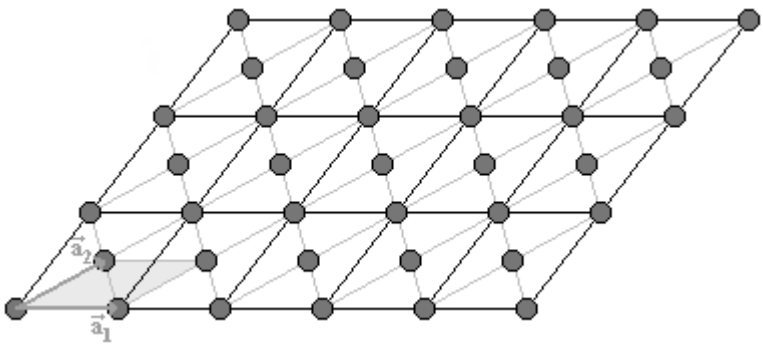

Figure 7 A two-dimensional crystal structure obtained from the structure from Fig. 4 by placing additional atoms in the centers of each unit cell of type I. The vectors $\vec{a}_1$ and $\vec{a}_2$ define a unit cell of the resulting structure which contains one atom.

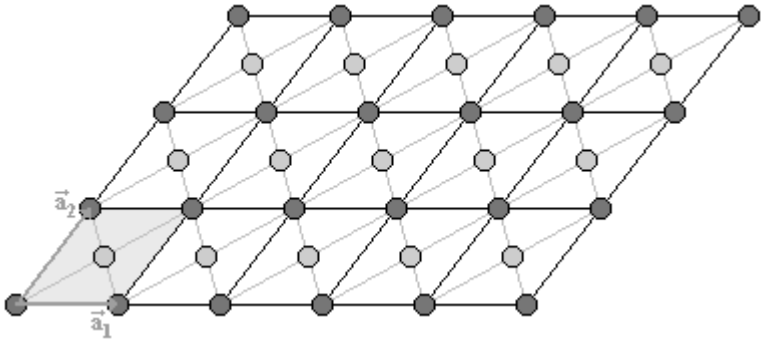

Figure 8 A two-dimensional crystal structure made up of two types of atoms. The unit cell, defined by vectors $\vec{a}_1$, $\vec{a}_2$, has 2 atoms.

however, this time not in the middle of the parallelogram, but in a position with less symmetry as it is shown in Fig. 9. In this case, the smallest atomic basis also contains two atoms but this time they are of the same type. We can observe in Fig. 9 that this crystal structure can be considered a superposition of two identical crystal substructures which are structures from Fig. 4.

Next, we will consider two more examples of two-dimensional crystal structures, namely, the honeycomb and the two-dimensional hexagonal structures. Figure 10 shows the honeycomb structure with a conventional primitive cell that contains two atoms. This is the smallest atomic basis for the honeycomb structure. In Fig. 10, we considered two choices for the initial point of the basis vectors $\vec{a}_1$ and $\vec{a}_2$. In each case, the location of the lattice points with respect to the atoms is different. In one case, the lattice

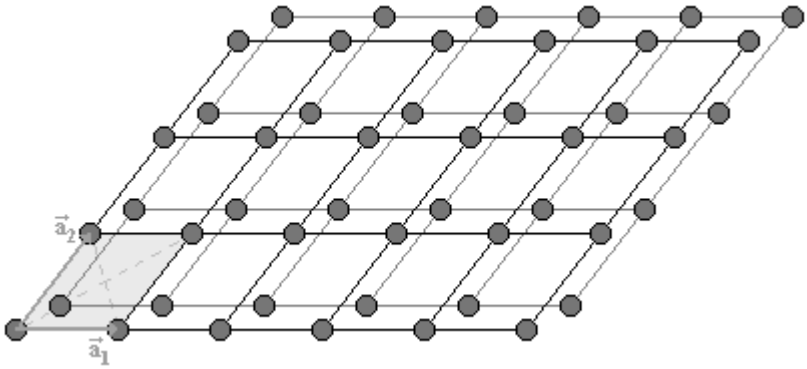

Figure 9 A two-dimensional crystal structure. The primitive cell of the lattice, defined by vectors $\vec{a}_1$ and $\vec{a}_2$, has 2 atoms.

points overlap with the centers of atoms and in the other case, they overlap with the centers of the hexagons. Later we will show that the choice of the initial point of the basis vectors is relevant in the description of a crystal structure.

In Fig. 11 we show a lattice for the honeycomb structure from Fig. 10. This lattice is a two-dimensional hexagonal lattice. The vectors $\vec{a}_1$ and $\vec{a}_2$ defined in Fig. 10 are the basis vectors of this lattice and they define a conventional primitive cell which has the shape of a rhomb.

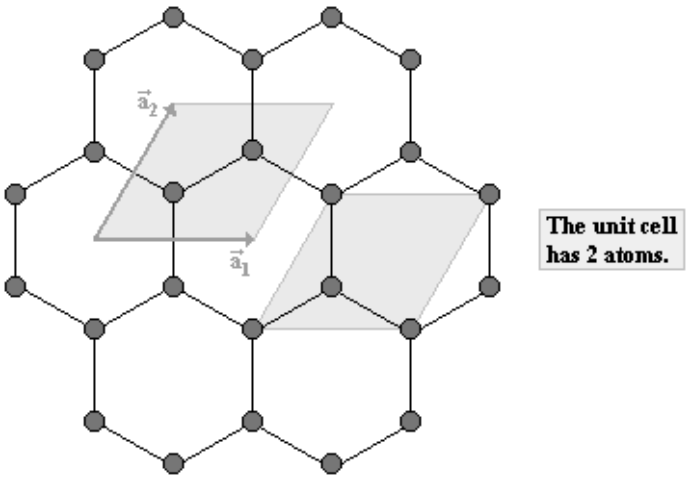

Figure 10 The honeycomb structure. In the figure are shown two positions of the unit cell with respect to the atoms of the structure.

The points of the infinite lattice shown in Fig. 11 are sixfold rotation points and the geometric centers of the equilateral triangles (building blocks of the hexagons) are threefold rotation points. If the lattice points for the structure that is shown in Fig. 10 overlap with the centers of the honeycombs then the sixfold rotation points of the lattice overlap with the sixfold rotation points of the honeycomb structure. However, if we place the lattice points in the centers of atoms, then the sixfold rotation points of the lattice overlap with the threefold rotation points of the honeycomb structure and half of the threefold rotation points of the lattice overlap with the sixfold rotation points of the honeycomb structure.

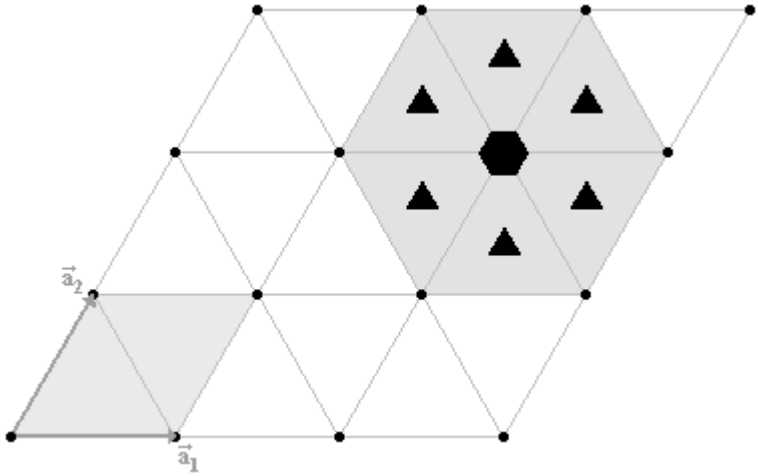

Figure 11 A hexagonal lattice for the honeycomb structure. The basis vectors $\vec{a}_1$ and $\vec{a}_2$ have been defined in Fig. 10. The points of the infinite lattice are sixfold rotation points and the geometric centers of the equilateral triangles overlap with the threefold rotation points of the lattice. In the figure, we also show the graphical symbols for the threefold and sixfold rotation points.

If we now place an additional atom (of the same type) in the center of each hexagon from Fig. 10, then the honeycomb structure transforms into a hexagonal (also known as triangular) structure. The smallest basis of the new structure has one atom, since the primitive translation vectors can be chosen in the way shown in Fig. 12.

The examples of two-dimensional lattices considered here show that the lattice has not only translation symmetry but also point symmetry. A point transformation is a geometric transformation that leaves at least one point invariant (rotations, reflections, etc.). The rotation points overlap with lattice nodes and also other high symmetry points of the lattice. The lattices proposed for structures shown in Figs. 4, 7, 8, and 9 have twofold rotation points. If the basis of the two-dimensional crystal structure has only one atom, then the structure has the *n*-fold rotation points of the same order of rotations as its lattice. The *n*-fold rotation points of the lattice and the structure overlap when the lattice points overlap with the centers of atoms. This can occur also in the case when the basis has more than one atom, but only in the case when the basis atoms are placed in points of high symmetry (see Fig. 8). In general the point symmetry of a crystal structure is lower than the symmetry of its lattice (see e.g. Fig. 9). The fact that the honeycomb structure with two-atom basis has sixfold rotation points (like its

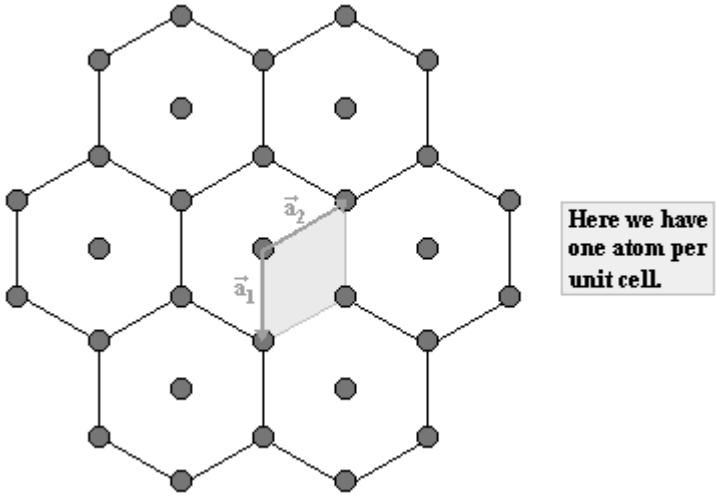

Figure 12 A two-dimensional hexagonal (also known as triangular) structure. The primitive unit cell is defined by vectors $\vec{a}_1$ and $\vec{a}_2$.

lattice) results from the very particular location of the basis atoms in the space lattice.

Let us now show that the presence of translation symmetry implies that there are only one-, two-, three-, four-, and sixfold rotation points in a two-dimensional crystal structure or lattice. We will explain this using Fig. 13. In this figure, we make rotations of the basis vector $\vec{a}_1$ and the opposite to it, $-\vec{a}_1$, by the same angle $2\pi/n$ ($n \in \mathbb{Z}$) but in opposite directions and the

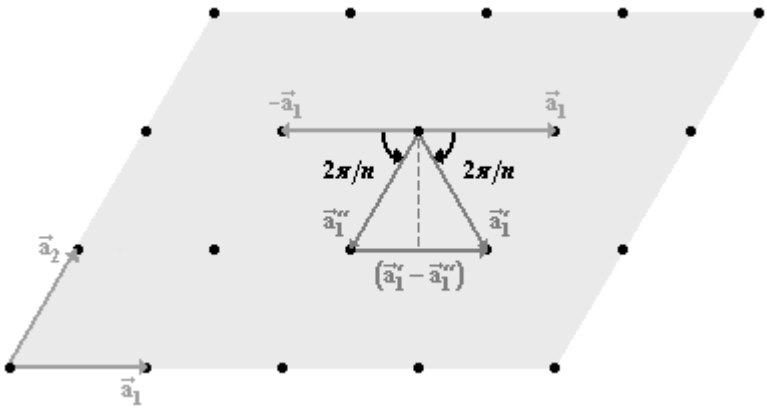

Figure 13 A construction made using basis vector $\vec{a}_1$ and the opposite to it, $-\vec{a}_1$, to show that that there are only one-, two-, three-, four-, and sixfold rotation points in a two-dimensional crystal structure or lattice.

difference of the rotated vectors is shown in the figure. The translation symmetry requires that the difference, $\left(\vec{a}_1' - \vec{a}_1''\right)$, be a multiple of vector $\vec{a}_1$, what imposes certain condition on the integer number n. We have

$$\begin{cases} \vec{a}_1' - \vec{a}_1'' = m\vec{a}_1 \\ 2a_1 \cos\left(2\pi/n\right) = ma_1 \end{cases}, \text{ where } m \in \mathbb{Z}. \tag{I.3}$$

From the above we obtain

$$\cos\left(2\pi/n\right) = \frac{1}{2}m \tag{I.4}$$

and the possible values of integer m and $\cos\left(2\pi/n\right)$ are

$$m = 0, \pm 1, \pm 2 \text{ and } \cos\left(2\pi/n\right) = 0, \pm\frac{1}{2}, \pm 1, \tag{I.5}$$

respectively. Therefore, from (I.5) we obtained that the only rotations that can be performed are those by the angles

$$\frac{2\pi}{1}, \frac{2\pi}{2}, \frac{2\pi}{3}, \frac{2\pi}{4}, \frac{2\pi}{6}. \tag{I.6}$$

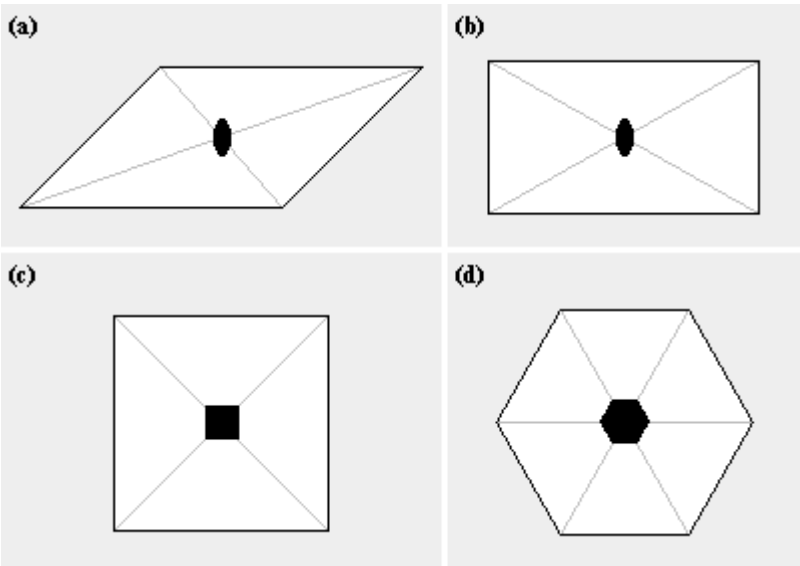

Figure 14 Graphical symbols for the rotation points that overlap with the geometric centers of the following plane figures: **(a)** parallelogram, **(b)** rectangle, **(c)** square, and **(d)** regular hexagon.

From the above we can finally conclude that in the lattice, there are only allowed one-, two-, three-, four-, and sixfold rotation points.

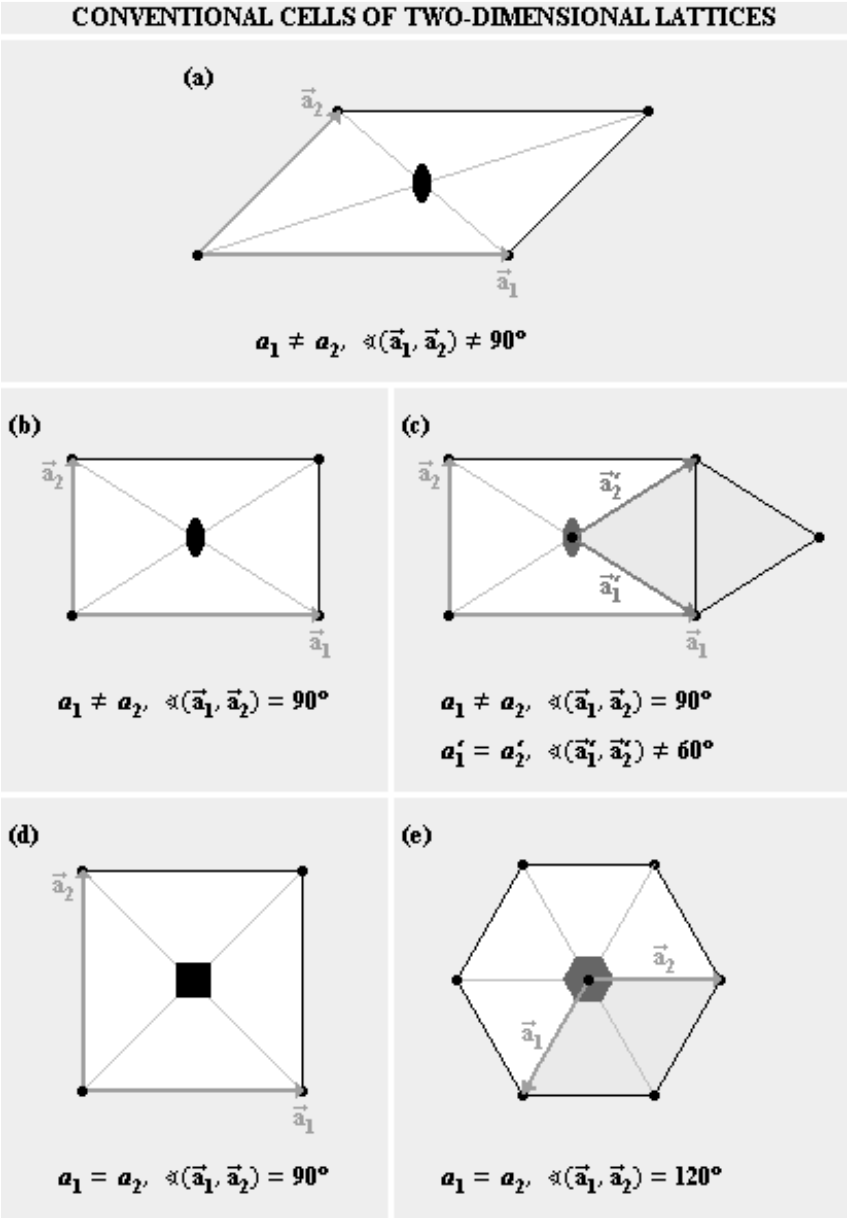

Figure 15 Conventional cells that have the same point symmetry as the corresponding infinite lattices and the conventional primitive cells if different, for the five lattices existing in two dimensions: **(a)** oblique, **(b)** rectangular, **(c)** centered rectangular, **(d)** square, and **(e)** hexagonal.

We will now identify the possible two-dimensional lattices taking into account the limitations for the rotation points described above. We can see, on the example of the considered here lattices, that it is possible to identify finite volumes of the space lattice which have the same point symmetry as the infinite lattice. Let us consider the smallest such volumes. In the case of the lattices for crystal structures from Figs. 4, 7, 8, and 9 the volumes are the primitive cells defined by vectors $\vec{a}_1$ and $\vec{a}_2$, while in the case of the hexagonal lattice the smallest such volume is the hexagon (see Fig. 11). Each of these volumes represents a conventional cell of the lattice, which has the same point symmetry as the infinite lattice.

Let us first consider the rotations about the points that overlap the geometric centers of some plane figures. In Figs. 14a and 14b we show the graphical symbol for the twofold rotation points that are in the centers of a parallelogram and a rectangle, respectively. We can also see in Figs. 14c and 14d that the geometric centers of a square and of a regular hexagon represent fourfold and sixfold rotation points, respectively, that are labeled with the corresponding graphical symbols in those figures.

There are five different two-dimensional types of lattices, which are classified in four crystal systems: oblique, rectangular, square, and hexagonal. Due to the limitations for the rotation points described above the parallelogram, rectangle, square, and hexagon represent the only conventional cells that have the same point symmetry as the corresponding infinite lattices. Each of the geometric figures shown in Fig. 14 represents one (or two) of the crystal systems. Furthermore, Fig. 15 shows the conventional cells that have the point symmetry of the infinite lattice and the conventional primitive cells if different, for the five lattice types that exist in two dimensions: oblique, rectangular, centered rectangular, square, and hexagonal (see Figs. 15a-15e).

4. Problems

Exercise 1 Figure 16 shows a hexagonal lattice.

a.) What lattice will be obtained if we place an additional point in the geometric center of each equilateral triangle in Fig. 16? Draw an example of primitive translation vectors for the new lattice.

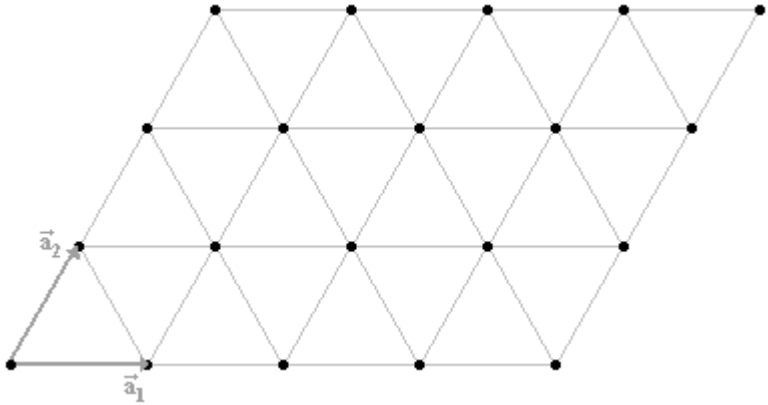

Figure 16 A hexagonal lattice.

b.) What crystal structure will be obtained if we attach to each lattice point a basis that has two identical atoms in the positions given by vectors $\vec{r}_1 = \vec{0}$ and $\vec{r}_2 = 2(\vec{a}_1 + \vec{a}_2)/3$? Draw this structure.

c.) If, instead of using identical atoms, we use in b.) a basis consisting of one boron and one nitrogen atom, then the resulting structure will be an isolated atomic sheet of the α phase of boron nitride (α-BN). What is the order of the highest order rotation point in the two-dimensional boron nitride structure? Draw this structure and show the highest order rotation points.

Exercise 2 In Fig. 17a, we show a conventional cell that has the point symmetry of an infinite two-dimensional crystal structure composed of two types of atoms. Draw the smallest unit cell that can reproduce this structure. How many atoms of each type are in this cell? Repeat all the above for the conventional cell shown in Fig. 17b.

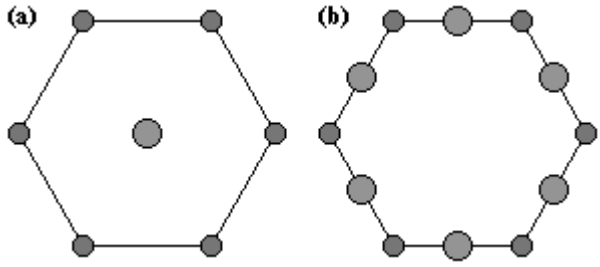

Figure 17 Conventional cells that have the same point symmetry as the two-dimensional infinite structures composed of two types of atoms.

Exercise 3 Figure 18 shows a unit cell for a two-dimensional lattice.

a.) What type of lattice is this?

b.) Draw a conventional primitive cell for this lattice.

c.) Draw the conventional unit cell which has the point symmetry of the infinite lattice.

Exercise 4 Show graphically that the honeycomb structure shown in Fig. 10 is nothing more than the superposition of two hexagonal substructures shifted one with respect to the other by a vector $(\vec{a}_1 + \vec{a}_2)/3$.

Exercise 5 Using the hexagonal lattice from Fig. 16 draw the vector $(\vec{a}_1' - \vec{a}_1'')$ defined in Fig. 13 for all rotations (by angles $2\pi/n$) allowed in a hexagonal lattice. Find the value of the integer *m* which satisfies Eq. (I.4) in each case.

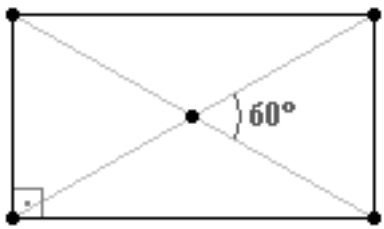

Figure 18 Unit cell for a two-dimensional lattice.

II. THREE-DIMENSIONAL CRYSTAL LATTICE

1. Introduction

In the case of a three-dimensional lattice, a primitive unit cell has the shape of a parallelepiped defined by three non collinear and not all in the same plane primitive translation vectors $\vec{a}_1$, $\vec{a}_2$, $\vec{a}_3$. The most general example of a unit cell is shown in Fig. 19.

The translation symmetry of an infinite two- or three-dimensional lattice imposes certain restrictions on its point symmetry elements, what was shown in the previous chapter for the case of a two-dimensional lattice.

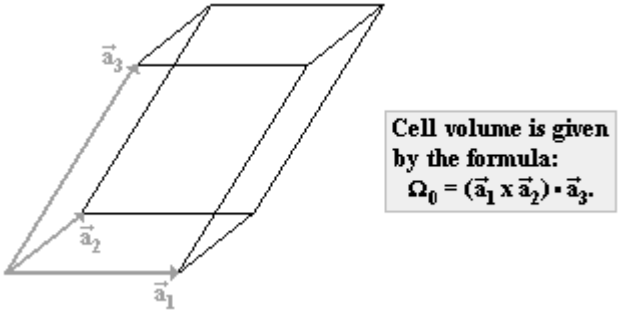

Figure 19 A unit cell of a three-dimensional lattice.

The allowed orders of symmetry axes in a three-dimensional lattice are the same as the orders of symmetry points in two dimensions, it means 1, 2, 3, 4, and 6. As a consequence, in two and three dimensions only certain lattice types are possible. In order to find them in three dimensions, we will proceed in a similar way as it was done for the two-dimensional case. First, we will consider certain finite three-dimensional figures whose symmetry axes are of the orders that are allowed in an infinite lattice.

2. Examples of Symmetry Axes of Three-Dimensional Figures

An object which has one or more symmetry axes of orders 1, 2, 3, 4, or 6 may have the shape of such a solid figure as parallelepiped, regular

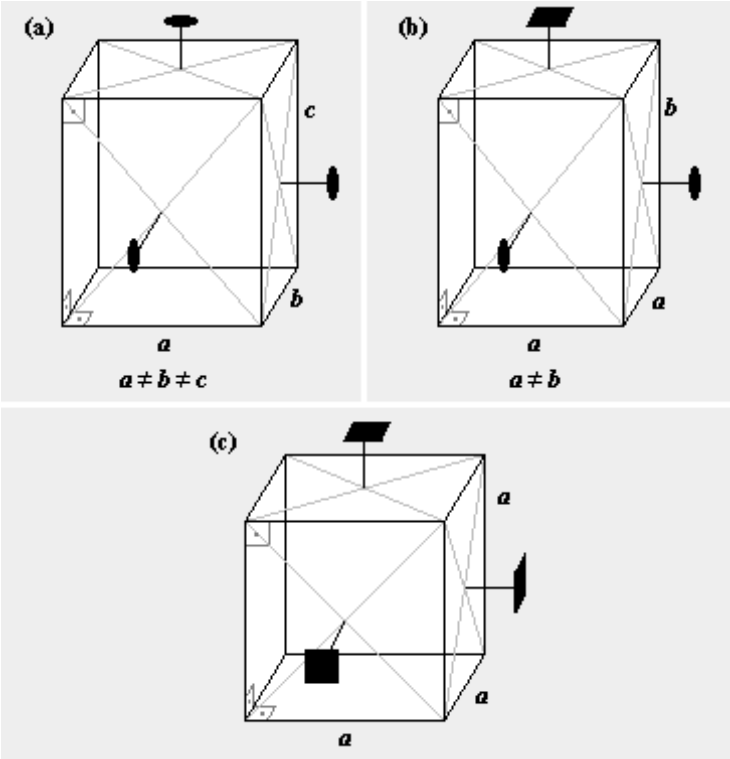

Figure 20 Some rotation axes of three solid figures: **(a)** rectangular prism, **(b)** square prism, and **(c)** cube.

tetrahedron or octahedron, or hexagonal prism. When the point symmetry of an infinite lattice is such that the highest order of the *n*-fold symmetry axis is only one, a parallelepiped of the lowest possible symmetry (see Fig. 19) represents a solid figure that has the same point symmetry as the lattice. In Fig. 20 we show other parallelepipeds whose shapes allow for the presence of two- and (or) fourfold symmetry axes. We can see in this figure the rotation axes that cross the geometric centers of the parallelepiped faces. In each case, they are the rotation axes of the highest order. We will show later that in the case of a cube (Fig. 20c) two- and threefold axes are also present.

The parallelepipeds shown in Fig. 20 represent conventional unit cells that have the same point symmetry as an important number of infinite lattices. The symmetry center of a parallelepiped overlaps with its geometric center. This is a common property of all point symmetry elements. Obviously, the orders of rotation axes and the number of axes of the same order depend on the shape of the parallelepiped. For example, a cube

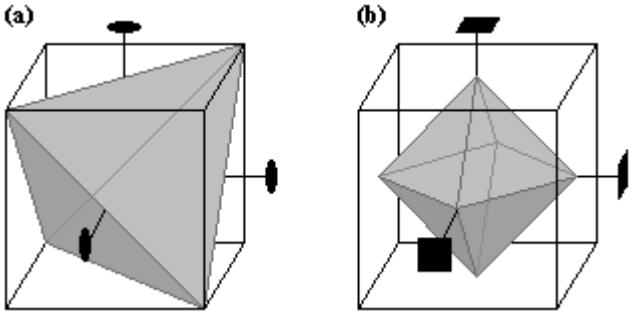

Figure 21 A regular tetrahedron **(a)** and a regular octahedron **(b)** inscribed in a cube.

(shown in Fig. 20c) has three fourfold axes. Each of them is defined by the geometric centers of two square faces, parallel one to each other. The cube has a total of 13 rotation axes. Namely, besides the three fourfold axes shown in Fig. 20c it still has two- and threefold axes. The case of the cube will be considered in more details later.

As we can see in Fig. 21 a regular tetrahedron and a regular octahedron can be inscribed in a cube. A tetrahedron has three mutually perpendicular twofold rotation axes instead of the fourfold axes of the cube (see Fig. 21a). Each of them is defined by the centers of its two edges. A tetrahedron does not represent a unit cell of any lattice, but it is relevant in the description of

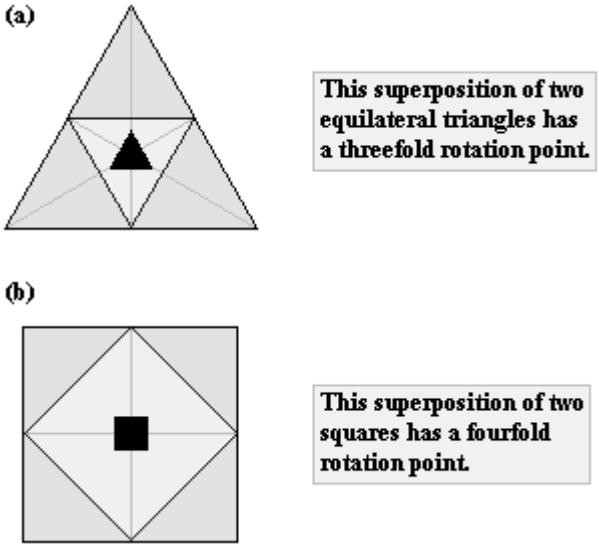

Figure 22 Symmetry points of a superposition of plane figures: **(a)** two equilateral triangles and **(b)** two squares.

important crystal structures (especially in the description of their symmetry). A regular octahedron, contrary to the tetrahedron, has the same three mutually perpendicular fourfold rotation axes that the cube has (see Fig. 21b) with the difference that in the case of an octahedron a fourfold axis is defined by two vertices and in the case of the cube by the geometric centers of two faces (the number of octahedron vertices agrees with the number of cube faces and *vice versa*).

The solid figure which has a sixfold rotation axis takes on the shape of a regular hexagonal prism that represents the unit cell of the same point symmetry as that of an infinite hexagonal lattice in three dimensions. This will be considered in more details later.

Before continuing with the three-dimensional case, we will look shortly at the symmetry points of a superposition of plane figures. The superposition of two equilateral triangles with a common geometric center has a threefold rotation point. This is shown in Fig. 22a. A similar superposition of two squares has a fourfold rotation point (see Fig. 22b). Both examples will be helpful in farther consideration of the rotation axes in some three-dimensional lattices.

3. Symmetry Axes of a Cube

Let us now continue with the consideration of the possible rotation axes in a cube. First we will look at the twofold rotation axes. Each of them is defined by the centers of two edges as it is shown in Fig. 23. So, the cube has a total of 6 twofold axes.

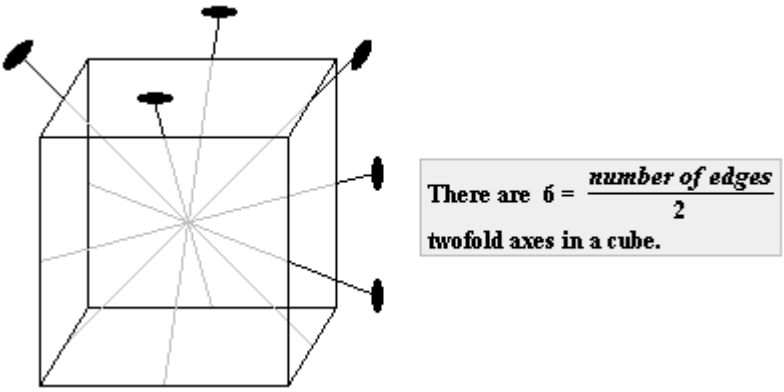

Figure 23 Six twofold rotation axes of a cube.

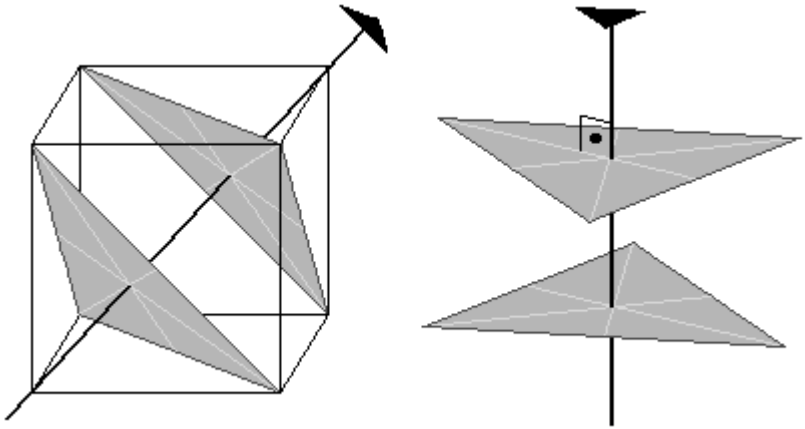

Figure 24 Each diagonal of a cube represents one of its threefold rotation axis.

It is easy to show that the body diagonals of the cube represent its threefold axes. We can see in Fig. 24 that the displayed body diagonal connects two opposite cube vertices. The remaining 6 vertices form two groups, with 3 vertices each, that represent the vertices of two equilateral triangles. Each of the triangles is lying in a plane orthogonal to the diagonal and its geometric center overlaps with the point where the diagonal intersects the plane of the triangle. It is obvious that after rotating the cube by an angle $2\pi/3$ (or its multiples), the new positions of the cube vertices (those out of the axis) overlap with some "old" positions of the vertices. Therefore, this transformation leaves the cube invariant. Besides the axis shown in Fig. 24, there are 3 more threefold axes in the cube, that is, as

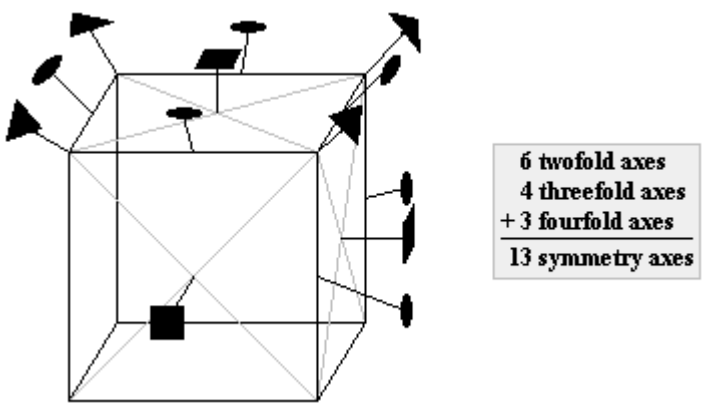

Figure 25 The 13 rotation axes of a cube.

many as the number of body diagonals. In conclusion, a cube has a total of 13 rotation axes. All of them are shown in Fig. 25.

4. Symmetry Axes of a Set of Points

Now, we will concentrate our attention on a system consisting of a set of 8 points (or atoms) located at the vertices of a cube. The symmetry axes of this set of points are the same as the symmetry axes of the cube. If we add one additional point in the middle of the cube, then the symmetry of the resulting system will remain the same, since this point will be a common point of all the axes and also other symmetry elements. Also, if we add

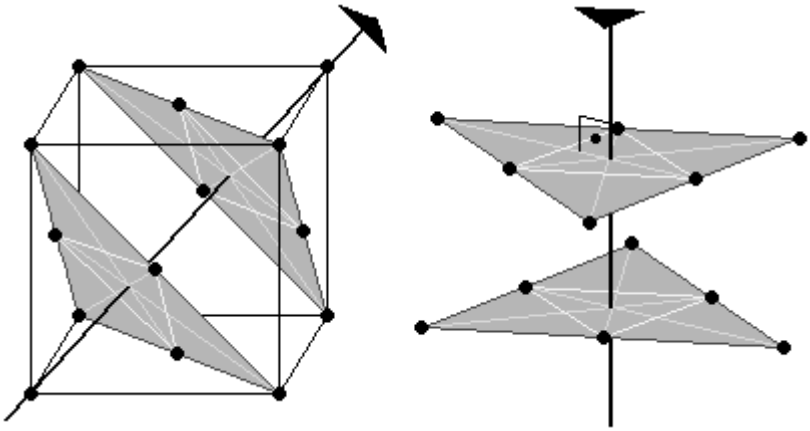

Figure 26 The system of 14 points placed at the vertices and in the geometric centers of the faces of a cube have the same threefold rotation axes as the cube.

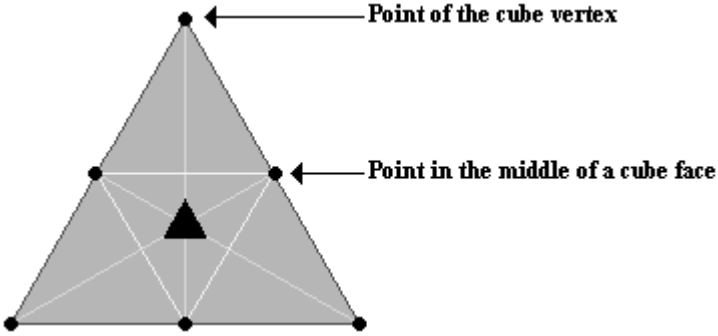

Figure 27 Axial view of one of the triangles from Fig. 26.

points in the middle of the faces of the cube, then the symmetry of this new 14-point system (shown in Fig. 26) will still remain the same as in the system consisting of only 8 points. For example, it is easy to see, comparing Figs. 24 and 26, that the threefold axes are present in this 14-point system. The six new points will form two groups of three points each, which are located in the middle of the triangle edges, as appears in Fig. 26. The axial view of one of the triangles from Fig. 26 is shown in Fig. 27.

Let us now consider the fourfold rotation axes in the case of the 14-point system in consideration. We can observe in Fig. 28 that, of the total of six points in the middle of the faces of the cube, two are on the axis and the remaining four represent vertices of a square lying in a plane orthogonal to the axis. If we project the 14 points on a plane orthogonal to the axis, then we will obtain a superposition of two squares shown on the

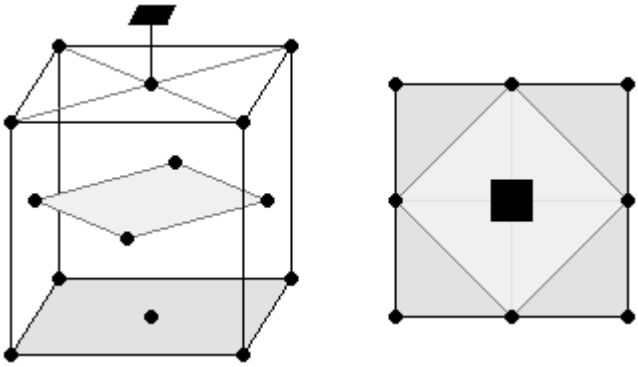

Figure 28 Fourfold rotation axis of a system consisting of 14 points located at the vertices and centers of the faces of a cube.

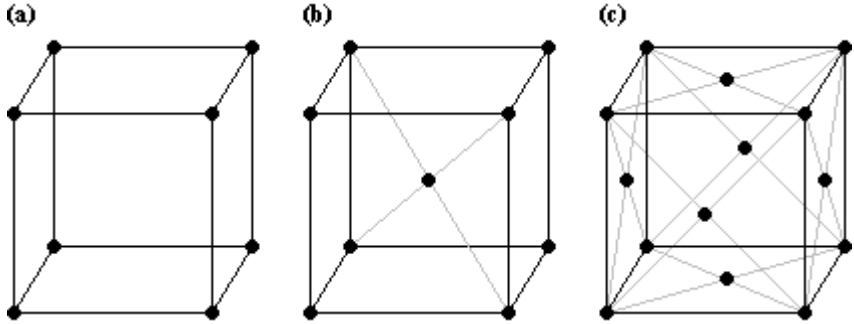

Figure 29 Three systems consisting of: **(a)** 8 points at the vertices of a cube, **(b)** 9 points at the vertices and the geometric center of a cube, and **(c)** 14 points at the vertices and face centers of a cube. Each set of points has the same 13 rotation axes as a cube.

right of Fig. 28. Thus we can say that the 14-point system has the same three fourfold rotation axes as the cube. Besides that, the system of points has six twofold axes. Finally, we can conclude that in the three cases described above, and shown in Fig. 29, we have the same 13 symmetry axes as were identified before in the cube.

5. Crystal Systems

In this section, we will learn about the crystal systems in three dimensions. To a given crystal system belong all the lattices that have the same point symmetry. However, the distribution of lattice points in space may be different in each of the lattices. In three dimensions, there are only 7 lattice point symmetries, called *holohedries*, and each of them defines one crystal system. Every lattice belonging to a given crystal system has in general its own conventional unit cell that possesses the same point symmetry as an infinite lattice but, since the symmetry of each cell is the same, we can propose one of them as a conventional cell for the crystal system. In Fig. 30 we show conventional cells for the 7 crystal systems existing in three dimensions, pointing out in each case the highest order symmetry axis. If there is more than one such axis it is also shown in the figure.

The conventional cells shown in Fig. 30 are defined by the basis vectors $\vec{a}_1$, $\vec{a}_2$, $\vec{a}_3$ parallel to the main symmetry axes, if there are any in the lattices belonging to the crystal system. In the triclinic system, there are no symmetry axes at all or, more precisely, there are only onefold axes. Thus, no basis vector is fixed by symmetry (see Fig. 30a) and $\vec{a}_1$, $\vec{a}_2$, $\vec{a}_3$ are just three non collinear and not all in the same plane primitive translation vectors of a triclinic lattice. There are no special restrictions on the triclinic conventional cell parameters (lattice constants a_1, a_2, a_3 and anges $\sphericalangle(\vec{a}_1,\vec{a}_2)$, $\sphericalangle(\vec{a}_1,\vec{a}_3)$, $\sphericalangle(\vec{a}_2,\vec{a}_3)$) since the onefold axes are present in a parallelepiped of any shape. The parallelepiped shown in Fig. 30a is the conventional cell for the triclinic system.

In the case of the monoclinic system only one symmetry axis is of the order higher than one. This is shown in Fig. 30b, where in the conventional cell for the monoclinic system is highlighted one twofold axis with the basis vector $\vec{a}_3$ parallel to it. The restriction $\sphericalangle(\vec{a}_1,\vec{a}_3)=\sphericalangle(\vec{a}_2,\vec{a}_3)=90°$ guarantees the presence of this unique symmetry axis.

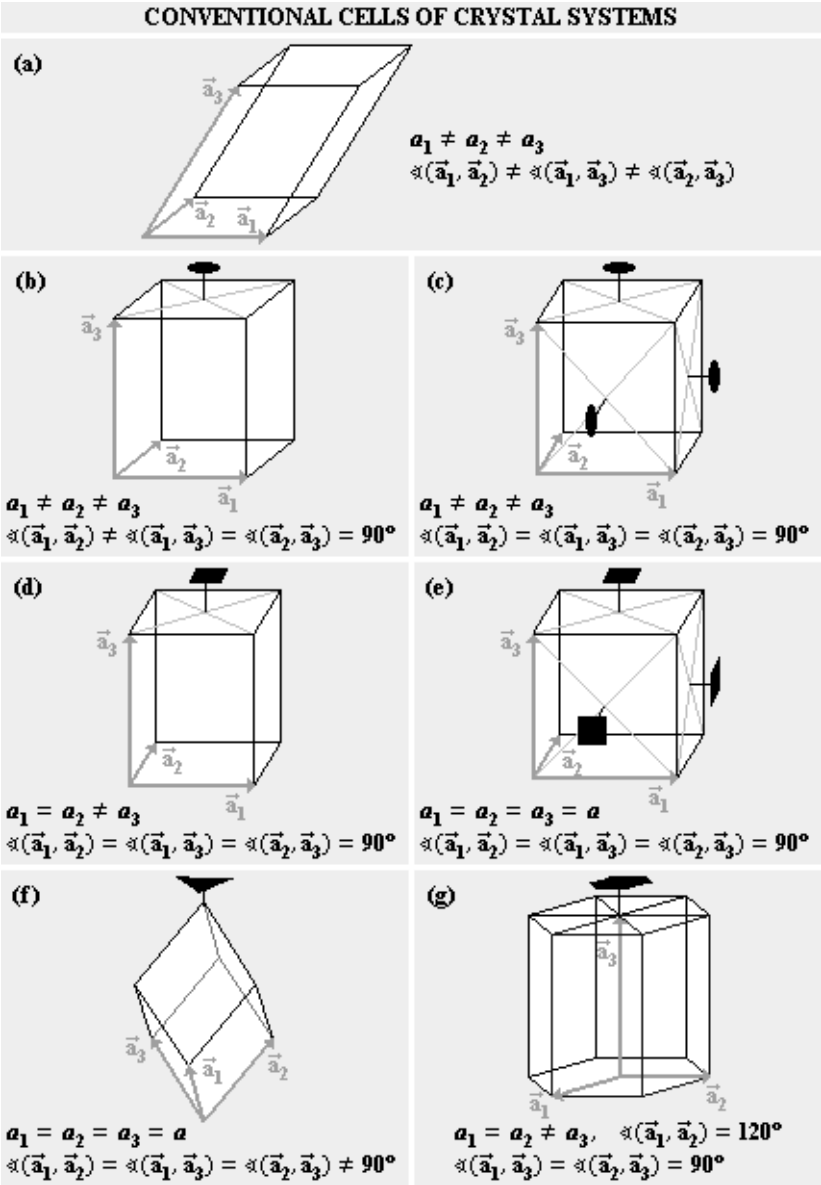

Figure 30 Conventional cells, of the most general shape, for the 7 crystal systems in three dimensions: **(a)** triclinic, **(b)** monoclinic, **(c)** orthorhombic, **(d)** tetragonal, **(e)** cubic, **(f)** trigonal, and **(g)** hexagonal.

In the lattices belonging to the orthorhombic, tetragonal, and cubic systems three mutually perpendicular symmetry axes coexist and the basis

vectors $\vec{a}_1$, $\vec{a}_2$, $\vec{a}_3$ are parallel to them. Figs. 30c and 30e show the conventional cells and the three twofold and fourfold rotation axes for the orthorhombic and cubic systems, respectively, while Fig. 30d shows the conventional cell and a fourfold rotation axis present in lattices of the tetragonal system. The remaining symmetry axes (not shown in Fig. 30d) are twofold. The restrictions for the conventional cell parameters are summarized in Table 1. These constrains guarantee the presence of three mutually perpendicular symmetry axes of the orders specified in Figs. 30c-30e.

The lattices with only one threefold or sixfold symmetry axis belong to the trigonal or hexagonal systems, respectively. A solid figure that possesses a sixfold symmetry axis has the shape of a hexagonal prism shown in Fig. 30g. In Fig. 30g is also shown a parallelepiped whose volume represents $1/3$ of the volume of the hexagonal prism. This parallelepiped is a conventional cell for the hexagonal system. Its basis vector $\vec{a}_3$ is parallel to the sixfold symmetry axis and the basis vectors $\vec{a}_1$ and $\vec{a}_2$ are lying in a plane orthogonal to this symmetry axis. The restrictions pointed out in Table 1 guarantee the presence of a sixfold symmetry axis in the lattices belonging to the hexagonal system. In Fig. 31 we show that the conventional cell for the trigonal system and the hexagonal prism are related. This will be explained in more details later. The restrictions on the rhombohedral cell parameters given in Table 1 guarantee the presence

Table 1 Restrictions on conventional cell parameters for each crystal system. The following abbreviations are used: $\sphericalangle(\vec{a}_1,\vec{a}_2)=\alpha_{12}$, $\sphericalangle(\vec{a}_1,\vec{a}_3)=\alpha_{13}$, $\sphericalangle(\vec{a}_2,\vec{a}_3)=\alpha_{23}$.

Crystal system	**Restrictions on conventional cell parameters** a_1, a_2, a_3, **and** α_{12}, α_{13}, α_{23}
Triclinic	None
Monoclinic	$\alpha_{13}=\alpha_{23}=90°$
Orthorhombic	$\alpha_{12}=\alpha_{13}=\alpha_{23}=90°$
Tetragonal	$a_1=a_2$ $\alpha_{12}=\alpha_{13}=\alpha_{23}=90°$
Cubic	$a_1=a_2=a_3$ $\alpha_{12}=\alpha_{13}=\alpha_{23}=90°$
Trigonal	$a_1=a_2=a_3$ $\alpha_{12}=\alpha_{13}=\alpha_{23}$
Hexagonal	$a_1=a_2$ $\alpha_{12}=120°$, $\alpha_{13}=\alpha_{23}=90°$

of a threefold symmetry axis. Of course in the case when

$$\sphericalangle(\vec{a}_1,\vec{a}_2)=\sphericalangle(\vec{a}_1,\vec{a}_3)=\sphericalangle(\vec{a}_2,\vec{a}_3)=90°$$

we are in the presence of a cube and this threefold symmetry axis coincides with one of the four threefold axes of the cube.

To summarize, we can say that the order and the number of the highest order symmetry axes characterize a crystal system. All the highest order symmetry axes for each of the 7 crystal systems are shown in Fig. 30.

6. Conventional Cell for the Trigonal System

The conventional cell for the trigonal system takes on the shape of a rhombohedron. This rhombohedron can be constructed in a hexagonal prism, what is shown in Fig. 31. We can see in that figure that two vertices of the rhombohedron are located in the centers of the hexagonal prism bases and the other 6 form two groups with 3 vertices each. The plane defined by the three vertices of one group is parallel to the prism bases, what means that these vertices are at the same distance from a base. The distance between the three vertices which are closer to the top base and this base is the same as the distance between the vertices from the other group and the bottom base, and represents $1/3$ of the prism height c (see Fig. 31).

The positions of the vertices belonging to each of the two groups can be determined easily as their projections on the plane of the nearer prism base

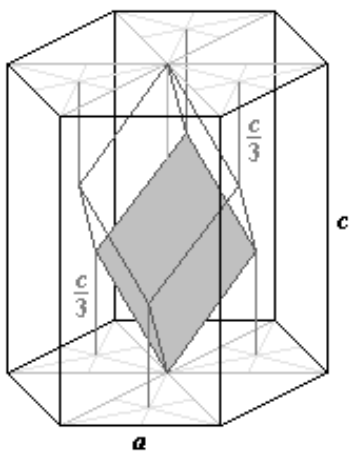

Figure 31 Rhombohedron constructed inside a hexagonal prism.

(bottom or top) coincide with the geometric centers of three equilateral triangles, what is shown in Fig. 31. We can also see in this figure that these triangles are not next to each other and the three triangles of the bottom base do not coincide with those of the top base.

7. The 14 Bravais Lattices

7.1. Introduction

In this section, we will describe all the three-dimensional lattices or more strictly speaking lattice types. If we place lattice points at the vertices of each parallelepiped that represents the conventional cell of one of the seven crystal systems, then we obtain 7 different lattices. All the points placed at the vertices of a cell contribute with 1 point to this cell. This is explained in Fig. 32 on the example of a cubic cell. A point placed in a vertex of a cube belongs to 8 cubes (4 of which are shown in Fig. 32), so $1/8$ of it belongs to each cube. Since there are 8 points at the vertices of the cube, they contribute with 1 point to it and the cell is primitive.

A French scientist, Bravais (second half of the XIX century), demonstrated that if we place an additional point in the geometric center or additional points on the faces of the parallelepipeds representing conventional cells of the seven crystal systems (in such a way that the set of points has the same symmetry as the parallelepiped), then we will obtain 7 new lattices or strictly speaking lattice types. Therefore, we have a total of 14 lattice types in three dimensions. It will be shown later that 11 of them belong to the monoclinic, orthorhombic, tetragonal, or cubic crystal systems. Each of the remaining crystal systems (triclinic, trigonal, and hexagonal) has only one lattice type. In the case of each of the 7 new lattices, the parallelepiped, which represents the unit cell that has the same

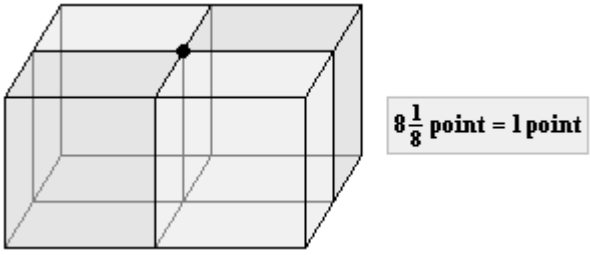

Figure 32 A $1/8$ of the point placed in each vertex of a cubic cell belongs to this cell.

symmetry as the infinite lattice, has more than one lattice point. Therefore, this unit cell represents a non primitive cell of the lattice while a primitive cell of such a lattice does not have its point symmetry.

Next, we will build the 7 new lattices mention above which are called the centered Bravais lattices.

7.2. The Triclinic System

In the case of the triclinic system, there is only one lattice type. The arguments are very simple. Since in the case of the triclinic system there are no restrictions on its conventional cell parameters, a primitive cell of any triclinic lattice represents a conventional cell of the triclinic system. By placing additional points out of the vertices of the conventional cell, we transform a primitive cell of one triclinic lattice onto a non primitive cell of another triclinic lattice, but of course both lattices are of the same type since a primitive cell of this new lattice represents another conventional cell for the triclinic system.

7.3. The Monoclinic System

In Fig. 33a, we have placed lattice points at the vertices of the conventional cell for the monoclinic system shown in Fig. 30b. This cell can be centered in several different ways as shown in Figs. 33b-33d and in Fig. 34. In all cases, the set of lattice points has the same point symmetry as the conventional cell of the monoclinic system. Note that in Figs. 33 and 34 we have changed the notation for the cell parameters, and now we are using a, b, c instead of a_1, a_2, a_3. The cells from Figs. 33 and 34 have their unique symmetry axes parallel to the c edges. Consequently, we speak of the setting with unique axis c (for short c-axis setting). In the case of the C-face centered cell, shown in Fig. 33b, the centering lattice points are in the cell bases (orthogonal to the c-edge). Figs. 33c and 33d show the same cell, but this time body and all-face centered, respectively. There are still two more options for placing the additional lattice points within the conventional cell of the monoclinic system. This is shown in Figs. 34a and 34b for the A-face centered and B-face centered cells, respectively. The symbols for the centering types of the cells shown in Figs. 33 and 34 are listed in Table 2.

Let us now investigate to which monoclinic lattice types belong the centered cells shown in Fig. 33. In Fig. 35, we demonstrate that in the lattice shown in Fig. 33b we can find a primitive cell of the same type as the cell from Fig. 33a, so this is, in fact, a primitive monoclinic lattice. It can be also

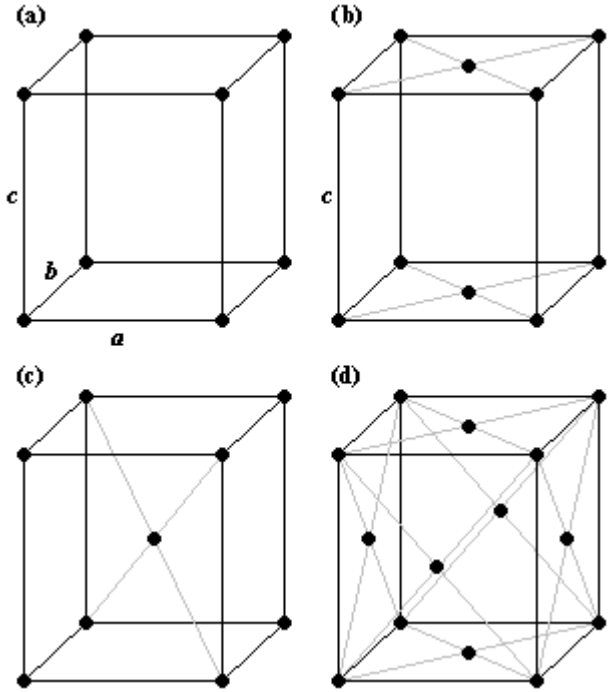

Figure 33 **(a)** Conventional primitive cell for the simple monoclinic lattice. In the figure, we have also drawn the cell from (a) centered in three different ways: **(b)** *C*-face centered, **(c)** body centered, and **(d)** all-face centered. The *c*-axis setting is assumed.

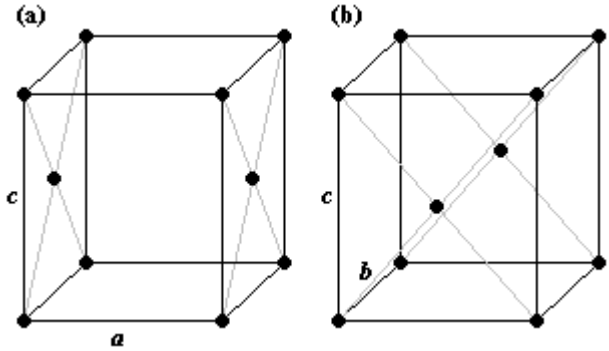

Figure 34 The cell from Fig. 33a centered in two different ways: **(a)** *A*-face centered and **(b)** *B*-face centered. The *c*-axis setting is assumed.

demonstrated (see Fig. 36) that in the lattice from Fig. 33d, there is a body centered cell of the same type as the cell from Fig. 33c, so this is a body centered monoclinic lattice. From all the above, we can conclude that

Table 2 Symbols for the centering types of the cells shown in Figs. 33 and 34.

Symbol	Centering type of a cell	Number of lattice points per cell
P	Primitive	1
A	*A*-face centered	2
B	*B*-face centered	2
C	*C*-face centered	2
I	Body centered	2
F	All-face centered	4

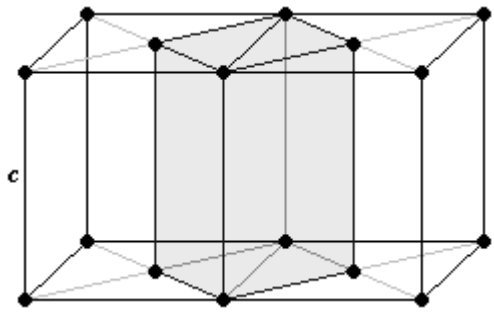

Figure 35 A primitive unit cell of the same type as the cell shown in Fig. 33a, located inside the monoclinic lattice from Fig. 33b. The *c*-axis setting is assumed.

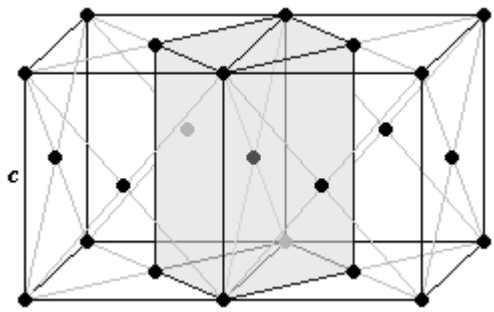

Figure 36 A body centered unit cell of the same type as the cell shown in Fig. 33c, placed inside the monoclinic lattice from Fig. 33d. The *c*-axis setting is assumed.

in Fig. 33 we have four cells belonging to only two types of monoclinic lattices, for which the arrangements of the lattice points are shown in Figs. 33a and 33c.

Next, we will check the cases shown in Fig. 34. In each lattice type plotted in this figure, we can find a body centered monoclinic cell. This is demonstrated in Fig. 37 for the lattice from Fig. 34b. Thus, in the

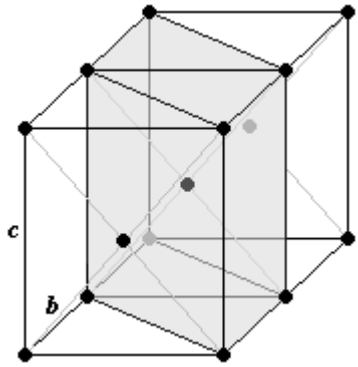

Figure 37 A body centered unit cell of the same type as the cell shown in Fig. 33c, located inside the monoclinic lattice from Fig. 34b. The *c*-axis setting is assumed.

monoclinic lattice shown in this figure, there are two different conventional monoclinic cells (body centered and *B*-face centered) that contain the same number of lattice points, so we may consider this lattice as a *B*-face centered or a body centered. Similarly, the monoclinic lattice from Fig. 34a may be considered as an *A*-face centered or a body centered. Therefore, if we assume the *c*-axis setting, then the *A*-face centered, *B*-face centered, and the body centered monoclinic lattices are mutually equivalent. In conclusion, there are only two types of monoclinic lattices, the primitive one and one of the following three lattices: *A*-face centered, *B*-face centered, or body centered. The *B*-face centered lattice is selected to represent the centering type of the monoclinic lattice (if the *c*-axis setting is assumed). The symbols of the two monoclinic lattice types are then *mP* and *mB*. However, in the literature we can find more often the case when the *b*-axis setting is assumed, and then the *mA*, *mC*, and *mI* lattices are equivalent. In this case, the *mC* lattice is selected to identify the centering type of the monoclinic lattice.

In the case of the *mB* (*c*-axis setting) or *mC* (*b*-axis setting) lattices the smallest cell that has the point symmetry of the infinite lattice contains 2 lattice points, while the primitive cells of these lattices do not have their point symmetry.

7.4. The Orthorhombic System

In the same way, as it was done in Sec. II.7.3 for the monoclinic system, we can place the lattice points within the conventional cell for the orthorhombic system. The resulting set of points will have the same point

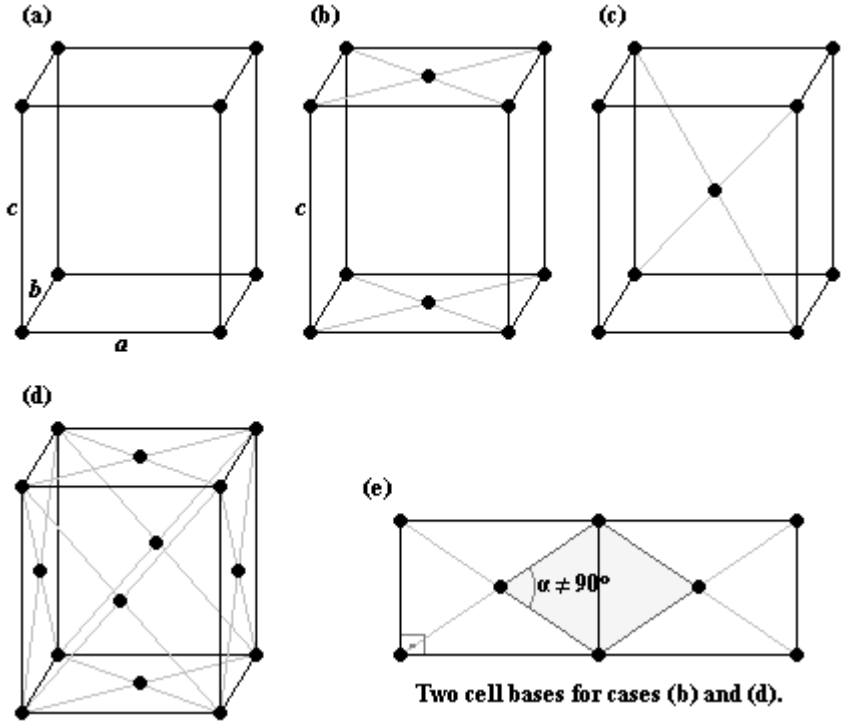

Figure 38 (a) Conventional primitive unit cell of the simple orthorhombic lattice. In the figure, we have also drawn the cell from (a) centered in three different ways: **(b)** *C*-face centered, **(c)** body centered, and **(d)** all-face centered. Figure **(e)** shows two bases for two adjacent cells from (b) and (d). The base of a primitive (or body centered) cell of the lattice shown in (b) (or (d)) is highlighted in (e).

symmetry as the cell. Since the three edges in the conventional cell for this system are mutually orthogonal, only the cases described in Fig. 38 will be considered. The rest of the cases, with *A*- and *B*-face centered cells, do not lead to any new lattice types. Contrary to the monoclinic system, this time, neither the case from Fig. 38b nor the case from Fig. 38d match the cases described in Figs. 38a and 38c, respectively, since neither a primitive nor a body centered unit cells with edges mutually orthogonal are present in the lattices shown in Figs. 38b and 38d, respectively. Therefore, we can conclude that in the case of the orthorhombic system, there are four types of lattices: primitive (*oP*), *C*-face centered (*oC*), body centered (*oI*), and all-face centered (*oF*).

7.5. The Tetragonal System

The conventional unit cell of the tetragonal system, instead of having a rectangle at the base (as it was the case of the orthorhombic system), has a square. For this system, we have to analyze the same types of centering of its conventional cell, as those shown in Figs. 38b-38d for the orthorhombic system. Thus, the *C*-face centered, body centered, and all-face centered tetragonal cells will be considered. Here, as before, the *c* edge is orthogonal to the cell base. The presence of a fourfold axis parallel to the *c* edge excludes the possibility of having *A*- and *B*-face centered cells in tetragonal lattices. It is easy to demonstrate that now the lattice represented by the *C*-face centered tetragonal unit cell is effectively a primitive lattice and the lattice represented by the all-face centered tetragonal unit cell is just a body centered lattice. This is shown in Fig. 39, where we have displayed two bases of a *C*-face centered or all-face centered tetragonal unit cells. One of those bases is labeled as I, whereas the square marked as II is the base of a primitive or body centered tetragonal cell.

To conclude, we can say that in the case of the tetragonal system, there are two types of lattices: *tP* and *tI*.

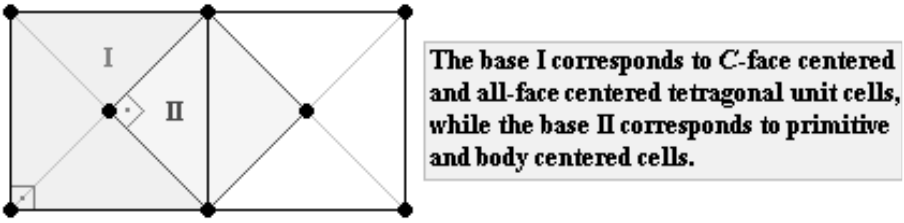

Figure 39 Two bases (labeled as I) of two adjacent *C*-face centered and all-face centered tetragonal unit cells. The base labeled as II corresponds in one case to a primitive tetragonal unit cell and in the other case to the body centered tetragonal cell.

7.6. The Cubic System

We now move to the case of a cubic system. The search for the possible lattices belonging to this system will be held using again Fig. 38. This time, the only relevant cases are those described in Figs. 38a, 38c, and 38d, since, due to the point symmetry, those are the only cases that can be *a priori* expected in the lattices of the cubic system (remember that in the present consideration all the cells shown Fig. 38 are cubes). In the cubic lattice with

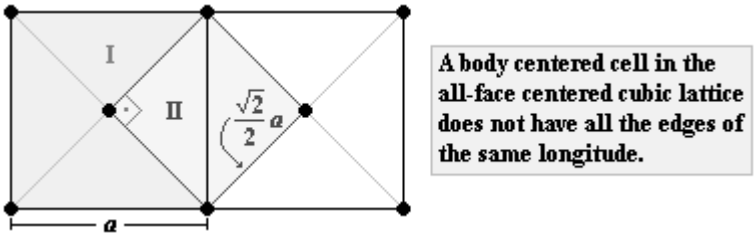

Figure 40 Two bases (labeled as I) of two adjacent all-face centered cubic unit cells. The base labeled as II corresponds to a noncubic body centered unit cell.

the same arrangement of lattice points as shown in Fig. 38d, it is excluded the presence of a cubic body centered unit cell, what is explained in Fig. 40.

Lastly, we can conclude that in the case of the cubic system, there are 3 types of lattices: *cP*, *cI*, and *cF*. The primitive cubic lattice is also called simple cubic (*sc*) and the body and all-face centered cubic lattices are commonly abbreviated as *bcc* (body centered cubic) and *fcc* (face centered cubic), respectively.

7.7. The Trigonal and Hexagonal Systems

There is only one type of lattices, namely, *hR* and *hP* in the trigonal and hexagonal systems, respectively. Later we will explain the origin of the symbol *hR* used for the trigonal lattice.

Finally, we may say that there are all together 14 types of lattices in three dimensions, called the Bravais lattices. The 14 Bravais lattices are shown in Fig. 41.

7.8. Symbols for Bravais Lattices

In Table 3 are summarized the symbols for the 14 Bravais lattices. We can observe in this table, that the lattices are classified in 6 crystal families, that are symbolized by lower case letters *a*, *m*, *o*, *t*, *h*, and *c* (see column two of Table 3). The second classification is according to the discussed by us 7 crystal systems. We can see in the table that in three dimensions the classifications according to crystal families and crystal systems are the same except for the hexagonal family, which collects two crystal systems: trigonal and hexagonal. The two parts of the Bravais lattice symbol are: first, the symbol of the crystal family and second, a capital letter (*P*, *S*, *I*, *F*, *R*) designating the Bravais lattice centering. As a reminder, the symbol *P* is given to the primitive lattices. The symbol *S* denotes a one-face centered lattice (*mS* and *oS* are the standard, setting independent, symbols for the

Table 3 Symbols for the 14 Bravais lattices.

Crystal Family	Symbol	Crystal System	Bravais Lattice Symbol
Triclinic (anorthic)	*a*	Triclinic	*aP*
Monoclinic	*m*	Monoclinic	*mP* *mS* (*mA*, *mB*, *mC*)
Orthorhombic	*o*	Orthorhombic	*oP* *oS* (*oA*, *oB*, *oC*) *oI* *oF*
Tetragonal	*t*	Tetragonal	*tP* *tI*
Hexagonal	*h*	Trigonal (rhombohedral)	*hR*
		Hexagonal	*hP*
Cubic	*c*	Cubic	*cP* *cI* *cF*

one-face centered monoclinic and orthorhombic Bravais lattices, respectively). For the last case also the symbols *A*, *B*, or *C* are used, describing lattices centered at the corresponding *A*, *B*, or *C* faces. The symbols *F* and *I* are designated for all-face centered and body centered Bravais lattices, respectively. Finally, the symbol *R* is used for a trigonal lattice.

7.9. Conclusions

To conclude we can say that the carried out identification of the 14 Bravais lattices was nothing more than the classification of all the three-dimensional lattices in 14 groups. The lattices belonging to a given group have the same point symmetry. Besides that, they have the same number and location of the lattice points within the smallest unit cell, which has the point symmetry of the lattice. We could see that half of the Bravais lattices appear as centered ones. This means, the smallest unit cells, that have the same point symmetry as the infinite lattices, contain more than one lattice point. However, it is important to point out that for each of the 14 Bravais lattices it is possible to choose a unit cell that contains only one lattice point, it means, a primitive unit cell. The basis vectors, $\vec{a}_1$, $\vec{a}_2$, $\vec{a}_3$, that define such a cell are primitive translation vectors of the Bravais lattice. Finally, a Bravais lattice represents a set of points whose positions are given by vectors $\vec{R}$ defined as

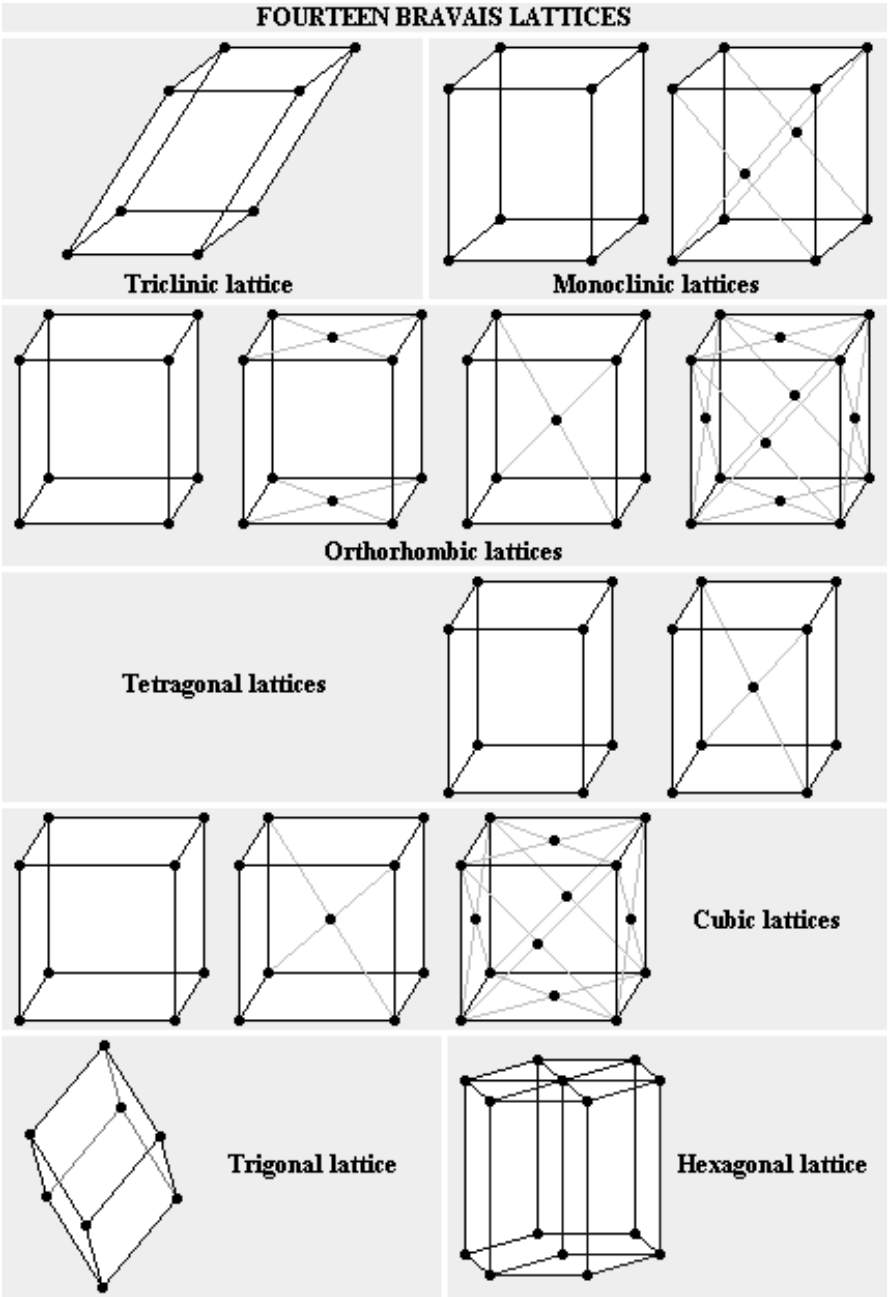

Figure 41 The 14 Bravais lattices. The conventional cells of the crystal systems are that from Fig. 30.

$$\vec{R} = n_1\vec{a}_1 + n_2\vec{a}_2 + n_3\vec{a}_3 , \qquad \text{(II.1)}$$

where $n_1, n_2, n_3 \in \mathbb{Z}$.

8. Coordination Number

Since all the lattice points in a Bravais lattice have equivalent positions in space, they have identical surroundings. Therefore, each point has the same number of NNs (points that are the closest to it) and this number, called the *coordination number*, is a characteristic of a given Bravais lattice. In the literature, we find more often an alternative definition in which the coordination number is the number of the NNs of an atom in a crystal (or molecule). Our definition, however, is more general, since we may think of substituting the lattice points with different objects like single atoms, or groups of atoms, or even molecules, and the definition still remains valid, since all these objects will have identical surroundings.

On occasions the information about the next nearest neighbors (NNNs) and even the third nearest neighbors (TNNs) of a lattice point is also important. Figure 42 shows the NNs, NNNs, and TNNs of a lattice point in the *sc* lattice. In this figure, the NNs of a lattice point placed in the center of a large cube (built of 8 smaller cubes) are placed at the vertices of a regular octahedron. Since the octahedron has 6 vertices, the coordination number for the *sc* lattice is 6. The NNNs are in the middle of the 12 edges of the large cube, so there are 12 NNNs of a lattice point in the *sc* lattice. The TNNs of the lattice point in consideration are at the vertices of the large

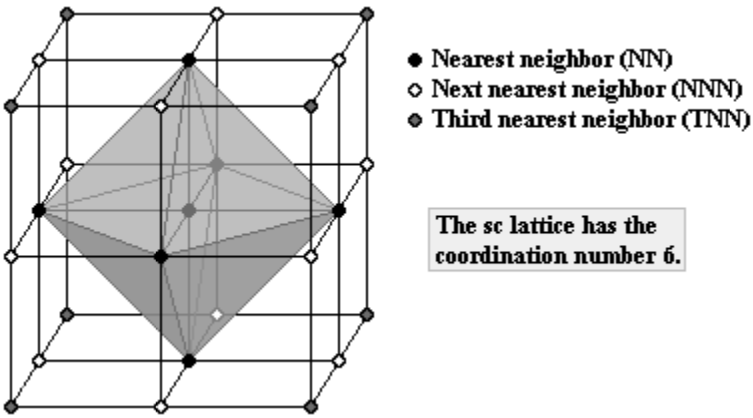

Figure 42 The NNs, NNNs, and TNNs of a lattice point in a *sc* lattice. The 6 NNs of a lattice point placed in the center of the large cube are at the vertices of the regular octahedron. The 12 NNNs are in the middle of the large cube edges and the 8 TNNs are in its vertices.

cube, so the number of them is 8. The NN distance in the *sc* lattice is equal to the lattice parameter *a*, the NNN distance is $\sqrt{2}a$, and the TNN distance is $\sqrt{3}a$.

9. Body Centered Cubic Lattice

Figure 43 shows three examples of a set of three primitive translation vectors that define the primitive unit cell of the *bcc* lattice. In these three cases at least one of the vectors involves two "types" of lattice points, namely, those from cube vertices and those from cube centers. This, of course, is essential in the case of a primitive cell, since with this cell it is possible to reproduce the entire lattice. The primitive cell defined by vectors $\vec{a}_1$, $\vec{a}_2$, $\vec{a}_3$ in Fig. 43c is shown in Fig. 44. In this figure, it is drawn a rhombohedron which represents the most symmetric primitive unit cell of the *bcc* lattice. We can also see in this figure that one diagonal of the rhombohedron is lying along one of the diagonals of the cube. Those diagonals represent a threefold axis of each cell. This is the unique threefold

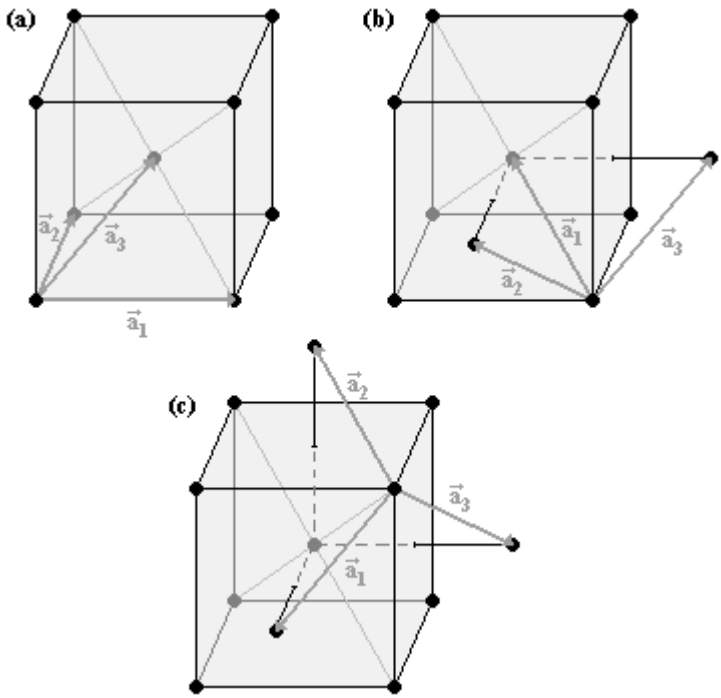

Figure 43 Three sets of three primitive translation vectors of the *bcc* lattice.

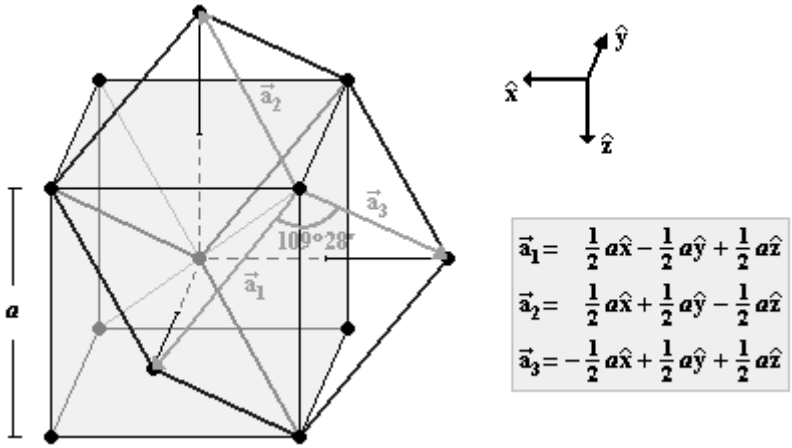

Figure 44 A primitive rhombohedral unit cell of the *bcc* lattice.

axis of the rhombohedron, while the cube has still three more such axes. The angles between the basis vectors $\vec{a}_1$, $\vec{a}_2$, $\vec{a}_3$ shown in Figs. 43c and 44 are the same:

$$\sphericalangle(\vec{a}_1,\vec{a}_2) = \sphericalangle(\vec{a}_1,\vec{a}_3) = \sphericalangle(\vec{a}_2,\vec{a}_3) = 109°28'.$$

Next, we will calculate the volume Ω_0 of the primitive unit cell and compare it with the volume of the cube. The volume of this cell is given by

$$\Omega_0 = (\vec{a}_1 \times \vec{a}_2)\cdot\vec{a}_3 = \begin{vmatrix} \hat{x} & \hat{y} & \hat{z} \\ \frac{1}{2}a & -\frac{1}{2}a & \frac{1}{2}a \\ \frac{1}{2}a & \frac{1}{2}a & -\frac{1}{2}a \end{vmatrix} \cdot \left(-\frac{1}{2}a\hat{x} + \frac{1}{2}a\hat{y} + \frac{1}{2}a\hat{z}\right),$$

$$= \left(0\hat{x} + \frac{1}{2}a^2\hat{y} + \frac{1}{2}a^2\hat{z}\right)\cdot\left(-\frac{1}{2}a\hat{x} + \frac{1}{2}a\hat{y} + \frac{1}{2}a\hat{z}\right) = \frac{1}{4}a^3 + \frac{1}{4}a^3 = \frac{1}{2}a^3 \tag{II.2}$$

and the volumes ratio is

$$\frac{V_{cube}}{\Omega_0} = \frac{a^3}{\frac{1}{2}a^3} = 2\,. \tag{II.3}$$

A primitive unit cell of the *bcc* lattice has one lattice point while the cubic cell has two points. The ratio, given by Eq. (II.3), between the cell volumes is equal to the ratio between the numbers of points belonging to them. Therefore, the same volume Ω_0 corresponds to each lattice point.

Let us now demonstrate that the two points that are within the *bcc* cubic unit cell have equivalent positions in the *bcc* lattice. This is shown and explained in Fig. 45. In Fig. 46 we show the NNs of a point of the *bcc* lattice. This lattice has a coordination number 8.

We will now consider the lattice points within the cubic cell of the *bcc* lattice. It is convenient sometimes to associate the point, being a sum of

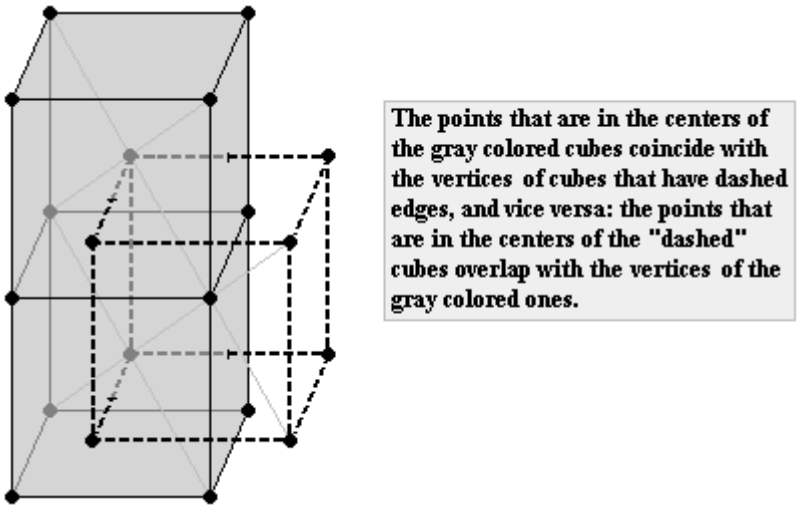

Figure 45 Demonstration of the equivalence of the two lattice points within the cubic unit cell of the *bcc* lattice.

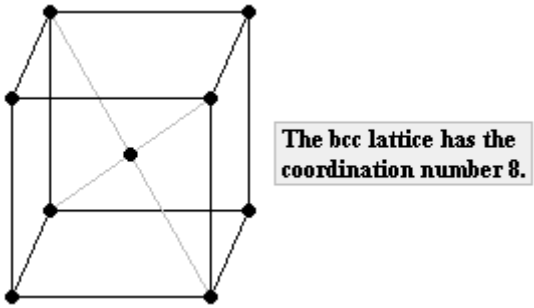

Figure 46 The lattice points from the vertices of the cubic unit cell of the *bcc* lattice represent the NNs of the lattice point that is in the center of the cell.

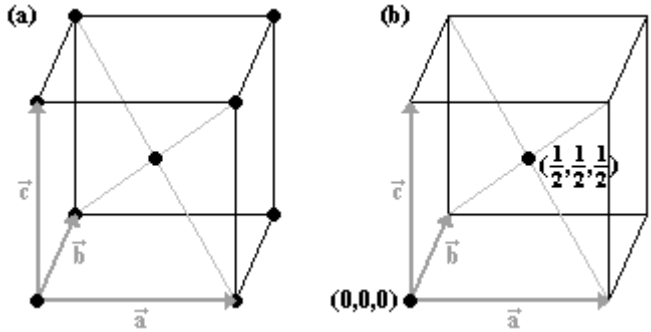

Figure 47 (a) A cubic cell of the *bcc* lattice. Each of the lattice points located at the vertices contributes with $1/8$ to the unit cell so the cell contains 2 lattice points. **(b)** Positions of the 2 points within the cubic cell. The point, which is a sum of eight fractions, is placed in the vertex of the cube that coincides with the origin of the cell. The coordinates are expressed in units of *a*.

eight fractions (see Fig. 47a), with only one of the vertices of the cube. Figure 47b shows such a point in the cube vertex that coincides with the initial point of the basis vectors $\vec{a}$, $\vec{b}$, $\vec{c}$. Its position is $(0,0,0)$. The position of the second lattice point within the cubic cell, given with respect to the $\vec{a}$, $\vec{b}$, $\vec{c}$ axes, is $(1/2,1/2,1/2)$, where the coordinates are expressed in units of *a*. The vector $\vec{t}=1/2\vec{a}+1/2\vec{b}+1/2\vec{c}$ represents one of the shortest translation vectors of the *bcc* lattice and it coincides with the vector $\vec{a}_3$ from Fig. 43a. In Figs. 43b and 43c there are shown other examples of the shortest translation vectors in the *bcc* lattice. At least one of such vectors has to appear in each set of basis vectors that define a primitive unit cell of this lattice (see Fig. 43), since both, the lattice point located in the center of the cubic cell and the point from its vertices, are then represented by the lattice point from vertices of the primitive unit cell.

10. Face Centered Cubic Lattice

First, let us consider the lattice points within the cubic unit cell of the *fcc* lattice. The two lattice points placed in the *A*-faces (orthogonal to the basis vector $\vec{a}$ in Fig. 48a) contribute to the cubic cell with half of the point each. We will represent these two fractions with one lattice point placed in the *A*-face that contains the origin of the basis vectors $\vec{a}$, $\vec{b}$, $\vec{c}$ (see Fig. 48b), that is, at the shortest distance from the origin. The position of this point is $(0,1/2,1/2)$, where the coordinates are expressed in units

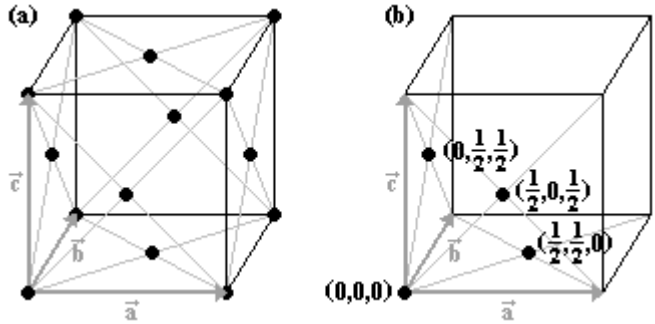

Figure 48 **(a)** All-face centered cubic unit cell of the *fcc* lattice. **(b)** Positions of the four lattice points within the cubic cell. The coordinates are expressed in units of *a*, which is the length of the cube edge.

of *a*, which is the length of the basis vectors. In the similar way, we can place the points in the *B*- and *C*-faces (see Fig. 48b). Finally, the positions of the four lattice points belonging to the cubic cell of the *fcc* lattice are: $(0,0,0)$, $(0,1/2,1/2)$, $(1/2,0,1/2)$, and $(1/2,1/2,0)$.

Figure 49 shows the most symmetric primitive unit cell of the *fcc* lattice. It is defined by the basis vectors $\vec{a}_1$, $\vec{a}_2$, $\vec{a}_3$. Each of them represents one of the shortest translation vectors of the *fcc* lattice. In the definition of the vectors $\vec{a}_1$, $\vec{a}_2$, $\vec{a}_3$ are involved all the four lattice points belonging to the cubic unit cell and this guarantees that the primitive cell can reproduce the entire lattice. The primitive unit cell shown in Fig. 49 takes on the shape of a rhombohedron that is inscribed in the cubic cell. The threefold axis of the rhombohedron coincides with one of the threefold axis of the cube. The lattice points that define this axis are at the vertices of the two cells, while the rest of the rhombohedron vertices coincide with the centers of the cube faces.

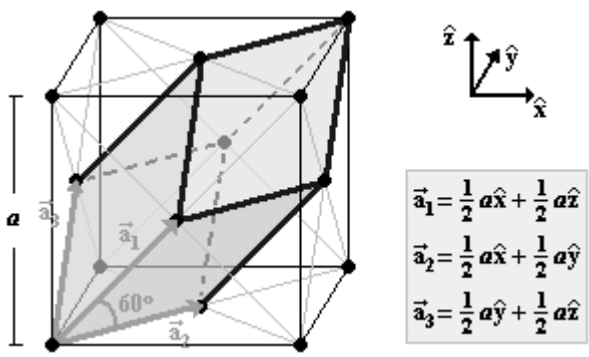

Figure 49 A primitive rhombohedral unit cell of the *fcc* lattice.

For the cell form Fig. 49 it is easy to show that

$$\sphericalangle(\vec{a}_1,\vec{a}_2)=\sphericalangle(\vec{a}_1,\vec{a}_3)=\sphericalangle(\vec{a}_2,\vec{a}_3)=60°\,. \tag{II.4}$$

Indeed, since $a_1=a_2=a_3=(\sqrt{2}/2)a$ we have that

$$\vec{a}_1\cdot\vec{a}_2=a_1a_2\cos\sphericalangle(\vec{a}_1,\vec{a}_2)=\frac{2}{4}a^2\cos\sphericalangle(\vec{a}_1,\vec{a}_2) \tag{II.5}$$

and using the vector coordinates we have also that

$$\vec{a}_1\cdot\vec{a}_2=a_{1x}a_{2x}+a_{1y}a_{2y}+a_{1z}a_{2z}=\frac{1}{4}a^2\,, \tag{II.6}$$

then comparing the two expressions for the scalar product $\vec{a}_1\cdot\vec{a}_2$, we obtain

$$\frac{2}{4}a^2\cos\sphericalangle(\vec{a}_1,\vec{a}_2)=\frac{1}{4}a^2 \;\Rightarrow\; \cos\sphericalangle(\vec{a}_1,\vec{a}_2)=\frac{1}{2}\,. \tag{II.7}$$

Repeating the same procedure as done in Eqs. (II.5-7), for all the vector pairs, we finally get Eq. (II.4). So the basis vectors $\vec{a}_1$, $\vec{a}_2$, $\vec{a}_3$ of a primitive rhombohedral unit cell of the *fcc* lattice are at angles of $60°$ to each other.

Let us now calculate the volume, Ω_0, of the primitive unit cell of the *fcc* lattice and compare it with the volume of the cubic cell. We have that

$$\begin{aligned}\Omega_0=\left(\vec{a}_1\times\vec{a}_2\right)\cdot\vec{a}_3&=\begin{vmatrix}\hat{x} & \hat{y} & \hat{z}\\ \frac{1}{2}a & 0 & \frac{1}{2}a\\ \frac{1}{2}a & \frac{1}{2}a & 0\end{vmatrix}\cdot\left(\frac{1}{2}a\hat{y}+\frac{1}{2}a\hat{z}\right)\\ &=\left(-\frac{1}{4}a^2\hat{x}+\frac{1}{4}a^2\hat{y}+\frac{1}{4}a^2\hat{z}\right)\cdot\left(\frac{1}{2}a\hat{y}+\frac{1}{2}a\hat{z}\right)=\frac{1}{8}a^3+\frac{1}{8}a^3=\frac{1}{4}a^3\,.\end{aligned} \tag{II.8}$$

The primitive unit cell has one lattice point while the cubic cell contains four lattice points, so the ratio between the volumes of these cells

$$\frac{V_{\text{cube}}}{\Omega_0}=\frac{a^3}{\frac{1}{4}a^3}=4 \tag{II.9}$$

is equal to the ratio between the numbers of lattice points in them.

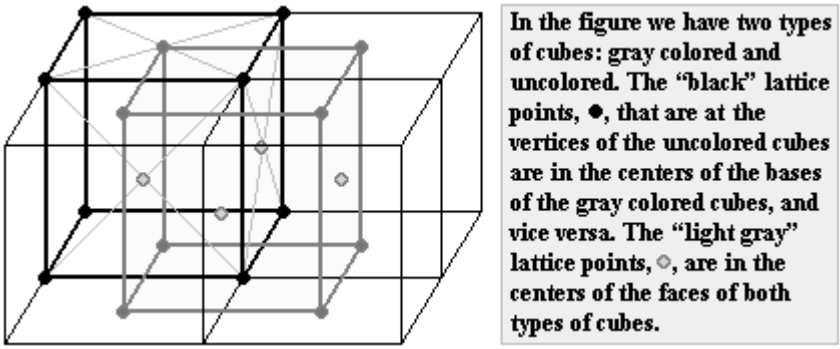

Figure 50 Demonstration of the equivalence of all lattice points in the cubic cell of the *fcc* lattice.

Next, we will demonstrate that different lattice points within the cubic unit cell of the *fcc* lattice have equivalent positions in this lattice. This is shown in Fig. 50. In the explanation we are using two sets of cubes. The second set of cubes (represented by a gray colored cube in Fig. 50) is obtained by translating the first one in the direction of a diagonal from its bases by half of the diagonal length. The correspondence of the lattice points in the two sets of cubes is explained in Fig. 50. Upon making a similar translation, but now in a plane which coincides with the side faces of one of the two sets of cubes, the result will be that the points that are in the middle of the faces of the two types of cubes (from the two sets) will occupy the positions of the points at the vertices. In this manner, we can demonstrate the equivalence between the positions of lattice points at the vertices and faces of the cube.

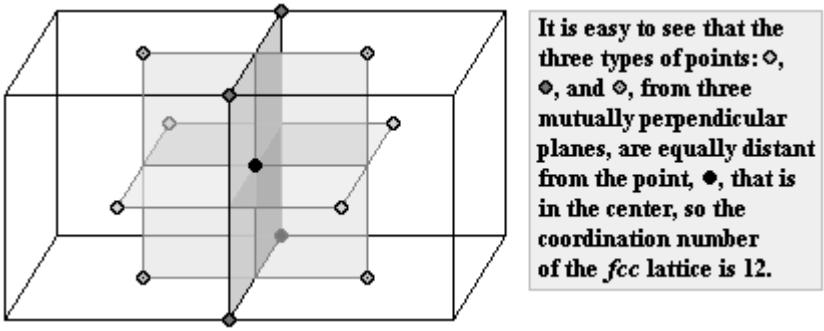

Figure 51 Nearest neighbors of a point in the *fcc* lattice.

Since all the lattice points in the *fcc* cubic lattice have equivalent positions, the neighborhood of each lattice point is the same and therefore, each point has the same number of NNs. We will consider the neighborhood of a lattice point from the face of a cube. This is shown in Fig. 51. As explained in this figure the coordination number of the *fcc* lattice is 12.

11. Rhombohedral Unit Cell in a Cubic Lattice

We have already learned in Secs. II.9 and II.10 that a rhombohedron represents a primitive unit cell of both the *bcc* and the *fcc* lattices. A cube, which is a primitive cell of the *sc* lattice, is also a particular case of a rhombohedron. However, a rhombohedron represents, at first, the conventional unit cell of the trigonal system, and now we know that when the basis vectors $\vec{a}_1$, $\vec{a}_2$, $\vec{a}_3$ of a primitive rhombohedral unit cell are at angles of $60°$, or $90°$, or $109°28'$ to each other, then this cell is a primitive cell of a lattice belonging to the cubic system, it means, possesses a higher point symmetry than the symmetry of a trigonal lattice. Moreover, the presence of a rhombohedral unit cell with its threefold symmetry axis in a cubic lattice is not surprising, since this lattice possesses threefold symmetry axes. As next we will show a centered rhombohedral unit cell in the *sc* lattice.

11.1. Rhombohedral Unit Cell of the *sc* Lattice

Besides of the primitive rhombohedral unit cells there are, of course, centered rhombohedral unit cells in lattices belonging to the cubic system.

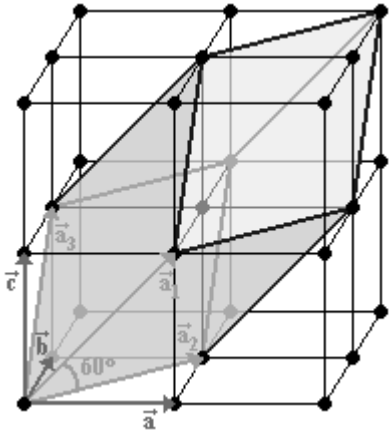

Figure 52 A body centered rhombohedral unit cell of the *sc* lattice.

Table 4 The characteristics of the two unit cells, shown in Fig. 52, of the *sc* lattice.

SIMPLE CUBIC LATTICE		
Unit cell type	**Cell parameters**	**Number of lattice points per cell**
Cubic *P*	a_c	1
Rhombohedral *I*	$a_r = \sqrt{2}a_c$, $\alpha_r = 60°$	2

Figure 52 shows such a unit cell of the *sc* lattice. This cell contains two lattice points.

Table 4 resumes information about the two types of unit cells shown in Fig. 52, that is, the cubic one defined by basis vectors $\vec{a}$, $\vec{b}$, $\vec{c}$ and the rhombohedral cell defined by vectors $\vec{a}_1$, $\vec{a}_2$, $\vec{a}_3$. The volume of the body centered rhombohedral cell is two times the volume of the primitive cubic cell (see the numbers of lattice points within each cell).

The positions of the two lattice points within the rhombohedral unit cell from Fig. 52 are shown in Fig. 53. One of them is placed in the origin of the cell and the position of the other is given by the vector $(1/2)(\vec{a}_1 + \vec{a}_2 + \vec{a}_3)$, where $\vec{a}_1$, $\vec{a}_2$, $\vec{a}_3$ are the axes of the rhombohedral unit cell defined in Fig. 52. The coordinates of the centering point are expressed in units of a_r ($a_r = |\vec{a}_1| = |\vec{a}_2| = |\vec{a}_3|$).

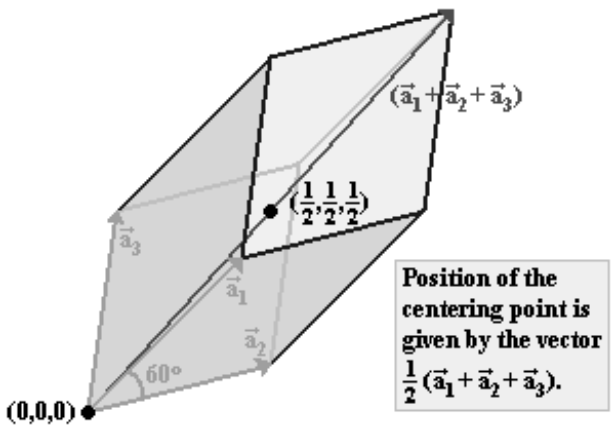

Figure 53 Positions of the two lattice points in the centered rhombohedral unit cell (defined in Fig. 52) of the *sc* lattice, given with respect to the $\vec{a}_1$, $\vec{a}_2$, $\vec{a}_3$ axes. The coordinates are expressed in units of a_r ($a_r = |\vec{a}_1| = |\vec{a}_2| = |\vec{a}_3|$).

11.2. Simple Cubic Crystal Structure

Let us now consider a *sc* monoatomic crystal structure. The *sc* lattice is an obvious option to describe this structure:

$$sc \text{ lattice } + \text{ 1-atom basis } = sc \text{ crystal structure}.$$

However, this is not the only Bravais lattice that we can propose to describe the *sc* crystal structure. The presence of a rhombohedral *I* unit cell, defined by the axes at angles of 60° to each other, in a monoatomic *sc* crystal structure suggests that the *sc* structure may be considered as a *fcc* lattice with an atomic basis composed of two atoms. This was already suggested in Fig. 52 by the distribution of lattice points within the large cubic cell. This cell may be considered as a cubic unit cell of the *fcc* lattice with 4 additional lattice points in it. It means, the number of lattice points belonging to the cubic *F* unit cell of the *sc* lattice is two times the number of lattice points in a cubic *F* unit cell of the *fcc* lattice. The same is true for the atoms in the monoatomic *sc* structure.

Let us now consider the *sc* crystal structure as the *fcc* lattice with two-atom basis:

$$fcc \text{ lattice } + \text{ 2-atom basis } = sc \text{ crystal structure}.$$

The centers of these atoms may overlap the two lattice points of the unit cell from Fig. 53 but, of course, the primitive rhombohedral unit cell of the *fcc* lattice contains only one lattice point, like it is shown in Fig. 54a. When the basis contains two atoms, the lattice points are frequently placed (with respect to the atoms of the crystal structure) in such a way that a lattice point is equidistant to the two basis atoms, what is shown in Fig. 54b. Then the origin of the unit cell changes from O to O′ and the cell contains 1 atom attached to its lattice point and another one that is attached to the lattice point belonging to a different unit cell.

We have shown here that the *sc* structure may be seen as a *fcc* lattice with 2-atom basis. However, it is of course more natural to choose the *sc* lattice when describing the monoatomic *sc* structure. In both cases, the lattices have the same point symmetry as the structure, but the lattice constant in *fcc* is two times the lattice constant in *sc*. As a consequence, in the *sc* lattice the volume of the *F*-centered cubic unit cell is 8 times larger than that of the cubic *P* cell. It should be noted that what we have learned in

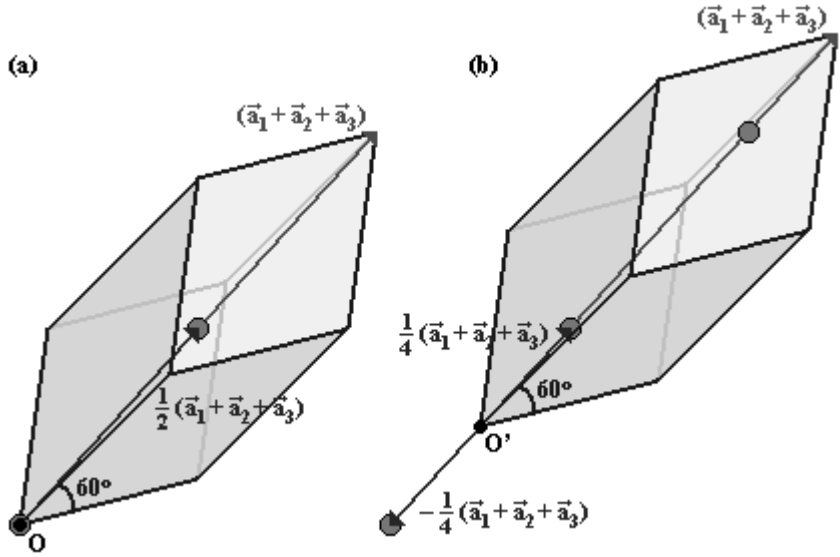

Figure 54 The *fcc* lattice used to describe the monoatomic *sc* structure. The figure shows a primitive rhombohedral unit cell of the *fcc* lattice with two-atom basis. Two locations of the basis atoms with respect to a lattice point are shown, where: **(a)** the lattice point coincides with the center of one of the basis atoms and **(b)** the lattice point is equidistant from the two basis atoms.

this section looks quite obvious and simple, but is very useful when it comes to analyze experimental and also theoretical results.

11.3. Interpretation of Data for As, Sb, Bi, and Hg

We will use now the considerations made in the previous section to show that the structures for arsenic, antimony, and bismuth are close to the *sc* structures. In order to do this, we have to realize, first, that a rhombohedron may be obtained by stretching a cube along one of its diagonals and this type of distortion applied to any cubic lattice changes it to a trigonal Bravais lattice. If such distortion would be present in the cells shown in Fig. 52, along their diagonals parallel to the vector $(\vec{a}_1+\vec{a}_2+\vec{a}_3)$, then the cube, defined by vectors $\vec{a}$, $\vec{b}$, $\vec{c}$, would become a rhombohedron with angles between the new $\vec{a}$, $\vec{b}$, $\vec{c}$ vectors slightly smaller than $90°$, and the rhombohedron defined by vectors $\vec{a}_1$, $\vec{a}_2$, $\vec{a}_3$ would be a different rhombohedron with angles between its axes slightly smaller than $60°$. The two cells (rhombohedral *P* and rhombohedral *I*) represent unit cells of a trigonal lattice that was obtained distorting the *sc* lattice.

Table 5 Experimental lattice parameters for arsenic, antimony, bismuth, and mercury. All this elements crystallize in trigonal crystal structures. The axes $\vec{a}_1$, $\vec{a}_2$, and $\vec{a}_3$ define a rhombohedral *P* unit cell that in the case of As, Sb, and Bi contains two atoms. The atoms are placed with respect to a lattice point like it is shown in Fig. 54b. In the case of Hg the basis is composed of one atom.

Element	**Lattice parameters** a_r **(Å),** α_r	**Number of atoms in a rhombohedral** ***P*** **unit cell**	**Coordinates of the basis atoms given in terms of vector** $(\vec{a}_1+\vec{a}_2+\vec{a}_3)$
As	$a_r = 4.13$ $\alpha_r = 54°10'$	2	$x = \pm 0.226$
Sb	$a_r = 4.51$ $\alpha_r = 57°6'$	2	$x = \pm 0.233$
Bi	$a_r = 4.75$ $\alpha_r = 57°14'$	2	$x = \pm 0.237$
Hg (5 K)	$a_r = 2.99$ $\alpha_r = 70°45'$	1	$x = 0$

The values for As, Sb, and Bi listed in Table 5 can be interpreted as follows. The three elements crystallize in trigonal crystal structures that are close to the *sc* structures. For each case Table 5 reports experimental data for a primitive rhombohedral unit cell of a trigonal lattice with an atomic basis composed of 2 atoms. The atoms are equidistant from a lattice point, like it was shown in Fig. 54b. The angles between the axes $\vec{a}_1$, $\vec{a}_2$, $\vec{a}_3$ are close to $60°$ and the positions of the basis atoms, $x(\vec{a}_1+\vec{a}_2+\vec{a}_3)$, with respect to a lattice point (see Fig. 54b) are close to $(\pm 1/4)(\vec{a}_1+\vec{a}_2+\vec{a}_3)$, which is the case of the *sc* crystal structure. Therefore, the crystal structures of the three elements are close to the *sc* structures.

Table 5 is reporting also the data for the crystal structure of mercury. This element crystallizes in the trigonal structure. The rhombohedral *P* unit cell contains 1 atom. If we consider this cell as a stretched cubic one then it is clear that the Hg crystal structure is far from the *sc* structure since the angle $\alpha_r = 70°45'$ is very different from $90°$ of a cubic *P* unit cell.

12. Trigonal Lattice

We know already that the conventional cell for the trigonal system (a rhombohedron) can be constructed inside a hexagonal prism (see Fig. 31). In such a construction, the sixfold symmetry axis of the hexagonal prism

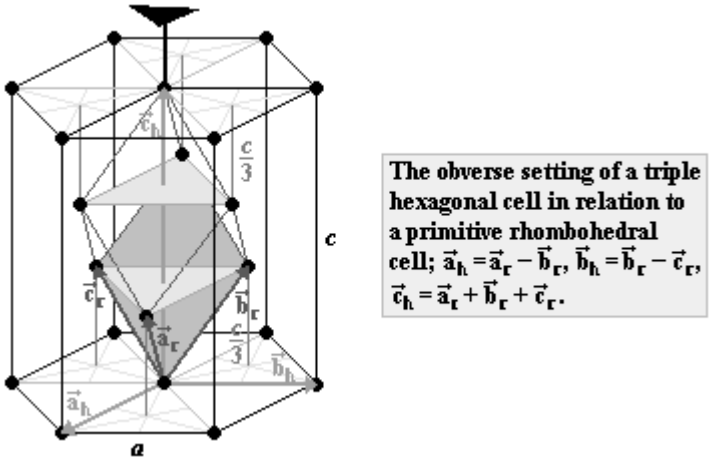

Figure 55 Primitive rhombohedral and a *R* centered hexagonal unit cells. A primitive trigonal lattice may be considered as a *R* centered hexagonal lattice. The centering points, within the hexagonal cell, reduce the sixfold symmetry axis of the hexagonal prism to a threefold symmetry axis.

becomes a threefold symmetry axis of the rhombohedron. We will see now that a trigonal lattice is just a centered hexagonal one. The presence of additional lattice points in a trigonal lattice, with respect to the hexagonal lattice, reduces the sixfold hexagonal prism axis to a threefold one, what is shown in Fig. 55. We can see in this figure that the trigonal lattice points that are inside the hexagonal prism define two equilateral triangles in planes orthogonal to the sixfold hexagonal prism symmetry axis. The axis is crossing these planes at the geometric centers of the triangles. Just such distribution of the trigonal lattice points, which are inside the hexagonal prism, reduces the sixfold axis of a hexagonal lattice to the threefold axis of a trigonal lattice. The basis vectors $\vec{a}_h$, $\vec{b}_h$, $\vec{c}_h$ in Fig. 55 define a rhombohedrally centered hexagonal unit cell for a trigonal lattice. This cell is called a *triple hexagonal unit cell* and contains three lattice points. A triple hexagonal cell for a trigonal lattice is also called a triple hexagonal cell *R* and the symbol of a trigonal lattice is just *hR*.

In Fig. 56a, we show the projections of the centering points of the triple hexagonal cell *R* from Fig. 55 on the cell base. Whereas, Fig. 56b shows the projections on the prism base of 6 trigonal lattice points that are inside the hexagonal prism from Fig. 55. In this figure O represents the origin of the triple hexagonal unit cell, defined by basis vectors $\vec{a}_h$, $\vec{b}_h$, $\vec{c}_h$. The coordinate of each point in the $\vec{c}_h$ axis is shown next to the lattice point

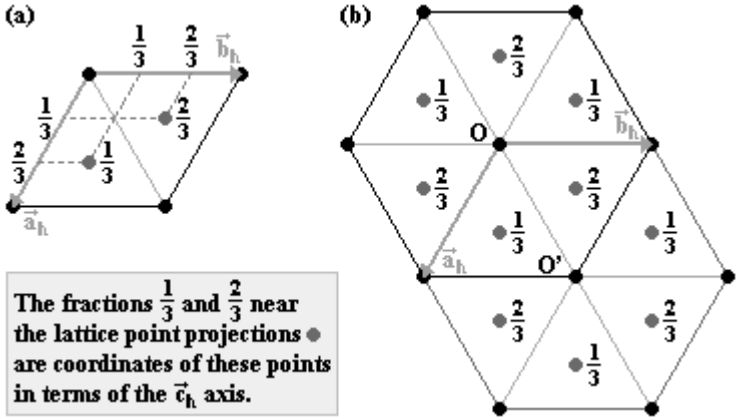

Figure 56 (a) Projections of the centering points of the triple hexagonal cell *R* from Fig. 55 on the base of the cell. The coordinates of these points are given in terms of the hexagonal axes $\vec{a}_h$, $\vec{b}_h$, $\vec{c}_h$. **(b)** Projections of the 6 points that are inside the hexagonal prism on its base. The coordinates of these points are given in terms of the $\vec{c}_h$ axis. The hexagonal prism base translated by a translation vector $\left(\vec{a}_h + \vec{b}_h\right)$ is also shown.

projection and is expressed in units of *c*. In Fig. 56b, there is also shown the base of the hexagonal prism in consideration translated by a translation vector $(\vec{a}_h + \vec{b}_h)$. For this case, the origin of the triple hexagonal unit cell changes from O to O'. We can see in Fig. 56b that by translating a trigonal lattice to a translation vector $(\vec{a}_h + \vec{b}_h)$ of the *R* centered hexagonal lattice, we obtain the same trigonal lattice.

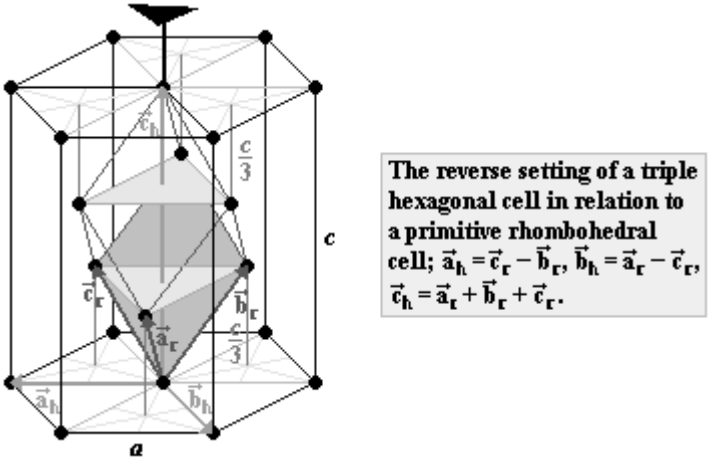

Figure 57 The reverse setting of a triple hexagonal cell in relation to the primitive rhombohedral cell.

The setting of the triple hexagonal unit cell in relation to the primitive rhombohedral unit cell is not unique. In Fig. 55 is shown the *obverse setting* of the triple hexagonal unit cell with respect to the primitive rhombohedral cell and in Fig. 56a, as we know, is displayed the projection of this cell onto the plane orthogonal to the $\vec{c}_h$ axis. If we propose the basis vectors $\vec{a}_h$, $\vec{b}_h$, $\vec{c}_h$ for the hexagonal cell in the way done in Fig. 57, then we obtain the *reverse setting* of a triple hexagonal unit cell in relation to the primitive rhombohedral cell. The positions of the centering points in a hexagonal cell depend on the setting in consideration.

Figure 58 shows two triple hexagonal cells *R*. The cell from Fig. 58a is in obverse setting in relation to the primitive rhombohedral cell, while the cell from Fig. 58b is in reverse setting with respect to the rhombohedral cell. Both figures show the positions of the three lattice points within the hexagonal unit cell *R*. We can observe that the coordinates of the centering points expressed in terms of the axes $\vec{a}_h$ and $\vec{b}_h$ are in each case different (of course, the vectors $\vec{a}_h$ and $\vec{b}_h$ are also different).

We have learned here that it is possible to describe a trigonal lattice in terms of the hexagonal axes. More strictly speaking, a trigonal lattice is just a *R* centered hexagonal lattice. Moreover, it is more convenient to see this lattice as a *R* centered hexagonal one since the hexagonal axes are easier to visualize. The relations between the basis vectors that define a rhombohedral cell and the ones that define a triple hexagonal cell *R* are

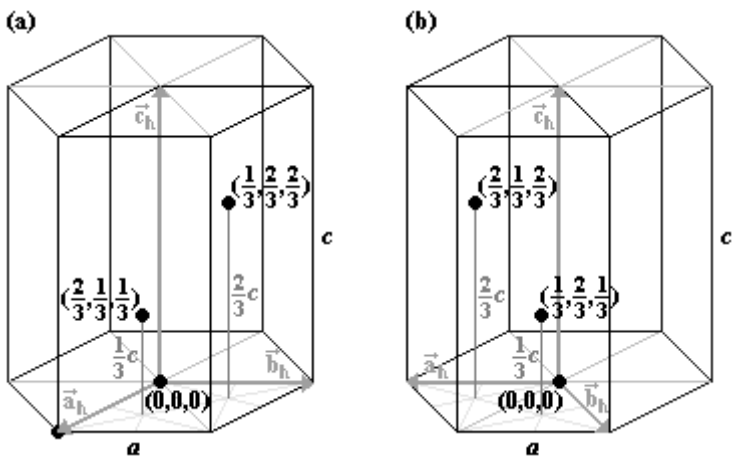

Figure 58 Positions of the three points within the triple hexagonal *R* unit cell **(a)** in obverse setting and **(b)** in reverse setting in relation to the primitive rhombohedral unit cell. The coordinates are expressed in units of *a* and *c*.

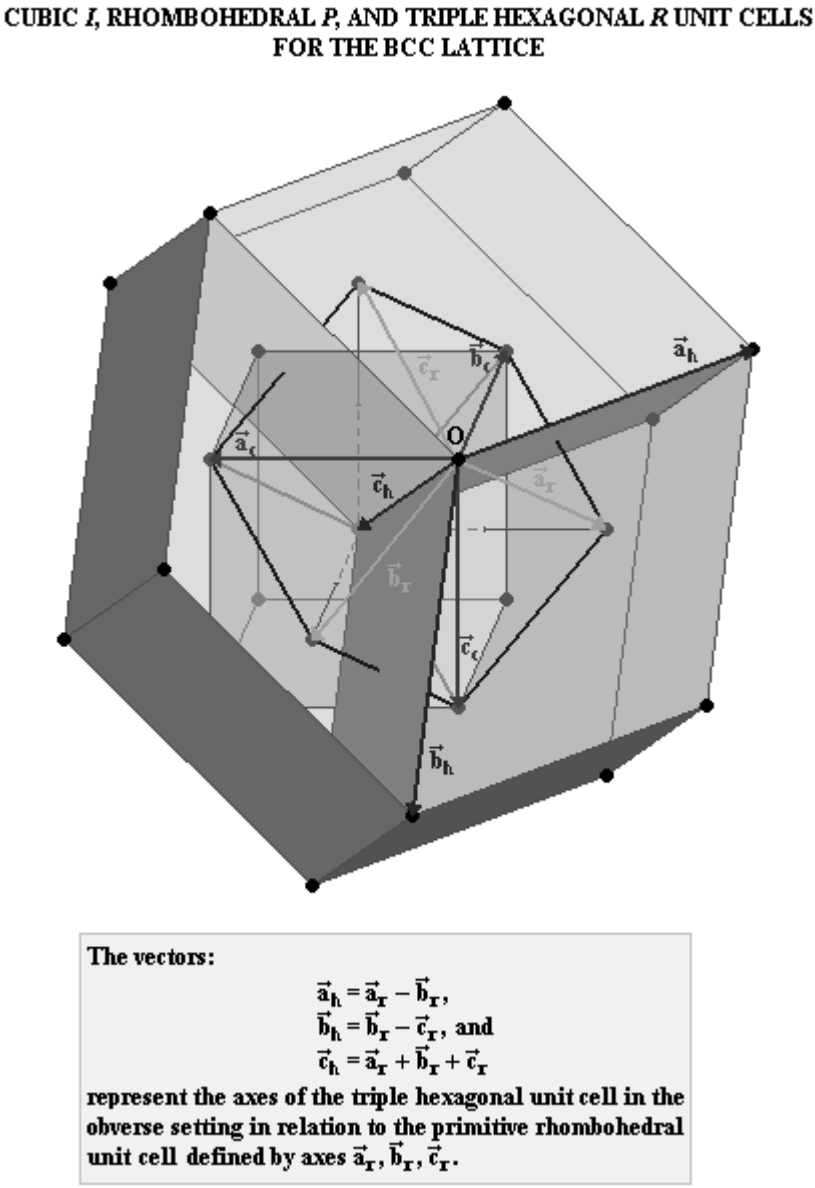

Figure 59 Three types of unit cells of the *bcc* lattice. Each of the three triple hexagonal *R* cells shown in the figure is defined by basis vectors $\vec{a}_h$, $\vec{b}_h$, and $\vec{c}_h$ or their linear combinations. Inside the hexagonal prism there is a rhombohedral *P* unit cell defined by basis vectors $\vec{a}_r$, $\vec{b}_r$, and $\vec{c}_r$. Besides that, there is a cubic *I* cell of the *bcc* lattice defined by vectors $\vec{a}_c$, $\vec{b}_c$, and $\vec{c}_c$. All three unit cells have the same origin O.

$$\vec{a}_h = \vec{a}_r - \vec{b}_r, \quad \vec{b}_h = \vec{b}_r - \vec{c}_r, \quad \vec{c}_h = \vec{a}_r + \vec{b}_r + \vec{c}_r,$$

in the case of the obverse setting and

$$\vec{a}_h = \vec{c}_r - \vec{b}_r, \quad \vec{b}_h = \vec{a}_r - \vec{c}_r, \quad \vec{c}_h = \vec{a}_r + \vec{b}_r + \vec{c}_r,$$

in the case of the reverse setting.

13. Triple Hexagonal Cell *R* in a Cubic Lattice

The centered cubic lattices (*bcc* and *fcc*) possess primitive rhombohedral cells so it is natural to introduce for them the triple hexagonal cells. Therefore, the *bcc* and *fcc* lattices may be described in terms of cubic, rhombohedral, and hexagonal axes by using cubic (body centered or all-face centered), primitive rhombohedral, and triple hexagonal *R* unit cells, respectively. In Fig. 59 we show the three types of cells of the *bcc* lattice by

Table 6 Basic information about three types of unit cells of the *bcc* lattice.

BODY CENTERED CUBIC LATTICE		
Unit cell type	**Cell parameters**	**Number of lattice points per cell**
Cubic *I*	a_c	2
Rhombohedral *P*	$a_r = \left(\sqrt{3}/2\right)a_c$ $\alpha_r = 109°28'$	1
Triple hexagonal *R*	$a_h = \sqrt{2}a_c$ $c_h = \left(\sqrt{3}/2\right)a_c$	3

Table 7 Basic information about three types of unit cells of the *fcc* lattice.

FACE CENTERED CUBIC LATTICE		
Unit cell type	**Cell parameters**	**Number of lattice points per cell**
Cubic *F*	a_c	4
Rhombohedral *P*	$a_r = \left(\sqrt{2}/2\right)a_c$ $\alpha_r = 60°$	1
Triple hexagonal *R*	$a_h = \left(\sqrt{2}/2\right)a_c$ $c_h = \sqrt{3}a_c$	3

putting them all together and with a common origin. Some information about those cells is listed in Table 6 and in Table 7 is listed the same information, but for the three types of unit cells of the *fcc* lattice.

14. Wigner-Seitz Cell

All primitive unit cells, for the case of centered Bravais lattices that we have considered until now, do not have the point symmetry of the lattice. However, each Bravais lattice has a primitive unit cell that has the point symmetry of the lattice. This cell is called the *Wigner-Seitz cell.*

14.1. Construction of the Wigner-Seitz Cell

The Wigner-Seitz cell like every primitive unit cell contains only one lattice point, but this point has a very particular location in the cell. It is placed in the geometric center of the cell and the region of space that is closer to that point than to any other lattice point defines the Wigner-Seitz cell. In order to obtain the Wigner-Seitz cell we have to identify, first, the NNs of a lattice point. The NNNs may also be involved in the construction of that cell and even the TNNs. This cell can be obtained in the following manner:

a.) First, any point of the lattice is chosen (the one that is going to be in the middle of the Wigner-Seitz cell).
b.) Second, we connect this lattice point with all the NNs by means of segments and draw median planes of the segments. In this manner a three-dimensional body, limited by these planes, is obtained.
c.) Last, we repeat the same work as in point b.), but with the NNNs. If the new planes reduce the volume of the region defined by the first planes, this new volume will be the Wigner-Seitz cell, if, of course, more distant neighbors (TNNs, fourth NNs, and so on) do not manage to limit this volume even more.

14.2. The Wigner-Seitz Cell of the *bcc* Lattice

Figure 60 shows the Wigner-Seitz cell of the *bcc* lattice. This cell has the shape of a tetradecahedron (a polyhedron with 14 faces). Eight of its faces are defined by 8 NNs and the rest of them by 6 NNNs. This tetradecahedron may be seen as a truncated regular octahedron. That is, the faces of the octahedron, which are defined by 8 NNs, are truncated by

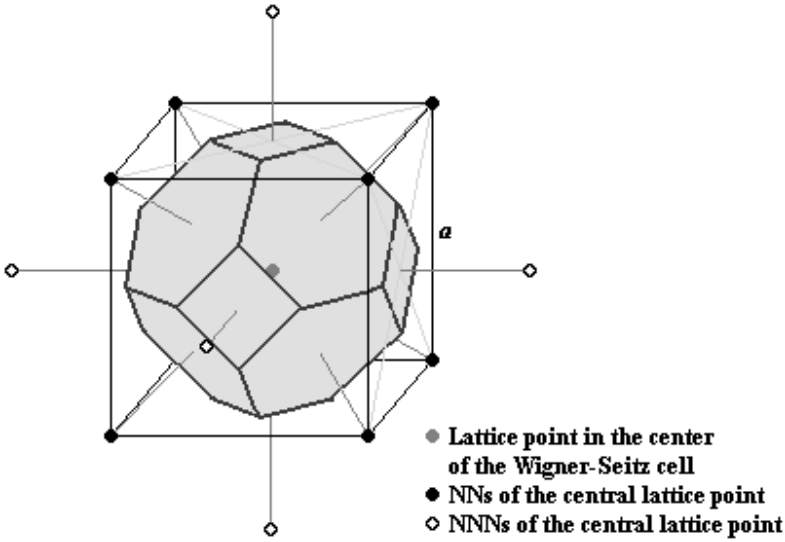

Figure 60 The Wigner-Seitz cell of the *bcc* lattice.

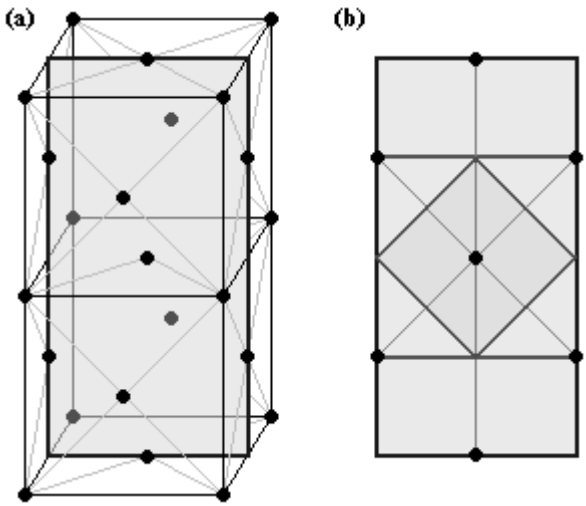

Figure 61 (a) A cross section of two cubic *F* cells of the *fcc* lattice. **(b)** Demonstration that in the construction of the Wigner-Seitz cell participate only the NNs of the lattice point belonging to the cell.

the 6 faces defined by the NNNs. This truncated octahedron has 6 square faces at a distance of $a/2$ from the middle of the Wigner-Seitz cell and 8 hexagonal faces at a distance of $\left(\sqrt{3}/4\right)a$ from the center. It is easy to identify, looking at the number, shape, and orientation of the faces of the

truncated octahedron, the 4 threefold axes and 3 fourfold axes that has the cubic unit cell of the *bcc* lattice (see Fig. 60).

14.3. The Wigner-Seitz Cell of the *fcc* Lattice

Figure 61a shows a cross section of two cubic *F* unit cells of the *fcc* lattice, in which there are 7 lattice points: the central one, 4 of its NNs, and 2 NNNs. The smallest square in Fig. 61b represents a cross section of the Wigner-Seitz cell. We demonstrate in this figure that in the construction of the Wigner-Seitz cell participate only the nearest neighboring lattice points. Since the number of the NNs in the *fcc* lattice is 12, its Wigner-Seitz cell has the shape of a dodecahedron. This is a rhombic dodecahedron, and it is shown in Fig. 62a. Figure 62b displays one of the 12 identical faces of this dodecahedron.

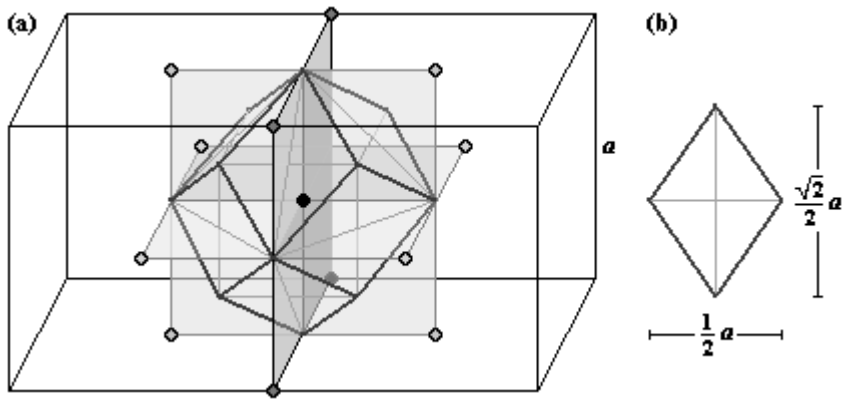

Figure 62 (a) The Wigner-Seitz cell of the *fcc* lattice. **(b)** A face of the dodecahedron shown in (a).

15. Problems

Exercise 1

a.) Draw all the rotation axes of the regular tetrahedron shown in Fig. 63a. In order to do that locate the positions of two points that define each axis. If it is necessary find these points graphically.

b.) Do the same for the regular octahedron shown in Fig. 63b.

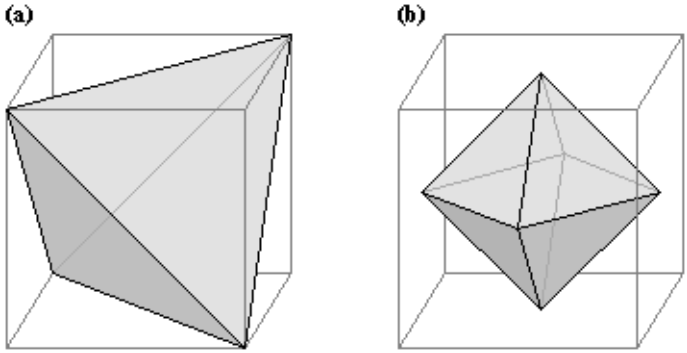

Figure 63 **(a)** A regular tetrahedron and **(b)** a regular octahedron.

Exercise 2 Figure 64 shows a truncated regular octahedron inscribed in a cube of edge length a, while the octahedron is inscribed in a cube of edge length $(3/2)a$. The faces of the two cubes are parallel to each other. We can see in this figure how the octahedron is truncated by the faces of the smaller cube with a tetradecahedron as a result. This tetradecahedron has 8 faces in shape of a regular hexagon (can you explain, why?) and 6 faces in shape of a square.

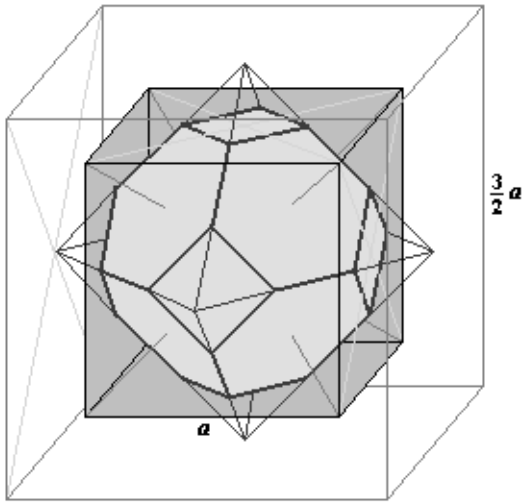

Figure 64 A tetradecahedron inscribed in a cube of edge length a. This tetradecahedron may be seen as a regular octahedron truncated by 6 faces of the smaller cube. The regular octahedron is inscribed in a cube of edge length $(3/2)a$ and has the same geometric center as the cube of edge length a.

a.) Draw all the rotation axes of the tetradecahedron (or truncated octahedron).
b.) Explain why the tetradecahedron from Fig. 64 does not have sixfold rotation axes.

Exercise 3 Show that the set of points from Fig. 65 has threefold and fourfold rotation axes. Follow the considerations of Sec. II.4 for the case of the set of 14 points.
***Hint*:** In Fig. 65 it is shown a regular hexagon defined by 6 of 27 lattice points, which is the set of points in consideration.

Exercise 4 Let us consider a threefold rotation axis of the set of 27 points from Fig. 65; 24 of them define 5 plane figures in planes orthogonal to the threefold axis. Find the edges of the plane figures and draw the superposition of their projections along this axis. Draw also the graphical symbol of the rotation point for this superposition.

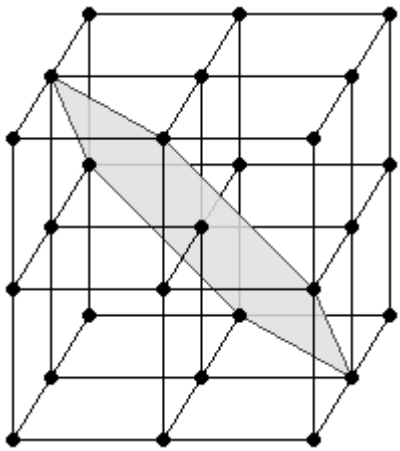

Figure 65 A set of 27 points located at the vertices of the 8 small cubes.

Exercise 5 Figure 66 shows a rhombohedron constructed inside a hexagonal prism of side a and height c. Two vertices of the rhombohedron are located in the geometric centers of the hexagonal bases and the other 6 form two groups of 3 vertices each. The positions of the vertices belonging to each group are described in Sec. II.6. Show that for $c/a = \sqrt{6}/2$ the rhombohedron takes on the shape of a cube.

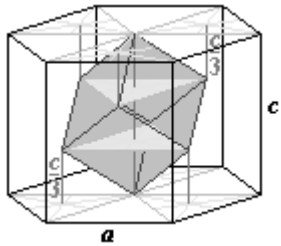

Figure 66 A rhombohedron constructed inside a hexagonal prism.

Exercise 6 In Fig. 67a it is shown a rhombohedron constructed inside a hexagonal prism of side *a* and height *c*. The rhombohedron is defined by the basis vectors $\vec{a}_1$, $\vec{a}_2$, $\vec{a}_3$.

a.) Show that the vector given by the sum $(\vec{a}_1 + \vec{a}_2 + \vec{a}_3)$ is lying along the longest diagonal of the rhombohedron and its longitude is *c*. Find the sum of the vectors graphically.

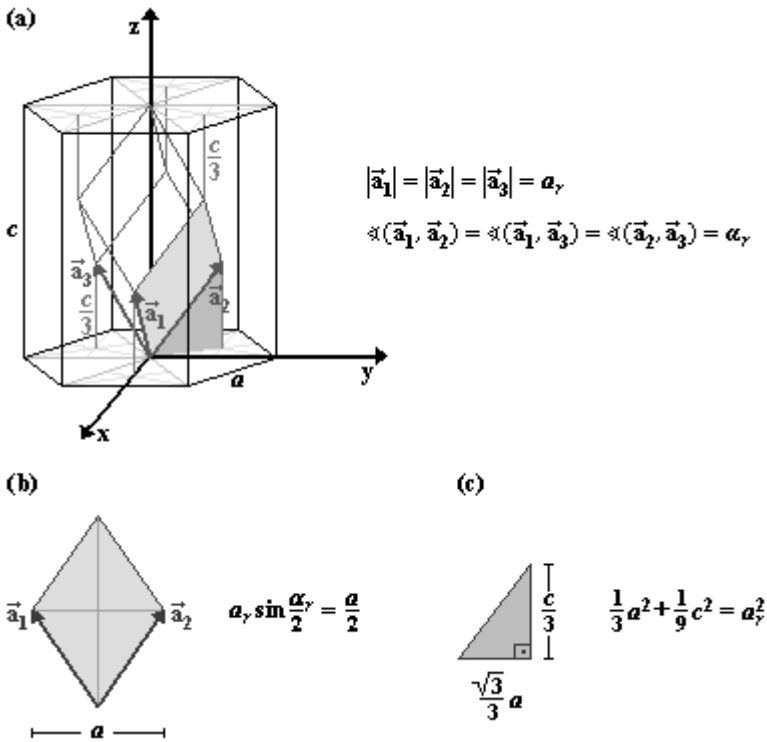

Figure 67 **(a)** A rhombohedron constructed inside a hexagonal prism of side *a* and height *c*. **(b)** The highlighted face of the rhombohedron from (a). **(c)** The right triangle highlighted in (a).

b.) Calculate the volume of the rhombohedron and compare it with the volume of the hexagonal prism.
***Hint*:** Show that the volume of the prism is 9 times the volume of the rhombohedron.

Exercise 7 Figure 67b shows the face of the rhombohedron that is highlighted in Fig. 67a. This face is defined by vectors $\vec{a}_1$ and $\vec{a}_2$. Figure 67c, in turn, displays the right triangle highlighted in Fig. 67a. This triangle is defined by the vector $\vec{a}_2$ and its projection onto the bottom base of the hexagonal prism.

a.) Using the plane figures from Figs. 67b and 67c, show that the relation between the parameters a_r, α_r that describe the rhombohedron and the parameters a, c that describe the hexagonal prism (in which this rhombohedron is inscribed) is the following

$$\begin{cases} a_r = \dfrac{1}{3}\sqrt{3a^2 + c^2} = \dfrac{a}{3}\sqrt{3 + (c/a)^2} \\ \sin\dfrac{\alpha_r}{2} = \dfrac{3}{2\sqrt{3 + (c/a)^2}} \end{cases}.$$

b.) Show that the c/a ratio is expressed only by the parameter α_r of the rhombohedron

$$\frac{c}{a} = \sqrt{\frac{9}{4\sin^2(\alpha_r/2)} - 3}\,.$$

Exercise 8 Figure 68 shows all the NNs, some of the NNNs and also some of the TNNs of a lattice point located in the center of the displayed *fcc* lattice with a lattice constant *a*.

a.) Show that the NNs, NNNs, TNNs, and also fourth and fifth nearest neighbors of a lattice point in the *fcc* lattice are at distances

$$\frac{\sqrt{2}}{2}a,\ \frac{\sqrt{4}}{2}a,\ \frac{\sqrt{6}}{2}a,\ \frac{\sqrt{8}}{2}a,\ \text{and}\ \frac{\sqrt{10}}{2}a\,,$$

from this point, respectively.

b.) Situate all the NNNs and the TNNs of the lattice point in consideration that fit in the empty cubes shown in Fig. 68.

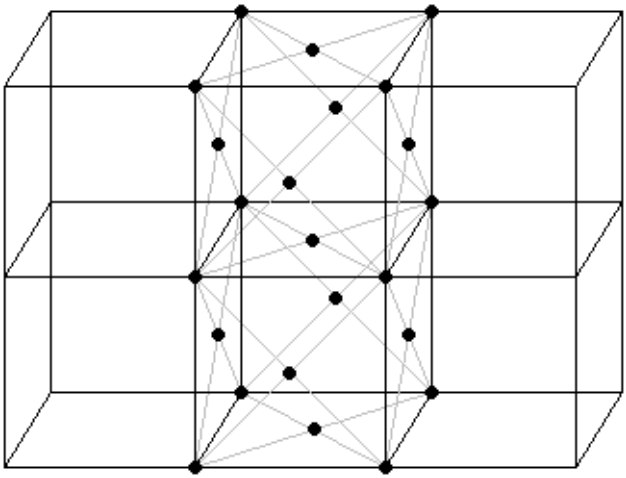

Figure 68 All the NNs, some of the NNNs, and also some of the TNNs of a lattice point located in the center of the displayed *fcc* lattice.

c.) Is it possible to estimate the number of the NNNs and the TNNs of a lattice point in the *fcc* lattice using the information obtained in point b.)?

Exercise 9 Show that the *A*-face centered, *C*-face centered, and body centered monoclinic lattices are equivalent in the case of the *b*-axis setting.

***Hint*:** In order to do this, find a body centered cell (with a shape of the conventional cell for the monoclinic system) for each of the lattices shown in Fig. 69.

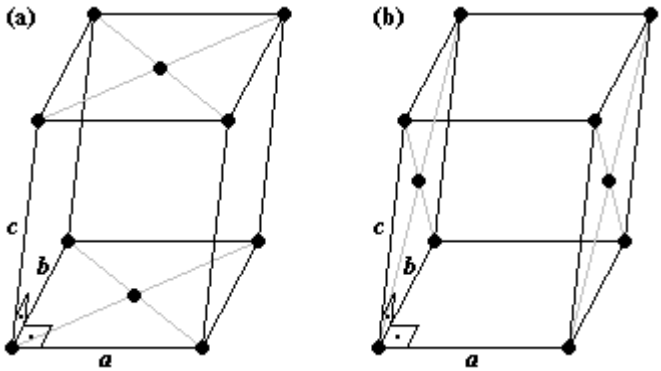

Figure 69 Two monoclinic lattices: **(a)** *C*-face centered and **(b)** *A*-face centered. The *b*-axis setting is assumed.

Exercise 10 Calculate the angles between the axes that define the primitive rhombohedral unit cell of the *bcc* lattice.
***Hint*:** Follow the steps shown in Sec. II.10 when calculating the angles between the axes that define the primitive rhombohedral unit cell of the *fcc* lattice.

Exercise 11 In the *sc* lattice from Fig. 70 draw the rhombohedral unit cell defined by axes with 109°28′ angles between them.
a.) What type of rhombohedral unit cell did you obtain?
b.) How many lattice points do belong to this cell?
c.) Calculate the volume of the rhombohedral unit cell and compare it with the volume of the primitive cubic cell.

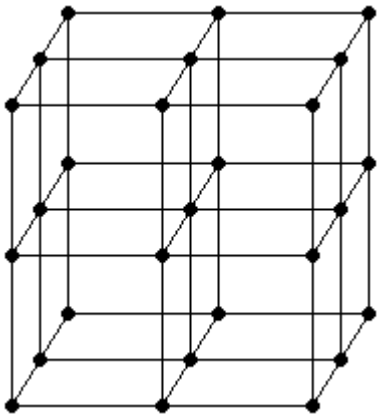

Figure 70 A simple cubic lattice.

Exercise 12 We know from Table 5 that mercury at 5 K crystallizes in a trigonal structure. Draw the hexagonal prism composed of three triple hexagonal *R* unit cells for the Hg crystal structure. Find first the parameters a and c for the hexagonal *R* cell using the data from Table 5 and then find the c/a ratio to draw the hexagonal prism of the Hg crystal structure in real proportions.
***Hint*:** See Exercise 7.

Exercise 13 Starting from Fig. 49 draw the hexagonal prism composed of the three triple hexagonal *R* unit cells for the *fcc* lattice. The resulting picture will contain the cubic *F*, rhombohedral *P*, and triple hexagonal *R* unit cells for the *fcc* lattice, all of them with a common origin.

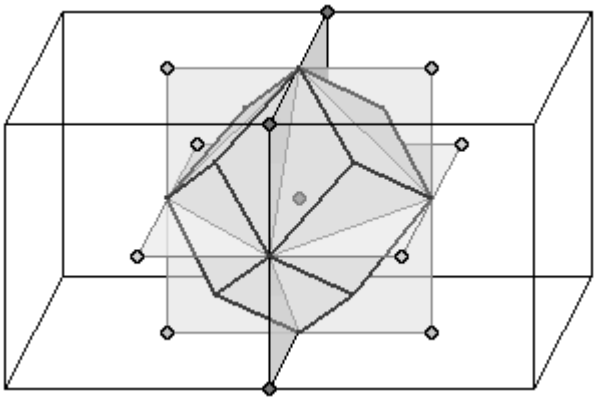

Figure 71 A regular dodecahedron.

Exercise 14

a.) Draw the fourfold axes of the regular dodecahedron shown in Fig. 71 (the Wigner-Seitz cell of the *fcc* lattice). How many such axes does it have?

b.) Draw a threefold axis of the dodecahedron. How many such axes does it have?

III. CRYSTAL STRUCTURES OF ELEMENTS

1. Introduction

In this chapter, we will consider the crystal structure of most metallic elements, nonmetals from column IV of the periodic table, and noble gases. More than 30 elements crystallize in two monoatomic crystal structures, *fcc* and *bcc*, at room temperature and normal pressure. There are also a large number of elements that crystallize in a structure that can be described by a hexagonal Bravais lattice but with two-atom basis. This is the so called hexagonal close-packed (*hcp*) crystal structure. To describe this structure, identical spheres are arranged in a regular array to minimize the interstitial volume. This close-packing of spheres may lead, however, to many different arrangements. One of them turns out to be nothing more than the *fcc* structure. Under normal conditions, more than 40% of the elements crystallize in the *hcp*, *fcc* and other close-packed crystal structures. All of them will be considered in this chapter.

In some sense, the idea of close-packing of spheres, to obtain crystal structures, coincides with the idea to consider atoms (or ions) as impenetrable hard spheres of a certain radius r. This model, even being so simple, is quite useful in the description of crystal structures. For example, it allows for the prediction of interatomic distances of new structures to a first approximation. The atomic radius is deduced from observed atomic separations in a set of crystals. However, the results may vary from set to set since the atomic separation depends on the type of chemical bonding. The principal bonds in crystals are: metallic, ionic, and covalent. The radius of an atom in the crystal of an element is given by half the observed minimal atomic separation.

The atomic radius depends on the kind of bond in the crystal because the nature of bonding is strongly connected to the spatial distribution of electrons. The degree of impenetrability of atoms (or ions) depends on their electronic configuration. The highest impenetrability is achieved in the case of atoms (or ions) with closed electron shells. This is, for example, the case of noble gases, positive ions of alkali metals (Li^+, Na^+, K^+, Rb^+, or Cs^+) or negative ions of the halogens (F^-, Cl^-, Br^-, or I^-). The high degree of impenetrability of such an atom (or ion) is a consequence of the Pauli

exclusion principle and a large energy gap existing between the lowest unoccupied atomic orbital and the highest occupied one.

The idea to consider an atom (or ion) as a hard sphere will be used frequently in this chapter.

2. Pearson Notation and Prototype Structure

The Pearson notation, together with the prototype structure, allows shorthand characterization of crystal structures. It consists of the symbol of the Bravais lattice corresponding to the structure in consideration followed by the number of atoms per conventional unit cell. Table 8 lists Pearson symbols for the 14 Bravais lattices. The assignation of the Pearson symbol to a crystal structure is not unique, it means, in general one Pearson symbol corresponds to more than one crystal structure. To achieve a unique identification of a crystal structure, to each structure type is assigned a representative (prototype) element or compound, in a proper phase, having that structure. The Pearson symbol together with the prototype structure identifies the crystal structure of a given element or compound. The

Table 8 Pearson symbols corresponding to 14 Bravais lattices. In these symbols *n* expresses the number of atoms per conventional unit cell. The last column gives examples of Pearson symbols which together with the prototype structures correspond to crystal structures of elements.

Crystal system	Bravais lattice symbol	Pearson symbol	Example of crystal structure
Triclinic (anorthic)	*aP*	*aPn*	
Monoclinic	*mP* *mS* (*mA*, *mB*, *mC*)	*mPn* *mSn*	*mP*4-γBi *mS*4-βBi
Orthorombic	*oP* *oS* (*oA*, *oB*, *oC*) *oI* *oF*	*oPn* *oSn* *oIn* *oFn*	*oP*8-αNp *oS*4-αU *oF*8-γPu
Tetragonal	*tP* *tI*	*tPn* *tIn*	*tP*4-βNp *tI*2-In
Trigonal (rhombohedral)	*hR*	*hRn**	*hR*1-αHg
Hexagonal	*hP*	*hPn*	*hP*2-Mg
Cubic	*cP* *cI* *cF*	*cPn* *cIn* *cFn*	*cP*1-αPo *cI*2-W *cF*4-Cu

*In the Pearson symbol *hRn*, the number of atoms, *n*, refers to the primitive rhombohedral unit cell.

examples listed in the last column of Table 8 correspond to crystal structures of elements.

3. The Filling Factor

The *filling factor* of a crystal structure is defined as the fraction of the total crystal volume filled with atoms considered hard spheres. Sometimes instead of filling factor the expressions "*atomic packing factor*" or "*packing fraction*" are used.

The filling factor gives us an idea how close "the atoms are packed" in the crystal structure. The closest packing of atoms is achieved when the number of NNs is the highest possible. In conclusion, the filling factor together with the coordination number give us an idea about the degree of filling the crystal volume with atoms, and, at the same time, tells us how close the atoms in a crystal are packed.

In order to calculate the filling factor, we have to know first the radii for atoms considered hard spheres. In the case of elements the radius is half the distance between NNs. To do the calculations, we can limit ourselves to the conventional unit cell of the crystal structure. The filling factor is defined as

$$filling\ factor = \frac{\begin{array}{c} volume\ occupied\ by\ atoms \\ (hard\ spheres)\ within\ the\ unit\ cell \end{array}}{cell\ volume}.$$

Below we will consider different crystal structures in which crystallize the elements. We will begin with the simple cubic structure.

4. Simple Cubic Structure

Pearson symbol: *cP*1, prototype: *α*-Po. Let us assume that the vertices of the cubic unit cell of the *sc* structure coincide with the centers of atoms. Figure 72 shows the plane of one of the faces of the cube with the cross sections of the atoms that, being considered hard spheres, are represented by circles on this plane. Each atom from a cube face has two of its NNs on this face. The NNs are at a distance equal to the lattice constant *a*. The atomic

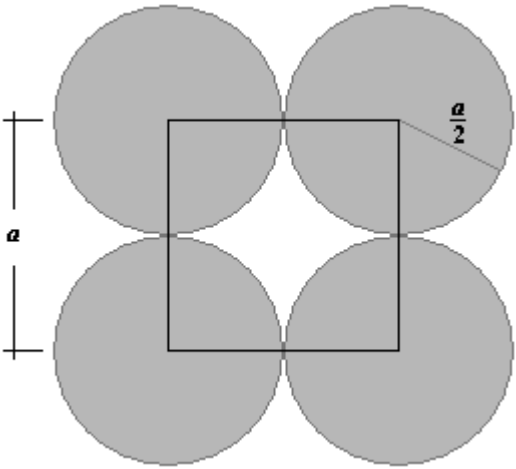

Figure 72 The plane that contains a face of a cubic unit cell of the *sc* structure with the cross sections of atoms considered hard spheres.

radius is equal to half of *a,* so the volume of the only one atom belonging to the cube is given by

$$V_{atom} = \frac{4}{3}\pi\left(\frac{a}{2}\right)^3 = \frac{\pi}{6}a^3 \qquad \text{(III.1)}$$

and the filling factor for the *sc* structure is the following:

$$\left(filling\ factor\right)_{sc} = \frac{\frac{\pi}{6}a^3}{a^3} = \frac{\pi}{6} \cong 0.52\,. \qquad \text{(III.2)}$$

The result for the filling factor shows that in the case of the *sc* structure about half of the crystal volume is filled with atoms and the other half corresponds to the interstices. Of course this is reflected also by the coordination number; the number of the NNs of an atom in the case of the *sc* structure is only 6. The next nearest neighbors (NNN) are already 12, but at the distance about 40% higher than the NNs. In conclusion, the interstitial volume in the *sc* crystal structure is quite large.

Under normal conditions, only one element, polonium in the α-phase, crystallizes in the *sc* structure. However, there are three elements, As, Sb,

and Bi (discussed already in the previous chapter) that crystallize in the trigonal structure, which is a slightly distorted *sc* structure.

5. Body Centered Cubic Structure

Pearson symbol: *cI*2, prototype: W. Now, we will see the case of the *bcc* structure. In this case, the atoms of the vertices of the cube are NNs of the atom that is in the center of the cube (see Fig. 73a), and those atoms are in contact with it. The point of contact between two atoms is found in a plane defined by two body diagonals of the cube, as it is shown in Fig. 73.

We can see in Fig. 73b that the atoms are in contact with each other only along the body diagonals of the cube, while, the atoms that are at the

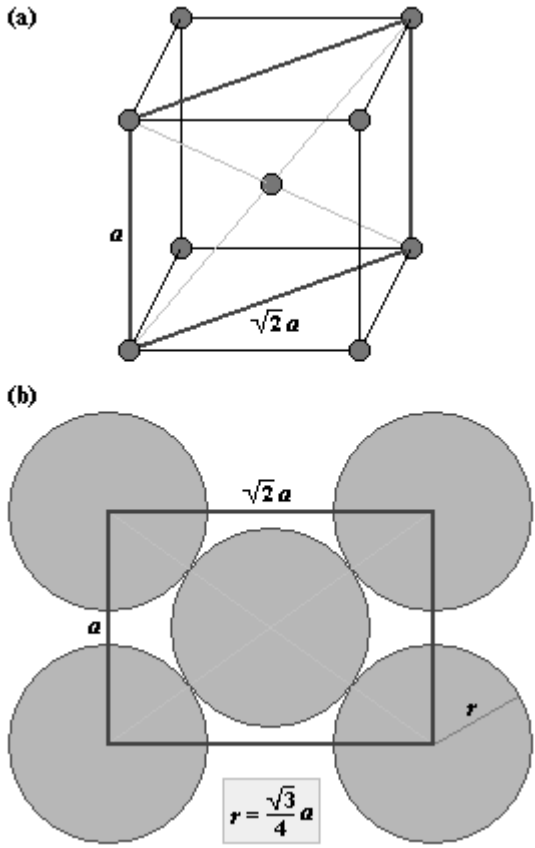

Figure 73 (a) Unit cell of the *bcc* structure. **(b)** A plane defined by two body diagonals of the cube shown in (a). In this plane, there are the points of contact between the central atom and its NNs.

vertices are at a distance greater than $2r$ (r – radius of the atom). There are two atoms in the cubic cell of the *bcc* structure, so the filling factor is

$$\left(filling\ factor\right)_{bcc} = \frac{2\frac{4}{3}\pi\left(\frac{\sqrt{3}}{4}a\right)^3}{a^3} = \frac{\sqrt{3}}{8}\pi \cong 0.68\,. \qquad \text{(III.3)}$$

Please note that the filling factor for the *bcc* structure is higher than that one for the *sc* structure. This is consistent with the fact that the number of NNs in *bcc* is also higher than in *sc* (8 and 6, respectively). Moreover, the distance of the 6 NNNs of an atom in the *bcc* structure differs from the distance of its NNs by less than 15%. Therefore, an atom in this structure has effectively 14 atoms close to it.

Table 9 reports lattice constants a for all elements that crystallize in the *bcc* structure at room temperature and normal pressure. All of them are metals. In this table, we can also find lattice constants for a number of metals that crystallize in the *bcc* structure at high temperatures and normal

Table 9 Lattice constants of elements that crystallize in the *bcc* structure at normal pressure. The data is provided at room temperature, unless otherwise specified.

Metal	*a* (Å)	Metal	*a* (Å)
α-Ba	5.023	**β-Pm**	4.100 (1163 K)
β-Ca	4.380 (773 K)	**β-Pr**	4.130 (1094 K)
δ-Ce	4.120 (1030 K)	**ε-Pu**	3.638 (773 K)
α-Cr	2.8847	**Ra**	5.148
α-Cs	6.141	**α-Rb**	5.705
β-Dy	4.030 (1654 K)	**β-Sc**	3.752 (1623 K)
α-Eu	4.5827	**β-Sr**	4.850 (887 K)
α-Fe	2.8665	**Ta**	3.3031
δ-Fe	2.9346 (1712 K)	**β-Tb**	4.070 (1562 K)
β-Gd	4.060 (1538 K)	**β-Th**	4.110 (1723 K)
K	5.321	**β-Ti**	3.3065 (1173 K)
γ-La	4.260 (1160 K)	**β-Tl**	3.882 (506 K)
β-Li	3.5093	**γ-U**	3.524 (1078 K)
δ-Mn	3.081 (1413 K)	**V**	3.024
Mo	3.147	**W**	3.1651
β-Na	4.291	**β-Y**	4.100 (1751 K)
Nb	3.3007	**γ-Yb**	4.440 (1036 K)
β-Nd	4.130 (1156 K)	**β-Zr**	3.609 (1135 K)
γ-Np	3.520 (873 K)		

pressure. Under normal conditions, these metals (with exception of Fe) crystallize in structures different from *bcc* and they will be considered later. One of them, manganese (α-Mn), crystallizes in a very complex structure due to its magnetic (antiferromagnetic) properties. This structure may be considered as *bcc* with 56 additional atoms, it means, in total 58 atoms per unit cell (Pearson symbol *cI58*). On the other hand, this supercell may be viewed as build of $3\times3\times3=27$ cubic *bcc* unit cells containing $2\times3\times3\times3=54$ atoms with still 4 additional atoms added. A number of these atoms are slightly shifted from the ideal positions in the small *bcc* unit cells. The NN interatomic distances in α-Mn, with lattice constant $a=8.9125$ Å (at 298 K), are in the range of 2.244-2.911 Å.

6. Face Centered Cubic Structure

Pearson symbol: *cF*4, prototype: Cu. We will now turn to the case of the *fcc* structure. The cubic unit cell of this structure is shown in Fig. 74a. The atom placed in the center of a face of the cube has 4 of its NNs at the vertices of this face. Figure 74b shows the plane of the front face of the cube with the cross sections of 5 atoms considered hard spheres. The points of contact between the atoms are found on the face diagonals.

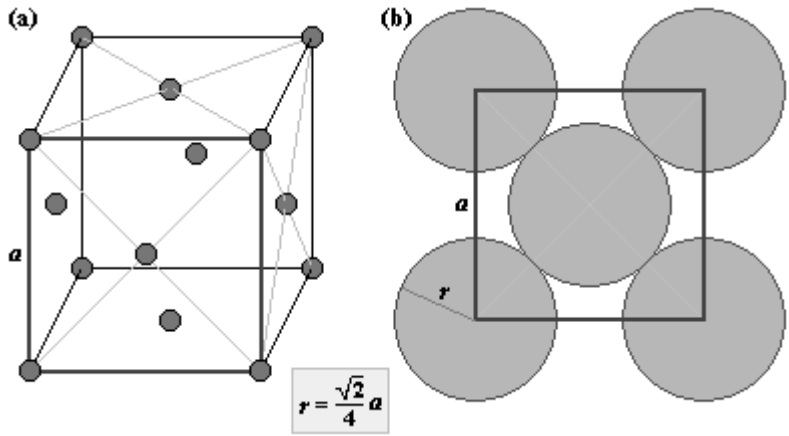

Figure 74 (a) Unit cell of the *fcc* structure. **(b)** Plane of the front face of the cube from (a) with the cross sections of 5 atoms considered hard spheres. The points of contact between the NNs are found in this plane.

In the case of the *fcc* structure, there are four atoms in the cubic cell, therefore the filling factor is

$$\left(\textit{filling factor}\right)_{fcc} = \frac{4\frac{4}{3}\pi\left(\frac{\sqrt{2}}{4}a\right)^3}{a^3} = \frac{\sqrt{2}}{6}\pi \cong 0.74\,. \qquad \text{(III.4)}$$

This filling factor is the largest one among the filling factors for the cubic structures and at the same time the larges one among the filling factors for all structures for the elements. In this case $3/4$ of the crystal volume is filled with atoms considered hard spheres and only $1/4$ is empty. The number of the NNs, equal to 12, is also the largest possible.

Table 10 Lattice constants of elements that crystallize in the *fcc* structure at normal pressure. The data is given at room temperature, unless otherwise specified.

Element	***a* (Å)**	**Element**	***a* (Å)**
Ac	5.311	***β*-La**	5.303 (598 K)
Ag	4.0861	***γ*-Mn**	3.863 (1373 K)
***α*-Al**	4.0496	**Ne**	4.462 (4.2 K)
Ar	5.311 (4.2 K)	**Ni**	3.5241
Au	4.0784	***α*-Pb**	4.9502
***α*-Ca**	5.5884	**Pd**	3.8901
***α*-Ce**	4.850 (77 K)	**Pt**	3.924
***γ*-Ce**	5.1610	***δ*-Pu**	4.637 (592 K)
***α*-Co**	3.569 (793 K)	**Rh**	3.803
Cu	3.6149	***α*-Sr**	6.084
Es	5.750	***α*-Th**	5.084
***γ*-Fe**	3.630 (1373 K)	**Xe**	6.309 (145 K)
Ir	3.8391	***β*-Yb**	5.4848
Kr	5.796 (96 K)		

Table 10 lists lattice constants *a* of all metals that crystallize at room temperature and normal pressure in the *fcc* structure. Besides that, in this table are also given the lattice constants of four noble gases (argon, krypton, neon, and xenon) and a number of metals that crystallize in the *fcc* structure at temperatures different from room temperature. A similar number of metallic elements crystallize in the *fcc* and *bcc* structures under normal conditions, what can be seen comparing Tables 9 and 10.

The *fcc* structure represents one of the close-packed structures. We will discuss them below.

7. Close-Packed Structures

The name "close-packed" refers to the way of packing the atoms in order to obtain the highest possible filling factor. To consider close-packed structures it is worthwhile to analyze first the manner of placing spheres of the same radius, in order for the interstitial volume to be as small as possible. For this purpose, the spheres are arranged in layers that are placed one on the top of the other in the way we will explain below. Each sphere within a layer is in contact with six others and a layer represents a two-dimensional close-packed hexagonal structure. The cross section of a layer is shown in Fig. 75. We will differentiate the holes existing between spheres of a layer as of type (a) or type (b) (see Fig. 75).

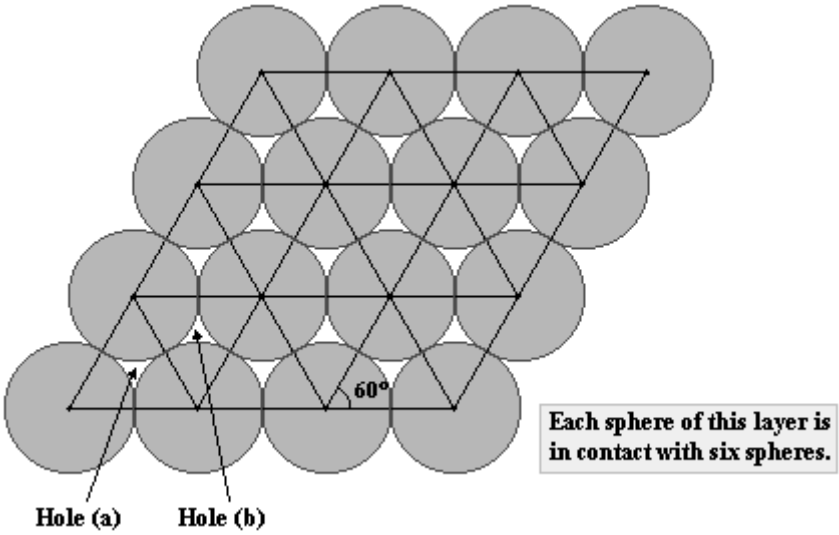

Figure 75 A close-packed layer of spheres that is a two-dimensional close-packed hexagonal structure.

Figure 76 shows the plane defined by centers of spheres of the first layer and the projection of centers of spheres of the second layer. The centers of the second layer spheres are above the centers of the holes of type (a) specified in Fig. 75. The spheres of the second layer just rest in the holes of type (a).

The centers of the holes of type (a) coincide with the geometric centers of the equilateral triangles shown in Fig. 76 (of course the same occurs in

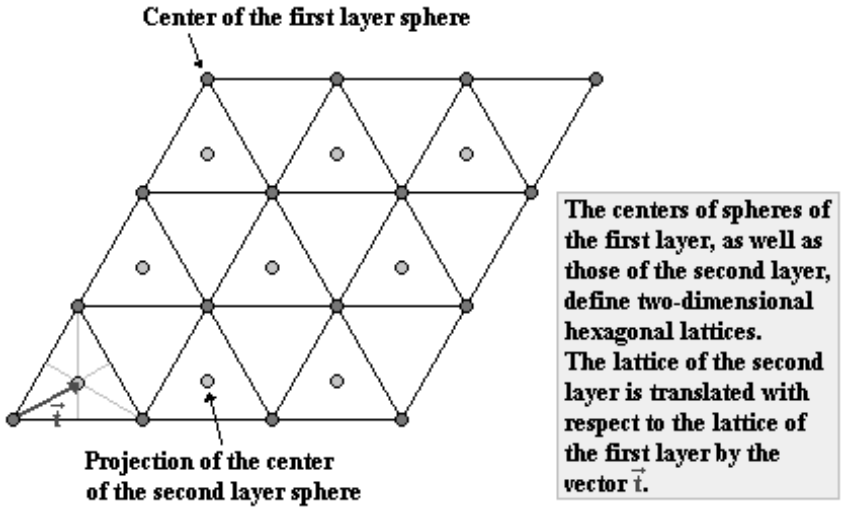

Figure 76 The centers of spheres of the first layer and the projection of the centers of spheres of the second layer in a close-packed arrangement of equal spheres.

the case of holes of type (b), see Fig. 77a). Therefore, each sphere of the second layer is in contact with three spheres of the layer below it.

The third layer can be placed in two ways as depicted in Fig. 77. In the case shown in Fig. 77a the centers of spheres of the third layer are above the centers of the holes of type (b) of the first layer, specified in Fig. 75, whereas in the case shown in Fig. 77b the spheres of the third layer lie directly above the spheres of the first layer.

We will show now that the close-packed arrangement displayed in Fig. 77a corresponds to the *fcc* structure. A part of Fig. 77a, with the cubic cell of the *fcc* structure, is drawn in Fig. 78. We can see in this figure that the *fcc* structure is of type **ABCABC…**, where **A**, **B**, and **C** denote three two-dimensional close-packed layers shifted horizontally one with respect to the other. The layer planes are orthogonal to a body diagonal of the cubic unit cell of this structure. The second layer, **B**, is shifted with respect to the first one, **A**, by vector $\vec{t}$, defined in Fig. 76. In this way, the spheres of the **B** layer are placed in holes of type (a), shown in Fig. 75, of layer **A**. The spheres of **C** layer are placed over the holes in the **A** layer not occupied by the spheres from **B** layer, it means, of type (b) in Fig. 75. The **C** layer is shifted with respect to the **A** layer by vector $2\vec{t}$, and with respect to the **B** layer by vector $\vec{t}$, so each sphere of the **C** layer is in contact with 3 spheres

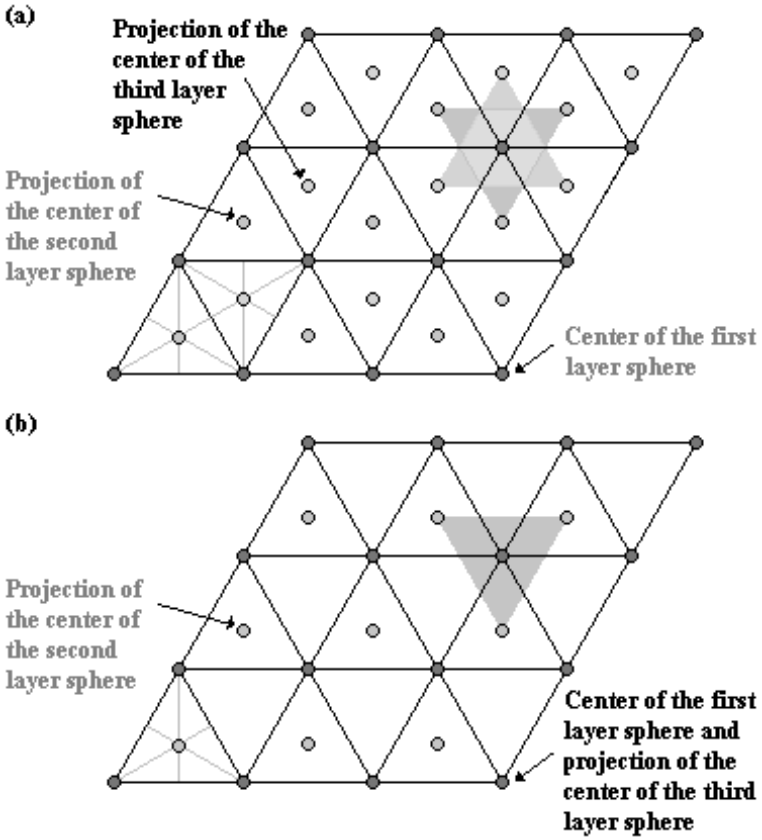

Figure 77 (a) and **(b)** show two close-packed arrangements of equal spheres. The case described in (a) differs from that one in (b) in the positions of spheres of the third layer with respect to the spheres of the first and second layers.

of the **B** layer. The spheres of the fourth layer lie directly above the spheres of the first one.

To conclude, we can say that in the case shown in Fig. 77a we have a *cubic close-packed* (*ccp*) structure that was already introduced as the *fcc* one. This is an **ABCABC…** type structure. Now it is easy to visualize the 12 NNs of an atom in the *fcc* structure; 6 of them belong to the layer in which is placed the atom in consideration, while half of the other 6 belong to the layer below and the other half to the layer above.

In the case shown in Fig. 77b we have a *hexagonal close-packed* (*hcp*) structure of an **ABAB…** type. Figure 79 shows a part of Fig. 77b together with the hexagonal prism. We can see in Fig. 79 that the *hcp* structure represents a hexagonal Bravais lattice with two-atom basis. Each atom in

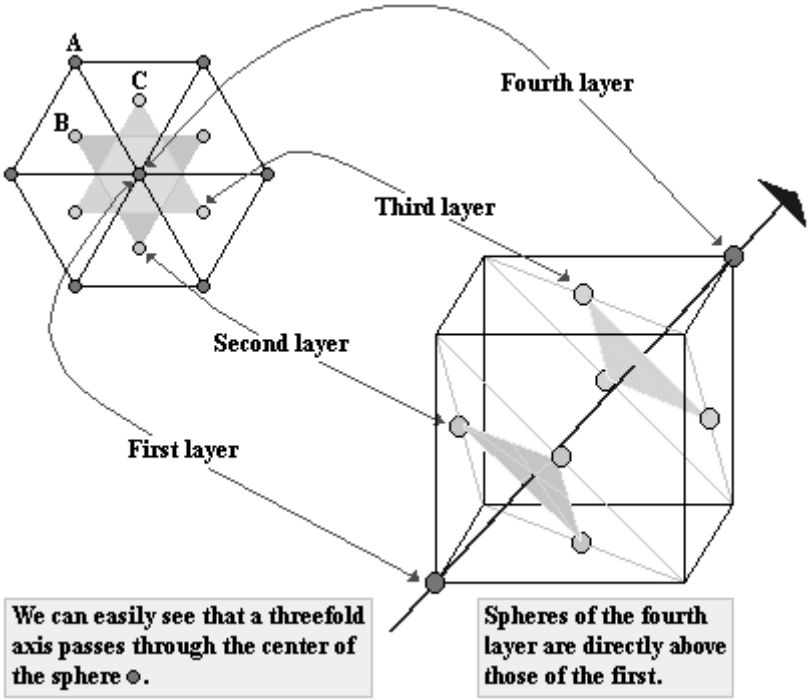

Figure 78 The *fcc* structure viewed as a close-packed structure (cubic close-packed). Three consecutive layers of this structure are marked as **A**, **B**, and **C**.

this structure has 12 NNs (as it is also the case for the *fcc* structure); 6 of them belong to the layer in which is placed the atom in consideration and the other 6 belong to the adjacent layers. The difference between *ccp* and *hcp* structures consists in the location of the NN atoms that belong to the adjacent layers. In the case of the *ccp* structure three of them occupy (a) holes and the other three (b) holes (specified in Fig. 75), present in the layer to which belongs the atom in consideration. In the case of the *hcp* structure these 6 NNs occupy holes of type (a): 3 from the top and 3 from the bottom side of the layer. Twelve is the maximum number of spheres that can be arranged to touch a given sphere. The *hcp* structure will be discussed in details later.

There is an infinite number of possible ways of close-packing equal spheres, since any sequence of **A**, **B**, **C** layers, with no two successive layers alike, represents a possible close-packing arrangement of equal spheres. Therefore, a close-packed structure can be obtained only if two consecutive layers are of a different type. In this case, each sphere touches 12 other spheres and this characteristic of all close-packed structures could be seen

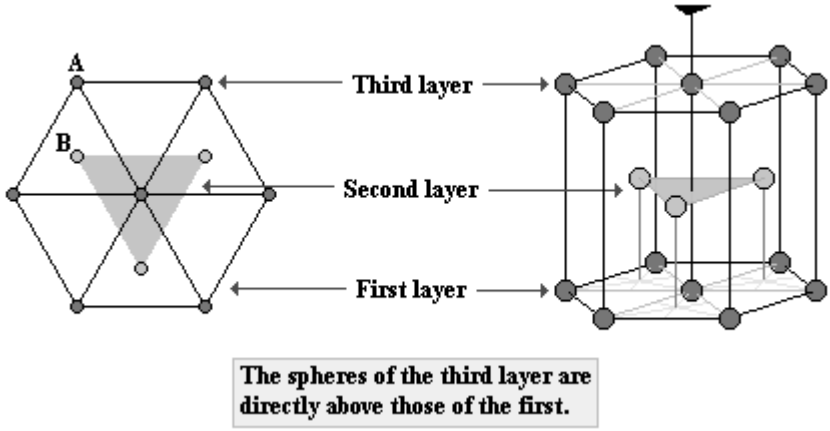

Figure 79 The **ABAB…** stacking of atomic layers in the *hcp* structure.

already in the case of *fcc* and *hcp* structures. Please note, that the only close-packed structure that represents a Bravais lattice with one-atom basis is the *fcc* structure.

Below we will give an example of a close-packed structure, different from the *fcc* and *hcp* structures, which has a layer sequence **ABACABAC…**. This structure is called a *double hexagonal close-packed* (*dhcp*) structure.

8. Double Hexagonal Close-Packed Structure

Pearson symbol: *hP*4; prototype: *α*-La. Two consecutive layers in the *dhcp* structure are of a different type, so it represents indeed one of the close-packed structures with the coordination number 12. Under normal conditions, in the *dhcp* structure crystallize 5 rare earth (RE) metals: lanthanum (α-La), cerium (β-Ce), praseodymium (α-Pr), neodymium (α-Nd),

Table 11 Lattice constants of lanthanides that crystallize in the *dhcp* structure under normal conditions. The data for δ-Sm correspond to room temperature and 4.0 GPa.

Element	*a* (Å)	*c* (Å)	*c*/*a*
***α*-La**	3.7740	12.171	2×1.61
***β*-Ce**	3.681	11.857	2×1.61
***α*-Pr**	3.6721	11.8326	2×1.61
***α*-Nd**	3.6582	11.7966	2×1.61
***α*-Pm**	3.65	11.65	2×1.60
***δ*-Sm (4.0 GPa)**	3.618	11.66	2×1.61

Table 12 Lattice constants of actinides that crystallize in the *dhcp* structure under normal conditions.

Element	a (Å)	c (Å)	c/a
α-Am	3.468	11.241	2×1.62
α-Cm	3.496	11.331	2×1.62
α-Bk	3.416	11.069	2×1.62
α-Cf	3.390	11.015	2×1.63

promethium (α-Pm), all of them lanthanides, and the following actinides: americium (α-Am), curium (α-Cm), berkelium (α-Bk), and californium (α-Cf). Cerium exhibits at room temperature and normal pressure two phases: beta and gamma (γ-Ce has the *fcc* structure, see Table 10). The phase transition from β-Ce to γ-Ce occurs close to the room temperature and β-Ce exists below this temperature. In Table 11 we have listed the experimental lattice parameters a and c for La, Ce, Pr, Nd, and Pm, obtained under normal conditions, and for δ-Sm obtained at room temperature and pressure 4.0 GPa, while Table 12 gives the experimental lattice parameters a and c for actinides obtained under normal conditions. The parameters a and c are defined in Fig. 80.

The hexagonal prism that represents a conventional unit cell of the *dhcp* structure, which has the same point symmetry as an infinite structure,

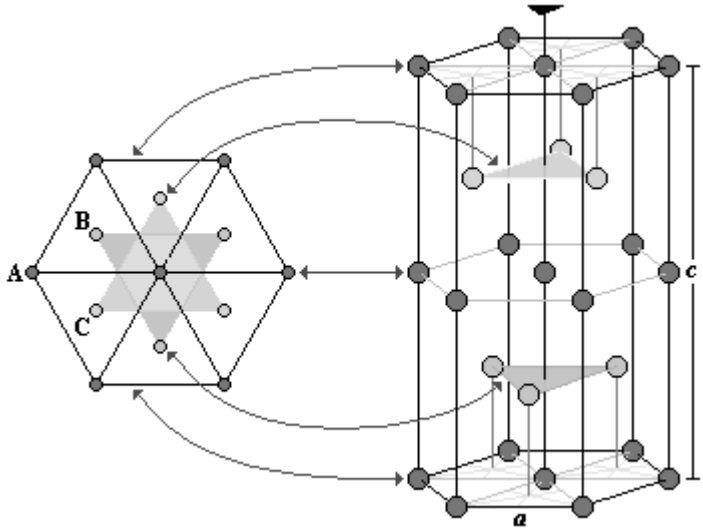

Figure 80 Double hexagonal close-packed structure. The **ABACABAC…** sequence of layers is shown.

is shown in Fig. 80. In this figure, we also show the sequence, **ABACABAC…**, of the two-dimensional *hcp* layers.

In the next section, we will consider the structure of samarium at room temperature and pressure (α-Sm).

9. Samarium Type Close-Packed Structure

Pearson symbol: *hR*3, prototype: *α*-Sm. Samarium in the alpha phase crystallizes in a complex close-packed structure with a layer sequence **ABABCBCACA…**. It means, represents the repetition of a unit consisting of 9 two-dimensional *hcp* layers, as can be seen in Fig. 81c. The smallest unit cell of this structure is rhombohedral (inscribed in the hexagonal prism from Fig. 81c), so the α-Sm structure is trigonal. Its rhombohedral unit cell contains 3 atoms, while the triple hexagonal cell contains 9 atoms. The cell parameters of the two unit cells, triple hexagonal and rhombohedral, are $a_h = 3.629\,\text{Å}$, $c_h = 26.207\,\text{Å}$ and $a_r = 8.996\,\text{Å}$, $\alpha_r = 23.22°$, respectively (at room temperature and normal pressure). About half of the RE metals crystallize at high pressure in the Sm-type structure. They are: yttrium (Y), gadolinium (Gd), terbium (Tb), dysprosium (Dy), holmium (Ho), erbium (Er), thulium (Tm), ytterbium (Yb), and lutetium (Lu). In the case of three of them (Y, Tb, and Dy) the following pressure-induced sequence of phase transitions is observed at room temperature:

$$hcp \rightarrow \text{Sm-type} \rightarrow dhcp \rightarrow fcc\,.$$

For yttrium, e.g., the experimentally determined transformations are: from *hcp* to Sm-type at 10-15 GPa, from Sm-type to *dhcp* at 25-28 GPa, and from *dhcp* to *fcc* at 46 GPa. A similar sequence, of pressure-induced phase transitions (at room temperature), is observed for Ho, Er, and Tm:

$$hcp \rightarrow \text{Sm-type} \rightarrow dhcp.$$

It is interesting to mention that the two sequences involve close-packed structures that are, to some degree, mutually related. The *dhcp* and Sm-type structures can be viewed as a certain mixture of the *hcp* and *ccp* (*fcc*) structures.

Figures 81 and 82 show hexagonal prisms for the four close-packed structures considered by us. The hexagonal prisms for the *hcp*, *dhcp*, and

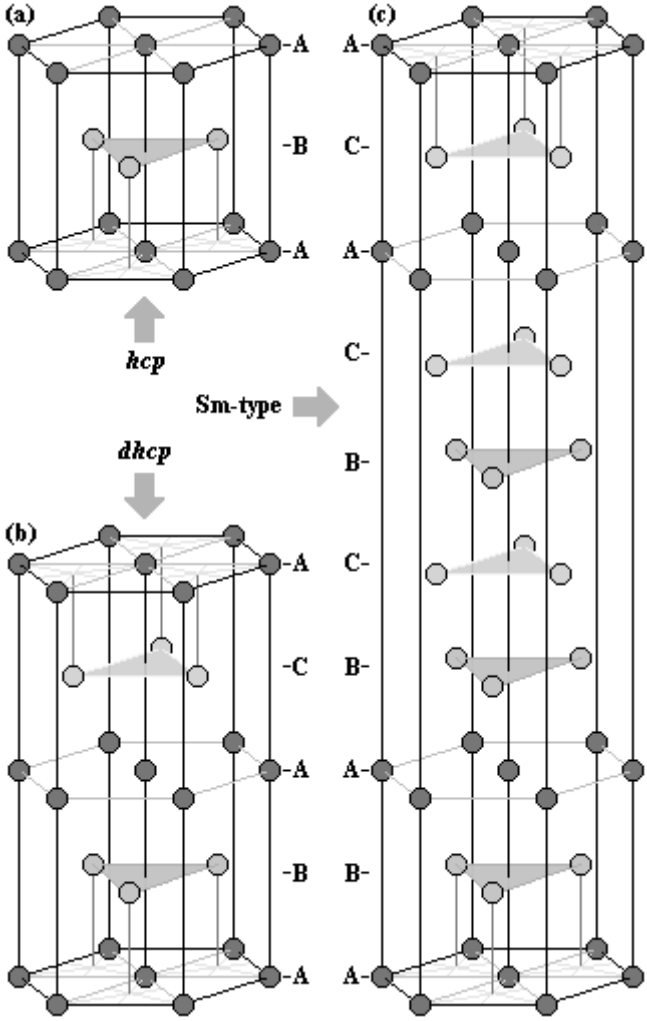

Figure 81 Hexagonal prisms for three of the four close-packed structures considered by us: *hcp*, *dhcp*, and Sm-type. In each case, the sequence of the two-dimensional *hcp* layers is shown. The hexagonal prism for the fourth close-packed structure (*ccp*) is displayed in Fig. 82.

Sm-type structures are drawn in Figs. 81a-81c, respectively, while in Fig. 82 is shown the hexagonal prism for the *fcc* structure. In each case, the sequence of the two-dimensional *hcp* layers is shown. The hexagonal prism displayed in Fig. 82 can reproduce the *fcc* structure, but has less symmetry (point symmetry) than an infinite *fcc* structure.

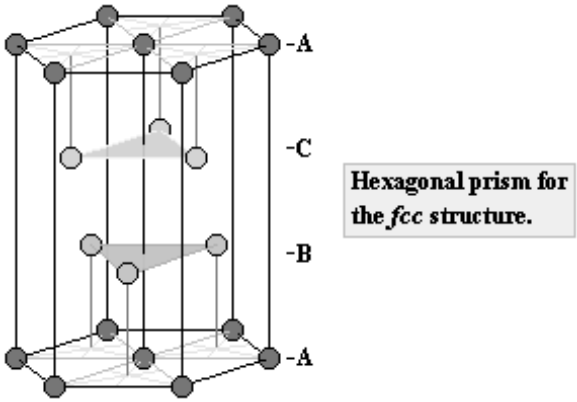

Figure 82 Hexagonal prism for the *ccp* (*fcc*) structure (the cell parameters ratio is $c / a = \sqrt{6}$, see Fig. 78). The sequence of layers **A**, **B**, and **C** is shown.

10. Hexagonal Close-Packed Structure

Pearson symbol: *hP*2, prototype: Mg. Now, we will analyze the hexagonal close-packed structure in more details. The hexagonal prism represents a conventional unit cell that has the same point symmetry as an infinite *hcp* structure. In this case, the highest order rotation axis is threefold. The hexagonal unit cell defined by vectors $\vec{a}$, $\vec{b}$, $\vec{c}$ in Fig. 83 can reproduce the whole *hcp* structure, as in the case of the simple hexagonal structure, but here it contains two atoms. The positions of the two atoms within the hexagonal unit cell are given in Fig. 84.

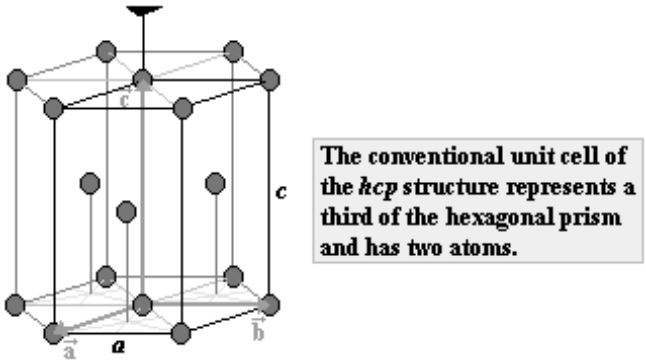

Figure 83 The conventional unit cell of the *hcp* structure defined by the basis vectors $\vec{a}$, $\vec{b}$, $\vec{c}$.

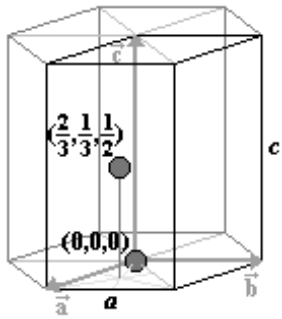

Figure 84 Positions of the two atoms within the hexagonal unit cell of the *hcp* structure. The coordinates are expressed in units of *a* and *c*.

We will now calculate the c/a ratio in an ideal case when the atoms considered hard spheres touch their NNs. Figure 85 shows the unit cell for this case. The three atoms marked as 1, 2, 3 (from the bottom base) and the three marked as 5, 6, 7 (from the top base) are the NNs of the atom marked as 4, and they are in contact with it. Likewise, atoms marked as 1, 2, 3 are in contact among themselves. As the distance between the centers of spheres 1 and 2 is *a*, so is the distance between the centers of spheres 1, 2, or 3 and the center of sphere 4.

To obtain the c/a ratio, we first derive the expression for the vectors $\vec{r}_{\parallel}$ and $\vec{r}_{\perp}$ that are the components of the position vector $\vec{r}$ of the center of the atom marked as 4 in Fig. 85. In Fig. 86 we show the plane of the rhombic

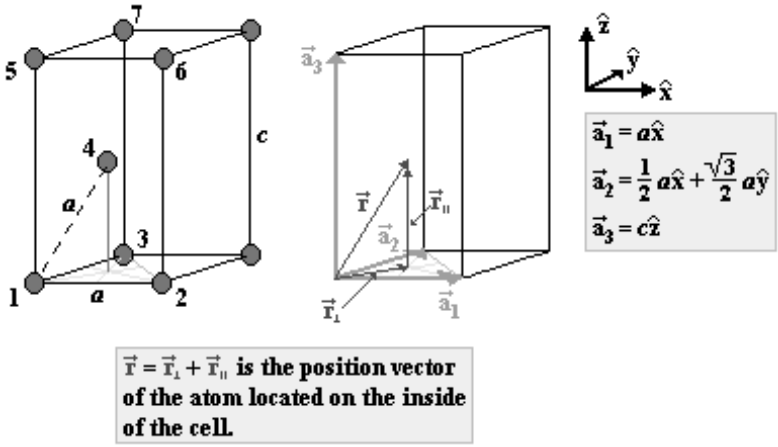

Figure 85 The 6 of 12 NNs of the atom marked 4 (the ones marked 1-3, and 5-7) located at the vertices of the hexagonal unit cell. The vector $\vec{r}$ gives the position of the atom marked as 4.

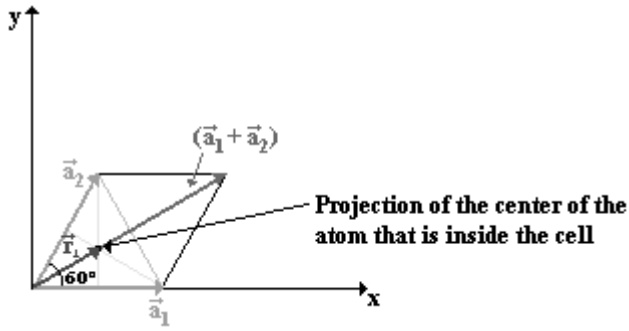

Figure 86 The base of the hexagonal unit cell shown in Fig. 85.

base of the hexagonal unit cell which contains $\vec{r}_\perp$. This vector can be expressed as a linear combination of basis vectors $\vec{a}_1$ and $\vec{a}_2$ (see Fig. 86). Vectors $\vec{r}_\parallel$ and $\vec{r}_\perp$ can be then written as

$$\begin{cases} \vec{r}_\parallel = \dfrac{1}{2}\vec{a}_3 \\ \vec{r}_\perp = \dfrac{1}{3}\left(\vec{a}_1 + \vec{a}_2\right) \end{cases}, \text{ where } \begin{cases} \vec{a}_1 = a\hat{x} \\ \vec{a}_2 = \dfrac{1}{2}a\hat{x} + \dfrac{\sqrt{3}}{2}a\hat{y} \\ \vec{a}_3 = c\hat{z} \end{cases}, \tag{III.5}$$

and can be expressed in terms of orthogonal versors as

$$\begin{cases} \vec{r}_\parallel = \dfrac{1}{2}c\hat{z} \\ \vec{r}_\perp = \dfrac{1}{2}a\hat{x} + \dfrac{\sqrt{3}}{6}a\hat{y} \end{cases}. \tag{III.6}$$

Finally, from (III.6) we obtain that vector $\vec{r}$ is

$$\vec{r} = \vec{r}_\perp + \vec{r}_\parallel = \frac{1}{2}a\hat{x} + \frac{\sqrt{3}}{6}a\hat{y} + \frac{1}{2}c\hat{z}\,. \tag{III.7}$$

Since the module of vector $\vec{r}$ is a (the distance between the centers of atoms 1 and 4), then

$$\left|\vec{r}\right| = \sqrt{\frac{a^2}{4} + \frac{3}{36}a^2 + \frac{c^2}{4}} = a\,, \tag{III.8}$$

and the c/a ratio is

$$\frac{c}{a} = \sqrt{\frac{8}{3}} \cong 1.633 \,. \qquad \text{(III.9)}$$

Therefore, in the ideal *hcp* structure the c/a ratio is about 1.63.

Table 13 lists lattice parameters *a* and *c* for all elements that crystallize in the *hcp* structure at room temperature and normal pressure. As in the case of *bcc* and *fcc* structures all of them are metals. The table reports also lattice parameters of other metals and also helium, obtained at conditions different from normal conditions. We can observe in the table that with exception of two metals, cadmium and zinc, for the rest of them the ratio c/a is quite close to the ideal value 1.63. The structures of cadmium and zinc are somewhat distorted from the ideal *hcp* structure. The NNs of an atom are not 12 but 6 (the ones from the same layer), while the other 6 atoms, which are placed in adjacent layers, are 10% farther away. However, the point symmetry of the *hcp* structure does not depend on the c/a ratio.

It is interesting to note that under normal conditions more than 25% of the elements crystallize in the *hcp* and *dhcp* structures. This information is given in Table 14.

Table 13 Lattice parameters of metals that crystallize in the *hcp* structure. The data is given at room temperature and normal pressure, unless otherwise specified. Values for helium (^{3}He and ^{4}He) are also included.

Element	*a* (Å)	*c* (Å)	*c*/*a*	Element	*a* (Å)	*c* (Å)	*c*/*a*
α-Be	2.286	3.585	1.57	**Os**	2.734	4.320	1.58
Cd	2.979	5.620	1.89	**Re**	2.761	4.458	1.62
ε-Co	2.507	4.069	1.62	**Ru**	2.706	4.282	1.58
α-Dy	3.5915	5.6501	1.57	**α-Sc**	3.3088	5.2680	1.59
α-Er	3.5592	5.5850	1.57	**β-Sm (723 K)**	3.663	5.845	1.60
α-Gd	3.6336	5.7810	1.59	**α´-Tb**	3.6055	5.6966	1.58
^{3}He (3.48 K, 0.163 GPa)	3.501	5.721	1.63	**Tc**	2.738	4.393	1.60
^{4}He (3.95 K, 0.129 GPa)	3.470	5.540	1.60	**α-Ti**	2.9503	4.6836	1.59
α-Hf	3.1946	5.0511	1.58	**α-Tl**	3.457	5.525	1.60
α-Ho	3.5778	5.6178	1.57	**α-Tm**	3.5375	5.5546	1.57
α-Li (78 K)	3.111	5.093	1.64	**α-Y**	3.6482	5.7318	1.57
α-Lu	3.5052	5.5494	1.58	**α-Yb**	3.8799	6.3859	1.65
Mg	3.2093	5.2107	1.62	**Zn**	2.644	4.9494	1.87
α-Na (5 K)	3.767	6.154	1.63	**α-Zr**	3.2317	5.1476	1.59

Let us now proceed to calculate the filling factor for the ideal *hcp* structure. The hexagonal unit cell volume is given by

$$\Omega_0 = \left(\vec{a}_1 \times \vec{a}_2\right)\cdot\vec{a}_3 = \begin{vmatrix} \hat{x} & \hat{y} & \hat{z} \\ a & 0 & 0 \\ \frac{1}{2}a & \frac{\sqrt{3}}{2}a & 0 \end{vmatrix} \cdot \left(c\hat{z}\right)$$

$$= \left(\frac{\sqrt{3}}{2}a^2\hat{z}\right)\cdot\left(c\hat{z}\right) = \frac{\sqrt{3}}{2}a^2 c = \sqrt{2}a^3, \text{ where } c = \sqrt{\frac{8}{3}}a, \quad \text{(III.10)}$$

then

$$\left(\textit{filling factor}\right)_{hcp} = \frac{2\frac{4}{3}\pi\left(\frac{a}{2}\right)^3}{\sqrt{2}a^3} = \frac{\sqrt{2}}{6}\pi \cong 0.74. \quad \text{(III.11)}$$

Note that we obtained the same result as in the case of the *fcc* (*ccp*) structure. This is the value of the filling factor for any close-packed structure. All of them characterize the maximum number, 12, of the NNs of an atom.

Under normal conditions, more than 40% of elements crystallize in three close-packed structures: *fcc*, *hcp*, and *dhcp*, what is shown in the periodic table of elements (see Table 14).

11. Interstices in Close-Packed Structures

We will now examine the *interstices* – empty spaces between atoms (hard spheres) – in close-packed structures. They are of two types: tetrahedral and octahedral. A tetrahedral interstice could be found already in Fig. 85. In this figure, the centers of spheres marked as 1, 2, 3, and 4 represent vertices of a tetrahedron. The edges of this tetrahedron are of the same longitude, $2r$ (where r is the sphere radius), so this is a regular tetrahedron. The empty space between the four spheres defining a tetrahedron is what we call a *tetrahedral interstice*. Spheres marked in Fig. 85 as 4, 5, 6, and 7 define another regular tetrahedron. The two tetrahedrons have different spatial orientation. The top view of the two types

Table 14 Crystal structures of all metals that crystallize in dense-packed structures (*fcc*, *hcp*, *dhcp*, Sm-type, and *bcc*) under normal conditions. The structures of noble gases at low temperatures are also included. The most stable forms of polymorphic elements are labeled with small Greek letters.

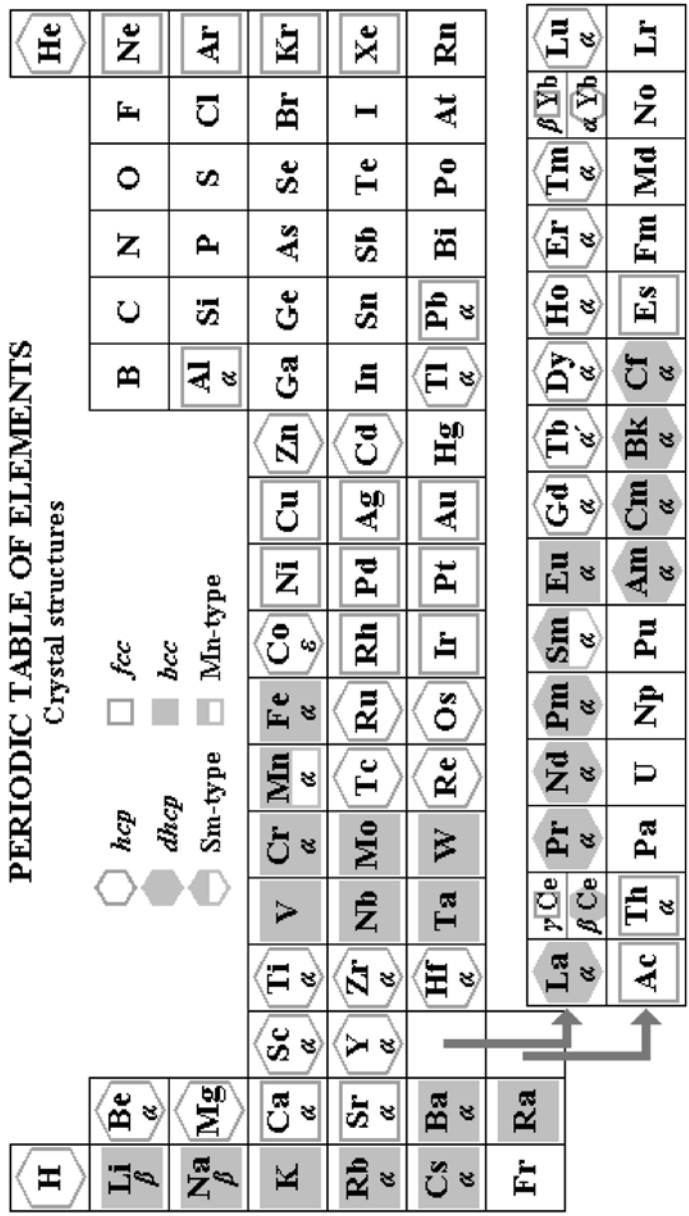

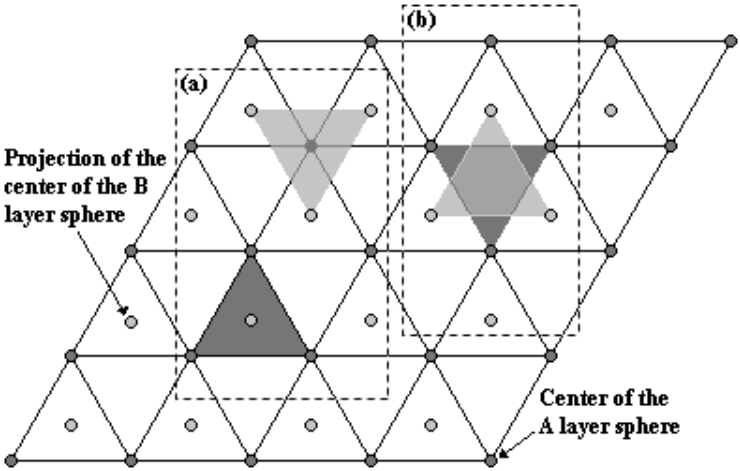

Figure 87 Centers of spheres of the **A** layer and projection of the centers of spheres of the **B** layer. **(a)** Three vertices and one vertex projection for one tetrahedron and one vertex and three vertex projections for the tetrahedron with the second spatial orientation are shown. **(b)** Top view of octahedron bases lying on **A** and **B** layers.

of tetrahedrons is shown in Fig. 87a, in which we have the plane of a hexagonal layer **A** and the projection of the centers of spheres of layer **B** on layer **A**. Three vertices of one of the tetrahedrons shown in this figure are found in layer **A** and the fourth in layer **B**. The opposite occurs for the tetrahedron with a second orientation in which three vertices are in layer **B** and the fourth in layer **A**.

A regular octahedron is visualized in Fig. 87b; three of its six vertices are placed in the **A** layer and the other three in the **B** layer. The empty space between the 6 spheres that define a regular octahedron represents the second type of interstices that are present between two different types of layers in a close-packed structure, the so called *octahedral interstices*. The octahedron edge length is $2r$ like in the case of the tetrahedron edges.

Let us show now interstices that are present in conventional unit cells for the two most common close-packed structures. Figure 88 shows three of the tetrahedral interstices present in a hexagonal prism which is a conventional unit cell of the *hcp* structure. Whereas, in Fig. 89 we show two of the tetrahedral and one octahedral interstices present in a cube that represents a conventional unit cell of *fcc* (*ccp*). There are crystal structures in which such interstices may be occupied by additional atoms. In general

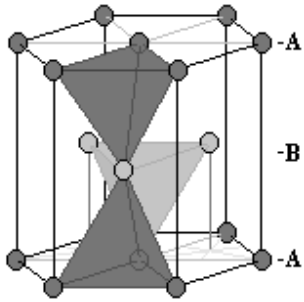

Figure 88 Three tetrahedral interstices inside a hexagonal prism which is a conventional unit cell that has the same point symmetry as the *hcp* structure. The sequence of layers **A** and **B** is shown.

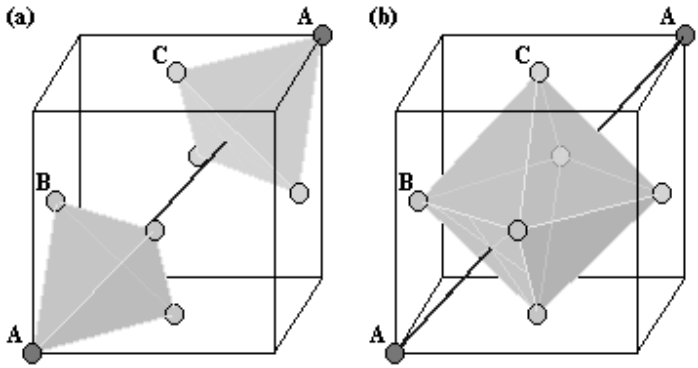

Figure 89 Two tetrahedral **(a)** and one octahedral **(b)** interstices in a cubic unit cell of the *fcc* (*ccp*) structure. The sequence of layers **A**, **B**, and **C**, orthogonal to a body diagonal of the cube, is shown.

these atoms are of another type than the atoms of the close-packed structure. This gives rise to a large number of compounds that can be described in terms of a close-packing of equal spheres. We will discuss this in details for binary compounds.

Summarizing, we have learned the following about close-packed structures:

a.) Three-dimensional close-packed structures are built of two-dimensional *hcp* layers of equal spheres (see Fig. 75). Each sphere of such a layer is in contact with 6 other spheres, which is the maximum possible number of NNs in two dimensions.

b.) The consecutive layers in a three-dimensional close-packed structure are shifted horizontally one with respect to the other, so we distinguish three types of layers: **A**, **B**, and **C**, defined in Fig. 78.

c.) As two consecutive layers are of a different type, the spheres of each layer rest in the holes of the layer below. Therefore, each sphere, apart from the 6 NNs in its own layer, has 3 NNs in each of the adjacent layers.

d.) There are tetrahedral and octahedral interstices between two consecutive layers of a close-packed structure.

We already know that metallic elements have the tendency to crystallize in close-packed structures. Moreover, noble gases also crystallize in those structures. The type of bonding between atoms of these elements gives preference for the coordination number 12, what is indeed achieved in a close-packed structure. Whereas, other types of bond (covalent or ionic) require 4, 6, or 8 NNs of an atom. The presence of tetrahedral and octahedral interstices in close-packed structures offers the possibility to form bonds with 4 or 6 NNs when an atom is placed inside a tetrahedral or octahedral interstice, respectively.

In general the atom (or ion) that is located inside the interstice pushes apart the atoms at the vertices of the tetrahedron or octahedron. As a consequence the *hcp* layers (**A**, **B**, **C**) do not represent any longer close-packed layers but only two-dimensional hexagonal structures. In these layers, the atoms do not touch each other and in addition the atoms from adjacent layers are not in contact with them. We will see this on the example of 4 elements that crystallize in the diamond structure. The atoms in this structure have 4 NNs.

The diamond structure represents a sequence of layers of **AABBCCAABBCC…** type, where each layer is a two-dimensional hexagonal (but not close-packed) structure. This sequence can be seen as a superposition of two equal sequences of **ABCABC…** type. It means that we are in presence of a superposition of two *fcc* structures. One of them is translated with respect to the other in such a way that the atoms of each of them occupy half of the tetrahedral interstices of the other. Thus, each atom has 4 NNs as is required in the case of pure covalent bonding. The diamond structure will be considered below in more details.

The **A**, **B**, **C** layers (two-dimensional hexagonal structures that are in general not close-packed) are present also in the case of various important

binary compounds. This will be shown in the next chapter on examples of compounds that crystallize in the zinc blende, wurtzite, NiAs, or NaCl structures. In general, in a binary compound, the atoms (ions) of a given type form a structure which is at the same time its substructure. Each of these substructures, in the case of structures mention above, represents a sequence of layers of **ABAB…** or **ABCABC…** type (or only of **AA…** type like in the case of cations in NiAs). In general, each layer (**A**, **B**, or **C**) represents a two-dimensional hexagonal structure, which is rarely a true close-packed layer.

When a three-dimensional structure is not really close-packed, it means, when an atom considered hard sphere is not in contact with 12 atoms closest to it, but it is still built of **A, B, C** (or **A** and **B**) layers in the way that two consecutive layers are of a different type, it is also called close-packed.

In zinc blende and wurtzite structures each substructure is of **ABCABC…** and **ABAB…** type, respectively, and the atoms of a given type occupy half of the tetrahedral interstices present in the other substructure. In NiAs the substructure of anions is of **ABAB…** type and the cations occupy its octahedral interstices, whereas NaCl is composed of substructures with a layer stacking **ABCABC…**. The ions from one substructure in NaCl occupy the octahedral interstices present in the other substructure. All these structures will be described in details in the next chapter.

12. Diamond Structure

Pearson symbol: *cF*8, prototype: C. Four elements, from column IV of the periodic table, crystallize in the diamond structure, namely: carbon, silicon, germanium and gray tin (which is one of the two allotropes of tin at normal pressure and temperature). The atoms of each of these elements have four electrons in the outermost shell (the so called valence shell). By completing this shell with four additional electrons those atoms can achieve a state of the highest stability. This stability is reached in the crystal of each of these elements in which an atom is surrounded by four neighboring atoms that in turn form covalent chemical bonds (represented schematically in Fig. 90) with it. In the diamond structure, each atom shares four electrons with its 4 NNs and each of these neighbors shares an electron with the atom under consideration. Therefore, all atoms can complete the 4 electrons that were lacking to achieve the highest stability.

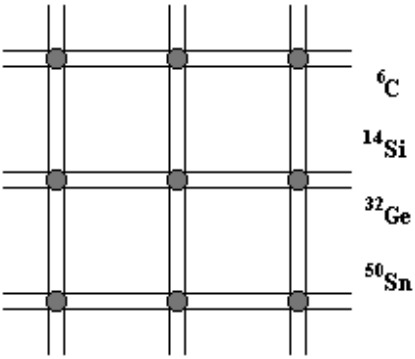

Figure 90 Two-dimensional schematic representation of covalent chemical bonds in the diamond structure.

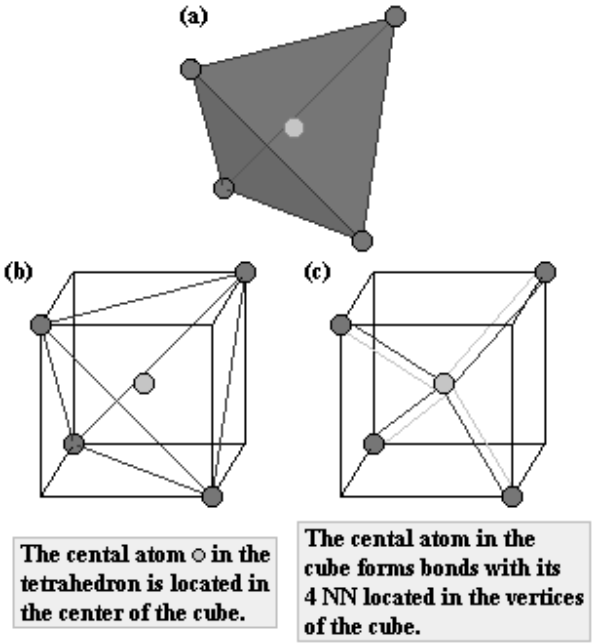

Figure 91 (a) A tetrahedron defined by the NNs of an atom in the diamond structure. **(b)** The tetrahedron from (a) inscribed in a cube. **(c)** Three-dimensional schematic representation of covalent bonds between an atom and its 4 NNs.

The neighborhood of an atom in the diamond structure is shown in Fig. 91. The four NNs of each atom of an element that crystallize in this structure are placed at the vertices of a regular tetrahedron that has the atom under consideration in the center, like it is shown in Fig. 91a. The regular

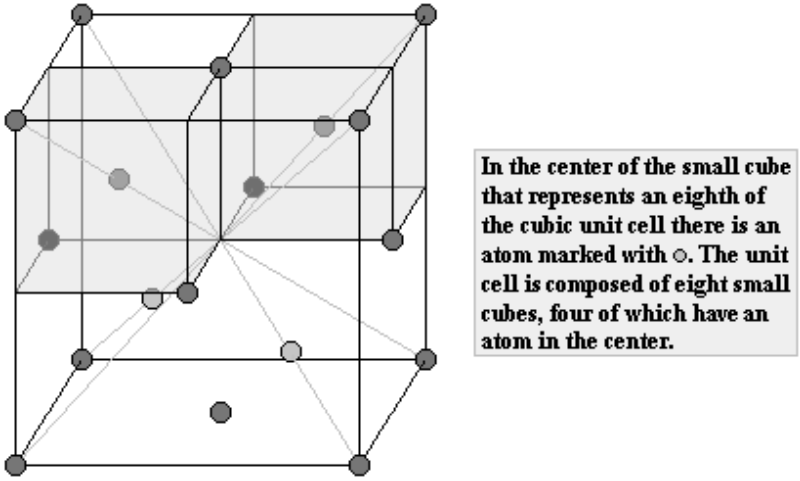

Figure 92 Two small cubes from Fig. 91b placed in two of the four possible positions inside a cubic unit cell of the diamond structure.

tetrahedron is easier to draw if we place it inside a cube, what was done in Fig. 91b. In addition, Fig. 91c shows a three-dimensional schematic representation of covalent bonds between an atom in the diamond structure and its 4 NNs.

We should observe that the cubic volume that we have drawn in Fig. 91b does not, of course, represent a unit cell of the diamond structure, since it does not have atoms in all its vertices. However, we can easily locate it within the cubic unit cell of this structure. Figure 92 shows two of the 4 possible positions of the small cube inside the diamond cubic unit cell. We may also observe in Fig. 92 that this unit cell is just the cubic unit cell of the *fcc* structure with 4 additional atoms placed inside (on the body diagonals). The distance between each additional atom and its nearest cube vertex is $1/4$ of the cube body diagonal, and those additional atoms occupy tetrahedral interstices present in the *fcc* cubic unit cell. We can see in Fig. 92 that in this cell, there is a total of 8 tetrahedral interstices and in the case of the diamond structure half of them are filled with atoms.

The tetrahedral interstices present in the *fcc* structure have been already considered by us in the previous section. In that opportunity, the *fcc* structure was seen as a sequence of two-dimensional *hcp* layers of **ABCABC…** type. In Fig. 89a, we have shown two examples of tetrahedral interstices present in the cubic cell of the *fcc* structure.

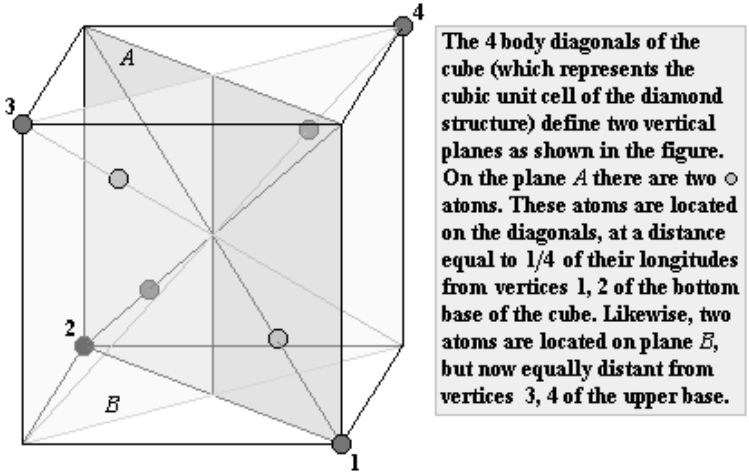

Figure 93 Relative positions of atoms belonging to the diamond structure. The 4 atoms that are inside the cubic unit cell are distributed in two vertical planes defined by the body diagonals of the cube.

To help visualize the positions of the 4 atoms that are inside of the cubic unit cell of the diamond structure, we have drawn in Fig. 93 two mutually orthogonal vertical planes ***A*** and ***B***. Each plane is defined by two body diagonals of the cube and the 4 atoms are placed on these diagonals in the way explained in this figure.

It is obvious that the neighborhood of each atom in the diamond structure is the same. This can be verified by drawing two cubic unit cells, I and II, in the diamond structure in such a way that cube II is shifted with respect to cube I along one of its body diagonals, to a segment equal in length to $1/4$ of the diagonal length. We obtain then that the atoms that are in the interior of cube I coincide with the vertices or centers of the faces of cube II, thus such atoms of cube II have the same neighborhood as the atoms on the diagonals of cube I. This is illustrated in 2D in Fig. 94, where we have plotted a plane with 12 atoms from certain region of the crystal. This plane includes a cross section of cube I with two atoms from the diagonals. One of these atoms is placed at a vertex of cube II and the other one at its face center. We can see in Fig. 94a that the atoms that are located on the body diagonals of the cubes have the same spatial distribution as the atoms from vertices and faces of cube I. It is also easy to observe in Fig. 94b the equivalence between the relative distributions of atoms of each

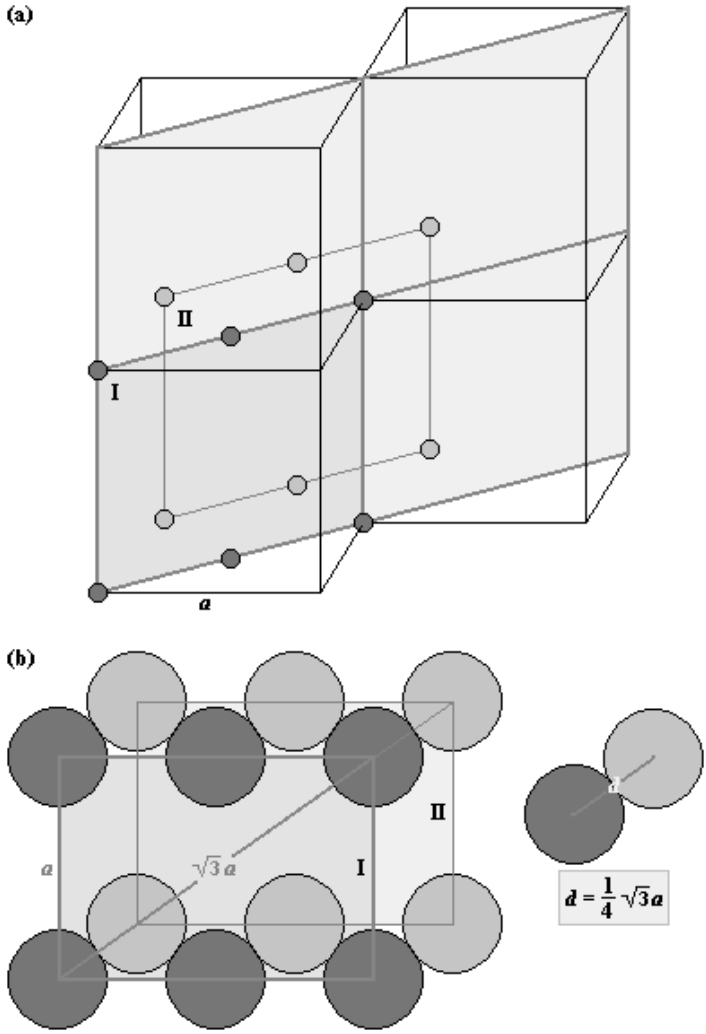

Figure 94 (a) Comparison of the distribution of atoms from vertices and faces of the cubic unit cells with those from their body diagonals in the diamond structure. **(b)** Cross sections of atoms (considered hard spheres) from (a) are shown. In this figure, the equivalency between the relative distributions of atoms of each type (those from vertices and faces of the cube and those from its diagonals) is visualized.

type (from the body diagonals and from the vertices and faces). Finally, we can say that it is the atomic arrangement in the diamond structure which

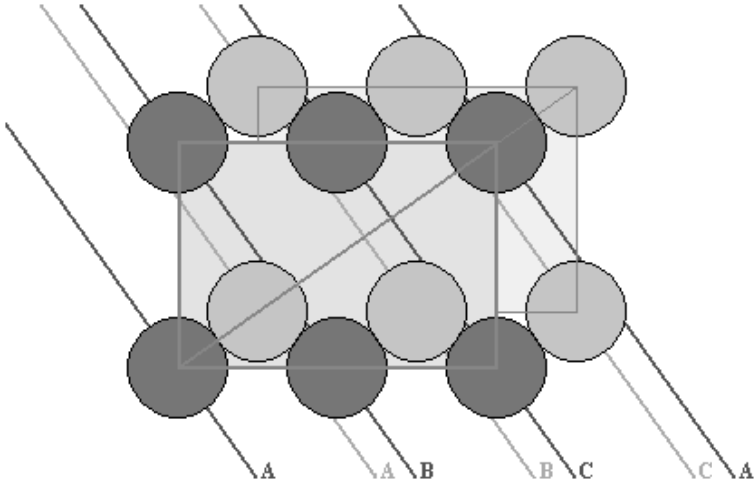

Figure 95 Left part of Fig. 94b with the cross sections of the **A**, **B**, and **C** layer planes added.

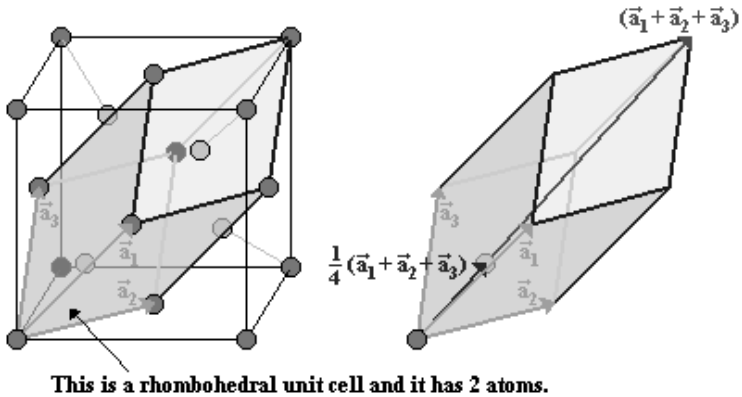

Figure 96 Cubic and rhombohedral unit cells for the diamond structure (left). In the figure, it is also shown the positions of the two atoms belonging to the rhombohedral unit cell (right).

allows each atom to be in the middle of a regular tetrahedron with 4 NNs (located at the vertices of the tetrahedron) that are covalently bonded to it.

To conclude, we can say that the diamond structure is just a superposition of two *fcc* substructures that are shifted one with respect to the other in the way described above. Each substructure may be seen as a sequence of layers of **ABCABC…** type and the two substructures are shifted one with respect to the other, to a segment shorter than the distance

between two consecutive layers in the substructures, in the direction orthogonal to the layer planes. Thus, the diamond structure represents indeed a sequence of layers of **AABBCCAABBCC…** type, what is easy to see in Fig. 95, where we have added the cross sections of the **A**, **B**, and **C** layer planes to Fig. 94b.

The smallest unit cell of the diamond structure is of the same shape as the primitive rhombohedral unit cell of the *fcc* structure, but in this case the cell contains 2 atoms as shown in Fig. 96. Therefore, the diamond structure can be seen as a *fcc* Bravais lattice with two-atom basis.

Finally, let us show the positions of atoms belonging to the diamond cubic unit cell. Figure 97a shows the coordinates of 8 atoms within the unit cell and Fig. 97b shows the projection of these atoms on the cell base. The coordinates of the 8 atoms, in Fig. 97a, are given in terms of the cubic axes $\vec{a}$, $\vec{b}$, $\vec{c}$, and the fractions near the atom projections in Fig. 97b represent the coordinates of these atoms in the $\vec{c}$ axis.

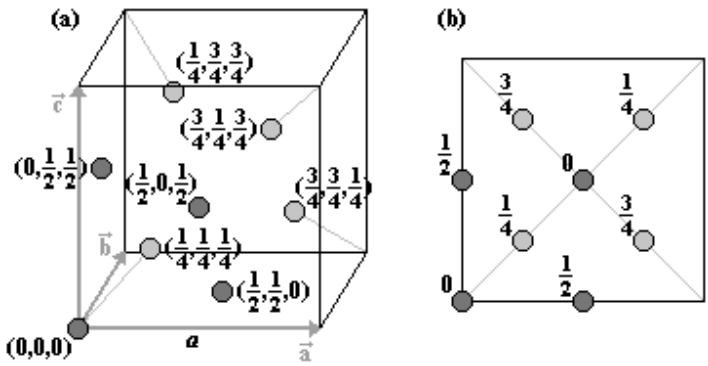

Figure 97 (a) Positions of the eight atoms within the cubic unit cell of the diamond structure. The coordinates are expressed in units of *a*. **(b)** Projection of atoms on the cell base. The fraction nearby the projection of an atom represents its coordinate in the $\vec{c}$ axis.

13. Atomic Radius

We have shown all along this chapter, on the examples of the most important crystal structures for elements, how to determine the atomic radius. As we remember, the atom is considered a hard, impenetrable sphere and its radius is given by half of the distance between NNs, which is

determined by the experimentally obtained lattice constant (or constants). The radius of such a sphere depends strongly on the type of bonding between atoms in a crystal. Until now we have considered metals, noble gases, and the elements from column IV of the periodic table. In each of those cases the bonding is different and the type of bonding determines the coordination number. We could observe that the metallic bonding prefers the coordination number 12. Some metals crystallize also in *bcc* structure with coordination number 8. The elements from column IV characterize pure covalent bonding, in case of which each atom requires 4 NNs. The predominantly ionic and partially ionic and partially covalent bonds appear in case of compounds and will be discussed on the examples of binary compounds in Chapter 4.

In Table 15 we list experimental lattice constants, NN interatomic distances, and covalent radii (all parameters obtained under normal conditions) of elements that crystallize in the diamond structure. The covalent radius for each element is calculated as half of the distance between NNs, *d*, determined by the experimental lattice constant *a* according to the expression

$$d = \frac{1}{8}\sqrt{3}a\,. \qquad \text{(III.12)}$$

In similar way, we have calculated the metallic radii for all metals that crystallize in structures with coordination number 12. Since the system of metallic radii is set up for the coordination number 12, for those metals that crystallize in the *bcc* structure, and therefore, have coordination number 8, we have made a correction (commonly used by chemists) consisting in increasing their radii by 3%.

Table 15 Lattice constants of elements that crystallize in the diamond structure under normal conditions. In addition, the NN distances, *d*, and the covalent radii, r_{cov}, are given.

Element	***a* (Å)**	***d* (Å)**	r_{cov} **(Å)**
C	3.5669	1.545	0.772
***α*-Si**	5.4306	2.352	1.176
***α*-Ge**	5.6574	2.450	1.225
***α*-Sn**	6.4892	2.810	1.405

Table 16 Nearest neighbor interatomic distances (in Angstroms) of metals that crystallize in dense-packed structures under normal conditions. The values have been calculated using the data from Tables 9-13. In the case of metals that crystallize in the *hcp*, *dhcp*, and Sm-type structures, we report two interatomic distances: the distance to the 6 NNs from the same layers and the distance to the 6 NNs from adjacent layers.

PERIODIC TABLE OF ELEMENTS

Nearest neighbor interatomic distances in Angstroms

H																	He
Li 3.039	Be 2.286 2.226											B	C	N	O	F	Ne
Na 3.716	Mg 3.209 3.197											Al 2.863	Si	P	S	Cl	Ar
K 4.608	Ca 3.952	Sc 3.309 3.254	Ti 2.950 2.896	V 2.619	Cr 2.498	Mn (2.244-2.91D)	Fe 2.482	Co 2.507 2.497	Ni 2.492	Cu 2.556	Zn 2.908 2.644	Ga	Ge	As	Se	Br	Kr
Rb 4.941	Sr 4.302	Y 3.648 3.557	Zr 3.232 3.179	Nb 2.858	Mo 2.725	Tc 2.738 2.706	Ru 2.706 2.650	Rh 2.689	Pd 2.751	Ag 2.889	Cd 2.979 3.295	In	Sn	Sb	Te	I	Xe
Cs 5.318	Ba 4.350		Hf 3.195 3.127	Ta 2.861	W 2.741	Re 2.761 2.740	Os 2.734 2.675	Ir 2.715	Pt 2.775	Au 2.884	Hg	Tl 3.457 3.408	Pb 3.500	Bi	Po	At	Rn
Fr	Ra 4.458																
			La 3.774 3.742	Ce 3.649	Pr 3.672 3.639	Nd 3.658 3.627	Pm 3.65 3.59	Sm 3.629 3.587	Eu 3.969	Gd 3.634 3.572	Tb 3.606 3.528	Dy 3.592 3.504	Ho 3.578 3.487	Er 3.559 3.467	Tm 3.538 3.447	Yb 3.878	Lu 3.505 3.434
			Ac 3.755	Th 3.595	Pa	U	Np	Pu	Am 3.468 3.451	Cm 3.496 3.478	Bk 3.416 3.398	Cf 3.390 3.378	Es 4.066	Fm	Md	No	Lr

Table 17 Metallic radii of metallic elements that under normal conditions crystallize in dense-packed structures (*fcc*, *hcp*, *dhcp*, Sm-type, and *bcc*). In the case of elements that crystallize in hexagonal close-packed structures the radius is half of the average value for the NN interatomic distance.

PERIODIC TABLE OF ELEMENTS
Metallic radii in Angstroms

H																	He
Li 1.565	Be 1.128											B	C	N	O	F	Ne
Na 1.914	Mg 1.602											Al 1.432	Si	P	S	Cl	Ar
K 2.373	Ca 1.976	Sc 1.641	Ti 1.462	V 1.349	Cr 1.287	Mn 1.26	Fe 1.278	Co 1.251	Ni 1.246	Cu 1.278	Zn 1.388	Ga	Ge	As	Se	Br	Kr
Rb 2.544	Sr 2.151	Y 1.801	Zr 1.603	Nb 1.472	Mo 1.404	Tc 1.361	Ru 1.339	Rh 1.345	Pd 1.375	Ag 1.445	Cd 1.568	In	Sn	Sb	Te	I	Xe
Cs 2.739	Ba 2.240		Hf 1.580	Ta 1.473	W 1.412	Re 1.375	Os 1.352	Ir 1.357	Pt 1.387	Au 1.442	Hg	Tl 1.716	Pb 1.750	Bi	Po	At	Rn
Fr	Ra 2.296																
			La 1.879	Ce 1.825	Pr 1.828	Nd 1.821	Pm 1.81	Sm 1.804	Eu 2.044	Gd 1.801	Tb 1.783	Dy 1.774	Ho 1.766	Er 1.757	Tm 1.746	Yb 1.939	Lu 1.735
			Ac 1.878	Th 1.797	Pa	U	Np	Pu	Am 1.730	Cm 1.744	Bk 1.704	Cf 1.692	Es 2.033	Fm	Md	No	Lr

The NN interatomic distances and metallic radii of all metals considered in this chapter are listed in Tables 16 and 17, respectively. We can observe in Table 16 that in the case of metals that crystallize in the *hcp*, *dhcp*, and Sm-type structures we are giving two values for the interatomic distances. The upper value corresponds to the distance of an atom to its 6 NNs located in the same layer to which the atom belongs, and the lower value corresponds to the distance to its 6 NNs from the adjacent layers. As we can see in Table 16 the two values are substantially different (by about 10%) only in the case of cadmium and zinc. The metallic radii reported in Table 17, for metals that crystallize in the hexagonal close-packed structures, were calculated using the average value for the NN distance.

14. Problems

Exercise 1 Calculate the filling factor for the diamond structure.

a.) Draw a cross section of the cubic unit cell for the diamond structure which contains the points of contact between the atoms considered hard spheres.

b.) Express the covalent atomic radius of the atom as a function of the lattice constant *a* and calculate the filling factor for the diamond structure.

c.) Make a comparison between the filling factor for the diamond structure and the filling factors for the *fcc* (or ideal *hcp*) *bcc* and *sc* structures. What is the coordination number in each case?

Exercise 2 Inside the hexagonal prism for the *dhcp* structure:

a.) Draw the hexagonal unit cell and the basis vectors $\vec{a}$, $\vec{b}$, $\vec{c}$ which define it.

b.) Find the positions of the atoms within the hexagonal unit cell. Express the coordinates of atoms in units of lattice constants *a* and *c*.

***Hint*:** A similar work was done for the *hcp* structure in Fig. 84.

Exercise 3 Gadolinium at room temperature and 44 GPa crystallizes in the triple hexagonal close-packed (*thcp*) structure which is a six-layered structure with a layer sequence **ABCBACABCBAC…**.

a.) Draw the hexagonal prism for this structure showing the layer sequence.

b.) Draw the hexagonal unit cell of the *thcp* structure with the basis vectors $\vec{a}$, $\vec{b}$, $\vec{c}$ that define it.

c.) In the similar way as it was done in Fig. 84 for the *hcp* structure, show the positions of the atoms within the hexagonal unit cell of the *thcp* structure. Express the coordinates of atoms in units of the lattice constants *a* and *c*.

d.) The experimental cell parameters of gadolinium at room temperature and 44 GPa are $a = 2.910\,\text{Å}$ and $c = 14.31\,\text{Å}$. Show that the crystal structure of Gd is nearly a perfect close-packed structure (each atom has its 12 NNs almost at the same distance to it).

***Hint*:** For that purpose show that the distance of an atom to its 6 NNs located in adjacent layers differs from the distance to the 6 NNs located within the same layer by less than 0.3%.

Exercise 4 Samarium under normal conditions (α-Sm) crystallizes in the trigonal structure. This structure may be seen as a

$$\textit{trigonal lattice} + 3\text{-}\textit{atom basis}$$
or as a
$$\textit{hexagonal lattice} + 9\text{-}\textit{atom basis}\,.$$

Figure 98 shows the hexagonal prism for α-Sm.

a.) Draw the rhombohedral unit cell of the α-Sm structure inside the hexagonal prism shown in Fig. 98.

b.) Draw a triple hexagonal unit cell of the α-Sm structure. What is the relation between the volume of this cell and the volume of the rhombohedral unit cell?

c.) How close is the α-Sm structure to an ideal close-packed structure? Express your answer in percentage.

***Hint*:** Use the experimental data given in Fig. 98 to calculate the c/a_h ratio, where *c* is the distance between every second layer in α-Sm.

Exercise 5 Show the positions of the atoms within a triple hexagonal unit cell of the α-Sm structure. Express the coordinates of those atoms in units of lattice constants a_h and c_h.

***Hint*:** See Exercise 4.

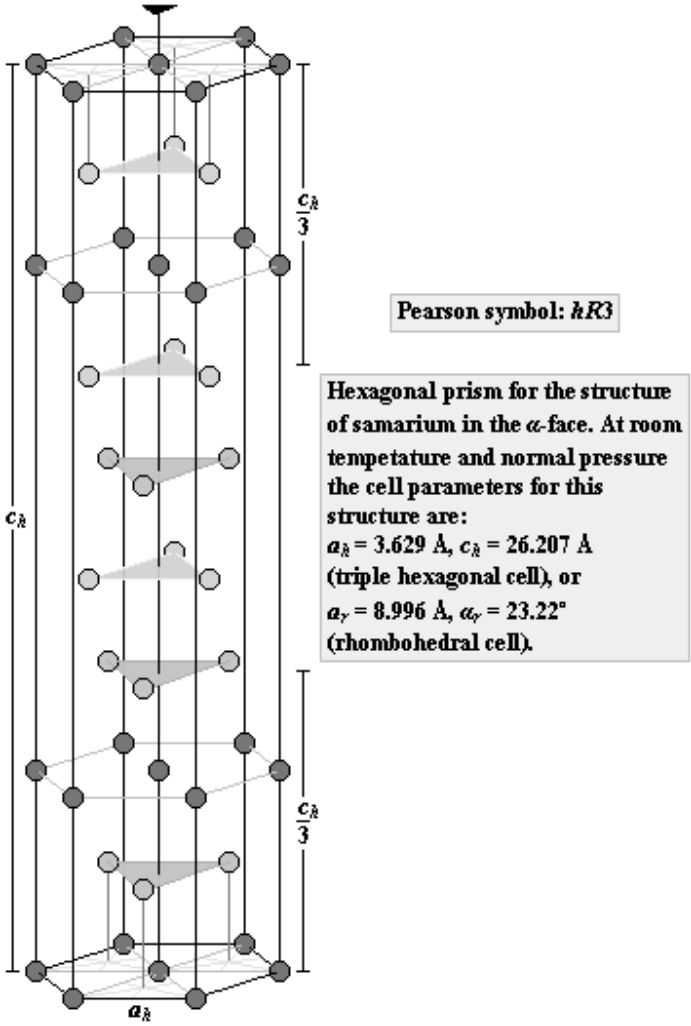

Figure 98 Hexagonal prism for the α-Sm structure.

Exercise 6 In the case of ytterbium the transition from the alpha to beta phase occurs in a broad temperature range near the room temperature. Tables 10 and 13 report the experimental lattice constants obtained for both phases at room temperature and normal pressure. Show that the average NN interatomic distance in α-Yb differs from the NN interatomic distance in β-Yb only by about 0.3%.

Exercise 7 For cerium the transition from the beta to gamma phase occurs in a broad temperature range near the room temperature. Tables 10 and 11 report the experimental lattice constants obtained for both phases under normal conditions. Show that the average NN interatomic distance in β-Ce differs from the NN interatomic distance in γ-Ce only by about 0.4%.

Exercise 8 Compare the NN interatomic distances of α-Fe at normal conditions and δ-Fe at 1712 K and normal pressure, both having *bcc* structure. The appropriate lattice constants should be taken from Table 9. Note that the volume of a solid usually increases with temperature and this is reflected by the positive value of the so called coefficient of thermal expansion.

Exercise 9 On the examples of metals for which we reported the experimental data for different phases, show that the NN interatomic distance derived from the experimental lattice constant of the *bcc* structure is smaller than the NN interatomic distance obtained from the data reported for close-packed structures, although the data for the *bcc* structure were obtained at higher temperatures. Compare the NN interatomic distances for the following cases:

a.) β-Ca (773 K) and α-Ca (room temperature),
b.) δ-Ce (1030 K) and γ-Ce (room temperature),
c.) δ-Fe (1712 K) and γ-Fe (1373 K),
d.) β-Li (room temperature) and α-Li (78 K),
e.) β-Na (room temperature) and α-Na (5 K).

The appropriate lattice constants are listed in Tables 9, 10, and 13.

IV. CRYSTAL STRUCTURES OF IMPORTANT BINARY COMPOUNDS

1. Introduction

In this chapter, we will consider important structures for binary compounds. As we could learn already on the examples of elements, the type of crystal structure depends significantly on the type of bonding between the NNs; at least the preference for the coordination number is determined by the type of bonds. Until now, we have discussed the structures of elements, mainly with metallic and covalent bonding. In the case of compounds, however, an important role plays the ionic bonding. In most cases the bonding is partially ionic and partially covalent. It means that the atoms are partially ionized and the atomic radii depend mainly on the degree of their ionization and also, however less, on the coordination number. The two types of ions in a binary compound have in general different radii and its crystal structure depends strongly on the cation to anion radius ratio.

2. The Ionic Radius Ratio and the Coordination Number

In this section, we will show the relation between the cation to anion radius ratio, r_+/r_-, and the number of NNs of a cation in a binary compound. The cations are in general smaller than the anions, so the r_+/r_- ratio is, in most cases, smaller than 1. The cation tries to surround itself with as many anions as possible and as closely as possible. The packing arrangement in most cases is such that the cations, considered hard spheres, are in contact with the anions, while the anions surround each cation without touching one another. Depending on the r_+/r_- ratio this can be achieved in different arrangements of ions, corresponding to different coordination numbers. Here, we will find the limiting radius ratio for the case of coordination number 4, on the example of the zinc blende structure.

In the zinc blende structure (also known as the sphalerite structure) crystallize binary compounds in which the contribution of covalent bonding to the interatomic bonds is important. Among them there is zinc sulphide in

the beta phase, β-ZnS, which gives the name to this structure. ZnS is an example of a binary compound in which the ionic bonding contributes in more degree than the covalent one (62%), but each ion has four NNs, what is a characteristic of covalent bonding. Both, Zn and S, have their NNs at the vertices of a regular tetrahedron with Zn or S in its center. This is shown in Fig. 99.

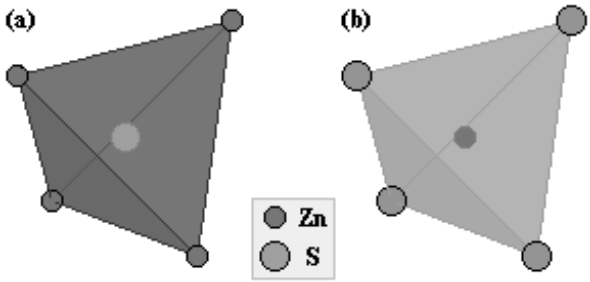

Figure 99 Zinc blende structure. **(a)** Regular tetrahedron defined by Zn cations with the S anion in its center. **(b)** Nearest neighbors of the Zn cation at the vertices of a regular tetrahedron.

It is easy to realize that the zinc blende structure has the same atomic arrangement as the diamond structure, but now the two *fcc* substructures are made of different ions. The cations occupy half of the tetrahedral interstices in the *fcc* anion substructure and *vice versa*. In Fig. 100 we show the cubic unit cell for the zinc blende structure. In this figure, we have also shown the diagonal cross section of the cube in which we can find the centers of the

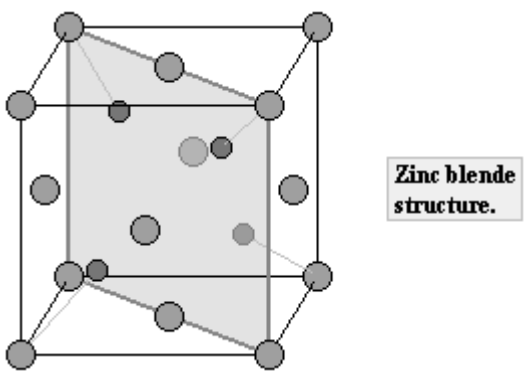

Figure 100 Unit cell for the zinc blende structure. A plane defined by two body diagonals of the cube is shown.

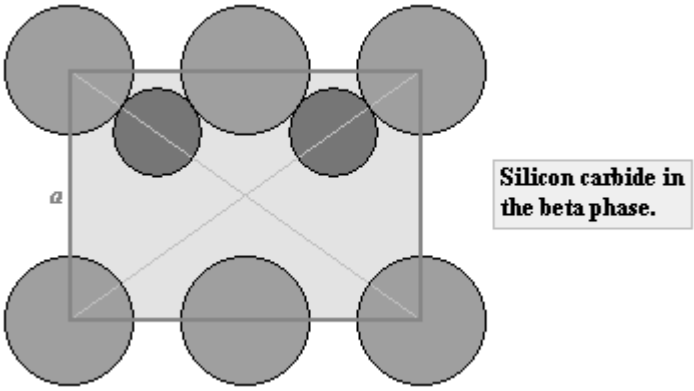

Figure 101 Cross section from Fig. 100 of the cubic unit cell for silicon carbide in the beta phase. Larger circles correspond to the cross sections of Si atoms and the smaller ones to the cross sections of C atoms.

NNs and the points of contact between them. As an example, the cross section for silicon carbide in the beta phase, β-SiC, is shown in Fig. 101. Silicon carbide is a IV-IV compound so it has a large covalent component in its bonds (82%). Therefore, in Fig. 101, we have drawn the circles, that represent the cross sections of Si and C atoms, with radii having the same ratio as for the covalent radii of the Si and C elements. The points of contact between neighboring atoms are found on the diagonals of the cube. We can observe in Fig. 101 that the Si atoms surround C atoms without touching one another. This is the typical situation in any zinc blende structure. The limiting case is achieved when the anions touch one another. This is shown in Fig. 102.

We see in Fig. 102 that the sum of the ionic radii is $1/4$ of the body diagonal longitude ($\sqrt{3}a$, where a is the cube edge)

$$r_- + r_+ = \frac{1}{4}\sqrt{3}a\,. \qquad \text{(IV.1)}$$

On the other hand, r_- is $1/4$ of the length of the cube face diagonal

$$r_- = \frac{1}{4}\sqrt{2}a\,, \qquad \text{(IV.2)}$$

so

$$\begin{cases} r_+ = \frac{1}{4}\sqrt{3}a - r_- = \frac{1}{4}(\sqrt{3}-\sqrt{2})a \\ r_- = \frac{1}{4}\sqrt{2}a \end{cases} \tag{IV.3}$$

and the radius ratio for the limiting case depicted in Fig. 102 is

$$\frac{r_+}{r_-} = \frac{\sqrt{3}-\sqrt{2}}{\sqrt{2}} = \frac{1}{2}\sqrt{6} - 1 \cong 0.225\,. \tag{IV.4}$$

It is obvious that only in cases when

$$\frac{r_+}{r_-} \geq 0.225 \tag{IV.5}$$

the cations are in contact with anions, otherwise a cation would occupy the central region of the tetrahedral interstice present in the anion substructure, without touching the anions. This situation rather does not occur as the structure would not be stable.

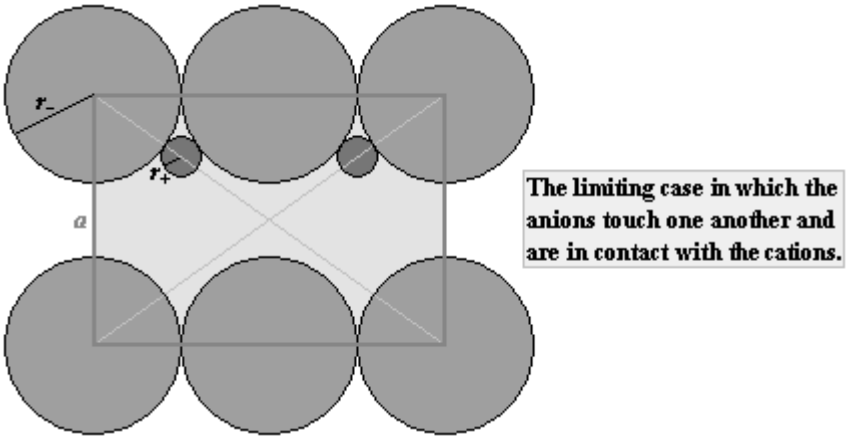

Figure 102 A plane defined by two body diagonals of the cubic unit cell for the zinc blende structure shown in Fig. 100. In the figure, we show the limiting case in which the anions, represented by larger circles, touch one another and are in contact with the cations (smaller circles).

In Table 18 we list the limiting radius ratios for different cation coordination numbers. This ratio for the coordination number 4 has been calculated above and the limiting radius ratios for the coordination numbers 6 and 8 will be calculated later. In Table 18 we also show the range for the radius ratio that would be expected for each coordination number and the possible crystal structures in which the cations have this coordination number. The ranges for the radius ratios are determined based on the fact that when r_+/r_- reaches the limiting value for the higher coordination number, the structures, in which the cation has this coordination number, become more stable. In practice only about 50% of cases can be classified according to the radius ratio ranges given in Table 18. This will be shown on the examples of alkali halides that crystallize in the NaCl structure.

Table 18 Expected radius ratio ranges for different cation coordination numbers. The crystal structures from the last column of the table will be fully described in this chapter.

Cation coordination number	Limiting values for r_+/r_-	Expected radius ratio range	Possible crystal structures
4	0.225	0.225 – 0.414	zinc blende, wurtzite, anti-fluorite
6	0.414	0.414 – 0.732	sodium chloride, nickel arsenide
8	0.732	0.732 – 0.999	cesium chloride, fluorite
12	1		

We are assuming in Table 18 that the r_+/r_- ratio is less than 1, what means that the cation is smaller than the anion, as it is the case in most compounds. In these cases, the cations, which occupy the interstices present in the anion substructure, are expected to touch the anions, what can be achieved in a structure for which the r_+/r_- ratio is larger than the limiting radius ratio for this structure. However, in occasions the situation is the opposite, the cations are larger than the anions, and then the r_-/r_+ ratio has to be considered in the way as r_+/r_- was in Table 18. This will be shown later, on the examples of some alkali halides.

We have already mentioned before that the ionic radii depend both on the degree of ionization of the atom and on the coordination number. The dependence on the coordination number is exemplified in Table 19. The comparison between the ionic radii and the metallic radius is also done in this table. We can observe the large difference between the values for the metallic and the ionic radii. We can also observe that, in the case of common

Table 19 Ionic radii for Na^+, K^+, and Ca^{2+}, for different coordination numbers. For comparison we have also listed the metallic radii for Na, K, and Ca taken from Table 17.

Element	Ionic radius (in Angstroms)				Metallic radius (in Angstroms)
	Coordination number				
	IV	VI	VIII	XII	XII
Na^+	0.99	1.02	1.18	1.39	
Na					1.91
K^+	1.37	1.38	1.51	1.64	
K					2.37
Ca^{2+}		1.00	1.12	1.34	
Ca					1.98

coordination numbers for binary compounds (IV, VI, and VIII), exists a quite large difference between the values for r_+ in the cases of coordination numbers IV and VI respect to the case of coordination number VIII.

3. Zinc Blende Structure

Pearson symbol: *cF*8, prototype: ZnS. In Fig. 103 we show two types of conventional unit cells for the zinc blende structure. The top part of this figure (Fig. 103a) shows two cubic cells that can be proposed for this structure: one with S ions and the other one with Zn ions at the vertices. The cubic unit cell has 8 ions (4 of each kind). In addition, in Fig. 103b we show a rhombohedral unit cell with two ions (one of each kind) belonging to it.

In the zinc blende structure crystallize compounds in which the covalent contribution to the bonds prevails over the ionic contribution or at least is significant. Among them there are III-V compounds, for which we have listed the experimental lattice parameters in Table 20. In this structure crystallize also compounds that contain a transition metal (TM) and an element from columns VI or VII of the periodic table. The lattice parameters for those compounds are given in Tables 21 and 22 for elements from columns VI and VII, respectively. Four II-VI compounds also crystallize in the zinc blende structure, although most of them, as we will see later, crystallize in the NaCl structure. They are: BeS, BeSe, BeTe, and BePo, and the lattice parameters for these compounds are listed in Table 21.

It was already mentioned in Sec. IV.2 that silicon carbide in the beta phase (β-SiC) also crystallizes in the zinc blende structure. The lattice

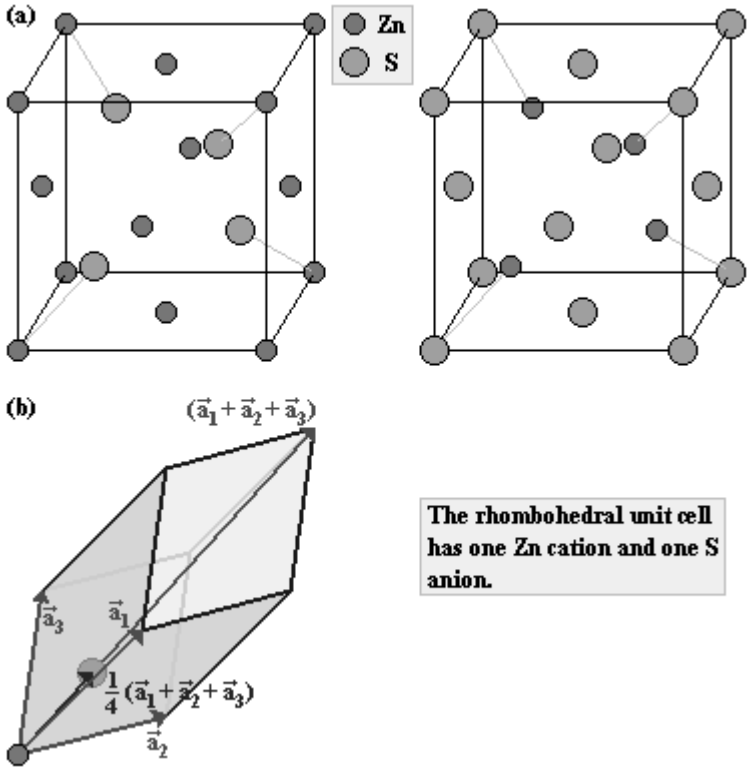

Figure 103 (a) Two cubic unit cells for the zinc blende structure of ZnS: one with Zn cations and the other one with S anions at the vertices. **(b)** A rhombohedral unit cell for the zinc blende structure with the two ions belonging to it.

Table 20 Lattice constants (in Angstroms) obtained under normal conditions for III-V compounds that crystallize in the zinc blende structure.

	N	P	As	Sb
B	BN (3.6159)	BP (4.5383)	BAs (4.777)	
Al		AlP (5.4625)	AlAs (5.656)	AlSb (6.1355)
Ga	GaN (4.511)	GaP (5.4504)	GaAs (5.65317)	GaSb (6.0961)
In		InP (5.847)	InAs (6.05836)	InSb (6.4794)

constant for this compound at normal conditions is 4.35845 Å. In Fig. 101, we had a plane defined by two body diagonals of the cubic unit cell for β-SiC, with the cross sections of the Si and C atoms drawn with the radii that have the same ratio as the ratio of the covalent radii for Si and C elements. It is interesting to mention that although silicon carbide has 18% of ionic contribution to its bonds, the sum of Si and C covalent radii (taken from Table 15), which is

$$r_{\mathrm{Si}} + r_{\mathrm{C}} = 1.176\ \text{Å} + 0.772\ \text{Å} = 1.948\ \text{Å},$$

is to within 3% equal to the sum of the Si and C radii obtained using Eq. (IV.1). This means that the amount (18%) of the ionic character of the bonds is almost not reflected in the sum of the Si and C radii.

In the diamond and zinc blende structures only half of the tetrahedral interstices present in the cubic unit cell are occupied with atoms or ions. We will show below an example of a structure that has the same conventional cubic unit cell but with all 8 tetrahedral interstices occupied with ions. This is the case of the calcium fluoride structure.

Table 21 Lattice constants (in Angstroms) obtained under normal conditions for compounds of Be-VI and TM-VI type that crystallize in the zinc blende structure.

	O	**S**	**Se**	**Te**	**Po**
Be		BeS (4.8624)	BeSe (5.1477)	BeTe (5.6225)	BePo (5.838)
Mn		β-MnS (5.601)	β-MnSe (5.902)	α-MnTe (6.338)	
Zn	ZnO (4.63)	β-ZnS (5.4109)	ZnSe (5.6676)	β-ZnTe (6.1037)	ZnPo (6.309)
Cd		β-CdS (5.8304)	CdSe (6.077)	CdTe (6.4809)	CdPo (6.665)
Hg		β-HgS (5.8537)	α-HgSe (6.0854)	α-HgTe (6.453)	

Table 22 Lattice constants (in Angstroms) obtained under normal conditions for compounds of TM-VII type that crystallize in the zinc blende structure.

	F	**Cl**	**Br**	**I**
Cu	CuF (4.255)	γ-CuCl (5.4202)	γ-CuBr (5.6955)	γ-CuI (6.05844)
Ag				γ-AgI (6.4991)

4. Calcium Fluoride Structure

4.1. Fluorite Structure

Pearson symbol: *cF*12, prototype: CaF_2. The calcium fluoride (CaF_2) structure, more commonly known as the fluorite structure, has its positive ions forming the *fcc* substructure and usually larger negative ions occupying tetrahedral interstices in this substructure. This is shown in Fig. 104a for CaF_2. Each F^- anion is placed in the center of a tetrahedral interstice and has 4 NNs (see also Fig. 105a). In Fig. 104b, we show the cubic unit cell for the CaF_2 structure with the anions in its vertices. We can see in this figure that

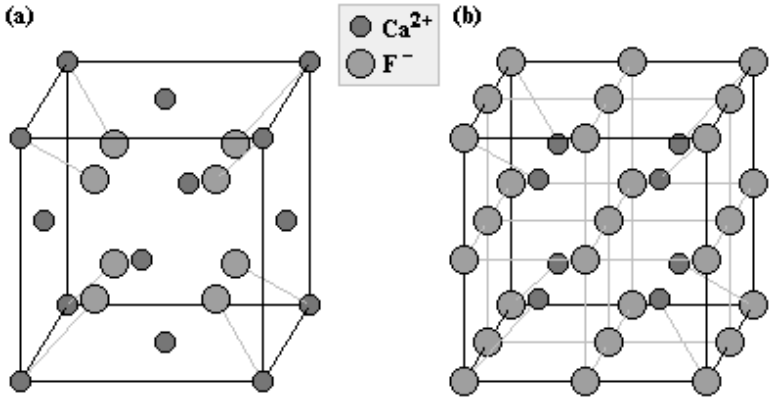

Figure 104 Cubic unit cells for the CaF_2 structure. In the cube vertices are placed Ca^{2+} cations in **(a)** and F^- anions in **(b)**.

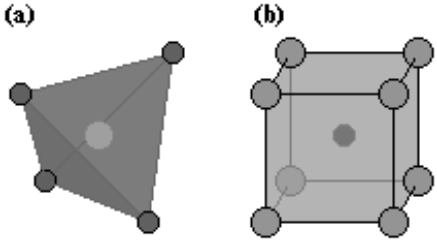

Figure 105 **(a)** Regular tetrahedron defined by the NNs of the F^- anion in CaF_2. **(b)** Cube defined by the NNs of the Ca^{2+} cation in CaF_2.

the anions define 8 small cubes with cations in their centers, therefore each Ca^{2+} cation, contrary to the anion, has 8 NNs, what is shown in Fig. 105b.

In addition to CaF_2, other II-VII compounds crystallize in the fluorite structure. They are listed at the top of Table 23. Among other examples of compounds that crystallize in this structure, we can mention hydrides, silicides, oxides, and fluorides of some TMs (mainly RE metals and actinides) and also lead difluoride in the beta phase (β-PbF_2) and polonium dioxide in the alpha phase (α-PoO_2). The experimental lattice constants, obtained under normal conditions for the compounds specified above, are listed in Table 23. This table allows to identify quickly which metals form compounds within a given group of hydrides, silicides, oxides, fluorides, or chlorides (see columns of the table) and also allows to see how many compounds with the fluorite structure can be formed by a given metal (see rows of the table).

Table 23 Lattice parameters (in Angstroms) obtained under normal conditions for II-VII compounds and hydrides, silicides, oxides, and fluorides of some TMs, all of them crystallizing in the fluorite structure. In addition, the data for β-PbF_2 and α-PoO_2 are included.

	H	**Si**	**O**	**F**	**Cl**
Ca				CaF_2 (5.46295)	
Sr				SrF_2 (5.7996)	$SrCl_2$ (6.9767)
Ba				BaF_2 (6.1964)	
Ra				RaF_2 (6.368)	
Sc	ScH_2 (4.78315)				
Co		$CoSi_2$ (5.365)			
Ni		$NiSi_2$ (5.406)			
Y	YH_2 (5.207)				
Zr			ZrO_2 (5.09)		
Nb	NbH_2 (4.566)				
Cd				CdF_2 (5.393)	
Pt	PtH_2 (5.517)				
Hg				HgF_2 (5.5373)	
Ce	CeH_2 (5.581)		CeO_2 (5.413)		
Pr	PrH_2 (5.516)		PrO_2 (5.392)		
Nd	NdH_2 (5.4678)				
Sm	SmH_2 (5.3773)				
Eu				EuF_2 (5.796)	
Gd	GdH_2 (5.303)				
Tb	TbH_2 (5.246)		TbO_2 (5.213)		
Dy	DyH_2 (5.2049)				
Ho	HoH_2 (5.165)				
Er	ErH_2 (5.1279)				
Tm	TmH_2 (5.0915)				
Lu	LuH_2 (5.0330)				
Th			ThO_2 (5.5997)		
Pa			PaO_2 (5.505)		
U			UO_2 (5.470)		
Np			NpO_2 (5.4341)		
Pu			PuO_2 (5.39819)		
Am			AmO_2 (5.3746)		
Cm			CmO_2 (5.368)		
Pb				β-PbF_2 (5.9463)	
Po			α-PoO_2 (5.637)		

When the ionic positions are reversed, and the anions and cations occupy the Ca^{2+} and F^- positions, respectively, we obtain the anti-fluorite structure, which will be considered below.

4.2. Anti-Fluorite Structure

Pearson symbol: *cF*12, prototype: Li_2O. In the anti-fluorite structure, the anions are in a *fcc* arrangement and the cations occupy all the tetrahedral interstices present in the anion substructure. This is shown in Fig. 106a. The cations have a coordination number 4. Figure 106b shows the cubic unit cell for the anti-fluorite structure with the cations at the vertices. We can observe in that figure that the 8 NNs of an anion are placed at the vertices of a small cube that represents one eight of the cubic unit cell. The NNs of a cation and an anion are shown in Figs. 107a and 107b, respectively.

In the anti-fluorite structure crystallize some alkali metals with elements from column VI of the periodic table, forming metal oxides, sulfides, selenides, and tellurides. They all are listed in Table 24. In Table 25 we list some II-III and II-IV compounds, and also phosphides of TMs that crystallize in the anti-fluorite structure.

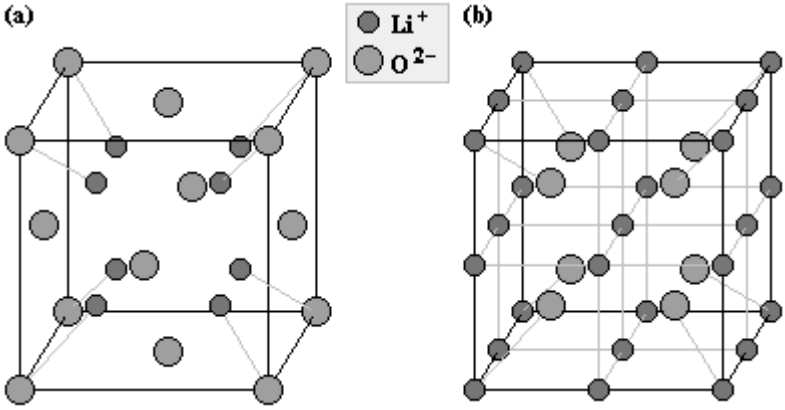

Figure 106 Cubic unit cells of Li_2O which crystallizes in the anti-fluorite structure. In the cube vertices are placed O^{2-} anions in **(a)** and Li^+ cations in **(b)**.

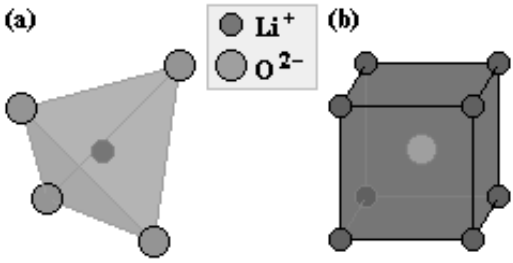

Figure 107 **(a)** Regular tetrahedron defined by the NNs of the Li^+ cation in Li_2O. **(b)** Cube defined by the NNs of the O^{2-} anion in Li_2O.

Table 24 Lattice constants (in Angstroms) obtained under normal conditions for I-VI compounds that crystallize in the anti-fluorite structure.

	O	**S**	**Se**	**Te**
Li	Li_2O (4.6114)	Li_2S (5.71580)	Li_2Se (6.0014)	Li_2Te (6.517)
Na	Na_2O (5.55)	Na_2S (6.5373)	Na_2Se (6.825)	Na_2Te (7.314)
K	K_2O (6.436)	K_2S (7.406)	K_2Se (7.676)	K_2Te (8.152)
Rb	Rb_2O (6.755)	Rb_2S (7.65)		

Table 25 Lattice constants obtained under normal conditions for some II-III and II-IV compounds, and also phosphides, all of them crystallizing in the anti-fluorite structure.

Compound	***a* (Å)**	**Compound**	***a* (Å)**
Be_2B	4.663	**Mg_2Sn**	6.765
Be_2C	4.3420	**Mg_2Pb**	6.815
Mg_2Si	6.351	**Rh_2P**	5.5021
Mg_2Ge	6.3894	**Ir_2P**	5.543

5. Wurtzite Structure

Pearson symbol: *hP*4, prototype: ZnS. Zinc sulphide and most of the binary compounds that crystallize in the zinc blende structure crystallize also in a hexagonal structure, the so called wurtzite structure. ZnS in the wurtzite structure is in the alpha phase (α-ZnS). The wurtzite structure is composed of two-dimensional hexagonal layers **A** and **B** and is of the **AABBAABB…** type, where one layer (**A** or **B**) corresponds to one kind of ions and another one to the other kind of ions, so in the case of α-ZnS we have:

$$\mathbf{A_{Zn}A_SB_{Zn}B_SA_{Zn}A_SB_{Zn}B_S\ldots}\ ,$$

whereas in the case of β-ZnS (ZnS in the zinc blende structure) we have:

$$\mathbf{A_{Zn}A_SB_{Zn}B_SC_{Zn}C_SA_{Zn}A_SB_{Zn}B_SC_{Zn}C_S\ldots}\ .$$

In Fig. 108 we show two hexagonal prisms for α-ZnS: one with Zn cations at the vertices (see Fig. 108a) and the other one with S anions at the vertices (see Fig. 108b). In this figure it is also easy to distinguish the two substructures of the wurtzite structure: that formed by cations and that

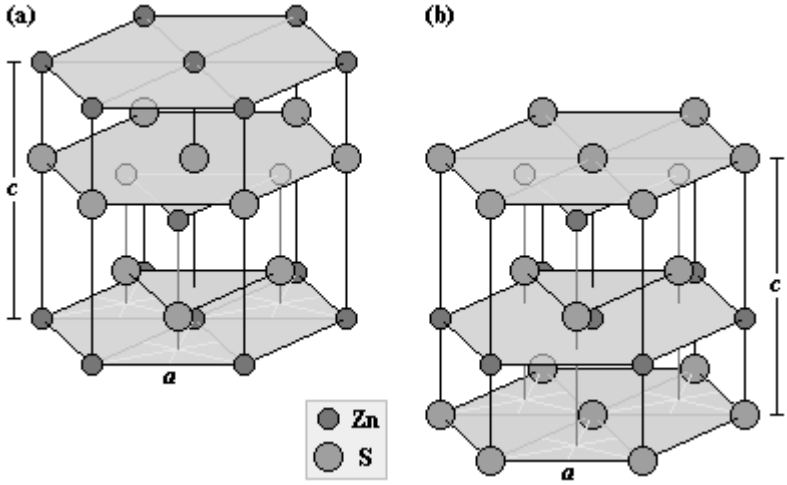

Figure 108 Hexagonal prism for ZnS in the wurtzite structure, with Zn cations at the vertices **(a)** and with S anions at the vertices **(b)**.

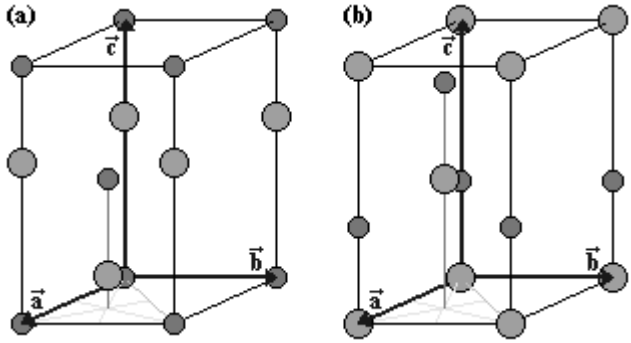

Figure 109 Two conventional unit cells for ZnS in the wurtzite structure: in **(a)** with Zn cations at the vertices and in **(b)** with S anions at the vertices.

formed by anions. Each substructure is a *hcp* structure. However, the ions in it do not touch each other, since the NNs of an ion in the wurtzite structure are of another type. Each ion from one substructure occupies a tetrahedral interstice from the other substructure.

The smallest volume that can reproduce the wurtzite structure is the hexagonal unit cell. Figure 109 shows two hexagonal cells for the wurtzite structure of ZnS, one with Zn cations at the vertices (see Fig. 109a) and the other one with S anions at the vertices (see Fig. 109b). The hexagonal unit cell for the wurtzite structure contains two ions of each type. We have

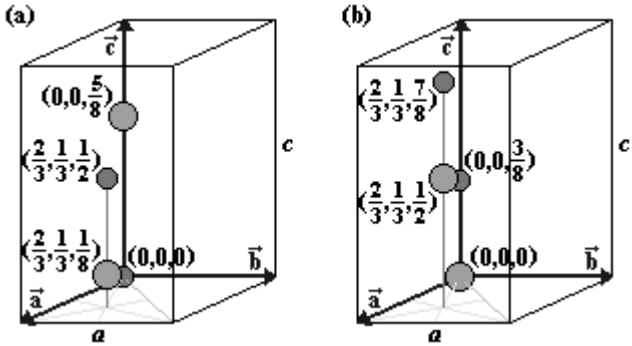

Figure 110 **(a)** and **(b)** show the positions of ions belonging to the unit cells from Figs. 109a and 109b, respectively. The coordinates are expressed in units of *a* and *c*.

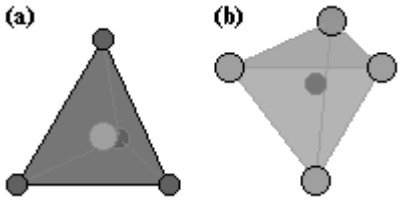

Figure 111 **(a)** A tetrahedron defined by the NNs of the S anion in α-ZnS. **(b)** A tetrahedron defined by the NNs of the Zn cation in α-ZnS. We can envision the tetrahedrons from (a) and (b) in both cells from Fig. 109.

shown in Fig. 110 the coordinates, given with respect to the $\vec{a}$, $\vec{b}$, $\vec{c}$ axes, of the four atoms belonging to each unit cell from Fig. 109.

Similarly to the zinc blende structure, each ion in the wurtzite structure has a tetrahedral arrangement of the four NNs, although the ionic contribution to their bonds is, in general, larger than the covalent one. This is shown in Figs. 111a and 111b for α-ZnS, where four NNs surround the S and Zn ions, respectively. These central ions and their NNs can be found inside the hexagonal cells from Fig. 109.

We will consider now an ideal case, when the tetrahedrons from Fig. 111 are regular. The parameters of the hexagonal unit cell, *a* and *c*, fulfill then the relation $c/a = \sqrt{8/3} \cong 1.633$, as in the case of an ideal *hcp* structure. The wurtzite structure of ZnS and many other binary compounds is very close to the ideal case. This can be seen in Table 26 where we list, in the last column of that table, the c/a ratios for compounds that crystallize in the wurtzite structure. In Fig. 112a, we show a regular tetrahedron defined by Zn cations, which is inside a hexagonal unit cell. The cations from the

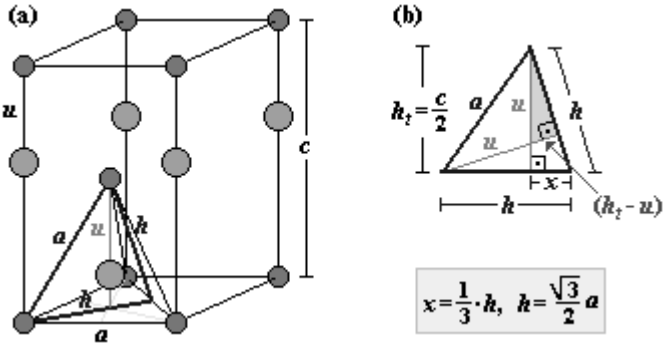

Figure 112 (a) A regular tetrahedron, defined by Zn cations, located inside a hexagonal unit cell for the wurtzite structure of ZnS. **(b)** A vertical cross section of the tetrahedron shown in (a). See text for detailed explanation.

tetrahedron vertices are the NNs of the S anion located in the center of the tetrahedron. We can also see in Fig. 112a that the distance, *u*, between NNs defines also the distance between layers $\mathbf{A_S}$ and $\mathbf{A_{Zn}}$, so the S *hcp* substructure is shifted with respect to the Zn substructure by *u* along the *c* axes.

Let us now express *u* as a function of the lattice parameters. In Fig. 112a, we show a vertical cross section of the regular tetrahedron that includes one of its edges *a* and two heights *h* of the tetrahedron faces, which are equilateral triangles. The three segments (*a*, *h*, *h*) define a triangle shown in Fig. 112b. Inside this triangle we highlighted a right triangle of sides $h_t - u$, $h - x$, and *u*. There is also a larger triangle that is similar to the highlighted one and have sides *x*, *h*, and h_t. The lengths of *x* is $h/3$. From the similitude of the last two triangles we have

$$\frac{h_t - u}{u} = \frac{x}{h} = \frac{\frac{1}{3}h}{h} = \frac{1}{3}, \tag{IV.6}$$

then

$$h_t - u = \frac{1}{3}u, \tag{IV.7}$$

finally

$$u = \frac{3}{4}h_t \underset{h_t = c/2}{\Rightarrow} u = \frac{3}{8}c. \tag{IV.8}$$

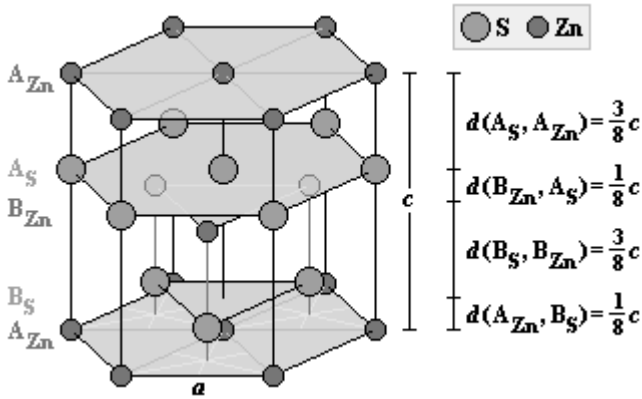

Figure 113 Hexagonal layers $\mathbf{A_S}$, $\mathbf{A_{Zn}}$, $\mathbf{B_S}$, and $\mathbf{B_{Zn}}$ in the wurtzite structure of ZnS. The distances between the consecutive layers are shown.

So, in an ideal wurtzite structure each atom has 4 NNs at a distance $(3/8)c$. As it was mentioned before, the same distance can be found between layers $\mathbf{A_S}$ and $\mathbf{A_{Zn}}$ and, of course, also layers $\mathbf{B_S}$ and $\mathbf{B_{Zn}}$. This is shown in Fig. 113 for the wurtzite structure of ZnS. In this figure, we show also that the distance between layers $\mathbf{A_{Zn}}$ and $\mathbf{B_S}$ or $\mathbf{B_{Zn}}$ and $\mathbf{A_S}$ is $(1/8)c$.

Each anion from layers $\mathbf{A_S}$ or $\mathbf{B_S}$ has 4 NNs located in adjacent $\mathbf{A_{Zn}}$ and $\mathbf{B_{Zn}}$ layers at a distance $(3/8)c$ (see Fig. 113), since the c/a ratio is for ZnS close to the case of an ideal wurtzite structure. The NNNs of an anion are 12 anions at a distance a: six from the layer to which belongs the anion in consideration and the other six from two adjacent layers in the substructure of anions. Since the anions do not touch each other, this substructure is not, of course, close-packed. The same analysis is valid for the substructure of Zn cations.

The experimental lattice parameters obtained under normal conditions for binary compounds that crystallize in the wurtzite structure are given in Table 26. We can observe that the c/a ratio, which is given in the last column of the table, is for each case close to that for the ideal case and as a consequence, there is a similarity between the hexagonal and cubic structures of these compounds, although the symmetry of both structures is different.

Let us now summarize important similarities and differences between the zinc blende and the ideal wurtzite structures:

a.) Looking at the NNs, we cannot tell whether it is zinc blende or wurtzite structure.

b.) In both cases, the NN and the NNN distances are very close in value. These values for the NNs of some compounds are listed in Table 27.
c.) The number (12) of NNNs is the same in both cases.
d.) There is a difference in the location of 3 NNNs. This will be explained in details below.

In both structures, zinc blende and wurtzite, each ion has 6 NNNs in the layer, let us say **A**, to which belongs. The other 6 of 12 NNNs belong to two adjacent layers in the substructure of the ion in consideration. In the case of the wurtzite structure, the adjacent layers are of **B** type, while in the case of the zinc blende structure one of them is of **B** type and the other one is of **C** type. Therefore, the 3 NNNs of an atom from layer **A**, that make the

Table 26 Lattice parameters, obtained under normal conditions, of binary compounds that crystallize in the wurtzite structure.

Compound	*a* (Å)	*c* (Å)	*c*/*a*
CuH	2.893	4.614	1.59
α-BeO	2.6967	4.3778	1.62
γ-MnS	3.987	6.438	1.61
γ-MnSe	4.12	6.72	1.63
γ-MnTe	4.48	7.32	1.63
γ-ZnO	3.25030	5.2072	1.60
α-ZnS	3.8227	6.2607	1.64
ZnSe	4.003	6.540	1.63
γ-ZnTe	4.31	7.09	1.65
α-CdS	4.1365	6.7160	1.62
CdSe	4.2999	7.0109	1.63
β-AgI	4.599	7.524	1.64
BN	2.555	4.21	1.65
AlN	3.11197	4.98089	1.60
GaN	3.1878	5.1850	1.63
InN	3.53774	5.7037	1.61
SiC	3.079	5.053	1.64

Table 27 Comparison between NN distances for zinc blende and wurtzite structures of some binary compounds. The values were obtained from the lattice parameters listed in Tables 20, 21, and 26.

Compound	NN distance (Å)	
	Zinc blende	Wurtzite
MnSe	2.555	2.52
MnTe	2.744	2.75
ZnSe	2.454	2.453
CdSe	2.631	2.629
GaN	1.953	1.944

difference between the two structures, are located in the **C** layer in the zinc blende structure and in the **B** layer in the wurtzite structure (in both cases in the substructure of the ion in consideration).

6. Nickel Arsenide Related Structures

6.1. NiAs Structure

Pearson symbol: *hP*4, prototype: NiAs. Similarly to the zinc blende and wurtzite structures, the nickel arsenide (NiAs) structure is related to a close-packed arrangement of ions. It is composed of anion and cation layers placed alternately one on the top of the other, in the way illustrated in Fig. 114. Each layer represents a two-dimensional hexagonal structure and a hexagonal prism is a conventional unit cell that has the same point symmetry as an infinite NiAs structure, but a sixfold symmetry axis of the prism is reduced here (as in the case of the wurtzite structure) to a threefold symmetry axis. In Fig. 114a, we show the hexagonal prism for the NiAs compound. In addition, we show in Fig. 114b the NiAs structure in the ideal case when $c/a = \sqrt{8/3}$. Such case has been already discussed before for the *hcp* and wurtzite structures. We can see in Fig. 114 that the *c*/*a* ratio for the

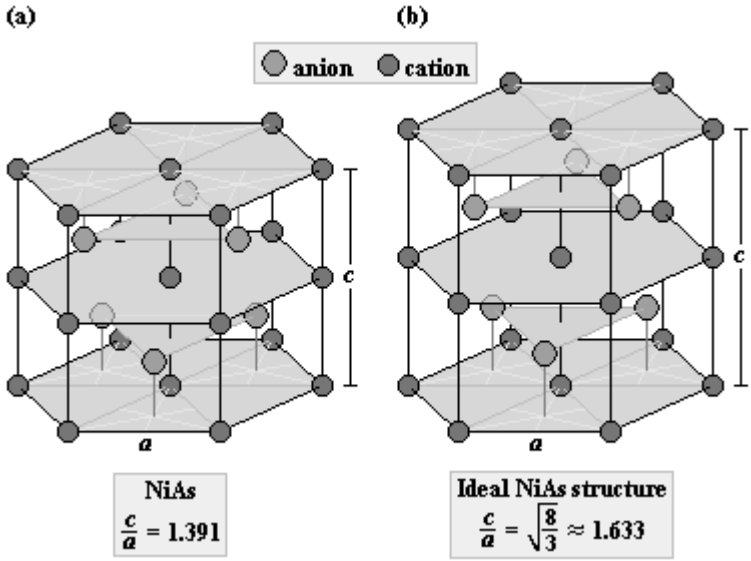

Figure 114 (a) Hexagonal prisms for the prototypical NiAs. **(b)** The NiAs structure for the ideal case when $c/a = \sqrt{8/3}$.

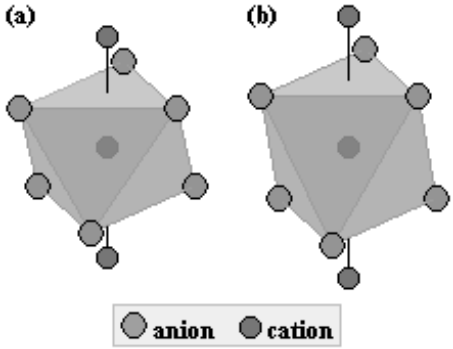

Figure 115 Octahedrons defined by anions that are the NNs of a cation **(a)** in the NiAs compound and **(b)** in the ideal NiAs structure. In this figure we also show the two nearest cations to the cation placed in the center of each octahedron.

prototypical NiAs differs 15% from the value that corresponds to the ideal case, while in compounds that crystallize in the wurtzite structure it nearly approaches the ideal ratio.

We can observe in Fig. 114 that 6 NNs of a cation located in the center of the hexagonal prism define an octahedron. This octahedron is shown in Fig. 115a for the NiAs compound. In the case of the ideal NiAs structure the octahedron is a regular polyhedron and is shown in Fig. 115b. In Fig. 115 we can also see two additional ions that are the closest cations to the cation placed in the center of each octahedron. In the case of the ideal NiAs structure, those cations are at a distance 15% longer than the distance to the NNs from the cation in consideration. However, in the case of the NiAs compound the distance from a cation to its nearest cations is only 3% longer than the distance to the NNs. It means that each cation in the NiAs compound has effectively 8 NNs (6 anions and 2 cations) all of them forming bonds with this cation (see Fig. 115a). It is also important to mention that the length of the Ni-Ni bond in the NiAs compound is, to within 1%, equal to the metallic bond length in the crystal of nickel. Therefore, we can expect that the Ni-Ni bonds, which we are describing here for the NiAs compound, are closer to the metallic bonds than to the ionic ones, since the Ni-Ni ionic bond would be longer than the Ni-Ni metallic bond.

In Fig. 116a, we show two hexagonal prisms for the NiAs structure: one with anions and another one with cations at the vertices of the prism. We observe in this figure that each cation from a cation layer lies directly over a cation from any layer below. Therefore, the cations form a simple

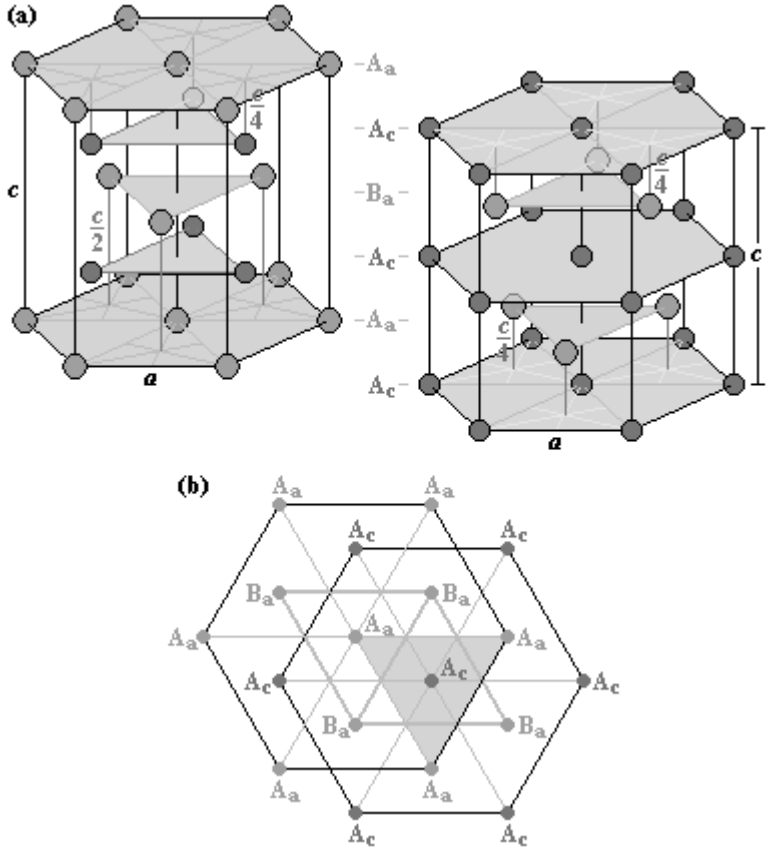

Figure 116 **(a)** Two hexagonal prisms for the NiAs structure: one with anions at the vertices and another one with cations at the vertices. **(b)** Projection of the centers of ions belonging to each hexagonal prism on the hexagonal base. We can observe that the triangles defined by the ions from the $\mathbf{B_a}$ layer have in each case from (a) different orientations with respect to the hexagonal prism base.

hexagonal substructure since each of their layers is of the same type. In Fig. 116 all cation layers are of **A** type and are labeled $\mathbf{A_c}$. In the case of anions, there are two types of layers (labeled $\mathbf{A_a}$ and $\mathbf{B_a}$ in Fig. 116) like in the case of the *hcp* structure, therefore the anions form a *hcp* substructure.

Let us now make a comparison between the neighborhood of a cation and an anion in the NiAs structure. We already know that there are tetrahedral and octahedral interstices between consecutive hexagonal layers of different types (see Fig. 87). This is the case of the *hcp* structure. In the case of the wurtzite structure half of the tetrahedral interstices, present in one *hcp* substructure, are occupied by ions belonging to the other

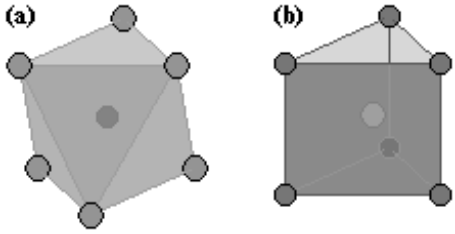

Figure 117 Octahedron defined by the NNs of a cation **(a)** and the trigonal prism defined by the NNs of an anion **(b)** in the NiAs structure.

substructure and the octahedral interstices are vacant. Also in the case of the zinc blende structure half of the tetrahedral interstices present in the *fcc* substructure of ions of one type are occupied by ions of the other type and the octahedral interstices remain vacant. Contrary to those cases, in the NiAs structure the cations occupy all octahedral interstices present in the *hcp* substructure of anions and the tetrahedral interstices are vacant. Turning now to the neighborhood of an anion in the NiAs structure, we can say that all cation layers are of the same type and between them, there are neither octahedral nor tetrahedral interstices. Each anion occupies the center of a trigonal prism, what can be seen in Fig. 114.

In Fig. 117 we have drawn the neighborhood of the two types of ions in the NiAs structure. Fig. 117a shows an octahedron with anions in its vertices. These anions are the NNs of a cation that is in the center of the octahedron. Similarly, Fig. 117b shows the NNs of an anion that is located in the center of a trigonal prism with cations at the vertices. In both cases the number of NNs is the same but the distribution of cations with respect to the anion is different from the distribution of anions with respect to the cation.

We will now calculate the value for the ideal c/a ratio. This was already done in Sec. III.10 for the *hcp* structure. In that opportunity, the calculations were based on the geometric characteristics of a regular tetrahedron defined by the NNs of an atom in the ideal *hcp* structure; the presence of such a tetrahedron inside the hexagonal unit cell of the *hcp* structure determines the c/a ratio in the ideal case. This time, in turn, we will calculate c/a using a regular octahedron defined by the NNs of a cation in the ideal NiAs structure.

As we already know, a regular octahedron may be inscribed in a cube. Figure 118 shows such a situation. The longitude of the cube body diagonal is equal to $(3/2)c$, what can be verified in the following way:

a.) The anion layers cross the body diagonal of the cube in the points that divide the diagonal in three segments of the same longitude.

b.) The distance between two consecutive anion layers is equal to $c/2$, so, taking into account point a.) we can conclude that the longitude of the body diagonal of the cube is equal to $3(c/2)=(3/2)c$.

From the considerations made in Fig. 118, we can conclude that, indeed, the octahedron defined by the NNs of a cation is a regular polyhedron when $c/a=\sqrt{8/3}$.

The smallest unit cell that can reproduce the NiAs structure may be of type (a) or (b) from Fig. 119. In both cases, the unit cell contains two anions

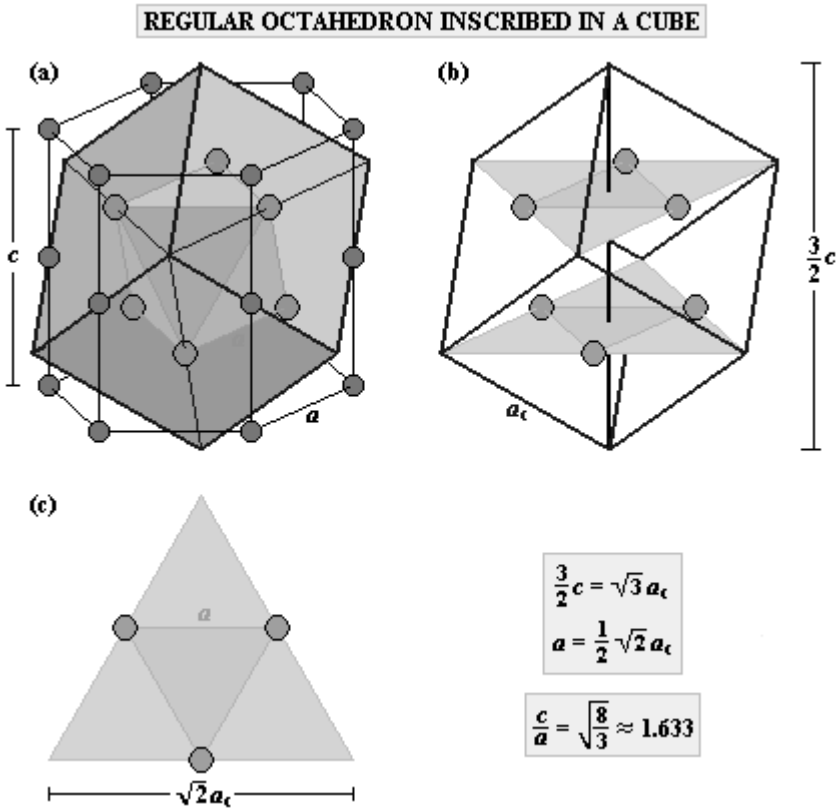

Figure 118 **(a)** Hexagonal prism for an ideal NiAs structure with the cations at the vertices. The regular octahedron defined by 6 anions located inside this prism is also shown. In addition, this octahedron is inscribed in a cube. **(b)** The cube defined in (a). The longitude of a body diagonal of the cube is expressed as a function of the lattice constant *c*. **(c)** One of the triangles shown in (b). In this figure we show the relation between the lattice constant *a* and the cube edge a_c.

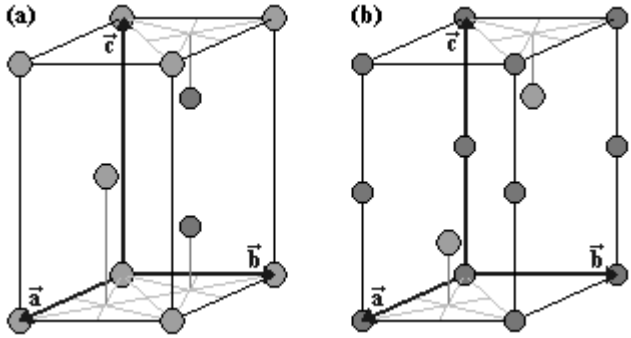

Figure 119 Two conventional unit cells for the NiAs structure: **(a)** with anions at the vertices and **(b)** with cations at the vertices.

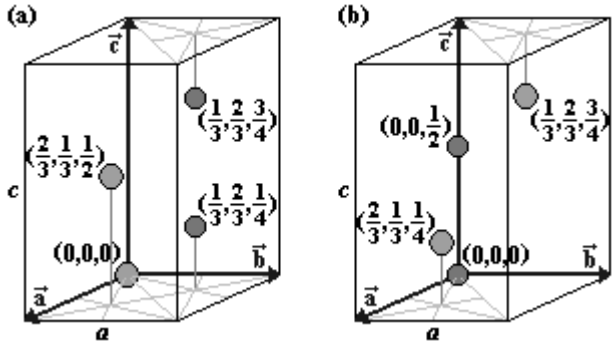

Figure 120 (a) and **(b)** show the positions of ions belonging to the unit cells from Figs. 119a and 119b, respectively. The coordinates are expressed in units of *a* and *c*.

and two cations. Figure 120 shows the coordinates, given with respect to the $\vec{a}$, $\vec{b}$, $\vec{c}$ axes, of the four ions belonging to each unit cell from Fig. 119.

Some binary compounds crystallize in the so called anti-NiAs structure that is the same as the NiAs structure, but with cations replaced by anions, and *vice versa*. Figure 121 shows the anti-NiAs structure on the example of the VP compound. We can see in this figure that now the vanadium cations form the *hcp* substructure, while the phosphorus anions are arranged in a simple hexagonal substructure.

In the NiAs structure crystallize compounds that contain TMs and elements from columns III, IV, V, or VI of the periodic table. The following compounds may be included:

Column III:
B: PtB*
Tl: NiTl

Column IV:
C: γ'-MoC**
Sn: FeSn, NiSn, CuSn, RhSn, PdSn, IrSn, PtSn, AuSn
Pb: NiPb, IrPb, PtPb*

Column V:
N: δ'-NbN,* ε-NbN**
P: TiP,** VP,* β-ZrP,** HfP**
As: α-TiAs,** β-TiAs,* MnAs, NiAs, α-ZrAs,** HfAs**
Sb: TiSb, VSb, CrSb, MnSb, FeSb, CoSb, NiSb, CuSb, PdSb, IrSb, PtSb
Bi: MnBi,* NiBi,* RhBi,* PtBi*

Column VI:
S: TiS, VS, CrS, β-FeS, CoS, α-NiS, NbS
Se: TiSe, VSe, CrSe, FeSe, CoSe, β-NiSe, RhSe, AuSe
Te: ScTe, TiTe, VTe, CrTe, α-MnTe, FeTe, CoTe, NiTe, ZrTe, RhTe, PdTe, IrTe
Po: MgPo**,** ScPo,* TiPo, NiPo, ZrPo, HfPo.

In the above classification, the compounds marked with one star crystallize in the anti-NiAs structure, whereas those marked with two stars in the TiAs structure, which will be discussed in the next section.

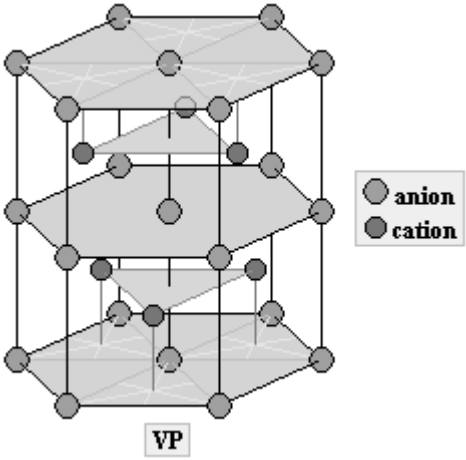

Figure 121 Anti-NiAs structure shown on the example of the VP compound.

Experimental lattice parameters for compounds that crystallize in the NiAs, anti-NiAs, or TiAs structures of TM-III, TM-IV, TM-V, and TM-VI types are listed in Tables 28–31, respectively. We can observe in Tables 28 and 29 that, with exception of γ'-MoC, all compounds crystallize with the c/a ratio much smaller than the ideal one ($\sqrt{8/3} = 1.633$). In the Table 30 more than half of the compounds contain metals from the group of iron. We can also observe in that table that the antimonides and bismuthides of TMs crystallize with the c/a ratio much smaller than the perfect one. In all such cases, the ions that occupy the octahedral interstices in the *hcp* substructure have indeed 8 NNs, like in the case of the Ni cation in NiAs.

We can observe in Table 31 that the iron group metals are present in more than $2/3$ of compounds listed there. The c/a ratios are in this table, for about half of the compounds, quite close to the ideal value, and the CrS, VSe, CrSe, FeSe, ScTe, α-MnTe, and MgPo compounds have the c/a ratio remarkably approaching that value.

Summarizing the data given in Tables 28-31, we can say that in the case of nickel arsenide related structures the values for c/a are in the wide range between 1.21 and 1.96. As a consequence the ions in these structures may have different number of NNs and NNNs. Let us see this on the example of a cation in the NiAs structure. For the lower-bound value of c/a each cation has 8 NNs (6 anions and 2 cations) and 6 cations as NNNs, while for the upper-bound value of the c/a ratio a cation in the NiAs structure has 6 anions as NNs and 8 NNNs (all of them cations).

Table 28 Lattice parameters, obtained under normal conditions, of PtB and NiTl that crystallize in the anti-NiAs and NiAs structures, respectively.

Compound	*a* (Å)	*c* (Å)	*c*/*a*
PtB*	3.358	4.058	1.21
NiTl	4.426	5.535	1.25

*anti-NiAs structure

Table 29 Lattice parameters obtained under normal conditions for compounds of TM-IV type that crystallize in the NiAs, anti-NiAs, or TiAs structures.

Compound	*a* (Å)	*c* (Å)	*c*/*a*	Compound	*a* (Å)	*c* (Å)	*c*/*a*
γ'-MoC**	2.932	10.97	2×1.87	**IrSn**	3.988	5.567	1.40
γ-FeSn	4.216	5.244	1.24	**PtSn**	4.104	5.436	1.32
NiSn	4.048	5.123	1.27	**AuSn**	4.3218	5.523	1.28
CuSn	4.198	5.096	1.21	**NiPb**	4.15	5.28	1.27
RhSn	4.340	5.553	1.28	**IrPb**	3.993	5.566	1.39
PdSn	4.378	5.627	1.29	**PtPb***	4.258	5.467	1.28

*anti-NiAs structure
**TiAs structure

Table 30 Lattice parameters obtained under normal conditions for compounds of TM-V type that crystallize in the NiAs, anti-NiAs, or TiAs structures.

Compound	*a* (Å)	*c* (Å)	*c*/*a*	Compound	*a* (Å)	*c* (Å)	*c*/*a*
δ´-NbN*	2.968	5.549	1.87	**CrSb**	4.115	5.493	1.33
ε-NbN**	2.9513	11.248	2×1.91	**MnSb**	4.140	5.789	1.40
TiP**	3.513	11.75	2×1.67	**FeSb**	4.072	5.140	1.26
VP*	3.178	6.222	1.96	**CoSb**	3.866	5.188	1.34
β-ZrP**	3.684	12.554	2×1.70	**NiSb**	3.9325	5.1351	1.31
HfP**	3.65	12.38	2×1.70	**CuSb**	3.874	5.193	1.34
α-TiAs**	3.642	12.064	2×1.66	**PdSb**	4.078	5.593	1.37
β-TiAs*	3.645	6.109	1.68	**IrSb**	3.978	5.521	1.39
MnAs	3.722	5.702	1.53	**PtSb**	4.126	5.481	1.33
NiAs	3.619	5.034	1.39	**MnBi***	4.290	6.126	1.43
α-ZrAs**	3.804	12.867	2×1.69	**NiBi***	4.07	5.33	1.31
HfAs**	3.765	12.680	2×1.68	**RhBi***	4.0894	5.6642	1.39
TiSb	4.1033	6.2836	1.53	**PtBi***	4.315	5.490	1.27
VSb	4.27	5.447	1.28				

*anti-NiAs structure
**TiAs structure

Table 31 Lattice parameters obtained under normal conditions for compounds of TM-VI type that crystallize in the NiAs or anti-NiAs structures. The values for MgPo are also included in the table.

Compound	*a* (Å)	*c* (Å)	*c*/*a*	Compound	*a* (Å)	*c* (Å)	*c*/*a*
TiS	3.299	6.380	1.93	**VTe**	3.942	6.126	1.55
VS	3.33	5.82	1.75	**CrTe**	3.978	6.228	1.57
CrS	3.419	5.55	1.62	**α-MnTe**	4.147	6.711	1.62
β-FeS	3.4436	5.8759	1.71	**FeTe**	3.800	5.651	1.49
CoS	3.374	5.187	1.54	**CoTe**	3.888	5.378	1.38
α-NiS	3.4395	5.3514	1.56	**NiTe**	3.965	5.358	1.35
NbS	3.32	6.46	1.95	**ZrTe**	3.953	6.647	1.68
TiSe	3.572	6.205	1.74	**RhTe**	3.987	5.661	1.42
VSe	3.66	5.95	1.63	**PdTe**	4.152	5.672	1.37
CrSe	3.71	6.03	1.63	**IrTe**	3.939	5.386	1.37
FeSe	3.62	5.92	1.64	**MgPo**	4.345	7.077	1.63
CoSe	3.62	5.286	1.46	**ScPo***	4.206	6.92	1.65
β-NiSe	3.6613	5.3562	1.46	**TiPo**	3.992	6.569	1.65
RhSe	3.642	5.486	1.51	**NiPo**	3.95	5.68	1.44
AuSe	4.12	5.39	1.31	**ZrPo**	4.031	6.907	1.71
ScTe	4.120	6.748	1.64	**HfPo**	4.058	6.717	1.66
TiTe	3.834	6.390	1.67				

*anti-NiAs structure

In the next section, we will describe the TiAs structure which is related to the NiAs structure.

6.2. TiAs Structure

Pearson symbol: *hP*8, Prototype: TiAs. In the TiAs structure, the anions are arranged in the *dhcp* substructure shown in Fig. 80 (Sec. III.8) and the cations occupy all octahedral interstices present in it. We can observe in Fig. 122 that the arrangement of ions in the down half of the hexagonal prism for the TiAs structure (see Fig. 122b) looks the same as the arrangement of ions in the hexagonal prism for the NiAs structure (see Fig. 122a). The sequence of the two-dimensional *hcp* layers in the TiAs structure is the following:

$$\mathbf{A_aA_cB_aA_cA_aB_cC_aB_cA_aA_cB_aA_cA_aB_cC_aB_c...},$$

where it is easy to separate the layer sequence $\mathbf{A_aB_aA_aC_aA_aB_aA_aC_a...}$ corresponding to the anion substructure from the layer sequence $\mathbf{A_cA_cB_cB_cA_cA_cB_cB_c...}$ for the cation substructure. In the last sequence, we can observe the presence of consecutive cation layers of both the same and different type, what marks the difference from the NiAs structure whose

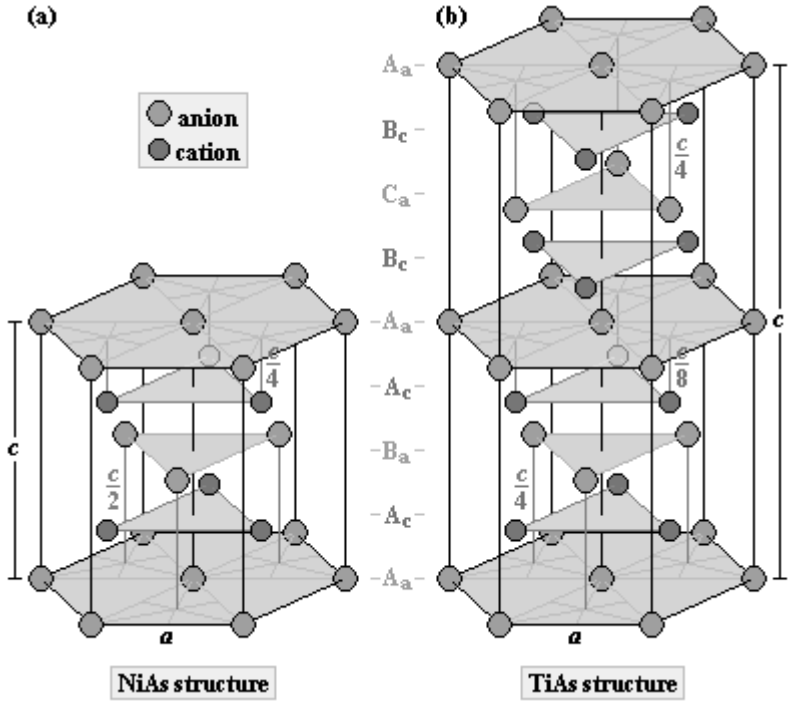

Figure 122 Hexagonal prisms: **(a)** for the NiAs structure and **(b)** for the TiAs structure. The lattice parameters, *a* and *c*, are shown in both cases.

cation substructure has all the layers of the same type. As a consequence, between consecutive layers of the TiAs cation substructure are present not only trigonal prism interstices, but also octahedral and tetrahedral interstices. Half of the trigonal prism interstices and all octahedral interstices are occupied by anions.

7. Sodium Chloride Structure

Pearson symbol: *cF*8, prototype: NaCl. We will now talk about the structure of sodium chloride. In those compounds that crystallize in this structure the ionic bonding prevails over the covalent one. Most of the binary compounds that have a high degree of ionicity in their bonds crystallize in this structure and among them the alkali halides which have over 90% of ionic contribution in their bonds.

In alkali halides the positive ion is one of the alkali metals (Li^+, Na^+, K^+, Rb^+, or Cs^+) and the negative ion is one of the halogens (F^-, Cl^-, Br^-, or I^-). Except for CsCl, CsBr, and CsI, all of them crystallize in the NaCl structure under normal conditions.

In the NaCl structure, each ion has six NNs and both, the anion and the cation, have their NNs at the vertices of a regular octahedron with the anion or cation in its center, what is shown, using as example the NaCl compound, in Fig. 123. The coordination number 6, which is higher than for the case of the zinc blende and wurtzite structures, allows to maximize the ionic bonding.

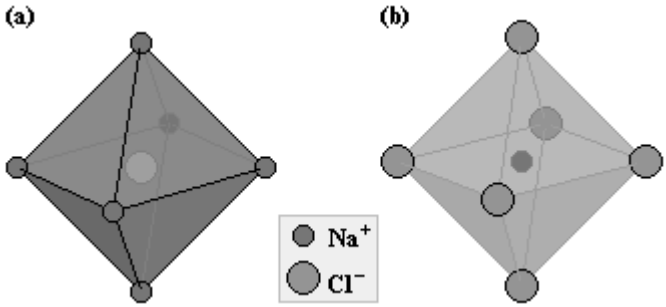

Figure 123 The structure of NaCl. **(a)** Regular octahedron defined by Na^+ cations with the Cl^- anion in its center. **(b)** Nearest neighbors of a Na^+ cation at the vertices of a regular octahedron.

The sodium chloride structure represents a sequence of two-dimensional hexagonal layers of

$$\mathbf{A_{Na}C_{Cl}B_{Na}A_{Cl}C_{Na}B_{Cl}A_{Na}C_{Cl}B_{Na}A_{Cl}C_{Na}B_{Cl}\ldots}$$

type. This sequence can be seen as a superposition of two subsequences of **ABCABC…** type, one for cations and another one for anions. The cation layers are displaced with respect to the anion layers in the way that each ion has 6 NNs.

Concluding, we can say that the NaCl structure is a superposition of two *fcc* substructures, each one for a given type of ions. Two cubic unit cells can reproduce this structure: one with anions at the vertices and the other one with cations at the vertices. These two cells are shown in Fig. 124a. In Fig. 124b, we show a rhombohedral unit cell with two ions (an anion

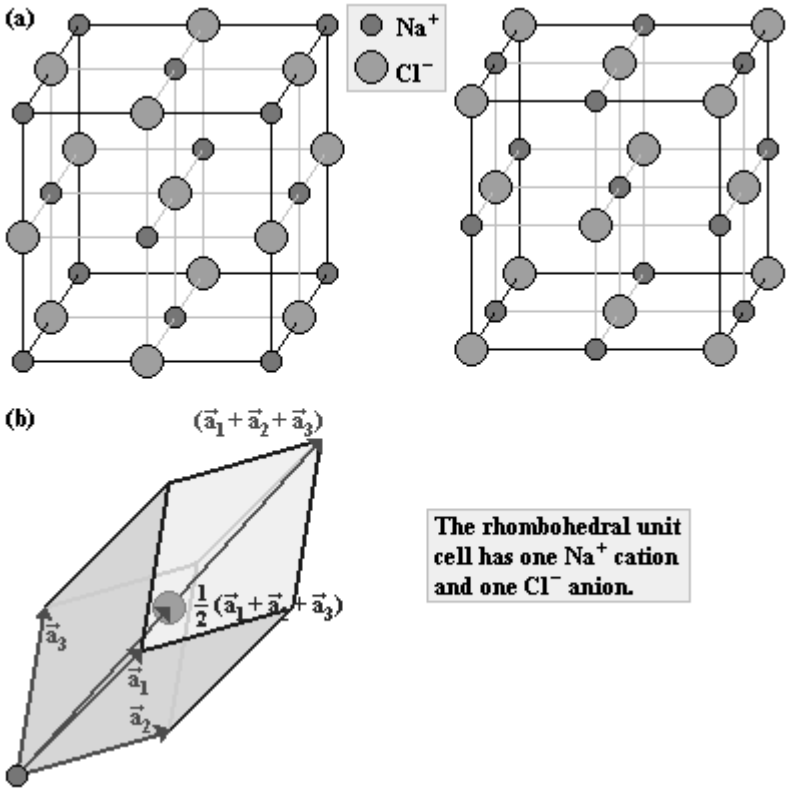

Figure 124 (a) Two cubic unit cells for the structure of sodium chloride: one with Na^+ cations at the vertices and the other one with Cl^- anions at the vertices. **(b)** A rhombohedral unit cell with two ions (one anion and one cation), which is the smallest unit cell that reproduces the NaCl structure.

and a cation) belonging to it, which is the smallest unit cell that reproduces the NaCl structure. The rhombohedron shown in Fig. 124b is the same as the primitive unit cell for the *fcc* lattice. Therefore, the sodium chloride structure can be considered a *fcc* Bravais lattice with two-atom basis consisting of one cation and one anion.

We can observe in Fig. 124a that the substructure of anions (cations) is displaced with respect to the substructure of cations (anions) along the cube edge by half of its lengths. Thus, an anion (cation) occupies an octahedral interstice in the cation (anion) substructure. Figure 125 illustrates the stacking of **A**, **B**, **C** layers for both types of ions in the cubic unit cell of NaCl. In this figure, the $\mathbf{A_{Na}C_{Cl}B_{Na}A_{Cl}C_{Na}B_{Cl}A_{Na}...}$ sequence of layers is shown. The layers are orthogonal to a body diagonal of the cube. In Fig. 126 we show the coordinates, given with respect to the $\vec{a}$, $\vec{b}$, $\vec{c}$ axes, of the eight ions belonging to the cubic unit cell shown on the left side of Fig. 124a.

In the next few tables we will list about 300 binary compounds that crystallize in the NaCl structure. This represents a significant percentage of the total number of compounds having that structure. We begin in Table 32 by report experimental lattice parameters for I-VII compounds and the silver halides. We can observe in this table that, with exception of CsCl, CsBr, and CsI, all other I-VII compounds have the NaCl structure. In Table 33 are given the lattice constants of II-VI, IV-VI, and V-VI compounds that crystallize in the NaCl structure. We can see in this table that nearly all compounds that contain one of the alkaline earth metals (magnesium, calcium, strontium, and barium) crystallize in this structure. In Tables 34 and 35 we report the lattice parameters for compounds of TM-VI, and TM-V

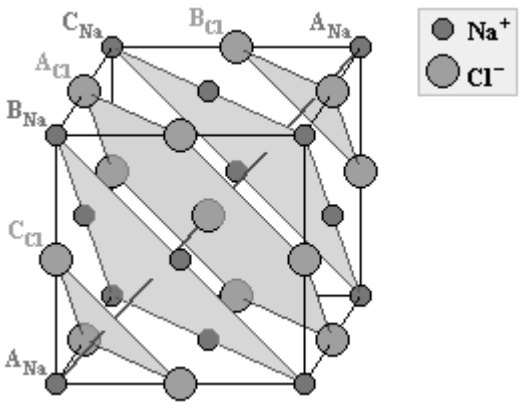

Figure 125 The sequence of two-dimensional hexagonal layers $\mathbf{A_{Na}}$, $\mathbf{B_{Na}}$, $\mathbf{C_{Na}}$, $\mathbf{A_{Cl}}$, $\mathbf{B_{Cl}}$, and $\mathbf{C_{Cl}}$ in the structure of NaCl.

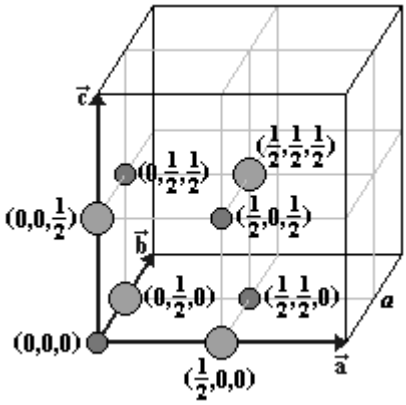

Figure 126 Positions of ions belonging to the cubic unit cell of the NaCl structure. The coordinates are expressed in units of *a*.

Table 32 Lattice parameters (in Angstroms), obtained under normal conditions, of alkali metal halides and silver halides that crystallize in the NaCl structure. In the table, it is also indicated which of the considered compounds crystallize in the CsCl or zinc blende structures.

	F	**Cl**	**Br**	**I**
Li	LiF (4.027)	LiCl (5.12952)	LiBr (5.5013)	α-LiI (6.0257)
Na	NaF (4.632)	NaCl (5.6401)	NaBr (5.9732)	NaI (6.4728)
K	KF (5.34758)	KCl (6.2952)	KBr (6.6005)	KI (7.0656)
Rb	RbF (5.6516)	RbCl (6.5810)	RbBr (6.889)	RbI (7.342)
Cs	CsF (6.014)	*CsCl*	*CsCl*	*CsCl*
Ag	AgF (4.92)	AgCl (5.5463)	AgBr (5.7721)	*zinc blende*

Table 33 Lattice parameters (in Angstroms), obtained under normal conditions, of II-VI and also some IV-VI and V-VI compounds that crystallize in the NaCl structure. In the table, it is also indicated which of the considered compounds crystallize in the wurtzite or NiAs structures.

	O	**S**	**Se**	**Te**	**Po**
Mg	MgO (4.2113)	MgS (5.20182)	MgSe (5.451)	*wurtzite*	*NiAs*
Ca	CaO (4.8105)	CaS (5.6948)	CaSe (5.916)	CaTe (6.356)	CaPo (6.514)
Sr	SrO (5.1615)	SrS (6.0198)	SrSe (6.2432)	SrTe (6.660)	SrPo (6.796)
Ba	BaO (5.539)	BaS (6.3875)	BaSe (6.593)	BaTe (7.0012)	BaPo (7.119)
Sn		SnS (5.80)	SnSe (5.99)	SnTe (6.320)	
Pb		PbS (5.9362)	PbSe (6.1243)	PbTe (6.4591)	PbPo (6.590)
Bi			BiSe (5.99)	BiTe (6.47)	

type, respectively. We can observe in Table 34 that nearly all chalcogenides of the RE metals and of the light actinides (thorium, uranium, neptunium, plutonium, and americium) crystallize in the NaCl structure. In this structure also crystallize oxides of the TMs, which are mainly from the iron group,

Table 34 Lattice parameters (in Angstroms) obtained under normal conditions for compounds of the TM-VI type that crystallize in the NaCl structure. In the table, it is also indicated which of the considered compounds crystallize in the NiAs or zinc blende structures.

	O	**S**	**Se**	**Te**	**Po**
Sc		ScS (5.19)	ScSe (5.398)	*NiAs*	*NiAs*
Ti	TiO (4.1766)	*NiAs*	*NiAs*	*NiAs*	*NiAs*
V	VO (4.073)	*NiAs*	*NiAs*	*NiAs*	
Cr	CrO (4.16)		*NiAs*	*NiAs*	
Mn	MnO (4.446)	α-MnS (5.2236)	α-MnSe (5.462)	*NiAs*	
Fe	FeO (4.326)	*NiAs*	*NiAs*	*NiAs*	
Co	CoO (4.264)	*NiAs*	*NiAs*	*NiAs*	
Ni	NiO (4.1771)	*NiAs*	*NiAs*	*NiAs*	*NiAs*
Y		YS (5.493)	YSe (5.711)	YTe (6.098)	
Zr	ZrO (4.62)	ZrS (5.1522)		*NiAs*	*NiAs*
Nb	NbO (4.212)	*NiAs*			
Rh			*NiAs*	*NiAs*	
Pd				*NiAs*	
Cd	CdO (4.6953)	*zinc blende*	*zinc blende*	*zinc blende*	*zinc blende*
Hf					*NiAs*
Ta	TaO (4.431)				
Ir				*NiAs*	
Pt	PtO (5.15)				
Au			*NiAs*		
Hg		*zinc blende*	*zinc blende*	*zinc blende*	HgPo (6.250)
La		LaS (5.854)	LaSe (6.066)	LaTe (6.429)	
Ce		CeS (5.779)	CeSe (5.9920)	CeTe (6.36)	
Pr		PrS (5.731)	PrSe (5.944)	PrTe (6.315)	
Nd		NdS (5.689)	NdSe (5.907)	NdTe (6.282)	
Sm	SmO (4.9883)	SmS (5.9718)	SmSe (6.202)	SmTe (6.594)	SmPo (6.724)
Eu	EuO (5.142)	EuS (5.9708)	EuSe (6.197)	EuTe (6.594)	EuPo (6.720)
Gd		GdS (5.565)	GdSe (5.76)	GdTe (6.139)	
Tb		TbS (5.5221)	TbSe (5.7438)	TbTe (6.1150)	TbPo (6.254)
Dy		DyS (5.489)	DySe (5.690)	DyTe (6.079)	DyPo (6.214)
Ho		HoS (5.465)	HoSe (5.680)	HoTe (6.049)	HoPo (6.200)
Er		ErS (5.422)	ErSe (5.656)	ErTe (6.063)	
Tm		TmS (5.412)	TmSe (5.688)	TmTe (6.346)	TmPo (6.256)
Yb	YbO (4.86)	YbS (5.687)	YbSe (5.9321)	YbTe (6.361)	YbPo (6.542)
Lu		LuS (5.355)	LuSe (5.572)	LuTe (5.953)	LuPo (6.159)
Th		ThS (5.6851)	ThSe (5.880)		
Pa	PaO (4.961)				
U	UO (4.92)	US (5.486)	USe (5.751)	UTe (6.155)	
Np	NpO (5.01)	NpS (5.527)	NpSe (5.8054)	NpTe (6.2039)	
Pu	PuO (4.958)	PuS (5.5412)	PuSe (5.7934)	PuTe (6.1774)	
Am	AmO (5.045)	AmS (5.592)		AmTe (6.176)	

Table 35 Lattice parameters (in Angstroms) obtained under normal conditions for the compounds of the TM-V type that crystallize in the NaCl structure. The data for some tin pnictides are also included. In addition, we indicate in the table which of the considered compounds crystallize in the NiAs or TiAs structures.

	N	**P**	**As**	**Sb**	**Bi**
Sc	ScN (4.44)	ScP (5.312)	ScAs (5.487)	ScSb (5.8517)	ScBi (5.954)
Ti	TiN (4.235)	*TiAs*	*NiAs and TiAs*	*NiAs*	
V	VN (4.1361)	*NiAs*		*NiAs*	
Cr	CrN (4.148)			*NiAs*	
Mn			*NiAs*	*NiAs*	*NiAs*
Fe				*NiAs*	
Co				*NiAs*	
Ni			*NiAs*	*NiAs*	*NiAs*
Cu				*NiAs*	
Y	YN (4.877)	YP (5.661)	YAs (5.786)	YSb (6.165)	YBi (6.256)
Zr	ZrN (4.585)	α-ZrP (5.263) *and TiAs*	β-ZrAs (5.4335) *and TiAs*		
Nb	δ-NbN (4.394), *NiAs, and TiAs*				
Rh					*NiAs*
Pd				*NiAs*	
Hf	HfN (4.52)	*TiAs*	*TiAs*		
Ta	*NiAs*				
Ir				*NiAs*	
Pt				*NiAs*	*NiAs*
La	LaN (5.301)	LaP (6.0346)	LaAs (6.151)	LaSb (6.490)	LaBi (6.578)
Ce	CeN (5.020)	CeP (5.909)	CeAs (6.072)	CeSb (6.420)	CeBi (6.5055)
Pr	PrN (5.155)	PrP (5.903)	PrAs (6.009)	PrSb (6.375)	PrBi (6.4631)
Nd	NdN (5.132)	NdP (5.838)	NdAs (5.9946)	NdSb (6.321)	NdBi (6.4222)
Sm	SmN (5.0481)	SmP (5.760)	SmAs (5.921)	SmSb (6.271)	SmBi (6.3582)
Eu	EuN (5.017)	EuP (5.7562)			
Gd	GdN (4.9987)	GdP (5.723)	GdAs (5.854)	GdSb (6.217)	GdBi (6.3108)
Tb	TbN (4.9344)	TbP (5.688)	TbAs (5.824)	TbSb (6.178)	TbBi (6.2759)
Dy	DyN (4.9044)	DyP (5.653)	DyAs (5.794)	DySb (6.154)	DyBi (6.2491)
Ho	HoN (4.8753)	HoP (5.626)	HoAs (5.769)	HoSb (6.131)	HoBi (6.228)
Er	ErN (4.842)	ErP (5.606)	ErAs (5.7427)	ErSb (6.106)	ErBi (6.2023)
Tm	TmN (4.8021)	TmP (5.573)	TmAs (5.711)	TmSb (6.087)	TmBi (6.1878)
Yb	YbN (4.7852)	YbP (5.555)	YbAs (5.698)	YbSb (6.079)	
Lu	LuN (4.7599)	LuP (5.533)	LuAs (5.680)	LuSb (6.0555)	LuBi (6.156)
Th	ThN (5.1666)	ThP (5.8324)	ThAs (5.978)	ThSb (6.318)	
Pa			PaAs (5.7560)		
U	UN (4.890)	UP (5.5883)	UAs (5.7767)	USb (6.203)	UBi (6.3627)
Np	NpN (4.897)	NpP (5.6148)	NpAs (5.8366)	NpSb (6.2517)	NpBi (6.370)
Pu	PuN (4.9049)	PuP (5.6613)	PuAs (5.8565)	PuSb (6.2375)	PuBi (6.2039)
Am	AmN (5.005)	AmP (5.7114)	AmAs (5.876)	AmSb (6.240)	AmBi (6.332)
Sn		SnP (5.5359)	SnAs (5.716)	SnSb (6.130)	

and oxides of the actinides mentioned above. In Table 34 we can also observe that the chalcogenides of TMs that are not RE metals often crystallize in the NiAs structure. Among compounds of the TM-VI type, there is also a small group of compounds that crystallize in the zinc blende structure, like CdPo and cadmium and mercury chalcogenides.

Similarly as in Table 34 are organized the experimental data in Table 35 for TM nitrides, phosphides, arsenides, antimonides, and bismuthides. As was the case in Table 34, in this table the compounds of the RE metals and that of the actinides crystallize in the NaCl structure, while those that contain other TMs prefer to crystallize in structures different from NaCl (NiAs or TiAs). Besides the values given in Tables 32-35, below we also list the lattice constants for alkali and some TM hydrides and also for TM borides and carbides:

Hydrides: LiH (4.0856 Å), NaH (4.880 Å), KH (5.704 Å), RbH (6.037 Å), CsH (6.376 Å), NiH (3.740 Å), and PdH (4.02 Å)

Borides: ZrB (4.65 Å), HfB (4.62 Å), and PuB (4.905 Å)

Carbides: ScC (4.51 Å), TiC (4.3186 Å), VC (4.182 Å), CrC (4.03 Å), ZrC (4.6828 Å), NbC (4.4691 Å), CeC (5.135 Å), HfC (4.63765 Å), TaC (4.4540 Å), ThC (5.346 Å), PaC (5.0608 Å), UC (4.9606 Å), NpC (5.005 Å), and PuC (4.731 Å).

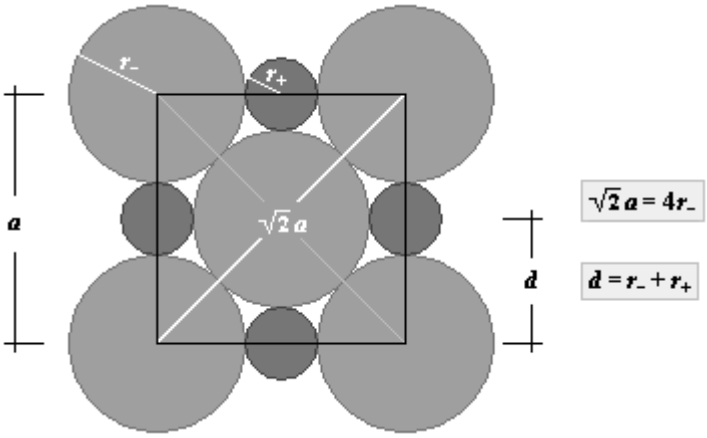

Figure 127 The plane of a face of the NaCl cubic unit cell with the cross sections of 9 ions considered hard spheres. The large ion, located in the center of the face, makes contact with its NNs (small spheres) and also with the NNNs (large spheres). The NN distance, *d*, is equal to the sum of the ionic radii, $r_- + r_+$.

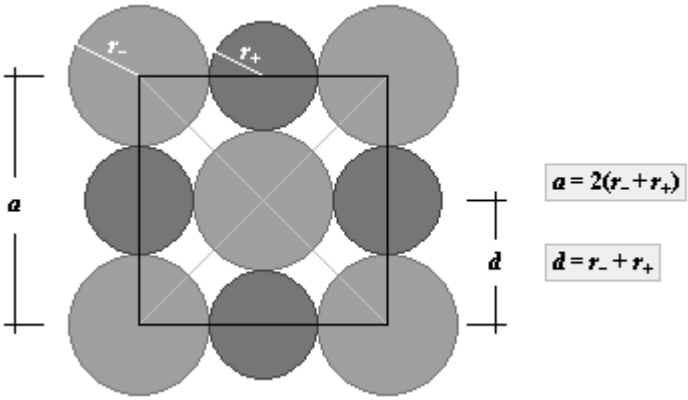

Figure 128 The same plane as in Fig. 127, but now the large ion, located in the center of the cube face, makes contact only with the NNs (small spheres). The NN distance, *d*, is equal to $r_- + r_+$.

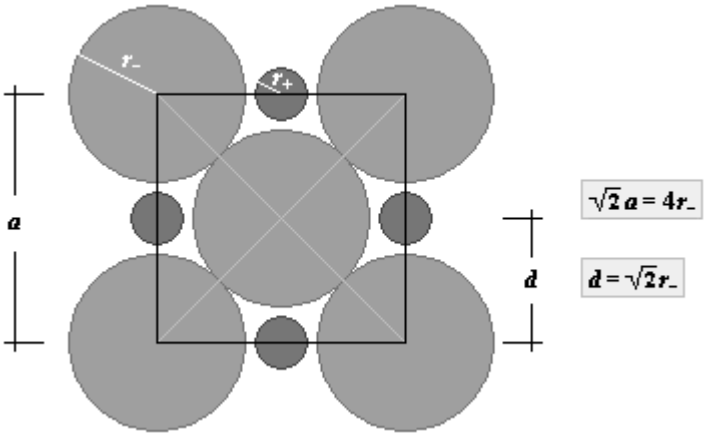

Figure 129 The same plane as in Figs. 127 and 128, but now the smaller ion is too small to make contact with larger ions and as a consequence the ion located in the center of the cube face makes contact only with its NNNs (large spheres). The NN distance, $d = \sqrt{2}r_-$, is defined only by the radius of the larger ion.

Let us now proceed to calculate the limiting radius ratio for the NaCl structure. We can see in Fig. 124a that 4 NNs of the Cl^- ion, placed in the center of a cubic unit cell face, are located in the centers of the face edges. Figures 127, 128, and 129 show the plane of one of the faces of the cube with cross sections of ions that, being considered hard spheres, are represented by circles on this plane. We can easily distinguish the following three cases:

a.) Each anion makes contact with its NNs (cations) and with the nearest anions as is shown in Fig. 127.
b.) Each anion makes contact only with its NNs (cations), see Fig. 128.
c.) Each anion makes contact only with the nearest anions as is illustrated in Fig. 129.

We will now proceed to calculate the r_+/r_- ratio for the case described in Fig. 127. We can see in this figure, that

$$2r_- + 2r_+ = a\,, \tag{IV.9}$$

as

$$\sqrt{2}a = 4r_-\,, \tag{IV.10}$$

then

$$2r_- + 2r_+ = \frac{4r_-}{\sqrt{2}} = 2\sqrt{2}r_- \tag{IV.11}$$

and finally

$$\frac{r_+}{r_-} = \sqrt{2} - 1 \cong 0.414\,. \tag{IV.12}$$

When $r_+/r_- = 0.414$, each anion touches both its NNs (cations) and the NNNs (anions). This is the limiting radius ratio for the NaCl structure which was already reported in Table 18. When the radius ratio is higher than the limiting one,

$$\frac{r_+}{r_-} > 0.414\,, \tag{IV.13}$$

each large ion makes contact only with the NNs (small ions) but not with the NNNs (see Fig. 128) and the structure is stable. In the opposite case, when the radius ratio is smaller than the limiting one, each large ion is in contact only with the NNNs (see Fig. 129). However, in principle, this situation would lead to a less stable structure and in this case a lower coordination number is expected.

We can see in Table 36, in which are given the data for alkali halides, that the listed there radius ratios are smaller than the limiting one,

$$\frac{r_+}{r_-} < 0.414\,, \tag{IV.14}$$

only for LiBr and LiI. In the rest of the alkali halides that have the NaCl structure, each ion touches its NNs that are of opposite sign. We can also observe in this table that in the case of KF, RbF, and CsF compounds the cation radius is larger than the anion radius and, as a consequence, the condition

$$\frac{r_-}{r_+} > 0.414 \tag{IV.15}$$

has to be considered instead of the condition given by Eq. (IV.13).

In Table 36 we list values for r_+/r_- or r_-/r_+ and $r_- + r_+$ or $\sqrt{2}r_-$, depending on the case in consideration. Those values were calculated using ionic radii given in the table. Table 36 contains also values for the distances, $d = a/2$, between the NNs, obtained using experimental lattice constants taken from Table 32. In those cases when the NNs touch each other, d should fulfill the equality

$$r_- + r_+ = d\,, \tag{IV.16}$$

what indeed happens to within 2% (see Table 36). This validates the concept of ionic radii, since the same radii can be used to calculate the interatomic distances for several compounds and those distances are very close to the experimental values obtained from the lattice constants.

In cases when the large ion makes contact only with its NNNs $(r_+/r_- < 0.414)$, the distance to the NNs fulfills the following equality

$$\sqrt{2}r_- = d\,. \tag{IV.17}$$

This happens with very good accuracy for LiBr, and LiI (see Table 36).

Finally, we can observe in Table 36 that about half of the compounds considered there have their ionic radius ratios r_+/r_- (or r_-/r_+) in the range from 0.414 to 0.732, which is the expected range for the NaCl structure (see Table 18). The LiBr and LiI compounds represent the exceptions, for which the zinc blende structure (or wurtzite) is predicted according to the ranges for ionic radius ratios listed in Table 18. The other exceptions, NaF, KF,

Table 36 Several values for alkali halides: **a.)** cation and anion radii (below the ion symbols), **b.)** ionic radius ratios (r_+/r_- or r_-/r_+), **c.)** sums of the ionic radii ($r_- + r_+$) in cases when $r_+/r_- > 0.414$ or $\sqrt{2}r_-$ in cases when $r_+/r_- < 0.414$, and **d.)** experimental values for the NN distances, $d = a/2$, where the lattice constants, a, are given in Table 32.

	Li^+ (0.76 Å)	**Na^+ (1.02 Å)**	**K^+ (1.38 Å)**	**Rb^+ (1.52 Å)**	**Cs^+ (1.67 Å)**
F^- (1.33 Å)	$\boldsymbol{r_+/r_- = 0.57}$ $r_- + r_+ = 2.09$ $d = 2.01$	$\boldsymbol{r_+/r_- = 0.77}$ $r_- + r_+ = 2.35$ $d = 2.32$	$\boldsymbol{r_-/r_+ = 0.96}$ $r_- + r_+ = 2.71$ $d = 2.67$	$\boldsymbol{r_-/r_+ = 0.88}$ $r_- + r_+ = 2.85$ $d = 2.83$	$\boldsymbol{r_-/r_+ = 0.80}$ $r_- + r_+ = 3.00$ $d = 3.01$
Cl^- (1.81 Å)	$\boldsymbol{r_+/r_- = 0.42}$ $r_- + r_+ = 2.57$ $d = 2.56$	$\boldsymbol{r_+/r_- = 0.56}$ $r_- + r_+ = 2.83$ $d = 2.82$	$\boldsymbol{r_+/r_- = 0.76}$ $r_- + r_+ = 3.19$ $d = 3.15$	$\boldsymbol{r_+/r_- = 0.84}$ $r_- + r_+ = 3.33$ $d = 3.29$	*cesium chloride structures*
Br^- (1.96 Å)	$\boldsymbol{r_+/r_- = 0.39}$ $\sqrt{2}r_- = 2.77$ $d = 2.75$	$\boldsymbol{r_+/r_- = 0.52}$ $r_- + r_+ = 2.98$ $d = 2.99$	$\boldsymbol{r_+/r_- = 0.70}$ $r_- + r_+ = 3.34$ $d = 3.30$	$\boldsymbol{r_+/r_- = 0.78}$ $r_- + r_+ = 3.48$ $d = 1.44$	
I^- (2.20 Å)	$\boldsymbol{r_+/r_- = 0.35}$ $\sqrt{2}r_- = 3.11$ $d = 3.01$	$\boldsymbol{r_+/r_- = 0.46}$ $r_- + r_+ = 3.22$ $d = 3.24$	$\boldsymbol{r_+/r_- = 0.63}$ $r_- + r_+ = 3.58$ $d = 3.53$	$\boldsymbol{r_+/r_- = 0.69}$ $r_- + r_+ = 3.72$ $d = 3.67$	

RbF, CsF, KCl, RbCl, and RbBr, have the radius ratios within the range corresponding to the CsCl structure.

In this section, we have learned that, among many other compounds, in the NaCl structure crystallize compounds of doubly ionized elements from columns II and VI of the periodic table, except for the beryllium compounds and MgTe. Geometric considerations, similar to that made for alkali halides, show that also in the case of II-VI compounds having the NaCl structure their ions may be considered, in good approximation, as hard impenetrable spheres of definite radii.

8. Cesium Chloride Structure

Pearson symbol: *cI*2, prototype: CsCl. In the NaCl structure (discussed in the previous section), the smaller in general cations are located in octahedral interstices (defined by 6 anions) present in the anionic *fcc* substructure. With the increase of the r_+/r_- ratio, a cubic interstice defined by 8 anions becomes a better option for the cations. This is the case of the cesium chloride (CsCl) structure, for which the limiting radius ratio is 0.732. The CsCl structure is a superposition of two simple cubic substructures. Both the cations and the anions occupy the cubic interstices present in each

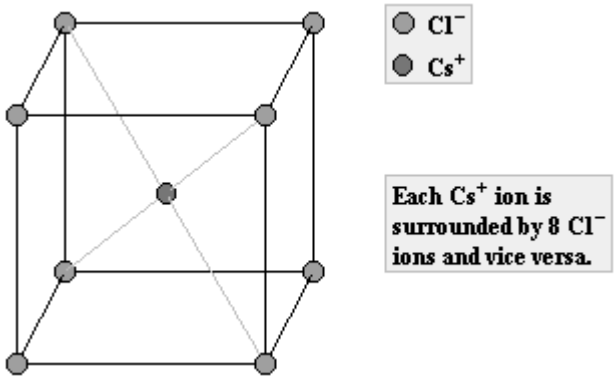

Figure 130 Conventional unit cell for cesium chloride.

substructure. In Fig. 130 we show the smallest unit cell for CsCl. The cell is a cube with one type of ions at the vertices and an opposite ion in the center.

One of the two principal groups of compounds that, under normal conditions, crystallize in the CsCl structure is formed by three cesium halides: CsBr, CsCl, and CsI, and also three thallium halides: TlBr, TlCl, and TlI. We can see in Table 36 that CsBr, CsCl, and CsI are the halides of the largest univalent ions (remember that these ions have somewhat different radii in the case of the coordination number 8). The other numerous group of

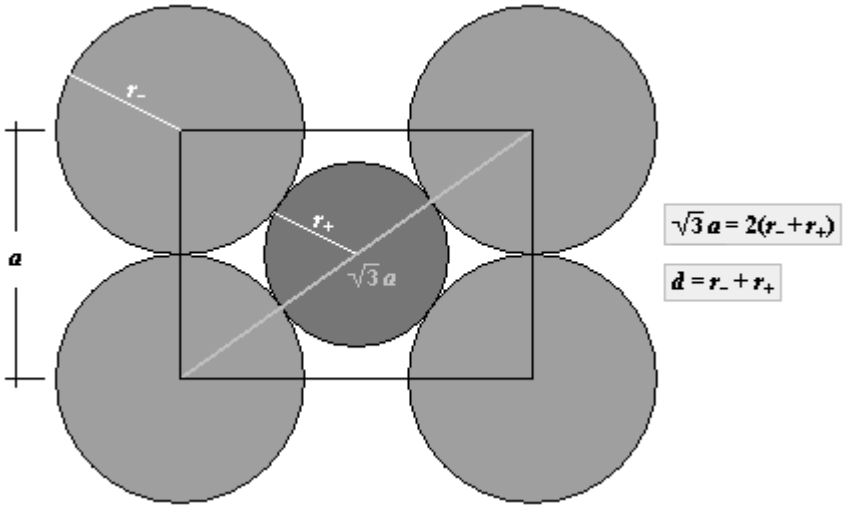

Figure 131 A plane defined by two body diagonals of the cube shown in Fig. 130. In this plane, there are the points of contact between the cation and its four NNs.

Table 37 Lattice parameters, obtained under normal conditions, of cesium and thallium halides that crystallize in the CsCl structure.

Compound	*a* (Å)	Compound	*a* (Å)
CsBr	4.286	**TlBr**	3.970
CsCl	4.123	**TlCl**	3.834
CsI	4.567	**TlI**	4.205

Table 38 Lattice parameters (in Angstroms) obtained under normal conditions for intermetallic compounds of the RE-Mg or RE-III type that crystallize in the CsCl structure. The elements in the compound symbols are listed alphabetically.

	Mg	Al	In	Tl
Sc	MgSc (3.597)	AlSc (3.450)		
Y	MgY (3.79)	AlY (3.754)	InY (3.806)	TlY (3.751)
La	LaMg (3.965)		InLa (3.985)	LaTl (3.922)
Ce	CeMg (3.899)	AlCe (3.86)		CeTl (3.893)
Pr	MgPr (3.888)	AlPr (3.82)	InPr (3.955)	PrTl (3.869)
Nd	MgNd (3.867)	AlNd (3.73)		NdTl (3.848)
Sm	MgSm (3.848)	AlSm (3.739)	InSm (3.815)	SmTl (3.813)
Eu				EuTl (3.975)
Gd	GdMg (3.824)	AlGd (3.7208)	GdIn (3.830)	GdTl (3.7797)
Tb	MgTb (3.784)			TbTl (3.760)
Dy	DyMg (3.776)	AlDy (3.6826)	DyIn (3.7866)	DyTl (3.743)
Ho	HoMg (3.770)		HoIn (3.774)	HoTl (3.735)
Er	ErMg (3.758)		ErIn (3.745)	ErTl (3.715)
Tm	MgTm (3.744)		InTm (3.737)	TlTm (3.711)
Yb			InYb (3.8138)	TlYb (3.826)
Lu	LuMg (3.727)			

compounds that crystallize in the CsCl structure is formed by intermetallic compounds.

Let us now calculate the limiting radius ratio for the CsCl structure. As in the case of the *bcc* structure, the ions that are at the vertices of the cube are the NNs of the ion that is in the center of the cube. Figure 131 shows a plane defined by two body diagonals of the cube with the cross section of a cation placed in the center and the cross sections of four anions placed at the vertices of the cube. We can see in the figure that the points of contact between the cation and the anions are on the body diagonals of the cube.

We can see in Fig. 131 that

$$2r_- + 2r_+ = \sqrt{3}a\,, \qquad \text{(IV.18)}$$

as $a = 2r_-$ then

$$2r_- + 2r_+ = 2\sqrt{3}r_- \qquad \text{(IV.19)}$$

and finally

$$\frac{r_+}{r_-} = \sqrt{3} - 1 \cong 0.732\,. \qquad \text{(IV.20)}$$

Table 39 Lattice parameters (in Angstroms) obtained under normal conditions for intermetallic compounds of the RE-TM type that crystallize in the CsCl structure. The elements in the compound symbols are listed alphabetically.

	Cu	**Zn**	**Rh**	**Ag**	**Cd**	**Au**	**Hg**
Sc	CuSc 3.256	ScZn 3.35	RhSc 3.206	AgSc 3.412	CdSc 3.513	AuSc 3.370	HgSc 3.480
Y	CuY 3.4757	YZn 3.577	RhY 3.410	AgY 3.6196	CdY 3.719	AuY 3.559	HgY 3.682
La		LaZn 3.759		AgLa 3.814	CdLa 3.904		HgLa 3.845
Ce		CeZn 3.696		AgCe 3.755	CdCe 3.855		CeHg 3.815
Pr		PrZn 3.678		AgPr 3.746	CdPr 3.829	AuPr 3.68	HgPr 3.799
Nd		NdZn 3.667		AgNd 3.716	CdNd 3.819	AuNd 3.659	HgNd 3.780
Sm	CuSm 3.528	SmZn 3.627	RhSm 3.466	AgSm 3.673	CdSm 3.779	AuSm 3.621	HgSm 3.744
Eu	CuEu 3.479	EuZn 3.808			CdEu 3.951		EuHg 3.880
Gd	CuGd 3.501	GdZn 3.609	GdRh 3.435	AgGd 3.6491	CdGd 3.748	AuGd 3.6009	GdHg 3.719
Tb	CuTb 3.480	TbZn 3.576	RhTb 3.417	AgTb 3.627	CdTb 3.723	AuTb 3.576	HgTb 3.678
Dy	CuDy 3.462	DyZn 3.562	DyRh 3.403	AgDy 3.609	CdDy 3.716	AuDy 3.555	DyHg 3.676
Ho	CuHo 3.445	HoZn 3.548	HoRh 3.377	AgHo 3.601	CdHo 3.701	AuHo 3.541	HgHo 3.660
Er	CuEr 3.430	ErZn 3.532	ErRh 3.361	AgEr 3.574	CdEr 3.685	AuEr 3.5346	ErHg 3.645
Tm	CuTm 3.414	TmZn 3.516	RhTm 3.358	AgTm 3.562	CdTm 3.663	AuTm 3.516	HgTm 3.632
Yb		YbZn 3.629	RhYb 3.347	AgYb 3.6787	CdYb 3.8086	AuYb 3.5634	HgYb 3.735
Lu		LuZn 3.491	LuRh 3.334		CdLu 3.640	AuLu 3.4955	HgLu 3.607

Table 40 Lattice parameters obtained under normal conditions for intermetallic compounds that crystallize in the CsCl structure. The elements are listed alphabetically in those compounds where at least one of the elements is a TM.

Compound	*a* (Å)	Compound	*a* (Å)	Compound	*a* (Å)
β-AgCd	3.332	**CaTl**	3.851	**HoIr***	3.383
AgGa	3.171	**CdSr**	4.003	**InNi**	3.093
β-AgLi	3.168	**CoFe**	2.857	**InPd**	3.246
β-AgMg	3.124	**CoGa**	2.880	**IrLu***	3.332
β-AgZn	3.1558	**CoHf**	3.164	**IrSc***	3.205
β-AlCo	2.864	**CoSc***	3.145	**LiTl**	3.435
AlFe	2.908	**CoTi**	2.995	**LuPd***	3.415
AlIr	2.983	**CoZr**	3.181	**MgRh**	3.099
β-AlNi	2.882	**β-CuPd**	2.988	**MgSr**	3.908
AlOs	3.001	**β-CuZn**	2.950	**MgTl**	3.635
AuCd	3.3232	**CuZr**	3.2620	**β-MnRh**	3.044
AuCs	4.262	**FeRh**	2.983	**NiSc***	3.171
AuMg	3.266	**FeTi**	2.976	**NiTi**	3.01
β-AuZn	3.1485	**FeV**	2.910	**OsTi**	3.07
BaCd	4.207	**GaIr**	3.004	**PdSc***	3.282
BaHg	4.125	**β-GaNi**	2.886	**PtSc***	3.268
BeCo	2.624	**GaRh**	3.0063	**RuSc***	3.203
BeCu	2.702	**GaRu**	3.010	**RuTi**	3.06
BeNi	2.6121	**HgLi**	3.287	**SrTl**	4.038
BePd	2.813	**HgMg**	3.448	**TlBi**	3.98
BeRh	2.740	**HgMn**	3.316	**ZnZr**	3.336
CaHg	3.759	**HgSr**	3.930		

*Intermetallic binary compounds where one of the elements is a RE metal

Equation (IV.20) gives the value for the limiting radius ratio for the CsCl structure. This value was already included in Table 18. In that limiting case each anion touches both its NNs (cations) and the NNNs (anions).

In Tables 37–40 we list the data for about 200 compounds that crystallize in the CsCl structure. Table 37 gives the lattice parameters for cesium and thallium halides, while Tables 38–40 report the data for intermetallic compounds. In those intermetallic compounds that are listed in Tables 38 and 39 one of the metallic elements is a RE metal. We can observe in these tables that the number of such compounds is significant. In the case of the intermetallic compounds in which at least one of the elements is a TM, we adopted the convention according to which the elements in compound symbols are listed alphabetically.

9. Problems

Exercise 1 How many cations and anions do belong to the cubic unit cell of the zinc blende structure? Draw this cell and the ions belonging to it. Find the position of each ion expressing its coordinates in units of the lattice constant a.

Exercise 2 Repeat Exercise 1, but now for the fluorite structure.

Exercise 3 Table 27 lists the distances of an ion to the NNs in MnSe, MnTe, ZnSe, CdSe, and GaN, for two crystal structures: zinc blende and wurtzite. These distances have been obtained using experimental lattice constants. Make a similar table with the distances, d_{NNN}, of an ion to the NNNs. Express, in percentage, the difference between d_{NNN} obtained for the zinc blende and wurtzite structures. In your calculations use the experimental lattice constants listed in Tables 20, 21, and 26.

Exercise 4

a.) Draw a hexagonal prism for β-ZnS, which crystallizes in the zinc blende structure. This prism should be able to reproduce the β-ZnS structure. Show on the figure two-dimensional *hcp* layers $\mathbf{A_{Zn}}$, $\mathbf{B_{Zn}}$, $\mathbf{C_{Zn}}$ and $\mathbf{A_S}$, $\mathbf{B_S}$, $\mathbf{C_S}$, and the distances between the consecutive layers.

***Hint*:** Similar work was done in Fig. 113 for the wurtzite structure of ZnS. See also Figs. 82, 94, and 95.

b.) How many ions of each type do belong to the hexagonal prism you have drawn in a.) and how many ions do belong to the hexagonal prism for the wurtzite structure?

Exercise 5 Let us consider 8 and 12 closest cations to a given cation in the NiAs and anti-NiAs structures, respectively. In the case of the NiAs structure the 8 cations can be divided, according to the distance to the cation in consideration, into two groups of 2 and 6 ions which are closer and more distant to the cation, respectively. Using similar criterion, the 12 cations considered in the anti-NiAs structure can be divided into two groups of 6 ions each. In each case the distances depend on the lattice constant ratio c/a.

a.) For the following compounds: VSb ($c/a = 1.28$), VSe ($c/a = 1.63$), VS ($c/a = 1.75$), and TiS ($c/a = 1.93$), that crystallize in the NiAs structure, calculate the two closest cation-cation distances, d^{I}_{VV} and

d^{II}_{VV} (or d^{I}_{TiTi} and d^{II}_{TiTi}). For each compound, compare the obtained distances expressing the difference in percentage. How does this difference change with the increase of the c/a ratio? How many NNNs has a cation in each compound? Use the lattice constants a and c from Table 30 for VSb and from Table 31 for TiS, VS, and VSe.

***Hint*:** When calculating the number of NNNs assume that whenever d^{I}_{VV} and d^{II}_{VV} (or d^{I}_{TiTi} and d^{II}_{TiTi}) differ by less than 10%, then the ions at both distances are NNNs. On the other hand, if the shortest distance differs from the distance of a cation to its nearest anions by less than 10%, then the cations at such a distance join the group of NNs of the cation in consideration.

b.) Do a similar work as in a.) for the anti-NiAs structure on the example of the following compounds: PtB ($c/a = 1.21$), ScPo ($c/a = 1.65$), δ'-NbN ($c/a = 1.87$), and VP ($c/a = 1.96$). How many NNNs has each Pt ion in the PtB compound (and also V ion in the VP compound)? To which two-dimensional *hcp* layer do those ions belong? Answer similar questions for the ScPo and δ'-NbN compounds. Use lattice constants a and c from Table 28 for PtB, from Table 30 for δ'-NbN and VP, and from Table 31 for ScPo.

***Hint*:** To determine the number of the NNNs of a given cation use the criterions suggested in the *Hint* of a.).

Exercise 6 In the case when the lattice constant ratio c/a is much smaller than 1.633, each cation in the NiAs structure has indeed 8 NNs: 6 anions and 2 cations.

a.) Show that the above is true, to within 3% of the NN interatomic distance, for the following compounds: CuSb ($c/a = 1.34$), PdSb ($c/a = 1.37$), IrSb ($c/a = 1.39$), and IrTe ($c/a = 1.37$). Use lattice constants a and c from Table 30 for CuSb, PdSb, and IrSb and from Table 31 for IrTe.

b.) Compare the cation-cation distances d_{CuCu}, d_{PdPd}, and d_{IrIr}, calculated in a.), with the distances $d^{element}_{\mathrm{CuCu}}$, $d^{element}_{\mathrm{PdPd}}$, and $d^{element}_{\mathrm{IrIr}}$, respectively, between Cu, Pd, and Ir NNs in the crystals of these elements. Confirm that in each case d_{XX} differ from $d^{element}_{\mathrm{XX}}$ by less than 2%. Use the NN interatomic distances for elements, listed in Table 16.

Exercise 7 Tables 30 and 35 report the experimental data obtained under normal conditions for ZrP in the beta (TiAs structure) and alpha (NaCl structure) phases, respectively.

a.) Calculate and compare the distances $d_{\mathrm{ZrP}}^{\mathrm{NaCl}}$ and $d_{\mathrm{ZrP}}^{\mathrm{TiAs}}$ between the NNs in the two structures.

b.) Calculate the distance, $d_{\mathrm{ZrZr}}^{\mathrm{NaCl}}$, between the NNNs in α-ZrP. Calculate also the distances $d_{\mathrm{ZrZr}}^{\mathrm{TiAs}}$ between a given Zr ion and the 10 closest Zr ions to it in β-ZrP. Compare the obtained distances with $d_{\mathrm{ZrZr}}^{\mathrm{NaCl}}$, expressing the differences in percentage. When making comparisons take into account the number of ions at each distance.

Exercise 8 Tables 30 and 35 report the experimental data obtained under normal conditions for δ'-NbN (anti-NiAs structure) and ε-NbN (TiAs structure), and δ-NbN (NaCl structure), respectively.

a.) Calculate and compare the NN distances: $d_{\mathrm{NbN}}^{\mathrm{NaCl}}$, $d_{\mathrm{NbN}}^{\mathrm{NiAs}}$, and $d_{\mathrm{NbN}}^{\mathrm{TiAs}}$, for the three structures.

b.) Calculate the distance between the NNNs in δ-NbN. Calculate also the two and three closest distances between the Nb ions in the anti-NiAs and TiAs structures, respectively.

***Hint*:** Draw the hexagonal prism with the Nb cations in its vertices to visualize better the location of the NNNs of a cation in the anti-NiAs structure.

c.) Compare the two distances obtained in b.) for the case of the anti-NiAs structure with the distance between the nearest Nb ions in δ-NbN. When making comparisons take into account the number of ions at each distance.

d.) Do the same as in c.) for NbN in the TiAs structure. Note that for this structure you have to consider the three closest distances between the Nb ions.

Exercise 9 Find the filling factors for the following compounds that crystallize in the NaCl structure: LiCl ($r_+/r_- = 0.42$), NaCl ($r_+/r_- = 0.56$), RbCl ($r_+/r_- = 0.84$), and KF ($r_-/r_+ = 0.96$). The cation radii, r_+, and the anion radii, r_-, are listed in Table 36 and the lattice parameters a for I-VII compounds are listed in Table 32.

a.) What is the relation between the values for the filling factor and the r_+/r_- (or r_-/r_+) ratio?

b.) What would be the value of the filling factor in the case when $r_+/r_- = 1$? Answer without doing any calculations.

Exercise 10 Prepare a similar table to Table 36 for II-VI compounds that crystallize in the NaCl structure. The radii of the double ionized elements from column II of the periodic table are: 0.72 Å for Mg^{2+}, 1.00 Å for Ca^{2+}, 1.18 Å for Sr^{2+}, and 1.35 Å for Ba^{2+}, and the radii for the double ionized elements from column VI are: 1.40 Å for O^{2-}, 1.84 Å for S^{2-}, 1.98 Å for Se^{2-}, and 2.21 Å for Te^{2-}. Show that the interatomic distance, *d*, expressed by the sum of ionic radii, $r_- + r_+$, if $r_+/r_- > 0.414$, or by $\sqrt{2}r_-$, if $r_+/r_- < 0.414$, agree to within 2% with the value obtained from the experimental lattice constant ($d = a/2$). The lattice parameters *a* for II-VI compounds are listed in Table 33.

V. RECIPROCAL LATTICE

1. Introduction

Crystal structures considered in previous chapters correspond to ideal crystalline materials, it means, refer to the cases when the atoms are in their equilibrium positions, what obviously represents the first approximation in the description of such materials. We know already that an infinite crystal structure possesses a translation symmetry which together with the point symmetry characterizes the lattice of a given structure. In this chapter, we will introduce the concept of the so called reciprocal lattice which has the same point symmetry as the crystal lattice (direct lattice) and plays an important role in the description of the physical properties of crystalline materials.

2. The Concept of the Reciprocal Lattice

The concept of the reciprocal lattice will be introduced starting from the fact that in an ideal infinite crystalline material the electrostatic potential produced by all the charges present in it is periodic with the periodicity of the crystal lattice. Let us denote the lattice translation vector as $\vec{a}_{\vec{n}}$. This vector can be expressed as a linear combination of three non collinear primitive translation vectors $\vec{a}_1$, $\vec{a}_2$, $\vec{a}_3$ or as a linear combination of the versors $\hat{a}_1$, $\hat{a}_2$, $\hat{a}_3$

$$\vec{a}_{\vec{n}} = n_1\vec{a}_1 + n_2\vec{a}_2 + n_3\vec{a}_3 = n_1 a_1\hat{a}_1 + n_2 a_2\hat{a}_2 + n_3 a_3\hat{a}_3, \qquad \text{(V.1)}$$

where $n_1, n_2, n_3 \in \mathbb{Z}$. A position vector $\vec{r}$ of any point in the crystal may be expressed in the $\hat{a}_1$, $\hat{a}_2$, $\hat{a}_3$ basis

$$\vec{r} = \xi_1\hat{a}_1 + \xi_2\hat{a}_2 + \xi_3\hat{a}_3, \qquad \text{(V.2)}$$

where the real numbers ξ_1, ξ_2, ξ_3 are coordinates of the vector in this basis.

In the approximation in which we are considering the crystalline material the $\vec{r}$ and $(\vec{r} + \vec{a}_{\vec{n}})$ points, shown in Fig. 132, are physically equivalent and as a consequence the electrostatic potential, $V(\vec{r})$, produced

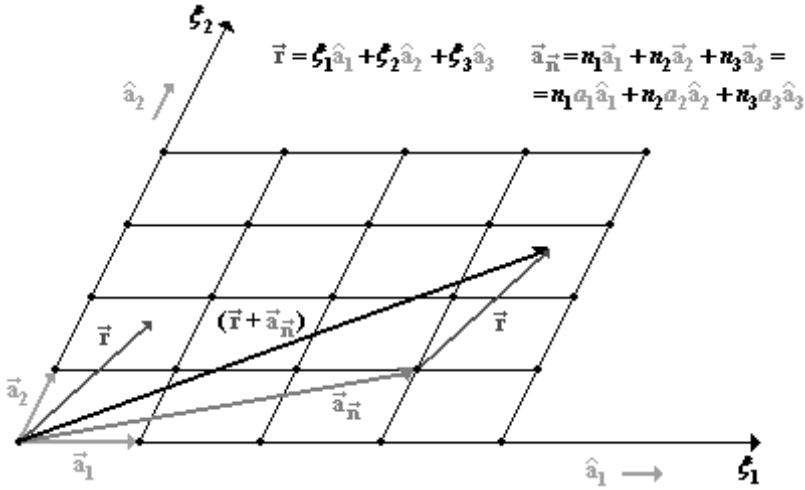

Figure 132 A two-dimensional crystal lattice. The points $\vec{r}$ and $(\vec{r} + \vec{a}_{\vec{n}})$ have equivalent positions in the infinite lattice.

by all the charges present in the crystal has the same value in both points

$$V(\vec{r}) = V(\vec{r} + \vec{a}_{\vec{n}}) . \tag{V.3}$$

That means the potential is periodic. Any periodic function can be expanded into its Fourier series. We will do that for $V(\vec{r})$ with respect to each of the components of the argument $\vec{r}$ in axes ξ_1, ξ_2, ξ_3, along of which the periodicity occurs. We have then

$$V(\vec{r}) = V(\xi_1, \xi_2, \xi_3) = \sum_{l_1=-\infty}^{\infty} \sum_{l_2=-\infty}^{\infty} \sum_{l_3=-\infty}^{\infty} V_{l_1 l_2 l_3} \exp\left[2\pi i \left(\frac{l_1 \xi_1}{a_1} + \frac{l_2 \xi_2}{a_2} + \frac{l_3 \xi_3}{a_3} \right) \right], \tag{V.4}$$

where l_1, l_2, l_3 are integer numbers and $V(\xi_1, \xi_2, \xi_3)$ is periodic with respect to each of its arguments ξ_1, ξ_2, ξ_3 with periods a_1, a_2, a_3, respectively. It is easy to show that the potential expressed in this way is indeed periodic. Since

$$\vec{r} + \vec{a}_{\vec{n}} = (\xi_1 + n_1 a_1)\ \hat{a}_1 + (\xi_2 + n_2 a_2)\ \hat{a}_2 + (\xi_3 + n_3 a_3)\ \hat{a}_3 , \tag{V.5}$$

we have

$$
\begin{aligned}
&V\left(\vec{\mathrm{r}}+\vec{\mathrm{a}}_{\vec{\mathrm{n}}}\right) \\
&= \sum_{l_1=-\infty}^{\infty}\sum_{l_2=-\infty}^{\infty}\sum_{l_3=-\infty}^{\infty} V_{l_1 l_2 l_3} \exp\left[2\pi i\left(\frac{l_1\left(\xi_1+n_1a_1\right)}{a_1}+\frac{l_2\left(\xi_2+n_2a_2\right)}{a_2}+\frac{l_3\left(\xi_3+n_3a_3\right)}{a_3}\right)\right] \\
&= \sum_{l_1=-\infty}^{\infty}\sum_{l_2=-\infty}^{\infty}\sum_{l_3=-\infty}^{\infty} V_{l_1 l_2 l_3} \exp\left[2\pi i\left(l_1n_1+l_2n_2+l_3n_3\right)\right]\cdot\exp\left[2\pi i\left(\frac{l_1\xi_1}{a_1}+\frac{l_2\xi_2}{a_2}+\frac{l_3\xi_3}{a_3}\right)\right] \\
&= \sum_{l_1=-\infty}^{\infty}\sum_{l_2=-\infty}^{\infty}\sum_{l_3=-\infty}^{\infty} V_{l_1 l_2 l_3} \exp\left[2\pi i\left(\frac{l_1\xi_1}{a_1}+\frac{l_2\xi_2}{a_2}+\frac{l_3\xi_3}{a_3}\right)\right]=V\left(\vec{\mathrm{r}}\right),
\end{aligned}
\tag{V.6}
$$

where we took into account that

$$
l_1n_1+l_2n_2+l_3n_3=\text{(integer number)} \;\Rightarrow\; \exp\left[2\pi i\left(l_1n_1+l_2n_2+l_3n_3\right)\right]=1\,. \tag{V.7}
$$

Now, we will make a transformation to an orthogonal coordinate system. The coordinates of the position vector $\vec{\mathrm{r}}$ in the orthogonal system shown in Fig. 133 can be expressed as a function of its coordinates given in the ξ_1 and ξ_2 axes

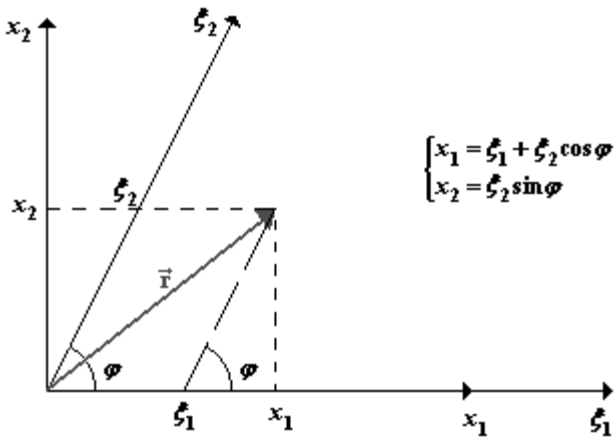

Figure 133 The relation between the components of the vector $\vec{\mathrm{r}}$ in the orthogonal and non orthogonal coordinate systems.

$$\begin{cases} x_1 = \xi_1 + \xi_2 \cos\varphi \\ x_2 = \xi_2 \sin\varphi \end{cases}. \tag{V.8}$$

The above represents a system of linear equations for ξ_1 and ξ_2. By solving for ξ_2 first and ξ_1 after, we find

$$\begin{cases} \xi_2 = \dfrac{1}{\sin\varphi} x_2 \\ \xi_1 = x_1 - \dfrac{\cos\varphi}{\sin\varphi} x_2 \end{cases} \Rightarrow \begin{cases} \xi_1 = x_1 - x_2 \cot\varphi \\ \xi_2 = x_2 \csc\varphi \end{cases}. \tag{V.9}$$

The formulas for ξ_1 and ξ_2 can be rewritten more generally as follows

$$\begin{cases} \xi_1 = a_{11}x_1 + a_{12}x_2, & \text{where} \quad a_{11} = 1 \text{ and } a_{12} = -\cot\varphi \\ \xi_2 = a_{21}x_1 + a_{22}x_2, & \text{where} \quad a_{21} = 0 \text{ and } a_{22} = \csc\varphi \end{cases}. \tag{V.10}$$

In a three-dimensional case, if the origins of the non orthogonal and orthogonal coordinate systems coincide, we have

$$\begin{cases} \xi_1 = a_{11}x_1 + a_{12}x_2 + a_{13}x_3 = \sum_{k=1}^{3} a_{1k}x_k \\ \xi_2 = a_{21}x_1 + a_{22}x_2 + a_{23}x_3 = \sum_{k=1}^{3} a_{2k}x_k \\ \xi_3 = a_{31}x_1 + a_{32}x_2 + a_{33}x_3 = \sum_{k=1}^{3} a_{3k}x_k \end{cases}, \tag{V.11}$$

where the a_{ik} coefficients are determined by the angles between axes ξ_i and x_k.

We will now substitute ξ_1, ξ_2, ξ_3 given by Eqs. (V.11) into Eq. (V.4), then

$$V(\vec{\mathrm{r}}) = \sum_{l_1=-\infty}^{\infty} \sum_{l_2=-\infty}^{\infty} \sum_{l_3=-\infty}^{\infty} V_{l_1 l_2 l_3} \exp[2\pi i A], \tag{V.12}$$

where

$$A = \frac{l_1}{a_1}\sum_{k=1}^{3} a_{1k}x_k + \frac{l_2}{a_2}\sum_{k=1}^{3} a_{2k}x_k + \frac{l_3}{a_3}\sum_{k=1}^{3} a_{3k}x_k$$
$$= \left(\frac{l_1 a_{11}}{a_1} + \frac{l_2 a_{21}}{a_2} + \frac{l_3 a_{31}}{a_3}\right)x_1 + \left(\frac{l_1 a_{12}}{a_1} + \frac{l_2 a_{22}}{a_2} + \frac{l_3 a_{32}}{a_3}\right)x_2$$
$$+ \left(\frac{l_1 a_{13}}{a_1} + \frac{l_2 a_{23}}{a_2} + \frac{l_3 a_{33}}{a_3}\right)x_3 \tag{V.13}$$

and abbreviating

$$\begin{cases} b_1 = 2\pi\left(\dfrac{l_1 a_{11}}{a_1} + \dfrac{l_2 a_{21}}{a_2} + \dfrac{l_3 a_{31}}{a_3}\right) \\ b_2 = 2\pi\left(\dfrac{l_1 a_{12}}{a_1} + \dfrac{l_2 a_{22}}{a_2} + \dfrac{l_3 a_{32}}{a_3}\right) \\ b_3 = 2\pi\left(\dfrac{l_1 a_{13}}{a_1} + \dfrac{l_2 a_{23}}{a_2} + \dfrac{l_3 a_{33}}{a_3}\right) \end{cases} \tag{V.14}$$

we obtain

$$V(\vec{\mathrm{r}}) = \sum_{l_1=-\infty}^{\infty}\sum_{l_2=-\infty}^{\infty}\sum_{l_3=-\infty}^{\infty} V_{l_1 l_2 l_3} \exp\left[i\left(b_1 x_1 + b_2 x_2 + b_3 x_3\right)\right]. \tag{V.15}$$

From this point on, the summation over l_1, l_2, l_3 will be replaced by the summation over discreet parameters b_1, b_2, b_3, determined by the l_k $(k = 1,2,3)$ according to Eqs. (V.14). Moreover, it will be helpful to consider b_i ($i = 1,2,3$) as coordinates of a certain vector $\vec{\mathrm{b}}$ in the orthogonal coordinate system. In this manner

$$b_1 x_1 + b_2 x_2 + b_3 x_3 = \vec{\mathrm{b}} \cdot \vec{\mathrm{r}} \tag{V.16}$$

and then

$$V(\vec{\mathrm{r}}) = \sum_{b_1}\sum_{b_2}\sum_{b_3} V_{b_1 b_2 b_3} \exp\left[i\left(b_1 x_1 + b_2 x_2 + b_3 x_3\right)\right] = \sum_{\vec{\mathrm{b}}} V_{\vec{\mathrm{b}}} \exp\left(i\vec{\mathrm{b}} \cdot \vec{\mathrm{r}}\right). \tag{V.17}$$

The components of vector $\vec{b}$ are given by Eqs. (V.14), however, it is convenient to determine the formula for this vector again, starting from the condition of periodicity of the crystal potential, which guides us to the following conclusion:

$$\left.\begin{aligned} V\left(\vec{r}+\vec{a}_{\vec{n}}\right) &= \sum_{\vec{b}} V_{\vec{b}} \exp\left[i\vec{b}\cdot\left(\vec{r}+\vec{a}_{\vec{n}}\right)\right] \\ &= \sum_{\vec{b}} V_{\vec{b}} \exp\left[i\vec{b}\cdot\vec{r}\right]\cdot\exp\left[i\vec{b}\cdot\vec{a}_{\vec{n}}\right] = V\left(\vec{r}\right) \\ &\text{and} \\ V\left(\vec{r}\right) &= \sum_{\vec{b}} V_{\vec{b}} \exp\left[i\vec{b}\cdot\vec{r}\right] \end{aligned}\right\} \Rightarrow \exp\left[i\vec{b}\cdot\vec{a}_{\vec{n}}\right]=1\,. \tag{V.18}$$

This means that in order for the potential to be periodic with periods $\vec{a}_{\vec{n}}$, the following equality has to be achieved

$$\exp\left[i\vec{b}\cdot\vec{a}_{\vec{n}}\right]=1\,. \tag{V.19}$$

It is easy to see that Eq. (V.19) implies the periodicity of the function $\exp\left(i\vec{b}\vec{r}\right)$, since

$$\begin{gathered} \exp\left[i\vec{b}\cdot\left(\vec{r}+\vec{a}_{\vec{n}}\right)\right] = \exp\left(i\vec{b}\cdot\vec{r}\right)\cdot\exp\left(i\vec{b}\cdot\vec{a}_{\vec{n}}\right) = \exp\left(i\vec{b}\cdot\vec{r}\right) \\ \Downarrow \\ \exp\left[i\vec{b}\cdot\left(\vec{r}+\vec{a}_{\vec{n}}\right)\right] = \exp\left(i\vec{b}\cdot\vec{r}\right) \end{gathered} \tag{V.20}$$

and *vice versa*, (V.20) implies Eq. (V.19). In conclusion, the potential $V\left(\vec{r}\right)$ can be expressed as a function of plane waves $\exp\left(i\vec{b}\cdot\vec{r}\right)$ which are periodic with the periodicity of the lattice. Next, we will use Eq. (V.19) to find the expression for the vector $\vec{b}$ that characterizes such plane waves. We have

$$\exp\left[i\vec{b}\cdot\vec{a}_{\vec{n}}\right]=1 \;\Rightarrow\; \vec{b}\cdot\vec{a}_{\vec{n}} = (\text{integer number})\cdot 2\pi, \;\text{ for all vectors } \vec{n} \tag{V.21}$$

and using Eq. (V.1) we obtain

$$\begin{aligned}\vec{b}\cdot\vec{a}_{\vec{n}} &= \vec{b}\cdot\left(n_1\vec{a}_1 + n_2\vec{a}_2 + n_3\vec{a}_3\right)\\ &= n_1\left(\vec{b}\cdot\vec{a}_1\right) + n_2\left(\vec{b}\cdot\vec{a}_2\right) + n_3\left(\vec{b}\cdot\vec{a}_3\right),\\ &= (\text{integer number})\cdot 2\pi \end{aligned} \tag{V.22}$$

for all possible $n_1, n_2, n_3 \in \mathbb{Z}$. The condition given by Eq. (V.22) is satisfied only if

$$\begin{cases}\vec{b}\cdot\vec{a}_1 = 2\pi\cdot g_1\\ \vec{b}\cdot\vec{a}_2 = 2\pi\cdot g_2\,,\ \text{where}\ g_1, g_2, g_3 \in \mathbb{Z}.\\ \vec{b}\cdot\vec{a}_3 = 2\pi\cdot g_3\end{cases} \tag{V.23}$$

The above represents three scalar equations for three components of vector $\vec{b}$. To solve these equations, instead of using the orthogonal coordinate system, we are going to express vector $\vec{b}$ as a linear combination of three non collinear vectors defined in the following manner:

$$\vec{a}_1\times\vec{a}_2,\ \vec{a}_2\times\vec{a}_3,\ \vec{a}_3\times\vec{a}_1. \tag{V.24}$$

We have then

$$\vec{b} = \alpha\left(\vec{a}_1\times\vec{a}_2\right) + \beta\left(\vec{a}_2\times\vec{a}_3\right) + \gamma\left(\vec{a}_3\times\vec{a}_1\right), \tag{V.25}$$

where the scalars α, β, and γ are coefficients of the linear combination. The task of solving Eqs. (V.23) consists now in finding the expression for the α, β, γ coefficients. To this end we substitute Eq. (V.25) into Eqs. (V.23) and obtain

$$\begin{cases}\vec{b}\cdot\vec{a}_1 = \beta\left(\vec{a}_2\times\vec{a}_3\right)\cdot\vec{a}_1 = 2\pi\cdot g_1\\ \vec{b}\cdot\vec{a}_2 = \gamma\left(\vec{a}_3\times\vec{a}_1\right)\cdot\vec{a}_2 = 2\pi\cdot g_2\\ \vec{b}\cdot\vec{a}_3 = \alpha\left(\vec{a}_1\times\vec{a}_2\right)\cdot\vec{a}_3 = 2\pi\cdot g_3\end{cases} \Rightarrow \begin{cases}\beta\Omega_0 = 2\pi\cdot g_1\\ \gamma\Omega_0 = 2\pi\cdot g_2\\ \alpha\Omega_0 = 2\pi\cdot g_3\end{cases}, \tag{V.26}$$

since

$$\left(\vec{a}_1\times\vec{a}_2\right)\cdot\vec{a}_3 = \left(\vec{a}_2\times\vec{a}_3\right)\cdot\vec{a}_1 = \left(\vec{a}_3\times\vec{a}_1\right)\cdot\vec{a}_2 = \Omega_0. \tag{V.27}$$

From (V.26) we finally obtain the following expressions for the coefficients α, β, γ

$$\alpha = 2\pi \frac{g_3}{\Omega_0},\ \beta = 2\pi \frac{g_1}{\Omega_0},\ \gamma = 2\pi \frac{g_2}{\Omega_0}, \tag{V.28}$$

then vector $\vec{b}$ has the following formula

$$\begin{aligned} \vec{b} &= g_3 2\pi \frac{(\vec{a}_1 \times \vec{a}_2)}{\Omega_0} + g_1 2\pi \frac{(\vec{a}_2 \times \vec{a}_3)}{\Omega_0} + g_2 2\pi \frac{(\vec{a}_3 \times \vec{a}_1)}{\Omega_0}, \\ &= g_1 \vec{b}_1 + g_2 \vec{b}_2 + g_3 \vec{b}_3 \end{aligned} \tag{V.29}$$

where

$$\vec{b}_1 = 2\pi \frac{(\vec{a}_2 \times \vec{a}_3)}{\Omega_0},\ \vec{b}_2 = 2\pi \frac{(\vec{a}_3 \times \vec{a}_1)}{\Omega_0},\ \vec{b}_3 = 2\pi \frac{(\vec{a}_1 \times \vec{a}_2)}{\Omega_0}. \tag{V.30}$$

We obtained that vector $\vec{b}$ is a linear combination of vectors $\vec{b}_1$, $\vec{b}_2$, $\vec{b}_3$, defined by Eqs. (V.30), with integer coefficients g_1, g_2, g_3. We have then a set of discreet vectors $\vec{b}$ and this makes them similar to vectors $\vec{a}_{\bar{n}}$, defined by Eq. (V.1), that go from one point to any other of the crystal lattice (direct lattice). In analogy to $\vec{a}_{\bar{n}}$ we define vectors $\vec{b}_{\bar{g}}$ as

$$\vec{b}_{\bar{g}} = g_1 \vec{b}_1 + g_2 \vec{b}_2 + g_3 \vec{b}_3,\ \ g_1, g_2, g_3 \in \mathbb{Z}. \tag{V.31}$$

It is convenient to call lattice a set of points generated by all possible vectors $\vec{b}_{\bar{g}}$. This lattice is called the reciprocal lattice and vectors $\vec{b}_1$, $\vec{b}_2$, $\vec{b}_3$ are its primitive translation vectors. From Eqs. (V.30) we can see that they are defined by vectors $\vec{a}_1$, $\vec{a}_2$, $\vec{a}_3$ that are three non collinear primitive translation vectors of the direct lattice. The primitive translation vectors of the reciprocal lattice define the unit cell of this lattice, which is shown in Fig. 134.

In conclusion, we can say that the plane waves $\exp(i\vec{b}_{\bar{g}} \cdot \vec{r})$, in which the periodic crystal potential was expanded, are characterized by the translation vectors $\vec{b}_{\bar{g}}$ of the reciprocal lattice. The relation between the reciprocal and direct lattices is such that the translation vectors of the reciprocal lattice define the plane waves that have the periodicity of the direct lattice. So we have that

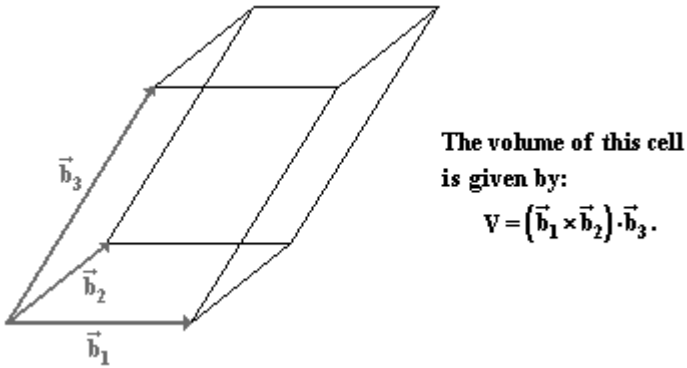

Figure 134 The unit cell of a reciprocal lattice defined by the primitive translation vectors $\vec{b}_1, \vec{b}_2$, and $\vec{b}_3$.

$$\exp(i\vec{b}_{\vec{g}} \cdot (\vec{r} + \vec{a}_{\vec{n}})) = \exp(i\vec{b}_{\vec{g}} \cdot \vec{r}), \tag{V.32}$$

what, at the same time, guarantees the periodicity of the crystal potential $V(\vec{r})$.

It can be easily proved that

$$\vec{a}_i \cdot \vec{b}_k = 2\pi\delta_{ik} = \begin{cases} 0, & \text{for } i \neq k \\ 2\pi, & \text{for } i = k \end{cases} \tag{V.33}$$

and we will use this property of vectors $\vec{a}_i$ and $\vec{b}_k$ to calculate the volume of the unit cell of the reciprocal lattice. Since $\vec{b}_3 = 2\pi(\vec{a}_1 \times \vec{a}_2)/\Omega_0$, we have

$$\begin{aligned} V &= (\vec{b}_1 \times \vec{b}_2) \cdot \vec{b}_3 = \frac{2\pi}{\Omega_0}(\vec{b}_1 \times \vec{b}_2) \cdot (\vec{a}_1 \times \vec{a}_2) \\ &= \frac{2\pi}{\Omega_0}\left[(\vec{b}_1 \cdot \vec{a}_1)(\vec{b}_2 \cdot \vec{a}_2) - (\vec{b}_1 \cdot \vec{a}_2)(\vec{b}_2 \cdot \vec{a}_1)\right] = \frac{(2\pi)^3}{\Omega_0}, \end{aligned} \tag{V.34}$$

where we have used the identity

$$(\vec{A} \times \vec{B}) \cdot (\vec{C} \times \vec{D}) = (\vec{A} \cdot \vec{C})(\vec{B} \cdot \vec{D}) - (\vec{A} \cdot \vec{D})(\vec{B} \cdot \vec{C}), \tag{V.35}$$

which is true for any three vectors and in the last step, we have used the relations given by Eq. (V.33). We can see from (V.34) that the volume of the unit cell of the reciprocal lattice is equal to the inverse of the volume of the unit cell of the direct lattice multiplied by factor $(2\pi)^3$.

3. Examples of Reciprocal Lattices

We will now give some examples of reciprocal lattices. As a first example, we will consider the triclinic lattice.

3.1. Reciprocal of the Triclinic Lattice

We can see in Fig. 135 that the reciprocal of a triclinic lattice is also triclinic. As we remember from Chapter II, there are no restrictions on the lengths of the unit cell edges or on their interaxial angles in a triclinic lattice. Given that the reciprocal of a triclinic lattice is also triclinic, the same is true for the reciprocal lattice.

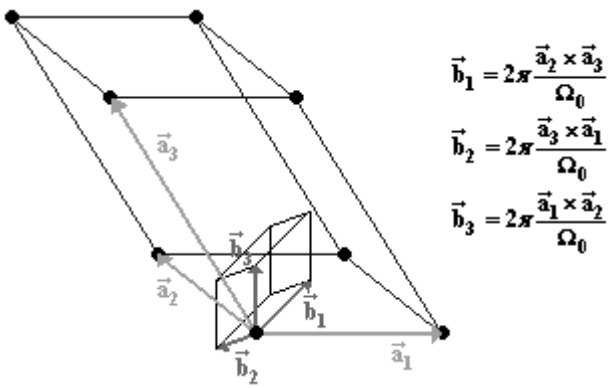

Figure 135 Primitive unit cell of the reciprocal of the triclinic lattice. In the figure, we show also the primitive unit cell for the direct lattice.

Each of the $\vec{b}_i$ vectors (which define a primitive unit cell of the reciprocal lattice, see Fig. 135) is orthogonal to the plane defined by two of the three vectors $\vec{a}_1$, $\vec{a}_2$, $\vec{a}_3$, which are the generators of the direct lattice. It should be noted that the dimensions of the cells in Fig. 135 are not comparable since the unit of a_i is meter and that of b_i is inverse meter.

We will consider now two more lattices, which belong to the cubic crystal system.

3.2. Reciprocal of the Simple Cubic Lattice

The primitive unit cell of the reciprocal of the *sc* lattice has a cubic shape, so this reciprocal lattice is also simple cubic. This is shown in

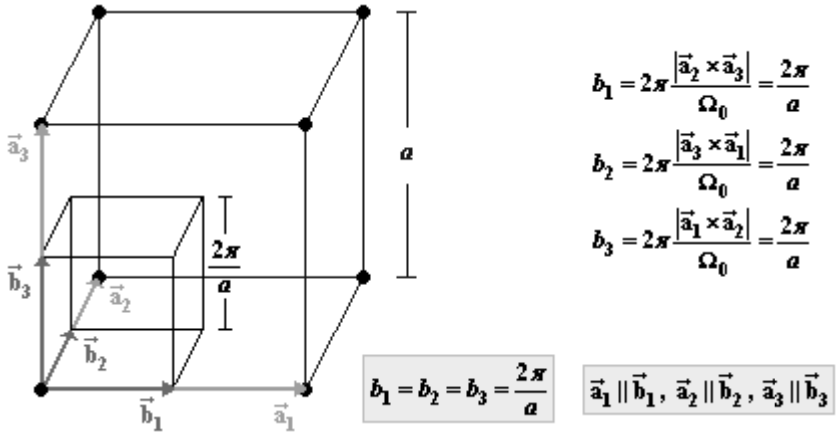

Figure 136 Cubic unit cells of the *sc* lattice and its reciprocal lattice.

Fig. 136. The volume of the unit cell of the reciprocal lattice is given by the expression

$$\mathrm{V} = b_1 \cdot b_2 \cdot b_3 = \frac{(2\pi)^3}{a^3} = \frac{(2\pi)^3}{\Omega_0}, \qquad \text{(V.36)}$$

where Ω_0 is the volume of the primitive unit cell for the direct lattice.

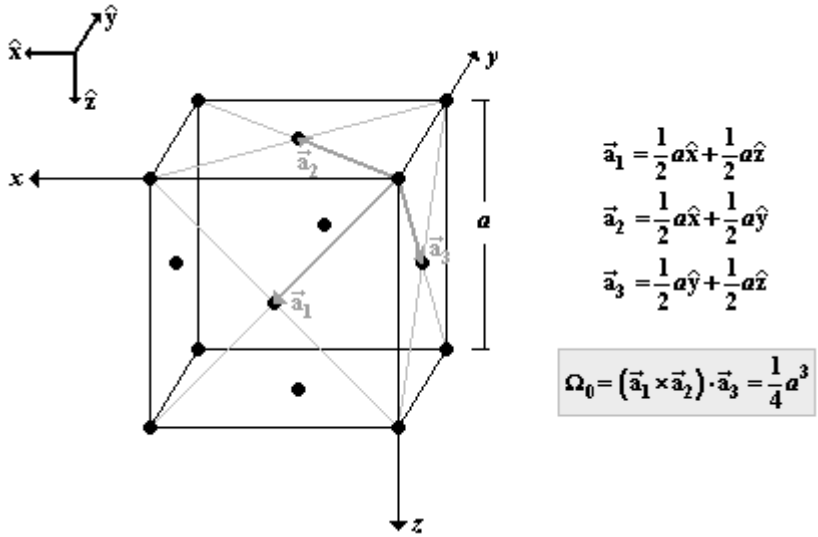

Figure 137 Cubic unit cell of the *fcc* lattice and the primitive translation vectors $\vec{a}_1$, $\vec{a}_2$, $\vec{a}_3$ that define a rhombohedral unit cell for this lattice.

3.3. Reciprocal of the Face Centered Cubic Lattice

Let us first remind some basics about the *fcc* lattice. The primitive translation vectors that define a rhombohedral unit cell for the *fcc* lattice are shown in Fig. 137. The volume of the rhombohedral unit cell is also given in this figure. The three non collinear primitive translation vectors for the reciprocal of the *fcc* lattice are calculated below. We have

$$\vec{b}_1 = 2\pi\frac{\vec{a}_2 \times \vec{a}_3}{\Omega_0} = \frac{2\pi}{\frac{1}{4}a^3}\begin{vmatrix} \hat{x} & \hat{y} & \hat{z} \\ \frac{1}{2}a & \frac{1}{2}a & 0 \\ 0 & \frac{1}{2}a & \frac{1}{2}a \end{vmatrix} = \frac{2\pi}{a}\hat{x} - \frac{2\pi}{a}\hat{y} + \frac{2\pi}{a}\hat{z}$$

$$\vec{b}_2 = 2\pi\frac{\vec{a}_3 \times \vec{a}_1}{\Omega_0} = \frac{2\pi}{\frac{1}{4}a^3}\begin{vmatrix} \hat{x} & \hat{y} & \hat{z} \\ 0 & \frac{1}{2}a & \frac{1}{2}a \\ \frac{1}{2}a & 0 & \frac{1}{2}a \end{vmatrix} = \frac{2\pi}{a}\hat{x} + \frac{2\pi}{a}\hat{y} - \frac{2\pi}{a}\hat{z} \quad . \quad \text{(V.37)}$$

$$\vec{b}_3 = 2\pi\frac{\vec{a}_1 \times \vec{a}_2}{\Omega_0} = \frac{2\pi}{\frac{1}{4}a^3}\begin{vmatrix} \hat{x} & \hat{y} & \hat{z} \\ \frac{1}{2}a & 0 & \frac{1}{2}a \\ \frac{1}{2}a & \frac{1}{2}a & 0 \end{vmatrix} = -\frac{2\pi}{a}\hat{x} + \frac{2\pi}{a}\hat{y} + \frac{2\pi}{a}\hat{z}$$

Using the above expressions for $\vec{b}_i$ it is easy to show that

$$b_1 = b_2 = b_3 = \sqrt{3\left(\frac{2\pi}{a}\right)^2} = \frac{2\pi\sqrt{3}}{a} \qquad \text{(V.38)}$$

and also

$$\sphericalangle\left(\vec{b}_1, \vec{b}_2\right) = \sphericalangle\left(\vec{b}_2, \vec{b}_3\right) = \sphericalangle\left(\vec{b}_1, \vec{b}_3\right). \qquad \text{(V.39)}$$

This means that the primitive unit cell of the reciprocal lattice has also a rhombohedral shape. If we now compare the expressions for vectors $\vec{b}_1$, $\vec{b}_2$, $\vec{b}_3$ given by Eqs. (V.37) with the expressions for the vectors $\vec{a}_1$, $\vec{a}_2$, $\vec{a}_3$ given in Chapter II for the *bcc* lattice (see the equations in Fig. 44) then we find that *bcc* is the reciprocal lattice of the *fcc* lattice with lattice constant $4\pi/a$ (see Fig. 138). It is also true that *fcc* is the reciprocal lattice of the *bcc* lattice.

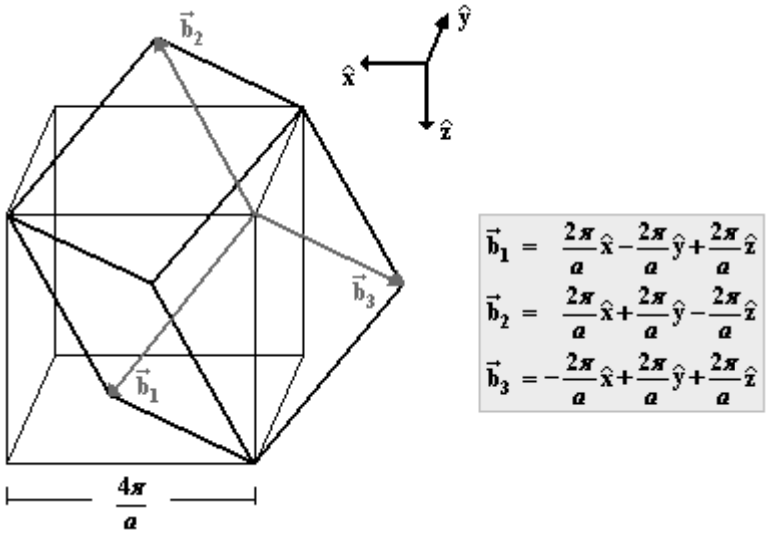

Figure 138 Primitive rhombohedral unit cell for the *bcc* reciprocal lattice. The cell is defined by primitive translation vectors $\vec{b}_1$, $\vec{b}_2$, $\vec{b}_3$ with coordinates given in the figure.

In Fig. 138 we have placed the rhombohedral unit cell and the cubic unit cell for the reciprocal of the *fcc* lattice. Note that vectors $\vec{b}_i$ go from a vertex of the cube shown in the figure towards three centers of the cubes adjacent to this cube (the ones that share a common vertex with this cube).

4. Problems

Exercise 1 Eq. (V.22) is reduced to the following form in the case of a two-dimensional lattice

$$\vec{b}\cdot\vec{a}_{\bar{n}} = n_1\left(\vec{b}\cdot\vec{a}_1\right) + n_2\left(\vec{b}\cdot\vec{a}_2\right) = (\text{integer number})\cdot 2\pi\,, \qquad \text{(V.40)}$$

for all possible $n_1, n_2 \in \mathbb{Z}$. The above represents the condition for translation vectors $\vec{b}$ of the reciprocal of a two-dimensional crystal lattice generated by primitive vectors $\vec{a}_1$ and $\vec{a}_2$. The condition given by Eq. (V.40) is satisfied only if

$$\begin{cases} \vec{b}\cdot\vec{a}_1 = 2\pi\cdot g_1 \\ \vec{b}\cdot\vec{a}_2 = 2\pi\cdot g_2 \end{cases}, \text{ where } g_1, g_2 \in \mathbb{Z}. \qquad \text{(V.41)}$$

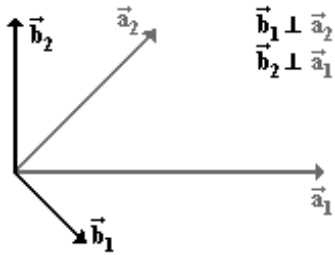

Figure 139 Vectors $\vec{a}_1$, $\vec{a}_2$ and $\vec{b}_1$, $\vec{b}_2$ that generate the two-dimensional direct and reciprocal lattices, respectively.

From Eqs. (V.41) we deduce that there are vectors $\vec{b}$ that are orthogonal to $\vec{a}_1$ or $\vec{a}_2$. Two such vectors are shown in Fig. 139. Let us denote those two vectors, that are primitive translation vectors, as $\vec{b}_1$ and $\vec{b}_2$.

a.) Show that the translation vector $\vec{b}$ of the reciprocal lattice has the following expression

$$\vec{b} = g_1\vec{b}_1 + g_2\vec{b}_2 , \qquad \text{(V.42)}$$

where g_1, g_2 are defined by Eqs. (V.41), and $\vec{b}_1$ and $\vec{b}_2$ are orthogonal to $\vec{a}_2$ and $\vec{a}_1$, respectively.

***Hint*:** Express the translation vector $\vec{b}$ as a linear combination of versors $\hat{b}_1$ and $\hat{b}_2$ with coefficients α and β

$$\vec{b} = \alpha\hat{b}_1 + \beta\hat{b}_2 , \qquad \text{(V.43)}$$

then find those coefficients and the expressions for the primitive translation vectors $\vec{b}_1$ and $\vec{b}_2$.

b.) For each of the five lattices existing in two dimensions draw the primitive unit cell for its reciprocal lattice (defined by the vectors $\vec{b}_1$ and $\vec{b}_2$ specified in a.)) together with the conventional primitive unit cell for the direct lattice shown in Fig. 15.

Exercise 2 Show that the primitive translation vectors $\vec{a}_1$, $\vec{a}_2$ and $\vec{b}_1$, $\vec{b}_2$ for a two-dimensional crystal lattice and its reciprocal, respectively, satisfy Eq. (V.33).

***Hint*:** Solve first point a.) in Exercise 1 in order to have the expressions for $\vec{b}_1$ and $\vec{b}_2$.

Exercise 3

a.) Show that the reciprocal of the *bcc* Bravais lattice (with lattice constant *a*) is the *fcc* lattice (with lattice constant $4\pi/a$).

b.) Using the primitive translation vectors for the *fcc* reciprocal lattice, obtained in a.), draw the primitive unit cell inside the cubic unit cell for this lattice.

Exercise 4 Prove that the reciprocal of a reciprocal lattice is its direct lattice.

***Hint*:** Substitute the expressions for $\vec{b}_1$, $\vec{b}_2$, $\vec{b}_3$ given by Eqs. (V.30) into the expressions for the primitive translation vectors of the reciprocal of a reciprocal lattice given by

$$2\pi\frac{(\vec{b}_2\times\vec{b}_3)}{V},\ 2\pi\frac{(\vec{b}_3\times\vec{b}_1)}{V},\ 2\pi\frac{(\vec{b}_1\times\vec{b}_2)}{V},$$

where V is the volume of the primitive unit cell of the reciprocal lattice. To simplify the result, make use of the vector identity

$$\vec{A}\times\left(\vec{B}\times\vec{C}\right)=\vec{B}\left(\vec{A}\cdot\vec{C}\right)-\vec{C}\left(\vec{A}\cdot\vec{B}\right)$$

and Eq. (V.34).

VI. DIRECT AND RECIPROCAL LATTICES

1. Introduction

A three-dimensional Bravais lattice may be seen as a set of two-dimensional lattices, whose planes are parallel to each other and equally spaced. Each of these planes represents a lattice plane of the three-dimensional Bravais lattice. The way of seeing a three-dimensional lattice as a set of two-dimensional lattices is not unique. A set of parallel, equally spaced lattice planes is known as a family of lattice planes. The orientation of the planes belonging to each family is given by the so called Miller indices. We will show in this chapter that the Miller indices represent the components of a translation vector of the reciprocal lattice which is orthogonal to the family of the lattice planes labeled with these indices. In the next section, we will learn how to obtain the Miller indices.

2. Miller Indices

We will show, first, examples of lattice planes in a given Bravais lattice. A lattice plane is defined by at least three non collinear lattice points. In Fig. 140 we can see four lattice planes with different orientations in the *sc* lattice.

Let us now introduce the Miller indices. They specify the orientation of a Bravais lattice plane (or the family of planes) in a very useful manner, what we will see later. The Miller indices, *h*, *k*, *l*, can be obtained as follows:

a.) From the family of lattice planes that are parallel to each other, we select a plane that crosses the lattice axes (defined by the primitive translation vectors $\vec{a}_1$, $\vec{a}_2$, $\vec{a}_3$) in the lattice points. The position vectors of these points, given in the non orthogonal reference system with axes along $\vec{a}_1$, $\vec{a}_2$, $\vec{a}_3$ (see Fig. 141), are $\vec{r}_1 = s_1\vec{a}_1$, $\vec{r}_2 = s_2\vec{a}_2$, $\vec{r}_3 = s_3\vec{a}_3$, where $s_1, s_2, s_3 \in \mathbb{Z}$.

b.) Next, we take the inverse values of the numbers s_1, s_2, s_3 and reduce them to the smallest integers with the same ratio, namely,

$$\frac{1}{s_1} : \frac{1}{s_2} : \frac{1}{s_3} = h : k : l \,. \qquad \text{(VI.1)}$$

The integer numbers with no common factors, h, k, l, obtained in this way are known as the Miller indices, which placed in parenthesis, (hkl), denote a family of lattice planes parallel to each other.

As a first example, we will use Eq. (VI.1) for the case shown in Fig. 141. For this case

$$\frac{1}{s_1}:\frac{1}{s_2}:\frac{1}{s_3}=\frac{1}{3}:\frac{1}{4}:\frac{1}{2}=4:3:6=h:k:l\,, \qquad \text{(VI.2)}$$

that is to say, the Miller indices of the plane represented in Fig. 141 are 4, 3, 6 and the plane is specified by (436). Let us next describe the cases shown in Figs. 140a-140d. In these figures, we can find four lattice planes in the *sc* lattice. The plane shaded in Fig. 140a includes a cube face. It intersects only the x axis in the point $\vec{r}_1 = 1\vec{a}_1$ (the other intercepts are at the "infinity"),

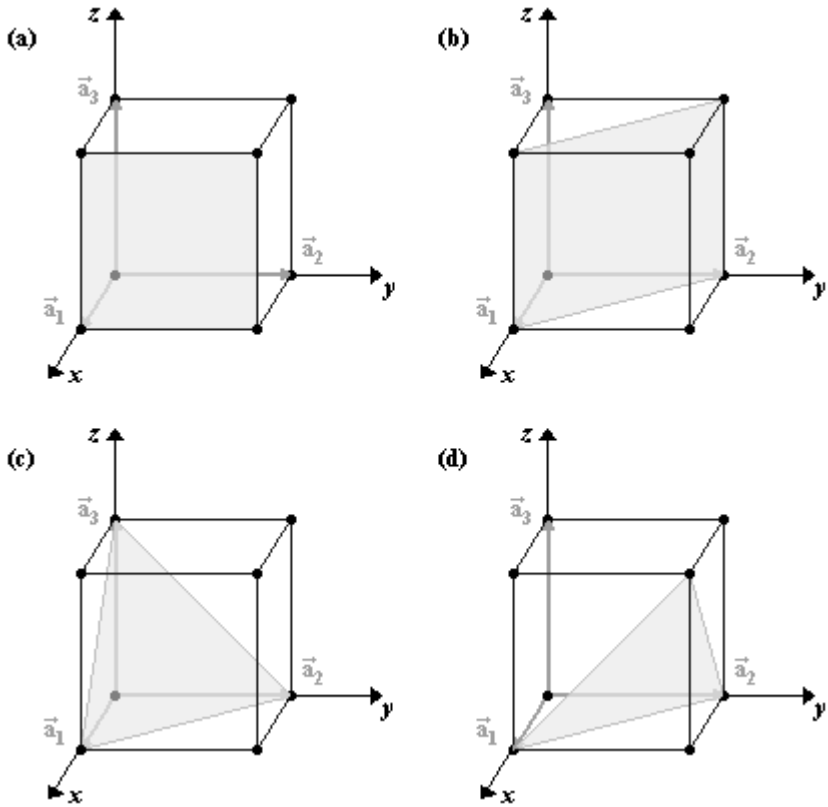

Figure 140 Four lattice planes with different orientations in the *sc* lattice.

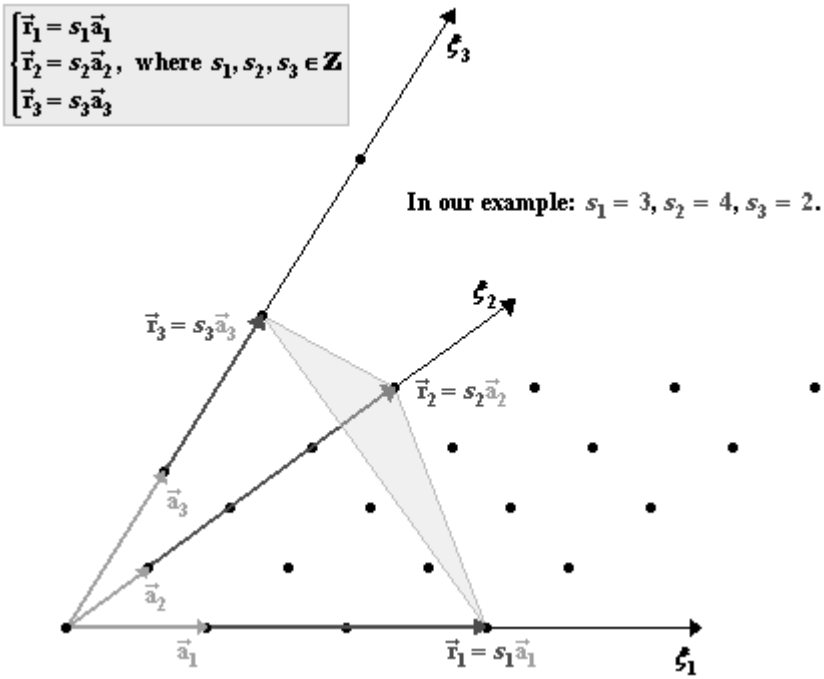

Figure 141 Three-dimensional crystal lattice generated by the primitive translation vectors $\vec{a}_1$, $\vec{a}_2$, $\vec{a}_3$. The lattice plane shown in the figure intersects the axes ξ_1, ξ_2, ξ_3 in the lattice points.

thus Eq. (VI.1) turns to the following form for this case:

$$\frac{1}{1}:\frac{1}{\infty}:\frac{1}{\infty}=1:0:0 \;\Rightarrow\; (hkl)=(100). \tag{VI.3}$$

In the similar way, we obtain the Miller indices for the rest of the planes shown in Fig. 140, namely,

$$\begin{aligned}
&\frac{1}{1}:\frac{1}{1}:\frac{1}{\infty}=1:1:0 \;\Rightarrow\; (hkl)=(110),\\
&\frac{1}{1}:\frac{1}{1}:\frac{1}{1}=1:1:1 \;\Rightarrow\; (hkl)=(111), \text{ and}\\
&\frac{1}{1}:\frac{1}{1}:\frac{1}{-1}=1:1:\bar{1} \;\Rightarrow\; (hkl)=(11\bar{1})
\end{aligned} \tag{VI.4}$$

for Figs. 140b-140d, respectively. The shaded plane in Fig. 140d intersects the z axis in the point $\vec{r}_3 = -1\vec{a}_3$ (see also Fig. 142). Due to the convention,

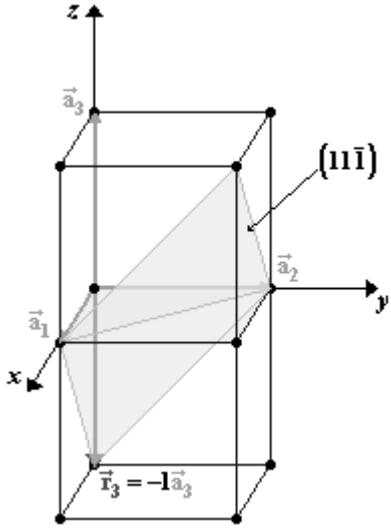

Figure 142 A complementary figure to Fig. 140d. In this figure is indicated the lattice point where the $(11\bar{1})$ plane crosses the *z* axis defined by the translation vector $\vec{a}_3$.

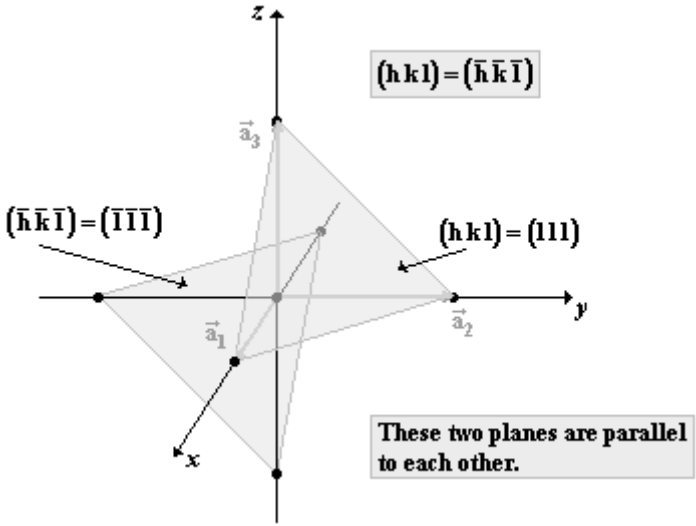

Figure 143 The (111) and $(\bar{1}\bar{1}\bar{1})$ planes in the *sc* lattice.

the negative Miller indices are written with a bar, it means, instead of -1 we have $\bar{1}$. From the definition of the Miller indices, it is easy to see that

$$\left(\bar{h}\ \bar{k}\ \bar{l}\right) = \left(hkl\right). \qquad \text{(VI.5)}$$

The equality (VI.5) is illustrated in Fig. 143 for the case of the (111) and $(\bar{1}\bar{1}\bar{1})$ planes in the *sc* lattice that are parallel to each other.

As we have learned, the Miller indices are used to identify a single lattice plane and also a family of planes parallel to each other. For a set of lattice planes (or a set of families of parallel lattice planes) that are equivalent by symmetry of the lattice, there is also a notation. Let us illustrate this on the example of the planes which include the three faces of the cubic unit cell for the *sc* lattice shown in Fig. 144. "Curly" brackets, $\{100\}$, designate the (100) plane together with the (010) and (001) planes that are equivalent by lattice symmetry to it. In general, the notation $\{hkl\}$ refers to the (hkl) planes and all other families of lattice planes that are equivalent to them by symmetry of the lattice.

Now, we will introduce a convention to specify a direction in a direct lattice. Such direction can be identified by the three components of vector $\vec{a}_{\bar{1}}$, which is the shortest one in this direction (see Fig. 145). In order to determine the components of this vector, we can take a vector $\vec{R}$ defined by two lattice points in the direction in consideration and make the reductions to the three smallest integers. For example, in Fig. 145 we have proposed $\vec{R} = 3\vec{a}_1 + 0\vec{a}_2 + 3\vec{a}_3$; next, we take the integer numbers that multiply the primitive translation vectors $\vec{a}_1$, $\vec{a}_2$, $\vec{a}_3$ and then reduce them to the smallest integers having the same ratio: $3:0:3 = 1:0:1$. In this manner, we can obtain the components of the vector $\vec{a}_{\bar{1}} = 1\vec{a}_1 + 0\vec{a}_2 + 1\vec{a}_3$, which is the shortest one in the lattice direction in consideration. The notation $[101]$, with square brackets instead of round brackets, is used to specify the lattice

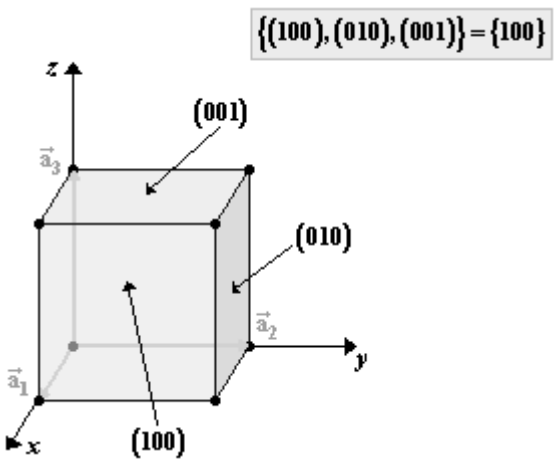

Figure 144 Three lattice planes in the *sc* lattice that are equivalent by symmetry of the lattice.

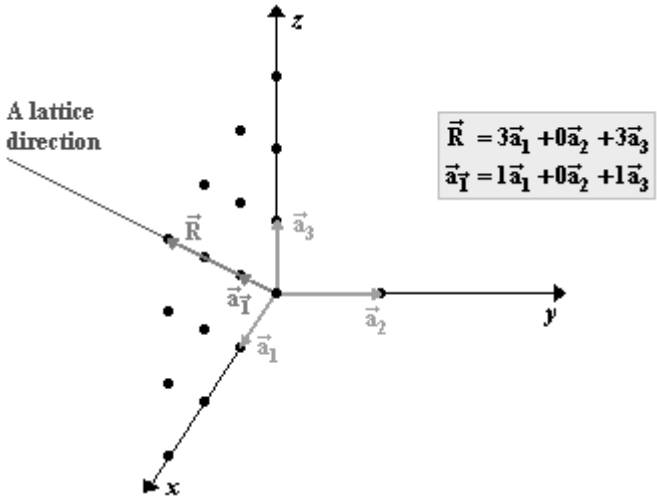

Figure 145 A lattice direction. The vector $\vec{a}_{\vec{l}}$ is the shortest one in this direction.

direction shown in Fig. 145. In general, the notation $[l_1 l_2 l_3]$ denotes a crystal lattice direction with the shortest translation vector $\vec{a}_{\vec{l}} = l_1\vec{a}_1 + l_2\vec{a}_2 + l_3\vec{a}_3$.

All directions that are equivalent to $[l_1 l_2 l_3]$ by lattice symmetry are denoted with the symbol $\langle l_1 l_2 l_3 \rangle$. Figure 146 shows an example of three equivalent directions, $[100]$, $[010]$, and $[001]$, in the *sc* lattice. The set of these directions, together with $[\bar{1}00]$, $[0\bar{1}0]$, and $[00\bar{1}]$, is denoted by $\langle 100 \rangle$.

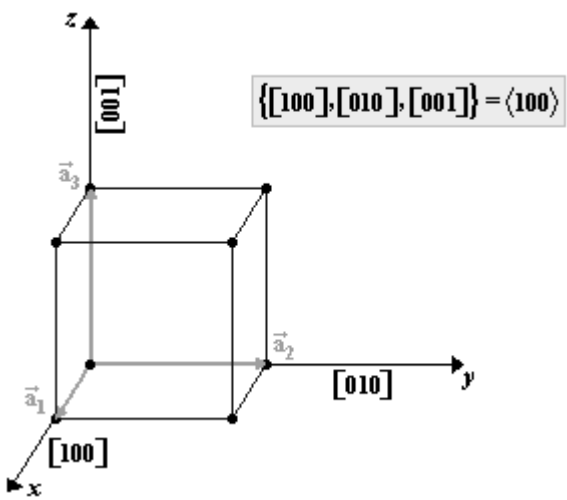

Figure 146 Three directions equivalent by lattice symmetry in the *sc* lattice.

3. Application of Miller Indices

We are going to describe now some of the properties of Bravais lattices with the aid of Miller indices.

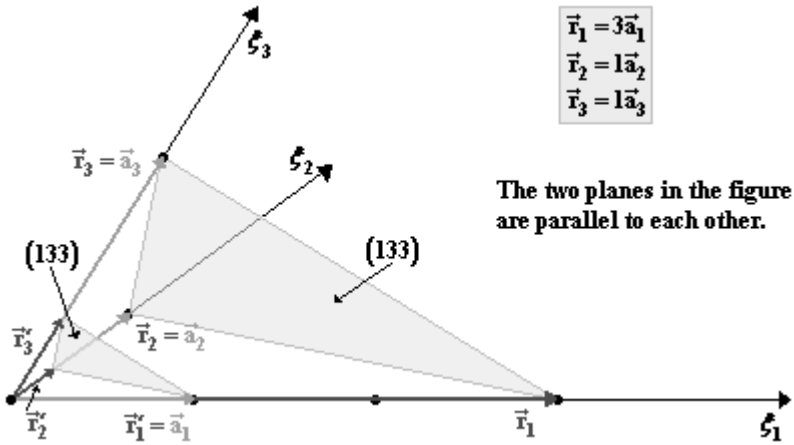

Figure 147 Two (133) lattice planes in a lattice generated by the primitive translation vectors $\vec{a}_1$, $\vec{a}_2$, $\vec{a}_3$.

Property 1

First, we will look for the positions of three points that define a lattice plane which is the closest to the plane that passes through the origin of the non orthogonal reference system, defined by the primitive translation vectors $\vec{a}_1$, $\vec{a}_2$, $\vec{a}_3$ (see Fig. 147). The vectors $\vec{r}_1$, $\vec{r}_2$, $\vec{r}_3$ shown in Fig. 147 give the positions of three lattice points. The lattice plane that intersects the ξ_1, ξ_2, ξ_3 axes in these points has the following Miller indices:

$$h:k:l = \frac{1}{3}:\frac{1}{1}:\frac{1}{1} = 1:3:3. \qquad \text{(VI.6)}$$

The other (133) lattice plane shown in Fig. 147 is the closest plane to the one that passes through the origin. This plane crosses the lattice axes in the points given by vectors

$$\begin{cases} \vec{r}_1' = 1\vec{a}_1 = \dfrac{\vec{a}_1}{h} \\ \vec{r}_2' = \dfrac{1}{3}\vec{a}_2 = \dfrac{\vec{a}_2}{k} \\ \vec{r}_3' = \dfrac{1}{3}\vec{a}_3 = \dfrac{\vec{a}_3}{l} \end{cases}. \tag{VI.7}$$

Therefore, the plane intersects the ξ_1, ξ_2, ξ_3 axes at the points $\vec{a}_1/h$, $\vec{a}_2/k$, $\vec{a}_3/l$, respectively. This general statement can be deduced from the geometric considerations related to the intercepts with the axes of equidistant and parallel to each other (hkl) planes.

Property 2

Next, we will show that the reciprocal lattice vector $\vec{b}_{hkl} = h\vec{b}_1 + k\vec{b}_2 + l\vec{b}_3$ is perpendicular to the (hkl) direct lattice plane. To demonstrate that, from all the planes of the (hkl) family, we will take the one that crosses the lattice axes (defined by the primitive translation vectors $\vec{a}_1$, $\vec{a}_2$, $\vec{a}_3$) in the points given by $\vec{a}_1/h$, $\vec{a}_2/k$, $\vec{a}_3/l$. The non collinear vectors $(\vec{a}_2/k - \vec{a}_1/h)$ and $(\vec{a}_2/k - \vec{a}_3/l)$ are on a (hkl) plane

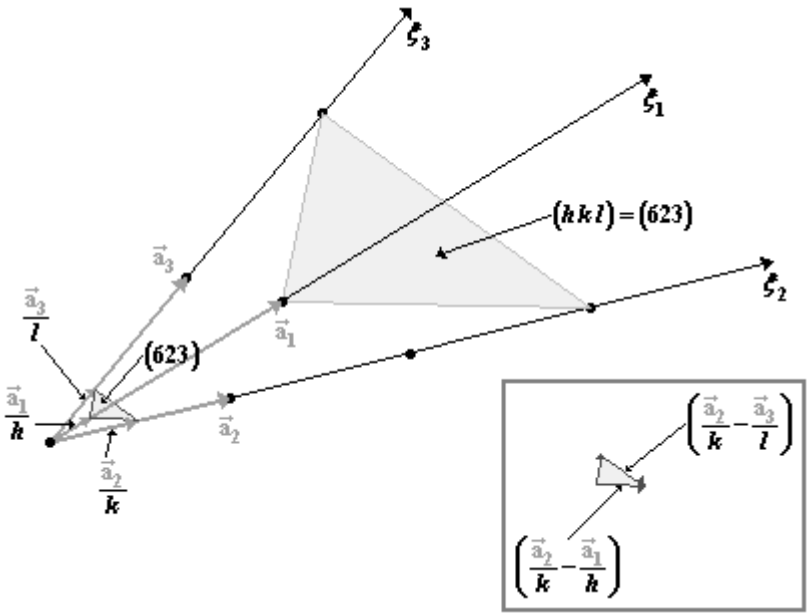

Figure 148 Two (623) lattice planes in a lattice generated by the primitive translation vectors $\vec{a}_1$, $\vec{a}_2$, $\vec{a}_3$.

that is the closest to the origin, what is illustrated for the case of the (623) plane in Fig. 148. It will suffice to show that $\vec{b}_{hkl} \perp \left(\vec{a}_2/k - \vec{a}_1/h\right)$ and $\vec{b}_{hkl} \perp \left(\vec{a}_2/k - \vec{a}_3/l\right)$ to be able to say that $\vec{b}_{hkl}$ is orthogonal to the family of (hkl) planes. We will calculate the following scalar products for this purpose

$$\begin{aligned} \vec{b}_{hkl} \cdot \left(\frac{\vec{a}_2}{k} - \frac{\vec{a}_1}{h}\right) &= \left(h\vec{b}_1 + k\vec{b}_2 + l\vec{b}_3\right) \cdot \left(\frac{\vec{a}_2}{k} - \frac{\vec{a}_1}{h}\right) = 2\pi - 2\pi = 0 \\ \vec{b}_{hkl} \cdot \left(\frac{\vec{a}_2}{k} - \frac{\vec{a}_3}{l}\right) &= \left(h\vec{b}_1 + k\vec{b}_2 + l\vec{b}_3\right) \cdot \left(\frac{\vec{a}_2}{k} - \frac{\vec{a}_3}{l}\right) = 2\pi - 2\pi = 0 \end{aligned} \quad . \qquad \text{(VI.8)}$$

In this manner, we have demonstrated that the vector $\vec{b}_{hkl}$ is indeed orthogonal to the family of (hkl) lattice planes. Concluding, we can say that the Miller indices, *h*, *k*, *l*, are the coordinates of the shortest reciprocal lattice vector $\vec{b}_{hkl} = h\vec{b}_1 + k\vec{b}_2 + l\vec{b}_3$, which is orthogonal to the (hkl) planes in the direct lattice. Of course, any vector that is a multiple of the $\vec{b}_{hkl}$ vector, $n\vec{b}_{hkl}$, is also orthogonal to the (hkl) plane. Certainly, if g_1, g_2, g_3, specified in Fig. 149, fulfill the relation $g_1 : g_2 : g_3 = h : k : l$, that is to say

$$\frac{g_1}{h} = \frac{g_2}{k} = \frac{g_3}{l} = n \in \mathbb{Z}, \qquad \text{(VI.9)}$$

then $\vec{b}_{\vec{g}} = n\vec{b}_{hkl}$ and the $\vec{b}_{\vec{g}}$ vector is orthogonal to the (hkl) plane. To conclude, we can say that the direction defined by the vector $\vec{b}_{hkl}$ in the reciprocal lattice corresponds to the (hkl) planes in the direct lattice. The vector $\vec{b}_{hkl}$ can be used to define a versor that is orthogonal to (*hkl*) planes

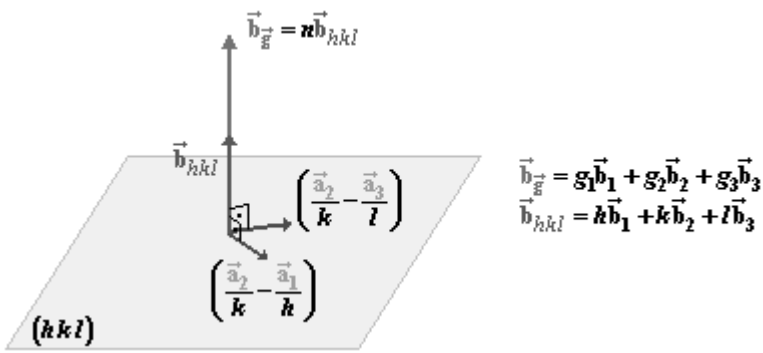

Figure 149 The direction given by the vector $\vec{b}_{hkl}$ in the reciprocal lattice is orthogonal to the family of (hkl) direct lattice planes.

$$\hat{\mathrm{n}}_{hkl} = \frac{\vec{\mathrm{b}}_{hkl}}{b_{hkl}} . \qquad \text{(VI.10)}$$

The versor given by Eq. (VI.10) specifies the orientation of a lattice plane denoted *(hkl)*.

Property 3

At last, we will calculate the distance between two consecutive (hkl) planes, d_{hkl}, using the vector $\hat{\mathrm{n}}_{hkl}$. To obtain the d_{hkl} parameter it is sufficient to project, for example, $\vec{\mathrm{a}}_1/h$ in the direction orthogonal to the (hkl) planes (as it is done in Fig. 150), that is to say

$$d_{hkl} = \frac{\vec{\mathrm{a}}_1}{h} \cdot \hat{\mathrm{n}}_{hkl} = \frac{\vec{\mathrm{a}}_1}{h} \cdot \frac{\left(h\vec{\mathrm{b}}_1 + k\vec{\mathrm{b}}_2 + l\vec{\mathrm{b}}_3\right)}{b_{hkl}} = \frac{2\pi}{b_{hkl}} . \qquad \text{(VI.11)}$$

This means that two consecutive planes of the family of (hkl) planes are at a distance which is equal to the inverse of the modulus of the $\vec{\mathrm{b}}_{hkl}$ vector multiplied by 2π.

As an example, let us now apply the formula that we obtained for d_{hkl} for the *sc* lattice. We will start with the family of the (100) lattice planes. The information about the vectors that generate the direct, $\vec{\mathrm{a}}_1$, $\vec{\mathrm{a}}_2$, $\vec{\mathrm{a}}_3$, and

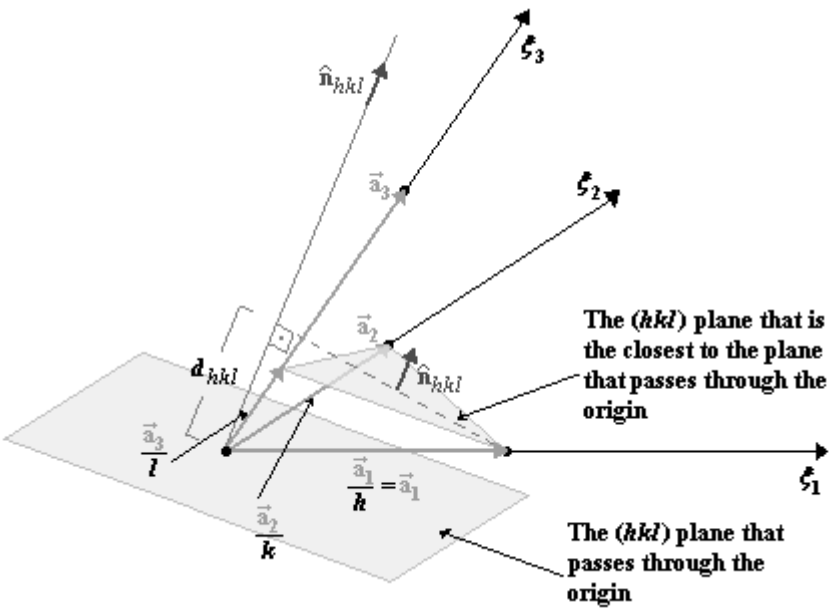

Figure 150 Two consecutive (hkl) planes. The direction orthogonal to these planes, defined by versor $\hat{\mathrm{n}}_{hkl}$, is shown. The distance, d_{hkl}, between these planes is also indicated.

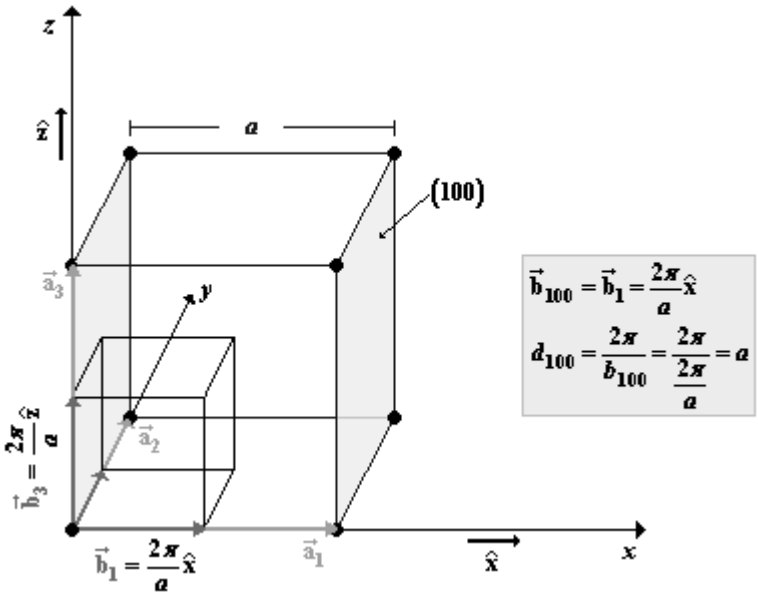

Figure 151 The (100) planes which include two cube faces that are parallel to each other in the *sc* lattice. The cubic unit cell defined by primitive translation vectors $\vec{b}_1$, $\vec{b}_2$, $\vec{b}_3$ of the reciprocal lattice is also shown. The translation vector $\vec{b}_{100} = \vec{b}_1$ is orthogonal to the (100) planes.

the reciprocal, $\vec{b}_1$, $\vec{b}_2$, $\vec{b}_3$, lattices is given in Fig. 151. We can see in this figure that $\vec{b}_1 \parallel \vec{a}_1$, $\vec{b}_2 \parallel \vec{a}_2$, and $\vec{b}_3 \parallel \vec{a}_3$. So the vector $\vec{b}_{100} = 1\vec{b}_1 + 0\vec{b}_2 + 0\vec{b}_3 = \vec{b}_1$ is indeed orthogonal to the (100) plane. The distance between two consecutive (100) planes, which include two cube faces that are parallel to each other, is $d_{100} = 2\pi/b_{100} = a$, it means, it is equal to the cube edge lengths as it should be.

As a second example, we will consider the family of planes that are orthogonal to a body diagonal of the cube that represents the cubic unit cell of the *sc* lattice. Two of these planes, denoted (111), are shown in Fig. 152. The figure shows also the cubic unit cell of the reciprocal lattice, generated by the primitive translation vectors $\vec{b}_1$, $\vec{b}_2$, $\vec{b}_3$, which were obtained using the primitive translation vectors $\vec{a}_1$, $\vec{a}_2$, $\vec{a}_3$. We can see in Fig. 152 that the vector $\vec{b}_{111}$ is parallel to the body diagonals of both cubes. So this vector is indeed orthogonal to the (111) direct lattice planes. The two (111) planes shown in Fig. 152 divide the body diagonal of the direct lattice unit cell in three segments of equal longitude. Thus the distance between these planes is equal to $1/3$ of the longitude of the diagonal of the cube:

$$d_{111} = \frac{1}{3}\sqrt{3}a = \frac{\sqrt{3}}{3}a\,. \qquad \text{(VI.12)}$$

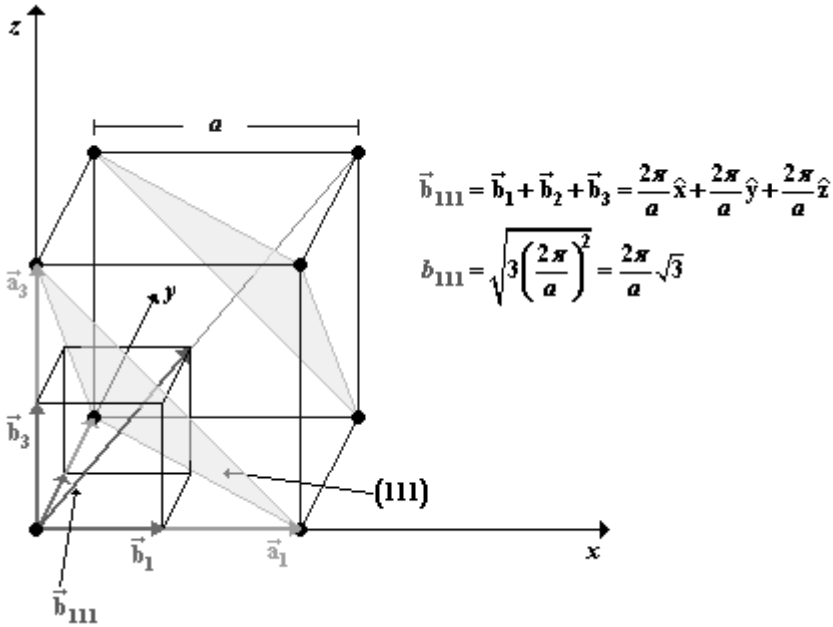

Figure 152 The cubic unit cells of the *sc* direct lattice and the reciprocal to it. The vector $\vec{b}_{111}$ of the reciprocal lattice is orthogonal to the (111) planes in the direct lattice.

The distance between the (111) planes calculated using Eq. (VI.11) is

$$d_{111} = \frac{2\pi}{b_{111}} = \frac{2\pi}{\frac{2\pi}{a}\sqrt{3}} = \frac{\sqrt{3}}{3}a\,. \qquad \text{(VI.13)}$$

This result agrees with d_{111} given by Eq. (VI.12), which we obtained from geometric considerations.

4. Problems

Exercise 1 In the *sc* lattice from Fig. 153

a.) draw five (111) lattice planes,

b.) draw all (221) lattice planes that contain at least two points from the (010) front large cube face. Place additional points on the z axis if necessary.

Does the (221) lattice plane that is the closest to the origin belong to the set of planes specified in b.)?

Exercise 2 For each case from Exercise 1 calculate the distance between two consecutive planes.

Exercise 3

a.) Without doing any calculations show that the consecutive lattice planes, orthogonal to body diagonals of the cubic unit cells of the *sc* and *fcc* lattices with the same lattice constant *a*, are at the same distance. Find this distance.
***Hint*:** Draw such lattice planes inside the cubic unit cells of the *sc* and *fcc* lattices (both having the same edge *a*).

b.) Check your result, obtained for the case of the *fcc* lattice in a.), calculating the distance in consideration using Eq. (VI.11).
***Hint*:** Use the primitive translation vectors that define the rhombohedral unit cell of the *fcc* lattice.

c.) Find the distance between the consecutive planes, orthogonal to a body diagonal of the cubic unit cell of the *bcc* lattice with the same lattice constant *a* as has the *fcc* lattice in b.), and compare it with d_{111} calculated there.

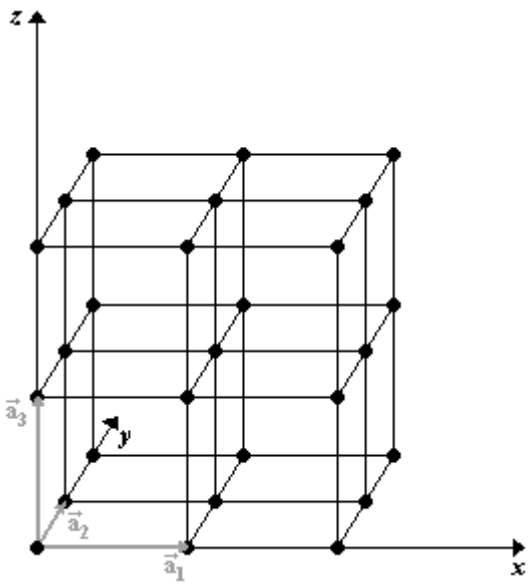

Figure 153 A simple cubic lattice, of lattice constant *a*, generated by the translation vectors $\vec{a}_1$, $\vec{a}_2$, $\vec{a}_3$.

***Hint*:** Choose appropriate primitive translation vectors for the *bcc* lattice.

Exercise 4 Figure 154 shows a two-dimensional lattice generated by the primitive translation vectors $\vec{a}_1$, $\vec{a}_2$ and four consecutive (41) planes in this lattice (Note, that in a two-dimensional lattice the planes are one-dimensional and are characterized by two Miller indices.). The Miller indices, 4 and 1, were calculated using the integer numbers s_1 and s_2 specified in Fig. 154:

$$\frac{1}{s_1}:\frac{1}{s_2}=\frac{1}{1}:\frac{1}{4}=4:1=h:k\,. \tag{VI.14}$$

It is also true that

$$s_1:s_2=\frac{1}{h}:\frac{1}{k}\,, \tag{VI.15}$$

thus the inverse of the Miller indices are at same ratio as s_1 and s_2. Due to Eq. (VI.7) the (41) lattice plane, that is the closest to the plane that passes through the origin, intersects the axes ξ_1 and ξ_2 in the points $(1/h)\cdot\vec{a}_1$ and $(1/k)\cdot\vec{a}_2$, respectively. It means, the intercepts of this lattice plane with the axes ξ_1 and ξ_2 are $1/h$ and $1/k$, respectively. Fig. 154 shows also three (41) planes whose intercepts with the ξ_1 axis represent the multiples of the smallest intercept, $1/h$, and are not larger than the integer s_1, that is

$$2\cdot\frac{1}{h},\ \ 3\cdot\frac{1}{h},\ \text{ and }\ 4\cdot\frac{1}{h}=s_1\,.$$

In similar way are obtained the intercepts of these planes with the ξ_2 axis, which are

$$2\cdot\frac{1}{k},\ \ 3\cdot\frac{1}{k},\ \text{ and }\ 4\cdot\frac{1}{k}=s_2\,.$$

The plane with integer intercepts s_1 and s_2 is the one that we usually use to determine the Miller indices.

a.) Show at least one more lattice point in each of the (41) lattice planes from Fig. 154 that have only one lattice point in the figure.

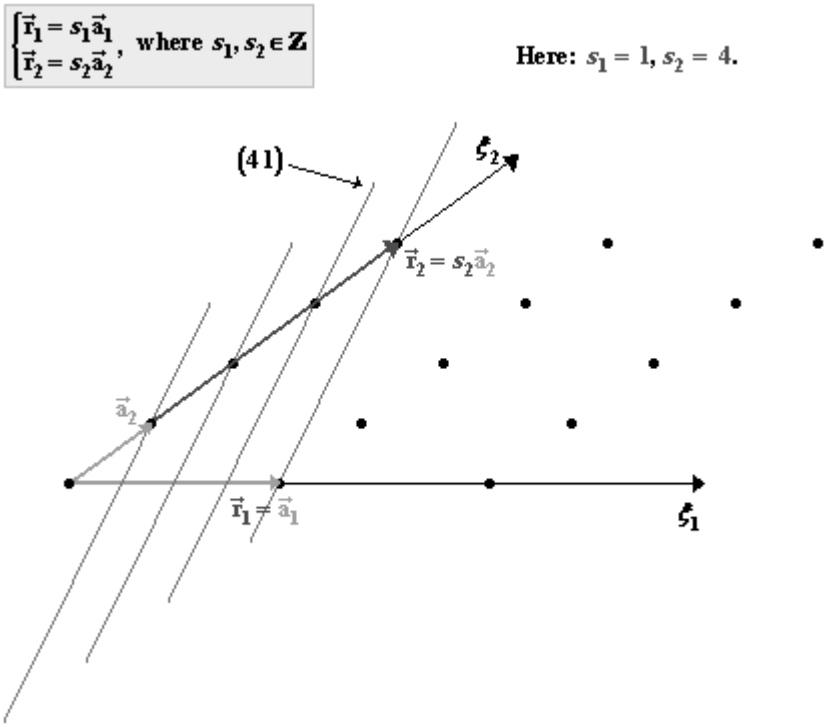

Figure 154 Two-dimensional crystal lattice generated by the primitive translation vectors $\vec{a}_1$, $\vec{a}_2$. In the figure four consecutive (41) lattice planes are shown.

b.) Find and draw (keeping proportions) the primitive translation vectors $\vec{b}_1$ and $\vec{b}_2$ of the reciprocal lattice and show graphically that the vector $\vec{b}_{41}$ is orthogonal to the (41) planes.
***Hint*:** To find the primitive translation vectors $\vec{b}_1$ and $\vec{b}_2$ follow the indications given in Exercise 1 from Chapter V.

REFERENCES

1. N. W. Ashcroft and N. D. Mermin, *Solid State Physics* (Holt, Rinehart and Winston, 1976).
2. J. D'Ans, R. Blachnik, E. Lax, and C. Synowietz, *Taschenbuch Für Chemiker und Physiker: Band 3: Elemente, Anorganische Verbindungen und Materialien, Minerale*, 4th ed. (Springer, 1998).
3. J. R. Davis, *Metals Handbook Desk Edition*, 2nd ed. (Taylor and Francis, 1998).
4. B. Douglas and S.-M. Ho, *Structure and Chemistry of Crystalline Solids* (Springer, 2006).
5. R. T. Downs and M. Hall-Wallace, *The American mineralogist crystal structure database*, American Mineralogist 88, 247 (2003).
6. P. Eckerlin and H. Kandler, *Structure Data of Elements and Intermetallic Phases* (Springer, 1971).
7. W. F. Gale and T. C. Totemeier, *Smithells Metals Reference Book*, 8th ed. (Elsevier, 2004).
8. C. Giacovazzo, *Fundamentals of Crystallography* (Oxford University Press, 1992).
9. S. Gražulis, D. Chateigner, R. T. Downs, A. F. T. Yokochi, M. Quirós, L. Lutterotti, E. Manakova, J. Butkus, P. Moeck, and A. Le Bail, *Crystallography open database – an open-access collection of crystal structures*, Journal of Applied Crystallography 42, 1 (2009).
10. T. Hahn, *International Tables for Crystallography*, 3rd ed. (Kluwer Academic Publishers, 1993).
11. T. Hahn and H. Wondratschek, *Symmetry of Crystals* (Heron Press, 1994);
12. M. Hellenbrandt, *The inorganic crystal structure database (ICSD) – present and future*, Crystallography Reviews 10, 17 (2004).
13. C. Kittel, *Introduction to Solid State Physics*, 5th ed. (Wiley, 1976).
14. W.-K. Li, G.-D. Zhou, and T. C. W. Mak, *Advanced Structural Inorganic Chemistry* (Oxford University Press, 2008).

15. D. R. Lide, *CRC Handbook of Chemistry and Physics*, 88th ed. (CRC Press, 2007).

16. W. Martienssen and H. Warlimont, *Springer Handbook of Condensed Matter and Materials Data* (Springer, 2005).

17. J. W. Martin, *Concise Encyclopedia of the Structure of Materials* (Elsevier, 2007).

18. L. R. Morss, N. M. Edelstein, J. Fuger, and J. J. Katz, *The Chemistry of the Actinide and Transactinide Elements*, 3rd ed. (Springer, 2006).

19. W. B. Pearson, *A Handbook of Lattice Spacings and Structures of Metals and Alloys* (Pergamon Press, 1958).

20. G. S. Rohrer, *Structure and Bonding in Crystalline Materials* (Cambridge University Press, 2001).

21. D. Sands, *Introduction to Crystallography* (Courier Dover Publications, 1993).

22. L. Smart and E. A. Moore, *Solid State Chemistry: An Introduction*, 3rd ed. (CRC Press, 2005).

23. R. J. D. Tilley, *Crystals and Crystal Structures* (Wiley, 2006).

24. E. Y. Tonkov and E. G. Ponyatovsky, *Phase Transformations of Elements Under High Pressure* (CRC Press, 2004).

25. R. W. G. Wyckoff, *The Structure of Crystals* (Read Books, 2007).

26. D. A. Young, *Phase Diagrams of the Elements*. (University of California Press, 1991).

INDEX

A

A-face 29, 31-2, 63
α-Mn 73
α-MnTe 114, 130-2
α-NiS 130, 132
α-PoO_2 115-16
α-Sm 81, 103-4
α-Yb 86, 104
α-ZnS 118, 120, 123
α-ZrP 139, 151
actinides 80, 115, 137, 140
Ag 74, 114
americium 80, 137
AmO 116, 138
anions 107-8, 110-11, 113-22, 124-9, 131, 133-6, 142, 144, 146, 148-50
antimonides 131, 140
antimony 49-50
arsenic 49-50
atomic basis 3-4, 6-7, 48, 50
AuSe 130, 132
axes 17-18, 20-4, 40, 42-3, 46-53, 58, 64-5, 98, 120-1, 129, 136, 154-6, 169-72, 175-6, 180, 182
  fourfold 19, 58, 65
  lattice 169, 175-6
  onefold 24
  sixfold 26, 50-1, 124
  threefold 18-19, 21, 23, 27, 39, 43, 46, 51, 58, 60, 65
  twofold 20, 24
axis, sixfold hexagonal prism 51

B

β-Ca 72, 105
β-Ce 79-80, 105
B-face 29, 31-2, 34
β-Li 72, 105
β-Na 72, 105
β-PbF_2 115-16
β-SiC 109, 112-13
β-Yb 74, 104
β-ZnS 114, 118, 149
Ba 116, 126
BAs 113, 137
basis atoms 9-10, 48-50
basis vectors 2-3, 5, 7-10, 24, 26, 36, 40, 42-4, 46-7, 51, 53-4, 83, 85, 102-3
  conventional 5
bcc (body centered cubic) 35, 39, 41-2, 46, 54-5, 67, 71-3, 86, 88, 101-2, 164-5, 181
BePo 112, 114
BeS 112, 114
BeSe 112, 114
BeTe 112, 114
Bi 49-50, 71, 130, 137
bismuth 49-50
bismuthides 131, 140
BN 113, 123
bonds 67, 91, 107, 109, 112-14, 120, 125, 134
  chemical 92-3
  covalent 91, 93-4, 99, 107-8
  ionic 107-8, 134
  metallic 99, 125
borides 140

Bravais lattice symbol 35
Bravais lattices 28, 35-8, 48, 56, 68, 77, 79, 98
  bcc 167
  centered 29, 36, 56
  hexagonal 67
  orthorhombic 36
  trigonal 49
BS 122, 149
BZn 122, 149

C

C-face 29, 31, 33-4, 43, 63
cadmium 86, 102, 140
CaF_2 114-16
calcium fluoride 114
californium 80
carbides 140
cations 92, 107-8, 110-11, 115-20, 125-9, 131, 133-6, 142, 144-6, 148-51
ccp (cubic close-packed) 77-8, 81-3, 87, 89-90
Cd 86, 116
CdPo 114, 140
CdSe 114, 123, 149
Ce 80, 147
cell 2, 4-6, 28-36, 39-44, 46-58, 64-5, 73, 80, 84, 90, 94, 98, 103, 119-21, 162-3, 165-6
  centered 29-30, 33-4, 63
  centered monoclinic 31, 36
  conventional 12-14, 24-9, 32-4, 37, 50, 63
  primitive rhombohedral 53, 55
cell parameters 29, 81
  conventional 24, 26, 29
  experimental 103
cell parameters ratio 83
cell volumes 4, 41, 69
  hexagonal unit 87
centering points 47, 51-2
centering type 29, 31
cerium 79-80, 105
cesium chloride 111, 144-5
chalcogenides 137, 140
Cl 134-6, 141, 144
compounds 90, 92, 99, 107, 111-15, 117, 120, 122-3, 125, 129-32, 134, 136-40, 143-6, 148-51
  binary 90, 92, 99, 107, 112, 118, 120, 122-3, 129, 134, 136, 148
  I-VI 118
  I-VII 136, 151
  II-III and II-IV 117-18
  II-VI 112, 144, 152
  II-VII 115-16
  intermetallic 146-8
  IV-VI 136-7
  V-VI 136-7
coordination number 38, 41, 46, 69-70, 79, 91, 99, 102, 107, 111-12, 117, 134, 142, 145
CoSb 130, 132
CoSe 130, 132
CrS 130-2
CrSb 130, 132
CrSe 130-2
CrTe 130, 132
crystal families 35-6
crystal lattice 153, 160, 166, 171, 183
crystal structure 1-7, 9, 13-15, 50, 67-70, 88-9, 103, 107, 109, 111, 117, 119, 121, 127, 135, 145

close-packed 67
Hg 50, 64
monoatomic 48, 67
one-dimensional 1
sc 48, 50, 69-70, 72, 102
three-dimensional 92
two-dimensional 4, 6-7, 9-10, 14
crystal systems 13, 24-8, 35, 37, 162
cubic 25-6, 34-5, 46
hexagonal 26, 35
monoclinic 24, 29, 32-3, 63
orthorhombic 32-4
tetragonal 26, 34
triclinic 24, 29
trigonal 26-7, 46, 50
crystalline materials 153
Cs 67, 134, 144, 149
CsBr 134, 136, 145-6
CsCl 134, 136-7, 144-6
CsI 134, 136, 145-6
Cu 73-4, 150
CuSb 130, 132, 150

D

dhcp (double hexagonal close-packed) 79-82, 86-8, 100-2, 133
dodecahedron 58, 65
regular 65
Dy 81

E

ε-NbN 132, 151
Er 81, 138-9, 146-7
Eu 116, 146
experimental data 50, 103, 105, 140, 143-4, 151

F

fcc (face centered cubic) 42-3, 45-6, 48-9, 63-5, 67, 73-4, 77-9, 81-3, 87-90, 97-8, 101-2, 108, 117, 127, 135, 181
Fe 73, 139
FeS 130, 132
FeSb 130, 132
FeSe 130-2
FeTe 130, 132
filling factor 69-70, 72-4, 87, 102, 151
fluorides 115-16

G

gadolinium 81, 102-3
GaN 123, 149
Gd 81, 103
graphical symbols 9, 13, 60

H

halides 136, 145
alkali 111, 134, 142-4
silver 137
thallium 145-6, 148
halogens 67, 134
hard spheres 68-70, 73-4, 84, 87, 92, 96, 102, 140-1
hcp (hexagonal close-packed) 67, 77-9, 81-4, 86-91, 100-2, 120-1, 124, 126-7, 129, 133

helium 86
hexagon 9, 11, 13, 59-60
  regular 13, 20, 59-60
hexagonal prism 18, 26-7, 50-2, 54, 60-2, 64, 77, 80-3, 89-90, 102-4, 118-19, 124-6, 128, 133, 149, 151
hexagonal structure 118, 124
  two-dimensional 75, 91-2
HfAs 130, 132
HfP 130, 132
HfPo 130, 132
Hg 49-50, 116
Ho 81, 86, 116, 138-9
hydrides 115-16, 140

I

interatomic distances 67, 73, 100, 102, 104, 143, 152
interstices 70, 87, 89-91, 94, 111, 117, 119, 134, 136
  cubic 144
  octahedral 89, 91-2, 126-7, 131, 133-4, 144
  tetrahedral 87, 89-92, 94, 108, 110, 114, 126-7, 134
  trigonal prism 134
Ir 74, 138-9
IrSb 130, 132, 150
IrSn 130
IrTe 130, 132, 150

K

KCl 137, 144
KF 137, 143, 151

L

La 79-80, 147
lanthanides 79-80
lattice 1-10, 12-15, 17-20, 24-6, 28-36, 38-9, 41-3, 45-9, 51-4, 56, 63-5, 160, 162-7, 170-6, 179, 181-2
  bcc 39-42, 54-8, 64, 164, 182
  centered 32, 34
  centered hexagonal 51, 53
  cubic 34, 46-7, 55, 64, 181
  direct 153, 160-3, 166-7, 177, 180
  fcc 43-5, 48, 55-8, 62-4, 136, 163-4, 167, 181
  fcc Bravais 136
  hexagonal 8, 13-15, 51-2, 103
  infinite 8-9, 12-13, 15, 17-18, 24, 29, 32, 36, 154
  monoclinic 29-32, 63
  orthorhombic 33
  primitive 34-5
  primitive cubic 35
  primitive monoclinic 29
  sc 46-9, 163, 169-73, 178-80
  tetragonal 34
  three-dimensional 17, 36, 169
  triclinic 24, 29, 162
  trigonal 35-6, 46, 49-53, 103
  two-dimensional 13, 15, 169, 182-3
  two-dimensional crystal 154
lattice constants 48, 72, 74, 80, 99, 102-3, 105, 113-14, 118, 128, 136, 143-4, 149-50, 164, 167, 181

experimental 99, 104-5, 115, 143, 149, 152
lattice direction 173-4
lattice nodes 9
lattice parameters 39, 86, 112, 116, 121, 123, 131-3, 137-9, 146-8, 151-2
experimental 50, 80, 112, 122, 131, 136
lattice planes 169-71, 173, 175-8, 180-3
family of 169, 173
lattice point symmetries 24
lattice points 2-9, 24, 28-9, 31-2, 36, 38-9, 41-51, 53, 55-8, 62-4, 169, 173, 175, 182
centering 29
lattice translation vector 153
lattice types 13, 28-9, 31
layer planes 76, 98
layers 75-8, 82, 86, 89-92, 97-8, 100, 102-3, 118, 121-6, 133-6
adjacent 78, 86, 91, 100, 102-3, 122-3
anion 128, 135
cation 124-7
close-packed 76, 91-2
consecutive 78-9, 91-2, 98, 122, 134, 149
hexagonal 89, 118, 122, 126, 135-6
sequence of 79-81, 83, 90-2, 97, 102, 133, 136
two-dimensional *hcp* 81, 94, 149-50
Li 67, 117-18, 134, 137, 144
Li_2O 117-18
LiBr 137, 143
LiCl 137, 151
LiI 137, 143
limiting radius ratio 107, 111, 141-2, 144, 146, 148
Lu 81, 116, 138-9, 146-7

M

mercury 50, 64
mercury chalcogenides 140
metal halides 137
metal oxides 117
metallic elements 67, 74, 91, 101, 148
metals 1, 72-4, 79, 86, 88, 99-100, 102, 105, 115, 131, 137, 140, 148
alkali 67, 117, 134
alkaline earth 136
iron group 131
MgPo 130, 132
Miller indices 169-73, 175, 177, 182
MnAs 130, 132
MnBi 130, 132
MnSb 130, 132
MnTe 123, 149
monoclinic cells 32

N

Na 67, 112, 134-5, 144
NaCl 92, 134, 136-7, 140-1, 151
Nb 72, 116, 138-40, 151
NbN 130, 132, 139, 150-1
NbS 130, 132

Ni 74, 116, 125, 131, 139
NiAs 92, 124-5, 127-8, 130-2, 137-40, 149, 151

NiBi 130, 132
nickel arsenide 111, 124, 131
NiPo 130, 132
NiSb 130, 132
NiTe 130, 132
NN interatomic distances 39, 99-102, 105, 123, 140-1, 150-1
NNN interatomic distances 39, 123
NNs (nearest neighbors) 38, 56-8, 69-74, 84, 90-4, 97-100, 102-5, 107-9, 117, 119-23, 125, 127-8, 131, 134-5, 140-6, 148-51
NNNs (next nearest neighbors) 38, 56-8, 62-3, 70, 72, 122-3, 131, 140-3, 148-51
noble gases 67, 74, 88, 91, 99
normal conditions 67, 70, 73-4, 80, 86-8, 99-101, 103, 105, 113-16, 118, 122-3, 131-2, 134, 137-9, 146-8, 151
normal pressure 67, 72, 74, 80-1, 86, 92, 104-5

O

octahedron 18, 20, 38, 56, 58-60, 89, 91, 125, 127-8, 134
  regular 19-20, 38, 58-9, 89, 127-8, 134
  truncated regular 56, 59
oxides 115-16, 140

P

packing fraction 69
parallelogram 5-7, 11, 13
Pb 116, 130, 137
Pd 74, 138, 150
PdSb 130, 132, 150
PdTe 130, 132
Pearson symbol 68-9, 71, 73, 79, 81, 83, 92, 112, 114, 117-18, 124, 133-4, 144
periodic table 67, 87, 92, 99, 112, 117, 129, 144, 152
periodicity 153-4, 158, 160-1
phase transitions 80-1
phosphides 117-18, 140
Po 116, 130, 137
polonium 70, 115
polyhedron 56, 128
  regular 125
Pr 116, 138-9, 146
prototype 68-9, 71, 73, 79, 81, 83, 92, 112, 114, 117-18, 124, 133-4, 144
prototype structure 68
Pt 74, 116, 150
PtB 130-1, 150
PtBi 130, 132

PtSb 130, 132
Pu 116, 138-9

R

Ra 72, 116
radii 67, 69-70, 72, 75, 98-9, 101, 107, 109, 113-14, 141, 143, 145, 151-2
  anion 143-4, 151

  atomic 67, 98, 102, 107
  cation 143
  covalent 99, 102, 109, 113

ionic 109, 111-12, 140, 143-4, 152
metallic 99, 102, 111-12
radius ratios 110-11, 142, 144
Rb 67, 118, 134, 137, 144
RbBr 137, 144
RbCl 137, 144, 151
RbF 137, 143-4
RE (rare earth) 79, 137, 140, 146-8
reciprocal lattice 153, 155, 157, 159-67, 169, 171, 173, 175, 177, 179-81, 183
reciprocal lattice vector 176
Rh 74, 138-9
RhBi 130, 132
rhombohedron 27, 39-40, 43, 46, 49-51, 60-2, 136
RhSe 130, 132
RhTe 130, 132
room temperature 67, 72, 74, 79-81, 86, 102-5
rotation axes 18-23, 58, 60
fourfold 20, 23-4, 26, 60
threefold 21-2, 60
twofold 20
rotation points 9, 11, 13, 20, 60
fourfold 20
highest order 14
n-fold 9
sixfold 8-10, 12-13
threefold 8-9
twofold 13

S

samarium 81, 103
Sb 49-50, 70, 113, 130, 139
sc (simple cubic) 35, 38-9, 46, 48-9, 64, 70, 72, 162, 170, 173-4, 179-81
ScPo 130, 132, 150
ScTe 130-2
Se 114, 118, 130, 137-8
setting 29, 35, 52-3, 63
b-axis 32, 63
c-axis 30, 32
obverse 53, 55
reverse 53, 55
Si 109, 113-14, 116
silicides 115-16
silicon carbide 109, 112-13
Sm 80, 82, 116, 138-9, 146-7
Sn 130, 137, 139
sodium chloride 111, 134-5
structure 1-10, 14-15, 48-50, 64, 67-84, 86-7, 89-99, 102-5, 107-53
anti-fluorite 111, 116-18
anti-NiAs 130-2, 149-51
bcc 71-2, 74, 99, 105, 146
close-packed 74, 81-2, 87, 89, 91, 102-3, 105
CsCl 144-8
cubic 74
dense-packed 88, 101
dhcp 79
diamond 91-9, 102, 108
fcc 67, 73-4, 76-7, 79-80, 82, 86, 91, 94
fluorite 114-17, 149
hcp 79, 83, 86-7, 102-3, 119
honeycomb 7-9, 15
NaCl 92, 111-12, 134-40, 142-4, 151-2
NiAs 124-7, 129-33, 140, 149-50

sc 69-71
Sm-type 81, 88, 100-2
sodium chloride 134-6
sphalerite 107
thcp 103
TiAs 131-3, 139, 151
two-dimensional boron nitride 14
wurtzite 92, 111, 118-20, 122-6, 134, 137, 143, 149
zinc blende 107-9, 112-14, 118, 120, 123, 127, 137-8, 143, 149
substructure 7, 92, 97-8, 108, 114, 117-19, 121-4, 126-7, 129, 135-6, 145
anion 92, 108, 111, 122, 127, 133, 136
cation 133-4, 136
cubic 144
fcc 114, 144
hcp 131
hexagonal 15, 126, 129
symmetry 2, 9, 11, 14, 17, 20, 22-4, 27-9, 33, 46, 122, 173
lattice 174
point 9, 12-15, 17-18, 24, 29, 32, 34, 36, 48, 56, 80, 82-3, 86, 90, 124, 153
translation 9-10, 17, 153
symmetry axes 17-18, 20, 22, 24, 26, 51, 124
symmetry axis, highest order 27, 81
symmetry center 18
symmetry points 9, 17, 19-20

T

Tb 81, 86
tetradecahedron 56, 59-60
tetrahedron 18-20, 87, 89, 91, 93-4, 97, 108, 120-1, 127
regular 19, 58-9, 87, 93, 97, 108, 115, 117, 120-1
thcp (triple hexagonal close-packed) 103
Ti 138-9
TiAs 130, 133-4, 139-40, 151
tin 92
tin pnictides 139
TiP 130, 132
TiPo 130, 132
TiSb 130, 132
TiSe 130, 132
TiTe 130, 132
Tm 81, 86, 116, 139, 146-7
TMs (transition metals) 81, 112, 114-17, 129, 131-2, 136-8, 140, 148
TNNs (third nearest neighbors) 38-9, 56, 62-3
translation vectors 4, 17, 24, 52, 153, 160, 164-6, 169, 172, 179, 181
primitive 1-2, 5-6, 9, 13, 36, 39, 160-1, 163-7, 169, 171, 173, 175-6, 179, 181-3
shortest 5, 42-3, 174
trigonal prism 127, 134
two-atom basis 9, 48-9, 67, 77, 98, 136

U

unit cell 6-8, 14-15, 31-3, 36, 47-50, 53-6, 64, 73, 81, 94-6, 98, 108, 120, 127-9, 135-6, 160-2

centered 35
centered cubic 43
centered hexagonal 51
centered rhombohedral 46-7
centered tetragonal 34
conventional 15, 18, 24, 34, 46, 68-9, 83, 89, 112, 119, 124, 129, 145
conventional primitive 5-6, 8, 12-13, 15, 30, 166
cubic 28, 41-5, 48, 69-70, 72-3, 76, 90, 94-5, 98, 109-10, 112-15, 117, 135-7, 163, 173, 179-81
diamond cubic 94
direct lattice 179
F-centered cubic 48
fcc cubic 94
hexagonal 51, 53, 83-5, 102-3, 119-20
NaCl cubic 136, 140
primitive 2-3, 5, 7, 13, 17, 29, 32, 36, 39-44, 46, 56, 136, 162-4, 166-7
primitive cubic 47, 64
primitive rhombohedral 40, 43-4, 46, 48-50, 53, 55, 64, 68
primitive tetragonal 34
rhombohedral 26, 46-7, 52-3, 64, 81, 97, 103, 112-13, 135, 163-5, 181

triple hexagonal 51-3, 55, 81, 103
UO 116, 138

V

VP 129-30, 132, 150
VSb 130, 132, 149-50
VSe 130-2, 149-50
VTe 130, 132

W

Wigner-Seitz cell 56-8, 65
wurtzite structure of ZnS 121-2, 149

Y

Y 81, 86, 116, 139, 146-7
Yb 72, 74, 81, 86, 104, 138-9, 146-7
ytterbium 81, 104
yttrium 81

Z

zinc 86, 102, 113, 124
zinc blende 92, 110-11, 122-4, 134, 137-8, 140, 149
zinc sulphide 107, 118
Zn 86, 108, 112-13, 118-22

ZnS 108, 112-13, 118-22, 149
ZnSe 114, 123, 149
Zr 116, 138-9, 151
ZrP 130, 132, 151
ZrPo 130, 132
ZrTe 130, 132